Минералдық шикізаттарды кешенді пайдалану

2 (329)

Комплексное Использование Минерального Сырья

Complex Use of Mineral Resources

The Journal "Complex Use of Mineral Resources" is included in the List of publications recommended by the Committee for Control in the Sphere of Education and Science of the Ministry of Education and Science of the Republic of Kazakhstan for the publication of the main results of scientific activities.
Owner: "Institute of Metallurgy and Ore Beneficiation" JSC

The Journal was re-registered by the Committee for State Control in the Sphere of Communication, Information and Mass Media of the Ministry of Information and Communication of the Republic of Kazakhstan.

Certificate № 16180-Ж since October 18, 2016

Crossref

Physico-chemical aspects of uranium extraction for investigation of underground well leaching control systems

[1]Turganaliev C.R., [2]Oryngozha E.E., [1,3]*Oringozhin E.S., [4]Nikulin V.V., [1]Alisheva Zh.N.

[1]Al-Farabi Kazakh National University, Almaty, Kazakhstan
[2]Almaty University of Power Engineering and Telecommunications named after Gumarbek Daukeyev, Almaty, Kazakhstan
[3]Institute of Mining named after Kunaev, Almaty, Kazakhstan
[4] State University of New York at Binghamton, Binghamton, NY, USA

* Corresponding author email: e24.01@mail.ru

ABSTRACT

This article gives the physical and chemical aspects of uranium extraction from the zones of reservoir oxidation using ultrasonic technology and the theoretical justification for the technology of in-situ borehole leaching (ISL) of uranium deposits in Kazakhstan. Kazakhstan has significant reserves, well-explored uranium deposits, developed uranium mining and processing capacities, as well as the current state of the world uranium market, which determine the prospects for the development of the uranium mining industry in Kazakhstan. Ore deposits of uranium deposits localized at the fronts of seam oxidation zones are largely similar in terms of the chemical composition of host rocks. *Fe, Al, Mg, Ca, K, and Na* are among the most widespread petrogenic elements of rock-forming minerals. Uranium is observed in association with iron, vanadium, selenium, molybdenum, rhenium, and other elements. Uranium mineralization is represented by exogenous (secondary) minerals – pitchblende and coffinite. In the general balance of uranium minerals, pitchblende is about 30%, and coffinite is about 70%. Nasturan ($xUO_2 \cdot yUO_3 \cdot z$) is represented by an association of tetravalent uranium dioxide and hexavalent uranium trioxide with a variable composition (UO_2+UO_3) - 65-85%, coffinite - tetravalent uranium silicate $USiO_4$.

Keywords: Physico-chemical aspects, recovery, uranium, theoretical substantiation, recovery, uranium, theoretical substantiation, in-situ leaching, wells.

	Information about authors:
Turganaliyev Saken Rahmatullayevich	*Candidate of Economic Sciences, Senior Lecturer, Al-Farabi Kazakh National University, Almaty, Kazakhstan, Al-Farabi Avenue, 71, 050040. Email: e24.01@mail.ru*
Oryngozha Yeraly Yernazuly	*Ph.D. doctoral student, Almaty University of Power Engineering and Telecommunications named after Gumarbek Daukeyev, Almaty, Kazakhstan, Baitursynov St., 126/1, 050013. Email: oryngozha_yeraly@mail.ru*
Oringozhin Ernaz Sovetovich	*Doctor of Technical Sciences, Chief Researcher of the Institute of Mining named after Kunaev, Professor of Al-Farabi Kazakh National University. Academician of the National Engineering Academy of the Republic of Kazakhstan., Almaty, Kazakhstan, Al-Farabi Avenue, 71, 050040. Email: e24.01@mail.ru*
Nikulin Vladimir Vladimirovich	*Ph.D., Associate Professor, State University of New York at Binghamton, ECE Dept., PO Box 6000, Binghamton, NY 13902-6000. Email: vnikulin@binghamton.edu*
Alisheva Zhanat Nurkuatovna	*Doctor Ph.D., Ass. Professor of al-Farabi Kazakh National University, Almaty, Kazakhstan, Al-Farabi Avenue, 71, 050040. Email: zhannat_86.2007@mail.ru*

Introduction

About 25% of the world's uranium reserves have been identified under the Republic of Kazakhstan. Uranium reserves are characterized by 75%. Of these, they are concentrated in deposits associated with regional zones of reservoir oxidation, which can be extracted by a relatively cheap and environmentally friendly in situ leaching method [1].

The development of the uranium mining industry in Kazakhstan is associated with the solution of key scientific and practical tasks. The modern uranium mining industry is characterized by high dynamism, the emergence of dangerous situations, in some cases radiation, and the need to make quick and effective decisions to eliminate them [[2], [3]]. The unique characteristics of each deposit require a certain amount of scientific research not only in the process of developing new deposits, but also in the application of well-known technological solutions. This situation objectively determines the high knowledge intensity of uranium mining production.

The analysis of the experience of exploitation of uranium deposits in the Chusar and Syrdarya regions shows the following [4]:

- In recent years, when developing large deposits (with optimal well placement grid sizes), a cellular arrangement of wells has been used;

- Reliable methods of well layout have not yet been developed, especially for deposits with complex structural conditions, such as the occurrence of ore bodies and hydraulic connections of aquifers;

- Well location schemes are selected on the basis of pilot tests and analogues.

The simplest, most effective and original method of developing hydrogen-containing uranium deposits is the method of underground borehole leaching. In principle, this leaching method can be successfully applied to the development of non-ferrous metal deposits in both underground and open-pit mining conditions [[1], [2], [3]].

Boreholes are the main technical facilities that provide an injection of a chemical or biochemical solution, control of its filtration process in the hydrogenous reservoir massif, uranium leaching processes, and delivery of productive solutions through pumping wells to the day surface for their processing. Thus, the system of boreholes for various purposes, drilled from the day surface to the depth of hydrogenous layers, is presented in the form of an underground mine.

For the opening of hydrogenous uranium deposits, the injection of biochemical solutions, as well as the pumping of productive solutions, are carried out using vertical wells. According to their purpose, they are divided into the following: technological, observational, control, and special [4].

In the exploitation of uranium deposits containing hydrogen, it is possible to use injection and extraction wells interchangeably. This means that each technological well can serve as both an extraction and injection well, allowing for a reversal in the direction of movement of working solutions in the productive horizon at a 180° angle. This reversal increases the degree of extraction of useful components from the deposit. The layout of technological wells, such as linear, areal, and combined, determines the scheme for opening the exploitation field of a hydrogenous uranium deposit.

Linear well arrangement systems consist of successively alternating rows of pumping and pumping wells over the area of deposits. Depending on the filtration coefficient and the homogeneity of the ore massif, the distances between rows and wells in a row vary widely (15-50 m or more). A production cell usually consists of two injections and one extraction well belonging to three consecutive rows.

In uranium deposits in the CIS (Commonwealth of Independent States) countries and other foreign countries, linear well arrangement systems were widely used, just as they are now. They are most effective in the development of extended hydrogenous uranium deposits composed of sedimentary, highly permeable ($K_F > 1.0$ m/day) ores and rocks and located in difficult hydrogeological conditions [[1], [5], [6], [7]].

Studies [[5], [7]] found that the most favorable of the tested is a linear system with a staggered arrangement of wells with a ratio of distances between wells in a row and between rows of 1:2, the least favorable is a system with a rectangular arrangement of wells with a ratio of distances of 1:1.

It is noted in [7] that in the domestic industry, a scheme of alternating linear rows of pumping and injection wells is mainly used with distances between wells in rows of 15–40 m, and between rows of 30–80 m. This well arrangement has a great advantage – the simplicity of construction and its operation. The most favorable for such a technological network are ore deposits of an elongated shape with good permeability. Depending on the specific conditions, the rows can be located along the strike or cross the strike. Under conditions of obtaining equal flow rates of pumping and injection wells ($Q0 = Q3$), the distance between wells in rows is also assumed to be the same.

Being in the group of actinides of the periodic system of elements by D.I. Mendeleev, the electronic structure of uranium, which determines the valence, is completed in the fifth shell from the top. Deep electrons, located on the fifth electronic level, due to the large atomic radius, are less firmly bound to the nucleus and, because of this, take part in the formation of valence bonds. Differences in the energy bonds of the electrons of the shells of the uranium nucleus are relatively small, but still exist, and this explains the multivalence of uranium. The main valence of uranium is 4, 5, 6. Variable valence leads to the formation of various complex compounds of uranium. Uranium mining by in-situ leaching through a system of wells drilled from the surface allows the most efficient exploitation of infiltration uranium deposits of in-situ and in-situ oxidation zones [[3], [7]].

When leaching in an acidic environment, uranium forms doubly charged uranyl cations (UO_2^{2+}), in an alkaline environment, uranate anions, and has a weak affinity for sulfur and a strong affinity for oxygen. As a result, simple and complex uranyl

sulfate ions are formed in HP solutions, depending on excess acidity. Additionally, in-situ leaching has a lower environmental impact compared to conventional mining methods. The use of injection and extraction wells allows for the control of the solution flow and prevents the release of harmful substances into the environment. The technology also reduces the amount of waste generated during the mining process, as only the useful components are extracted from the deposit.

However, there are also some challenges associated with in-situ leaching. One of the main challenges is the potential for groundwater contamination, which can occur if the solution used for leaching is not properly contained or if there are leaks in the well system. Another challenge is the potential for subsidence, which can occur if the pressure in the deposit is not properly maintained during the leaching process.

Overall, in-situ leaching is a promising technology for uranium mining, offering lower costs and environmental impacts compared to conventional mining methods. However, careful planning and monitoring are necessary to ensure the safe and effective extraction of uranium from hydrogenous deposits [8].

Research methods

Uranium compounds are relatively well soluble, which explains their migration ability with the formation of exogenous deposits of in-situ oxidation zones.

In solutions, uranium can exist in four valence states: U^{3+}, U^{4+}, U^{5+}, U^{6+} [1]. Aqueous solutions of salts of trivalent uranium are not very stable. Salts of tetravalent uranium form more stable solutions. Air oxygen oxidizes tetravalent uranium in aqueous solutions to hexavalent. Pentavalent uranium forms the uranyl radical (UO_2^+) in aqueous solutions in an extremely unstable form, which transforms into tetravalent and hexavalent uranium ions.

Quadrivalent uranium is slightly soluble in dilute solutions of sulfuric acid, and oxygen, permanganates, hydrogen peroxide, nitrogen-containing oxidizers, chlorine, chlorine-containing oxidizers, etc. can be used for its oxidation. Industrial applications are pyrolusite, melange, ferric iron salts, oxygen, and hydrogen peroxide [2]. For compounds of hexavalent uranium, the formation of the uranyl ion UO_2^{2+} is characteristic. Uranyl salts are highly hydrolyzed and have a pronounced acid reaction (pH 0.02M solutions of uranyl is 2.9) [[1], [4], [9]].

All salts are characterized by incomplete dissociation into ions.

In a sulfate medium, the uranyl ion is a strong complexing agent. In slightly acidic solutions with pH = 1-2, trisulfate and disulfate complex ions $[UO_2(SO_4)_3]^{4-}$ and $[UO_2(SO_4)_2]^{2-}$. In sulfate solutions, the ratio of simple and complex uranium ions depends on the excess acidity of the solution, the content of sulfate ions in it, and the concentration of uranium (Figure 1). For hexavalent uranium, the formation constants of the main complex ions in leaching solutions [[2], [6]]:

- for uranyl cation UO_2^{2+} - 5,0-6,5;
- for the neutral uranyl sulfate molecule $UO_2SO_4^0$ - 50-96;
- for uranyl disulfate anion $[UO_2(SO_4)_2]^{2-}$ - 320-900;
- for uranyl trisulfate anion $[UO_2(SO_4)_3]^{4-}$ - 2500.

An analysis of the graph shows that an increase in the acidity of the solution from pH = 3-3.5 to pH = 2-1.5 leads to a decrease in the content of the uranyl cation and, due to an increase in the content of sulfate ions, to a sharp increase in the complex ions of uranyl sulfate in the solution with the transition from a neutral molecule $UO_2SO_4^0$ to the anion of uranyl disulfate and uranyl trisulfate.
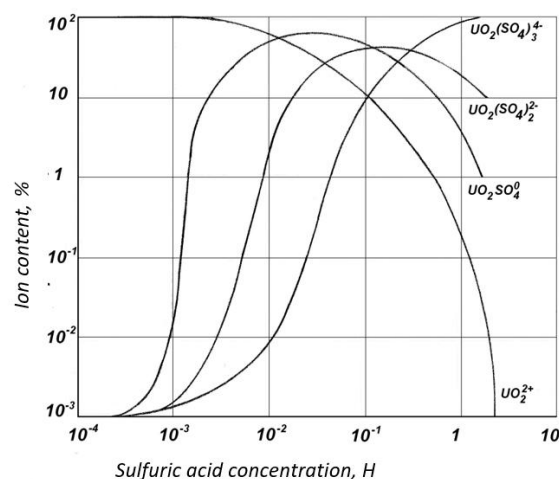
Figure 1 - Ionic composition of uranium compounds in sulfuric acid solutions at different acidity

Further, increase in acidity (up to pH=0.5-0.3) leads to a decrease in the content of $UO_2SO_4^0$; $[UO_2(SO_4)_2]^{2-}$, since in acidic solutions at pH < 2-1.5 the most stable form of uranium is the uranyl trisulfate anion $[UO_2(SO_4)_3]^{4-}$. If the solution is again raised to pH > 2.5, ion polymerization will appear with the formation of tri- and disulfate uranyl dimer $[UO_2O_5(SO_4)_3]^{4-}$, $[UO_2O_5(SO_4)_2]^{2-}$ due to hydrolysis of

complex ions, which leads to a significant increase in capacity of anion exchangers [[4], [10]].

Therefore, it is advisable to start uranium leaching in a mild mode at pH>2.5 (H_2SO_4 - 3.0-5.0 g/l), increasing the concentration in the uranyl sulfate solution to 50-60%. Then, increase the acidity of the solution to pH - 1.5-1.0 (H_2SO_4 - 10-15 g / l) and bring it to pH - 05.-0.3 (H_2SO_4 - 20-25 g / l), concentrating uranium in solution for uranyl trisulfate up to 95-100%. Then, at the outlet, quench the solution with soda to an acidity of pH - 2.5-4.0, facilitating the formation of well-sorbed uranyldimer trisulfate ions as much as possible.

In [10], the authors note that areal (cellular) well location systems are usually used to develop deposits confined to sedimentary layered heterogeneous ores and rocks of horizontal or slightly inclined occurrence, under conditions of relatively low water permeability of ores ($K_F \approx 0.1 \div 1$ m/day). These systems represent a uniform alternation of pumping and injection wells on the deposit area, forming cells (triangular, square, hexagonal, etc.) with small interwell distances ($8 \div 20$ m). In the CIS countries, the cellular arrangement of wells was rarely used.

With further involvement in the development by the IW method of more morphologically complex ore deposits with relatively low filtration coefficients (up to 1 m/day), large variability in the physicochemical properties of ores and host rocks, as well as when using high-rate pumps for pumping solutions, areal pumps (cellular) well layouts will be widely used.

In [[1], [11]] it is noted that cellular systems of wells are less common in domestic practice. So for isothermal ore deposits with relatively low, but allowing to obtain equal well flow rates ($Q_0 \approx Q_3$) permeability parameters of the massif, a square grid of alternating pumping and injection wells is taken.

For ore deposits of complex irregular shapes with low permeability parameters, it is advisable to use a hexagonal network of injection wells with a pumping well in the center of each cell. The ratio of debits in such a scheme $Q_o = 3Q_3$. Extraction wells are half as many as injection wells.

Other layouts of technological wells are also possible, in particular, triangular and pentagonal cells.

Bacterial leaching, also known as bioleaching, uses microorganisms to extract metals from ores. This method has several advantages over traditional mining methods, including lower energy consumption, reduced environmental impact, and higher metal recovery rates. Bacteria can be used to extract a wide range of metals, including copper, gold, silver, and uranium.

In the case of uranium, bacterial leaching can be used to extract the metal from low-grade ores that are not economically viable to mine using traditional methods. The process involves introducing bacteria into the ore deposit and allowing them to break down the minerals that contain the uranium. The uranium is then extracted from the solution using conventional methods.

The high efficiency of the method of bacterial leaching of gold from ore can be shown in the following example. In October 2001, the Polyus gold mining company announced that the first in Russia technological complex for extracting gold from ore using special bacteria was put into operation at one of the country's largest Olimpiada deposits, located 600 km north of the city of Kazan. Krasnoyarsk. Since 2002, Polyus has been annually giving the country 30 tons of gold. This is about a fifth of all precious metal mined in Russia. If we consider that 720 gold mining companies throughout the Magadan region mine 30 tons of gold per year, then one Polyus company replaces 720 companies, thanks to the use of bacterial leaching technology. The Polyus company employs only 1,000 people, while similar Western or Russian firms employ 11,000 workers.

Every year in the USA, 300 thousand tons of copper and 4 thousand tons of uranium are mined by leaching. Extensive research is being carried out on the extraction of Cu, Zn, Pb, Mn and other metals by leaching.

In addition, Kazatomprom officially stated that "depending on the configuration of the uranium ore body, two different types of landfill opening can be used: linear or hexagonal."

During the construction of uranium mines and their operation, the use of both triangular and hexagonal arrangements of technological wells causes large-scale economic damage, which is unacceptable.

One of the main advantages of bacterial leaching is its lower environmental impact compared to traditional mining methods. Bacteria do not produce toxic waste products, and the process does not require large amounts of water or energy. Additionally, bacterial leaching can be used to extract metals from ores that are too deep or too difficult to access using traditional mining methods.

However, there are also some challenges associated with bacterial leaching. One of the main challenges is ensuring that the bacteria are able to

survive and thrive in the harsh conditions of the ore deposit. This requires careful selection of the appropriate bacteria and optimization of the leaching conditions. Another challenge is controlling the leaching process to ensure that only the target metal is extracted and that other metals or contaminants are not released into the environment.

Overall, bacterial leaching is a promising technology for extracting metals from ores in a more environmentally friendly and cost-effective way. Further research and development are needed to optimize the process and ensure its safety and effectiveness in a range of mining conditions.

The main advantages of this method of in-situ uranium in-situ leaching compared to traditional mining methods of deposit development are as follows [12]:

– the possibility of involvement in the exploitation of poor and off-balance ore deposits with complex geological and hydrogeological conditions of occurrence, but having large reserves of uranium;

– significantly reduce capital investments and the time of putting deposits into operation;

– labor conditions are improved, the number of miners is reduced and labor productivity increases by 2.5 times;

– the negative impact of uranium mining on the environment is reduced.

The supply of the leaching brine is ensured by trunk pumps located in the pumping station, which can provide pressure up to 7 bar. The productive stratum is brought to the surface by submersible pumps installed in the pumping wells.

The peculiarity of the development system with piston wells is that all pumping wells work in a pulsating mode, during the cycle of changing the pumping and pumping modes (T) [[6], [7], [13]]:

- Cycle 1 - pumping wells of row 2 work for a given period (T) in injection mode, while pumping wells of row 1 work in pumping mode during the same period (T). All injection wells of row 2 are in operation, and all injection wells of row 1 are stopped.

- Cycle 2 - The injection wells of row 1 operate for a given period (T) in injection mode, while the injection wells of row 2 operate in pumping mode for the same period (T). All injection wells of row 1 are in operation, and all injection wells of row 2 are stopped.

In order to allow the pumping well to work in pumping and injection modes, it is necessary to install a sealed cap on the well casing and tie up each

pumping well with leaching solution distribution (LSD) and productive rastor reception (PRR) units with pipelines.

- leaching solution outlet (6), which is connected to the leaching solution distribution unit (LDSU);

- leaching solution pumping outlet (8), which is connected to the productive solution reception unit (PRR).

Injection mode:
- submersible pump in off-state;
- valve of this well in PRR in a closed position;
- valve of this well in LSD in the open position, which provides a supply of leaching rastor under pressure. The pressure is created in the leaching solution pumping station at the plant site.

Outflow mode:
- Valve of this well in LDSU in a closed position;
- Valve of given well in PRR in open position:

The submersible pump is in the off position, which ensures that the pay zone is lifted into the PRR and further into processing.

The radius of oxidized mining mass at a distance of 62.5 m between wells is taken from the ratio of 2/3 and is equal to 42 m. Such a radius allows to share 1/3 of the distance with adjacent wells.

Mathematical and physical models investigate one-dimensional filtration flows, while in real conditions the flows, as a rule, have multidimensional character, due to which the models do not objectively reflect the leaching process dynamics [[6], [14]].

Extrapolation of such modeling results to real conditions of this or that deposit, without production determination of parameters of uranium extraction process, is very conditional and, as a consequence, modeling data do not provide optimality of accepted technological decisions. In this regard, it is necessary to develop fundamentally new hydrodynamic models that take into account the multidimensional dynamics of the in-situ leaching process.

In most cases, the parameters used to design in-situ leaching facilities do not reflect the true picture of the development of uranium recovery in the specific conditions of the deposits under development, which leads to significant losses of productive solutions, failure to recover uranium from the subsurface and its contamination.

The actual sulfuric acid consumption for extraction of 1 kg of uranium is still significant and may reach hundreds or more kilograms due to the lack of accounting for the acid capacity of the host rock without ore.

There remain significant losses of solutions beyond the contours of the blocks (up to 20% or more).

The filtration zones of the pumping wells are colmatized within the radius of 1.5-2.5 m by clay particles and chemical sludge, which leads to the loss of up to 50.77% of the surplus head, obtained by level reduction, and negatively affects the productivity of the wells [[15], [16]].

There are no reliable instrumental methods of controlling the movement of geochemical, redox barriers.

Used pumps, relatively quickly fail due to abrasion of units by mechanical impurities, wear of stator motor sleeves, etc.

Up to 50% of injection wells fail during the first 23 years of operation due to failure of production strings integrity, filters destruction and poor insulation of annular space.

Not all the wells are equipped with the heads, preventing overflow of working solutions, which leads to contamination of the surface of in-situ leaching sites. In many cases there are no elementary flow meters, to say nothing of electrified valves for automatic regulation.

Uranium prices on the world market are rising, but uranium is mined under specific orders and, accordingly, the development of new deposits will be under orders.

NAC Kazatomprom has established permanent dosimetric monitoring and determines radiation levels in water, air, and dust [17].

Methods of intensification of in-situ leaching of uranium consist of raising the level of the aquifer, intensification of the leaching process, and differentiated supply of leaching solutions. As a result of the new methods of preparation and intensification of in-situ leaching, off-balance uranium deposit areas will be involved in development, reagent consumption will be reduced and the development of uranium deposits will be reduced. These research results will enable the following: uranium output per 1 km of deposit area will be differentiated by 20-30%; uranium production will be reduced by 15-20%; environmental safety of uranium production will be improved; the economic effect will amount to 60-80 mln tenge a year.

Discussion of results

In the leaching process, the reaction of the solvent with rock-forming minerals forms mobile geochemical barriers (acid-alkali and redox) with alternating acts of uranium dissolution and precipitation due to changes in pH and Eh of the environment. In this case, acids are used not only and not so much for uranium leaching but for the dissolution of rock-forming minerals, and in real conditions they may amount to tens and hundreds of kilograms per kilogram of uranium. The main acid-intensive minerals are carbonates (calcium, dolomite, magnesite) and some types of clay minerals.

Because of the consumption of H_2SO_4 for reaction with rock-forming minerals, its concentration front moves significantly slower than if only uranium leaching occurred. In this case, the concentration front of the dissolved uranium tends to overtake the acid front, but this does not happen, because as the acidity of the solution decreases at the acid concentration front, uranium hydrolysis and redeposition occur according to the scheme [17]:

$$UO_2^{2+} + OH^- = UO_2OH^+$$
$$UO^+ + OH^- = UO_2(OH)_2 \downarrow$$
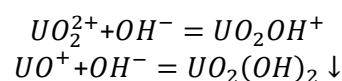
In this case, the concentration front of the acid plays the role of a mobile alkaline barrier. Then, when new portions of acid approach, the redeposited substance dissolves again, i.e. the reaction goes in the opposite direction. Repetitive steps lead to an increase in the concentration of H_2SO_4 at the mobile barrier to the saturation concentration.

It is not possible to determine the spatial and temporal position of the geochemical barrier under conditions of underground leaching by computational methods. Changes in parameters of pH and Eh, its ionic composition are monitored only by observation wells and at the outlet of pumping wells.

There are no in-situ leaching process models related to thermodynamics that answer the questions of spatial and temporal control of redox processes of uranium leaching in the deposits of formation oxidation zones yet. The creation of a generalized mathematical model of Redox potential control for these conditions remains an extremely difficult and, perhaps, as yet unsolvable task.

It is known that the Redox potential value is directly related to the concentration of the potential-determining components of the system:

$$E = E_o + \frac{0,059}{n} \ell g \frac{/O_к/}{/B_o/}.$$

From the point of view of potential-determining systems, the association of uranium and iron is of greatest interest at these deposits. The reaction between uranium and iron in an acidic environment goes in the direction of oxidation of uranium and reduction of iron.

Oxidation potentials for iron:

$$Fe \xrightarrow{-0,44} Fe^{2+} \xrightarrow{+0,771} Fe^{3+} \xrightarrow{<+1,9} FeO_4^{2-}.$$
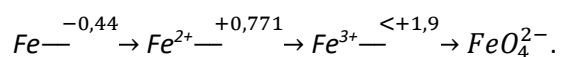
In turn, at Eh +0.35c the tetravalent uranium transforms into the hexavalent hydrated oxide $UO_2(OH)_2$ and then at Eh +0.407c into the hexavalent divalent cation-uranium form UO_2^{2+}.

The oxidation of uranium involving trivalent iron ions proceeds by the reaction $UO_2 + 2Fe^{3+} \rightarrow UO_2^{2+} + 2Fe^{2+}$, where uranium is oxidized to the hexavalent form and iron is reduced to the divalent form.

Under real conditions of underground uranium leaching, in addition to iron ions, the solution always contains other cations of variable valence and ions that affect the redox potential value. However, the role of these ions in establishing the redox potential, as compared to iron ions, is insignificant. Iron ions play the role of catalysts in the uranium oxidation process.

In the process of in-situ leaching, complexation has a great influence on changes in the oxidative environment. During acid leaching, in addition to uranyl sulfate complexes UO_2SO_4 ; $[UO_2(SO_4)_2]^{2-}$, $[UO_2(SO_4)_3]^{4-}$, about half of calcium, magnesium, and manganese are bound to sulfate complexes $CaSO_4^0$, $MgSO_4^0$, $MnSO_4^0$. Up to 80% of aluminum and over 90% of iron $FeSO_4^+$, $Fe(SO_4)_2$, $AlSO_4^+$, $Al(SO_4)_2^-$ are bound into sulfate complexes. The proportion of simple ions decreases as the total concentration in the solution of sulfate sulfur increases, pH and Eh change, and the content of free SO_4 ions decreases. Complexation causes the acidity of in-situ leaching solution to shift towards increasing pH value and to maintain the process of uranium oxidation and dissolution on geochemical barriers, the H_2SO_4 flow rate has to be increased.

However, taking into account the fact that in the process of multiple circulations of sulfuric acid solutions between pumping and injection wells, up to 0,05 mol/l and more of ferrous oxide sulfate $FeSO_4$ in divalent form (Fe^{2+}) is accumulated in circulating solutions, maintenance of redox potential at the required level can be maintained without additional consumption of sulfuric acid and other oxidizing reagents. For this purpose, one should pay attention to the effects of the chemical action of ultrasound.

It is known that the kinetics of sound-chemical reactions in liquid media (water, solutions) is determined by the rate of formation and expenditure of radicals.

It can be assumed that under ultrasonic action on recycled water solutions in the cavitation mode, water molecules, going to the excited state [[1], [13], [18]], split into H, OH radicals, ionized with the formation of hydrated electrons e_{ag}^- and further in the presence of dissolved oxygen transformed to HO_2, O_2^- и OH and H_2O_2. The formed hydroperoxide radicals are oxidized by Fe^{2+}:

$$HO_2 + Fe^{2+} + H^+ \rightarrow Fe^{3+} + H_2O_2,$$
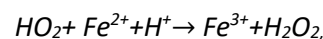
and the formed hydrogen peroxide H2O2 will additionally oxidize two Fe^{2+} ions by the reactions

$$H_2O_2 + Fe^{2+} + H^+ \rightarrow Fe^{3+} + OH + H_2O,$$
$$OH + Fe^{2+} \rightarrow Fe^{3+} + OH^-$$
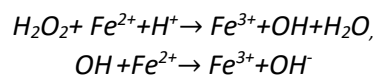
The equation of the chemical-acoustic yield of Fe^{3+}, in this case will be written as:

$$Fe^{(O_2)}(Fe^{3+}) = 3F_{HO_2}^{(O_2)} + F_{HO}^{(O_2)} + 2F_{H_2O_2}^{(O_2)}$$

Energy output $Fe^{(O_2)}(Fe^{3+})$ = 7,85.

Determination of the required number of productive solutions (V) at the annual capacity of the mine (P) 1000 tons of uranium per year and the average concentration (C) 70 mg/l uranium in the productive solutions (PS).

In all countries, including our country, uranium mining is carried out using underground in-situ leaching.

To develop each block, a linear system of three rows of wells is used: two rows of injection wells, and one row of withdrawal wells between them. There are 8 wells in each row.

In total, for one block there are 8 wells, the distance between them is assumed to be 25 m, the distance between the rows of wells is 50 m, and the number of injection and injection wells in the block is 3 × 8 = 24.

There are several methods of feeding chemical solutions into the block array in bacterial leaching. When applying the first method, a solution is used that contains special reagents that are capable of dissolving uranium and other metals, but do not interact with the rest of the components of the array. The solution passes through the porous structure of rocks and leaches uranium from the ore. The productive solution is then pumped to the surface and further processed to extract uranium.

The second method is used in IS technology and allows to extract uranium from hydrogen-containing deposits efficiently and economically. However, the second method is considered more efficient and environmentally friendly, as it allows you to extract more uranium from the ore and minimize the impact on the environment.

The chemical solution is an aqueous medium containing sulfuric acid at the rate of 3 g per liter of water.

The water in the solution becomes a good solvent, the chemical solution is heated to a temperature of 50-60 ° C. All these factors accelerate the leaching of uranium and other metals.

The third way.

A piston well is a well that can perform pumping and injection functions [18]. When using full piston wells, rows of spray wells are eliminated. After the beginning of the industrial application of advanced uranium purification technology from ores of permeable (water-intensive) deposits in the 50s of the last century, a kind of "boom" continues in the USA in all countries of the world to search for this type of deposits of uranium of sedimentary origin, the extraction of which is carried out in the simplest and therefore inexpensive way, known as the in-situ leaching method.

The essence of the technological scheme of this process is as follows.

Chemical or biochemical filtrates pumped through pumping wells are filtered through the holes and slits of the hydrogen plate to the nearest neighboring producing wells. During filtration, chemical solutions enriched to a concentration of uranium become "production solutions", which are pumped to the surface and transported to treatment facilities, where the production solution is subjected to absorption and desorption treatment, after which the uranium is extracted. To do this, a combination of various devices known as an adsorbent is used. It consists of absorption and regeneration columns, a tank for rich and dilute solutions, a tank for finishing chemical concentrates, a pump, a pipeline system and a set of auxiliary tanks for the preparation of solutions. filtration, neutralization of wastewater and mine treatment waters. In-situ filtration technology is most effective for the enrichment of hydrogenated uranium mines with filtration coefficients of more than 0.5 m/day.

Therefore, the scheme of underground filtration technology provides for the leaching of metallic uranium in the natural occurrence of an ore deposit. An indispensable condition for its use is the presence of aquifers on the roof and bottom of the ore formation. Among the various schemes of linear systems for the placement of technological hydrogen deposits, the most common in the practice of developing hydrogenated uranium deposits is a three-row system consisting of the first row of pumps, the second and third row of pumps. cargo pump. At the same time, the distance between the rows and wells in a row is 50 and 15 m or more, respectively. From the above it can be seen that the production cell usually consists of two injection wells and a production well between them, in three consecutive rows. In passive zones, during the operation of pumping wells, the previously permeable chemical solution will be partially filtered back into some pumping wells, which is unlikely, i.e. as soil-hydraulic screens [18]. The leakage of production solutions formed in the passive zones P1 and P2 towards the active zones A1 and A2 due to the pressure drop created by the operation of the pumps also occurs with significant losses.

In all mines of hydrogenous uranium deposits, linear well arrangements are widely used, consisting of successively alternating rows of pumping and pumping wells over the area of the deposit. A production cell usually consists of two injections and one extraction well belonging to three consecutive rows. In this case, a row of pumping wells is located between two rows of injection wells [[19],[20]].

The flow of the chemical solution supplied through the injection wells into the array of the hydrogenous reservoir is filtered in a circular area around each injection well. Both the chemical solution and the productive solution formed in the areas S_1 and S_2 cannot penetrate a number of pumping wells, since their return path is obstructed by the flows of chemical solutions supplied through the injection wells to the hydrogen reservoir mass. In addition, the pressure gradient created on the

suction side of the pump can have an effect at a distance of no more than 3-5 m.

Conclusions

This article describes the physical and chemical aspects of uranium extraction from the zones of reservoir oxidation using ultrasonic technology and the use of ISL technology in Kazakhstan has several advantages, such as reducing the environmental impact of mining activities, minimizing the need for surface infrastructure, and reducing the cost of production. The technology involves injecting a solution into the ore deposit through a borehole, which dissolves the uranium and other metals present in the deposit. The solution is then pumped back to the surface, where the metal is extracted.

The result of these works is the development of a technology for underground borehole leaching of uranium in Kazakhstan. To implement the ultrasonic method of acid-free increase in the redox potential of leaching solutions in industrial conditions, complex devices and high specific power of ultrasound are not required. Ultrasonic impact on the HP solution can be carried out in settling tanks using submersible magnetostrictive transducers with a flat radiating surface (PMS-6, PMS-38, etc.) and a frequency of up to 50 kHz, with a power consumption of 0.4 to 4 kW, or directly in sorption columns using ring magnetostrictive transducers operating at frequencies from 4 to 400 kHz with a power consumption of 2.5 to 10 kW, produced by the Taganrog and Tallinn machine-building plants.

ISL technology is one of the most effective methods for uranium mining, as it minimizes the loss and depletion of valuable minerals. The solution used in the process dissolves only the desired metals, leaving the rest of the minerals intact. This results in a higher recovery rate and a lower waste generation rate compared to traditional mining methods.

Accurate measurement and evaluation of the loss and depletion of valuable minerals are crucial for effective decision-making in mining operations. This information is used to determine the optimal mining method, estimate reserves, evaluate productivity, and optimize the development and production processes. In the simplest case, when a mineral with an average balance grade is lost, and the impoverishing rocks do not contain useful components, one ton of balance reserves can be represented as a rectangle, losses as part of this rectangle, and dilution as part of the rock added to the recoverable part of the balance reserves. At the same time, it must be borne in mind that the quality of the lost mineral and the quality of the impoverished rocks can be different. Therefore, in each specific case, it is necessary to take into account all the features of the geological structure of the deposit and the possible change in the quality of loss reserves and impoverishing rocks. For such cases, the term "contamination" introduced at the time, which characterizes only some addition to the recoverable balance reserves of the rock, is completely inappropriate.

For example, in ferrous metallurgy mines, the iron content in impoverishing rocks or off-balance ores usually ranges from 25 to 50% of its content in balance reserves. It is not clear what in such cases should be considered "garbage".

In the coal industry, the term "ash content" introduced instead of impoverishment does not fully characterize the quality of the mined coal. Therefore, the content of sulfur, phosphorus, moisture, etc. is additionally taken into account. All these qualitative indicators could be taken into account in one indicator - impoverishment, using an appropriate method for determining losses and impoverishment. The fact is that with the same ash content of the mined coal, its dilution can differ quite significantly, and vice versa.

The ash content can be significantly less than the dilution when the diluting rocks are carbonaceous shales with fairly high carbon content. In this case, dilution causes less damage than with rocks that do not contain carbon. Or, conversely, containing sulfur or phosphorus in large quantities than in balance reserves.

Consider an example. The excavation thickness of the seam is 1.3 m, the thickness of clean coal packs is 1.1 m, and the thickness of the rock layers is 0.2 m. In this case, the dilution determined by the direct method will be 68%. The rock layer is carbonaceous shale containing carbonaceous matter and having the following qualitative characteristics: ash content of 75%, sulfur content of 0.5%. With an ash content of clean coal packs of 12%, the ash content of the extracted rock mass is 6.8%, i.e. dilution will be 9.7%. With the sulfur content in clean coal packs, the sulfur content in the extracted rock mass will be %, i.e. as a result of the admixture of the rock layer, the sulfur content will decrease by 0.23%. When setting the price in mutual settlements between the mine and the processing plant, the coefficient of additional

payment (penalty) for a deviation of 1% from the base indicators for ash content is 2.5, and for sulfur 5.

When applying ultrasound to sorption columns, a double effect can be obtained - the intensification of sorption of uranium and the oxidation of Fe^{2+} to Fe^{3+}, to increase the redox potential of the solution leaving the sorption columns and sent to injection wells.

The use of ultrasonic technology to increase the oxidation potential of the HP circulating solution will significantly reduce the cost of sulfuric acid at uranium leaching facilities and significantly reduce the cost of its production.

Conflict of interest. The authors of this study do not cooperate with other publishers on this topic.

Жер асты ұңғымаларын шаймалауды басқару жүйелерін зерттеу үшін уран алудағы физика-химиялық аспектілер

[1]Турганалиев С.Р., [2]Орынгожа Е.Е., [1,3]*Орингожин Е.С., [4] Никулин В.В., [1]Алишева Ж.Н.

[1] әл-Фараби атындағы Қазақ ұлттық университеті, Алматы, Қазақстан
[2] Г.Даукеев атындағы Алматы энергетика және байланыс университеті, Алматы, Қазақстан
[3] Д.А.Қонаев атындағы Тау-кен институты, Алматы, Қазақстан
[4] Бингэмтон Нью-Йорк мемлекеттік университеті, Бингэмтон, Нью-Йорк, АҚШ

ТҮЙІНДЕМЕ

Бұл мақалада ультрадыбыстық технологияны қолдана отырып, қабаттың тотығу аймақтарынан уран алудың физика-химиялық аспектілері және Қазақстанның уран кен орындарын жерасты ұңғымалық шаймалау (ЖҰШ) технологиясының теориялық негіздемесі келтірілген. Қазақстанда қорлары бойынша елеулі, жақсы барланған уран кен орындарының, дамыған уран өндіру және өңдеу қуаттарының болуы, сондай-ақ әлемдік уран нарығының қазіргі заманғы конъюнктурасы Қазақстанның уран өндіру өнеркәсібін дамыту перспективасының жоғары екендігін көрсетеді. Қабаттың тотығу аймақтарының фронттарында локализацияланған уран кен орындарының кендері негізінен жанас жыныстардың химиялық құрамына ұқсас. Жыныстарды құрайтын минералдарда ең көп таралған петрогендік элементтерінің қатарына Fe, Al, Mg, Ca, K, Na жатады. Уран темір, ванадий, селен, молибден, рений және басқа элементтермен байланыста болады. Уранның минералдануы экзогендік (қайталама) минералдар – настуранмен және кофинитпен білінеді. Уран минералдарының жалпы балансында настуран шамамен 30%, кофинит шамамен 70% құрайды. Настуран ($xUO_2 \cdot yUO_3 \cdot z$) төрт валентті уран диоксиді мен алты валентті уран үш оксидінің ауыспалы құрамынан (UO_2+UO_3) – 65-85%, коффинит – $USiO_4$ төрт валентті уран силикатынан тұрады.

Түйін сөздер: физика-химиялық аспектілері, экстракциялар, уран, теориялық негіздеме, жер асты шаймалау, ұңғымалар.

Авторлар туралы ақпарат:	
Тұрғаналиев Сәкен Рахметуллаұлы	*Э.ғ.к., Әл-Фараби атындағы Қазақ ұлттық университеті, Алматы, Қазақстан. Email: e24.01@mail.ru*
Орынгожа Ералы Ерназұлы	*PhD докторанты, Г.Даукеев атындағы Алматы энергетика және байланыс университеті, Алматы, Қазақстан. Email: oryngozha_yeraly@mail.ru*
Орынгожин Ерназ Советович	*Техника ғылымдарының докторы, ҚР ҰИА академигі, Д.А.Қонаев атындағы Кен істері институтының «Жер қойнауын игерудің арнайы әдістері» зертханасының меңгерушісі. Әл-Фараби атындағы Қазақ ұлттық университетінің профессоры, Алматы, Қазақстан. Email: e24.01@mail.ru*
Никулин Владимир Владимирович	*PhD докторы, Нью-Йорк штаты Бингемтон университетінің доценті, ECE департаменті, PO Box 6000, Бингемтон, Нью-Йорк, 13902-6000. Email: vnikulin@binghamton.edu*
Алишева Жанат Нуркуатовна	*PhD докторы, Әл-Фараби атындағы Қазақ ұлттық университетінің доцент қ.а., Алматы, Қазақстан. Email: zhannat_86.2007@mail.ru*

Физико-химические аспекты извлечения урана для исследования систем управления подземного скважинного выщелачивания

[1]Турганалиев С.Р., [2]Орынгожа Е.Е., [1,3*]Орингожин Е.С., [4]Никулин В.В., [1]Алишева Ж.Н.

[1]*Казахский национальный университет им. Аль-Фараби, Алматы, Казахстан*
[2]*Алматинский университет энергетики и связи им. Г.Даукеева, Алматы, Казахстан*
[3]*Институт горного дела им. Д.А. Кунаева, Алматы, Казахстан*
[4] *Государственный университет Нью-Йорка в Бингемтоне, Бингемтон, Нью-Йорк, США*

АННОТАЦИЯ

В этой статье даны физико-химические аспекты извлечения урана из зон пластового окисления с использованием ультразвуковой технологии и теоретическое обоснование технологии подземного скважинного выщелачивания (ПСВ) урановых месторождений Казахстана. Наличие в Казахстане значительных по запасам, хорошо разведанных месторождений урана, развитых добывающих и перерабатывающих уран мощностей, а также современная конъюнктура мирового рынка урана предопределяют перспективу развития уранодобывающей промышленности Казахстана. Рудные залежи урановых месторождений, локализуемые на фронтах зон пластового окисления, во многом сходны по химическому составу вмещающих пород. К числу самых распространенных петрогенных элементов породообразующих минералов относятся *Fe, Al, Mg, Ca, K, Na*. Уран наблюдается в ассоциации с железом, ванадием, селеном, молибденом, рением и другими элементами. Урановая минерализация представлена экзогенными (вторичными) минералами – настураном и коффинитом. В общем балансе урановых минералов настуран составляет порядка 30%, коффинит порядка 70%. Настуран ($xUO_2 \cdot yUO_3 \cdot z$) представлен ассоциацией двуокиси четырехвалентного и трехокиси шестивалентного урана с переменным составом (UO_2+UO_3) – 65-85%, коффинит – силикатом четырехвалентного урана $USiO_4$.

Ключевые слова: физико-химические аспекты, извлечение, уран, теоретическое обоснование, подземное выщелачивание, скважины.

Информация об авторах:

Тұрғаналиев Сәкен Рахметуллаұлы	*К.э.н., Казахский национальный университет им. Аль-Фараби, Алматы, Казахстан. Email: e24.01@mail.ru*
Орынгожа Ералы Ерназулы	*Докторант PhD, Алматинский университет энергетики и связи им. Г.Даукеева, Алматы, Казахстан. Email: oryngozha_yeraly@mail.ru*
Орынгожин Ерназ Советович	*Д.т.н., академик НИА РК, заведующий лаборатории «Специальные методы разработки недр», Институт горного дела им. Д.А. Кунаева. Профессор Казахского национального университета им. Аль-Фараби, Алматы, Казахстан. Email: e24.01@mail.ru*
Никулин Владимир Владимирович	*Доктор PhD, доцент, Государственный университет Нью-Йорка в Бингемтоне, кафедра ECE, PO Box 6000, Бингемтон, NY 13902-6000. Email: vnikulin@binghamton.edu*
Алишева Жанат Нуркуатовна	*Доктор PhD, И.о. доцента Казахского Национального Университета им. Аль-Фараби Алматы, Казахстан. Email: zhannat_86.2007@mail.ru*

References

[1] Altaev ShA, Chernetsov GE, Oringozhin ES. Tekhnologiya razrabotki gidrogennykh uranovykh mestorozhdeniy Kazakhstana [Technology for the development of hydrogenous uranium deposits in Kazakhstan]. Almaty. 2003, 294. (in Russ.).

[2] Oryngozhin YeS, Yeremin NA, Metaxa GP, Alisheva ZhN. Underground uranium borehole leaching. News of the national academy of sciences of the Republic of Kazakhstan - Series of geology and technical sciences. 2020; 442(4):62-69. https://doi.org/10.32014/2020.2518-170X.85

[3] Tsoı SV, Oryngojın ES, Metaksa GP, Jangalıeva MJ, Alısheva ZhN, Oryngoja EE. Otsenka sushestvuiyshei tehnologii i razrabotka alternativnogo sposoba ekspluatatsii gidrogennyh uranovyh mestorojdenii [Evaluation of existing technology and development of an alternative method of exploitation of hydrogenous uranium deposits]. Aktualnye dostijeniya evropeiskoi nauki [Current achievements of European science]. 2018, 40-44. (in Russ.).

[4] Gagné-Turcotte R, Reynier N, Larivière D, Nail R, Zagrtdenov R, Goulet Ph. Impact of Variability in Precipitation Patterns on the Geochemistry of Pyritic Uranium Tailings Rehabilitated with Saturated Cover Technology. 2022; 2(2):385-401. https://doi.org/10.3390/mining2020020

[5] Otchet. Rezultaty gidrogeohimicheskih rabot na Sasyk-Kulskoi kotlovine za 1975-1977gody [Results of hydrogeochemical work on the Sasyk-Kul basin for 1975-1977]. Moscow. 1978, 26. (in Russ.).

[6] Otchet. İzvlechenie urana iz rapy ozera Sasyk-Kul metodami membrannoi tehnologii [Extraction of uranium from the brine of Lake Sasyk-Kul using membrane technology]. Moscow. 1983, 19. (in Russ.).

[7] Faizullin A. Podzemnoe i kuchnoe vyщelachivanie urana, zolota i drugih metallov [Underground and heap leaching of uranium, gold and other metals]. Ruda i metally [Ore and metals]. 2005; 1:407. (in Russ.).

[8]   Liu ShQ, Lin Zh, Li D, Li X, Kozan E, M. Masoud. Recent Research Agendas in Mining Equipment Management. 2022; 2(4): 769-790. https://doi.org/10.3390/mining2040043

[9]   Yunusov MM. Razykov ZA, Faizulloyev BG. Extraction of uranium from natural uranium-bearing waters of complex salt composition: Proceedings of the II International Scientific and Practical Conference: "Actual problems of uranium industry". Almaty. 2002.

[10] Mikhail V Dvoynikov, Sidorkin DI, Yurtaev SL, Grokhotov EI, Ulyanov D. Drilling of deep and ultra-deep wells for prospecting and exploration of new raw mineral fields. Journal of Mining Institute. 2022; 258:945-955. https://doi.org/10.31897/PMI.2022.55

[11] Tran TT, Lee MS. Use of ferric salt solutions as leaching agents of Co, Ni, Cu, Fe, and Mn from metallic alloys of spent lithium-ion batteries and separation of iron from the leaching solution. J. Min. Metall. Sect. B-Metall. 2022: 58(3): 405-415. DOI:10.2298/JMMB220311023T

[12] Vorobev AY, Metaxa GP, Bolenov YM, Metaxa AS, Alisheva ZN. Digitization of the mining industry. Concept and modern geotechnology. News of the National Academy of Sciences of the Republic of Kazakhstan, Series of Geology and Technical Sciences. 2019; 4(436): 121-127. https://doi.org/10.32014/2019.2518-170X.105

[13] Lewandowski KA, Kawatra SK. Binders for Heap Leaching Agglomeration, Minerals & Metall. Colorado, USA. 2009; 26:1-24. https://doi.org/10.1007/BF03403413

[14] Turaev NS. Himiya i tehnologiya urana [Chemistry and technology of uranium]. Rudy i metally [Ores and metals]. Moscow. 2006, 396. (in Russ.).

[15] Menkin LI, Tokarev VI, Trubin VK, et al. Reaktornye i poslereaktornye issledovaniya tvelov RBMK s uran-erbievym toplivom [Reactor and post-reactor studies of RBMK fuel rods with uranium-erbium fuel]. Atomnaya energiya [Atomnaya Energiya]. 1997; 83(6):426-429 (in Russ.).

[16] Bystrikov AA, Egorov AK, Ivanov VI, et al. Opyt ispol'zovaniya uran-erbiyevogo topliva na energoblokakh s RBMK [Experience in the use of uranium-erbium fuel in power units with RBMK]. Atomnaya energiya [Atomnaya Energiya]. 2006; 100(3):165-170. (in Russ.).

[17] Gromov BV. Vvedenie v himicheskuyu tehnologiyu urana [Introduction to the chemical technology of uranium]. Atomizdat. 1976, 336. (in Russ.).

[18] Metodicheskie rekomendatsii po primeneniyu klassifikatsii zapasov k mestorojdeniyam radioaktivnyh metallov [Guidelines for the application of the classification of reserves to deposits of radioactive metals]. Ministerstvo prirodnyh resursov RF [Ministry of Natural Resources of the Russian Federation]. Moscow. 2005, 68. (in Russ.).

[19] Razykov ZA, Gusakov EG, Marushchenko AA, et al. Uranovye mestorojdeniya Tadjikistana [Uranium deposits in Tajikistan] Khujand. 2001, 212. (in Russ.).

[20] Farkhutdinov IM, Khairullin RR, Soktoev BR, Zlobina AN, Chesalova EI, Farkhutdinov AM, Tkachev AV. Tkachev. Uranium in man-made carbonates on the territory of Ufa. Journal of Mining Institute. 2023; 2(260): 226-237. DOI: 10.31897/PMI.2023.

Demonstration of the feasibility and practical value of direct acoustic measurements in liquid metals

[1]*Kazhikenova S.Sh., [1]Shaikhova G.S., [1]Shaltakov S.N., [2]Belomestny D.

[1] Abylkas Saginov Karaganda Technical University, Karaganda, Kazakhstan
[2] Duisburg-Essen University, Duisburg, Germany

* Corresponding author email: sauleshka555@mail.ru

ABSTRACT

The temperature dependences of ultrasound absorption and propagation speed in simple semimetals, semiconductors, and semiconductor compounds have been studied in this article. Experimental and theoretical results testify to the microheterogeneity of semimetals and semiconductor melts. Generalization and analysis of experimental data on the absorption and propagation speed of ultrasound in melts based on D.I. Mendeleev periodic law clearly indicate the presence of micro-groups of atoms (clusters) in them, microheterogenizing melts of semimetals and semiconductors. The urgency of this problem is predetermined by the problem of the liquid state of matter. The dependence of ultrasound absorption and propagation speed on temperature is measured using several groups of samples in paper, each group is heated to a different temperature. It is proved that melts have clustered in their atomic matrix, and so melts with semiconductor properties are micro-inhomogeneous. These results are needed to scale melt sonication to an industrial scale and are needed to provide valuable new insights into temperature dependencies of ultrasound absorption.

Keywords: melts, atomic mass, ultrasonic melt, ultrasound absorption, temperature dependences, ultrasound propagation speed.

	Information about authors:
Kazhikenova Saule Sharapatovna	Doctor of Technical Sciences, Professor, Head of the Higher Mathematics Department of Abylkas Saginov Karaganda Technical University, Karaganda city, 100027, Nursultan Nazarbayev Avenue, 56. E-mail: sauleshka555@mail.ru
Shaikhova Gulnazira Serikovna	Candidate of Engineering Sciences, acting associate professor of the Higher Mathematics Department of Abylkas Saginov Karaganda Technical University, Karaganda city, 100027, Nursultan Nazarbayev Avenue, 56. E-mail: shaikxova_2011@mail.ru
Shaltakov Sagyndyk Nagashibayevich	Ph.D., acting associate professor of the Physics Department of Abylkas Saginov Karaganda Technical University, Karaganda city, 100027, Nursultan Nazarbayev Avenue, 56. E-mail: sagyndyk613@mail.ru
Belomestny Denis	PhD, Professor University of Duisburg-Essen, Forsthausweg 247057 Duisburg, Universitätsstraße 245141, Germany. E-mail: denis.belomestny@uni-due.de

Introduction

Semiconductor physics, including its technical applications, was limited to polycrystalline and rarely amorphous materials (such as selenium) until the middle 1940s. This was the time when the semiconductors theory foundations were laid, including the development of Wilson's impurity conductivity model and Schottky's theory of barrier layer. The subsequent development of semiconductor physics, physical chemistry, and related sciences has led to the fact that the use of liquid semiconductors in electronics as a raw material for microelectronics currently goes hand in hand with the new single-crystal materials growth and development, especially when creating high-speed processors for computer technology.

The hypothesis of the liquid's micro-heterogeneous structure arose as early as the 1920s. in connection with liquids using X-rays Stewart's studies [1]. Since then, this hypothesis has won many adherents among researchers. Methods have been developed for estimating the size of microheterogeneity, their volume fraction [[2], [3]], and calculating coordination numbers [4]. The special distinction was not between the melts of metals and semiconductors in this case. Micro-inhomogeneity extended to any melts from alkali metals to semiconductors. However, without having unambiguously interpreted experimental evidence, the hypothesis remained and had not only

adherents but also opponents. Among the works that deny the polycrystalline model of liquids is the work by a reference [5]. They are more inclined to see a fluctuation basis in individual phenomena.

A large number of works have been devoted to the study of electronic melts. Among them, the most ambitious are the extensive studies with employees of electrophysical, volumetric, viscometric, and acoustic studies [[6], [7]].

Recently, the study of liquid semiconductors, which is the subject of this work, continues to expand continuously due to progress in solid-state physics and semiconductor technology, as well as physical chemistry. In this case, structural research is of particular importance.

Ultrasonic processing is important and interesting. This is needed as a promising route to improving melt quality for scientific and industrial problems. The significance of this problem is predetermined by the matter liquid state problem. In this study, the ultrasound absorption and propagation speed and temperature are measured using multiple groups of melts and semiconductors, that were not widely also studied, since the high-temperature acoustic experiments technology with aggressive melts of semimetals and semiconductors complicated the research process. This study summarizes the results of the evaluation of ultrasound absorption and the propagation speed, for calculating the ultrasound propagation speed in solutions, studies of the nucleation, growth, and fragmentation of particles in liquid melts. It has been proven that melts with semiconductor properties are micro-inhomogeneous due to the existence of clusters in their atomic matrix. These results are needed to scale melt sonication to an industrial scale and are needed to provide valuable new insights into temperature dependences of ultrasound absorption and propagation speed in simple semimetals, semiconductors, and semiconductor compounds that have been studied by the authors. The application of absorption and propagation speed waves in electron melts is quite complex, and their interpretation requires the use of several mechanisms to describe process power, and the mechanical and microstructures properties [8]. In fact, the entire arsenal of modern experimental and theoretical physics is connected to the research of the physicochemical behavior of melts [[9], [10], [11], [12]]. Acoustic methods are the most promising among experimental methods for research of the matter liquid state. They are simple,

reliable, and highly sensitive to changes in matter structure and interatomic interaction.

The application of power ultrasound during liquid-to-solid transformation is believed to be an effective way to improve the solidification microstructures and mechanical properties [8]. In fact, the entire arsenal of modern experimental and theoretical physics is connected to the research of the physicochemical behavior of melts [9]. Acoustic methods are the most promising among experimental methods for research of the matter liquid state. They are simple, reliable, and highly sensitive to changes in matter structure and interatomic interaction.

The results of this research make it possible to predict the melt's elastic properties of simple substances and extend it to complex substances.

At present, the electrophysical, thermophysical, thermodynamic, and viscous properties of liquid semimetals and semiconductors based in the electronics industry have been widely studied.

However, the ongoing research in the field of studying these properties is not sufficient to solve the problem of the liquid semimetals and semiconductors structure. It is also impossible to obtain an unambiguous result by only structural research. In this aspect, it is known that «modern acoustic research methods are a powerful tool for obtaining information about the structure of melts and semiconductors» [10]. Melts and semiconductors were not widely also studied, since the high-temperature acoustic experiments technology with aggressive melts of semimetals and semiconductors complicated the research process [[8], [9], [10], [11], [12], [13]]. Our research includes
- the development of liquid semimetals and semiconductors structure model;
- experimental and theoretical studies of the propagation speed and absorption coefficient of ultrasound temperature dependences in liquid semimetals and semiconductors;
-regularities generalization of liquid metals, semimetals, and semiconductors structural properties.

The ultrasound absorption and propagation speed waves in electron melt are quite complex, and their interpretation requires the use of several mechanisms to describe this process. For example, to interpret the experimental dependence of the sound absorption coefficient in liquid sulfur, the authors of [64±67] used the relaxation theory [14],

which assumes a micro inhomogeneous structure of highly viscous liquids.

The $\frac{\beta}{f^2}$ polytherms behavior in the after-melting temperature range is associated with relaxation mechanisms in the high-temperature region by the authors, where the speed has a maximum value and the ultrasound absorption coefficient is minimal. The sound absorption coefficient practically does not change at higher temperatures, despite the fact that the speed has a minimum value.

It was noted in a reference [15] that $\frac{\beta}{f^2}$ depends on the frequency, namely, as the sound frequency increases, the absorption coefficient decreases. However, in a reference [16], in contrast to the reference [15], no frequency dependence was observed. The sound absorption value in liquid sulfur is proportional to the frequency square, i.e. $\beta \sim f^2$. The experimental ultrasound absorption coefficient exceeds the classical value 2 times, while in the reference [16] this process excess is 3 times.

The ultrasound absorption in liquid binary systems was studied by Abovitz and Gordon [17], where $\frac{\beta}{f^2}$ was measured for the first time in the mercury ± thallium system. As the authors of this work pointed out, the low melting point of the components of this system allowed them to operate at a high frequency (up to 270 MHz).

The ultrasound absorption coefficient in the mercury-thallium alloy decreases with increasing frequency, which indicates the presence of relaxations. The $\frac{\beta}{f^2}$ value decreases with increasing temperature and increases with increasing thallium concentration.

The authors conclude that the relaxation that occurs in mercury-thallium alloys under the periodic stresses action is a structural relaxation associated with a change in the average number of nearest neighbors of both types surrounding a given atom. Relaxation is characterized by diffusion rates.

Dzharzinsky and Litovits [18] showed that in melts of the *K-Na* system, the $\frac{\beta}{f^2}$ value increases as a temperature 473–673 K function at 30 and 70 MHz frequencies.

At the same time, the authors of the reference [15] at 30 MHz frequencies obtained the opposite sound absorption polytherm than at the same frequency. Perhaps this is due to the acoustic contact instability between the melt and the sound ducts. However, at higher temperatures, good agreement is observed between the experimental results of [15] and [19].

The work [19] also presents a relaxation sound absorption theory in associated liquids. Theoretical results qualitatively correctly describe the behavior of the absorption polytherm coefficient. Quantitatively, the sound absorption coefficient theoretical value differs by almost 100% from the experimental results.

The ultrasound absorption measurement in liquid sulfur was carried out in [15]. As is known from X-ray data, liquid sulfur consists of ring formations. Apparently, these features affect such liquid sulfur characteristics as viscosity and sound propagation speed. The sound speed polytherm in molten sulfur shows three regions with different sound speed temperature coefficients. The same feature is inherent in the sound absorption polytherm in molten sulfur [15]. The studies were carried out with high-purity sulfur at a 30–60 MHz frequency in the temperature range from the melting point to 673 K.

The $\frac{\beta}{f^2}$ temperature dependence is quite complex, there is a decrease in the ultrasonic wave absorption coefficient immediately after melting, which increases monotonically with increasing temperature. This includes the alkali metals and further all other simple metals that are densely packed in the solid state.

Two-component liquid-metal solutions with monotonically increasing ultrasound absorption polytherms should also be attributed to this class.

The second class includes melts in which the ultrasonic waves absorption polytherms do not increase monotonically with temperature. This class includes semimetals and semiconductors, which undergo significant structural changes during melting.

All melts with anomalous behavior of absorption polytherms and propagation rates (bismuth, antimony, tellurium, etc.) are characterized by the fact that structural changes in them continue in a certain temperature range after melting. This is especially pronounced in melts of tellurium, antimony, etc. The $\frac{\beta}{f^2}$ anomalous behavior temperature interval of these melts coincides with the after-melting temperature range [6].

Such a classification can be given for sound speed polytherms in electron melts. A similar classification of polyterms v_s is given in a reference [6]. According to their data, polytherms of ultrasonic propagation speed in *AlSb*, *GaSb*, and *InSb* melts can be assigned to the second class [6]. In these semiconductor compounds, an increase in the ultrasound speed is observed in the after-melting temperature range.

Thus, an available data analysis of the acoustic properties of experimental studies of electron melts shows that the behavior of the ultrasonic wave absorption polytherm and propagation speed is characterized by anomalies and features of semimetal and semiconductor melts acoustic properties.

This was the reason for separating these melts into electron melts separate classes. The entire set of experimental data on speed, density, and electrical properties [6], as well as the results of structural studies [7], show that this electron melts class exhibits changes in the short-range order structure upon heating.

Therefore, anomalies and features of melts, semimetals, and semiconductors' acoustic properties should be considered manifestations of structural changes.

Results and discussion

A hypothesis about the micro-inhomogeneous structure of liquids arose in connection with Stuart's research using X-rays in 1920. Micro-inhomogeneity extends to any melts from alkali metals to semiconductors. But the hypothesis remained a hypothesis since there were no interpreted experimental data. The ultrasonic generator used for experiments to any melts from alkali metals to semiconductors were interpreted experimental data.

Experimental and theoretical results testify to the microheterogeneity melts, which were interpreted for any melts by Doppler velocimetry.

Authors of this study solved different problems to obtain sufficient Doppler signals.

The first is the ultrasonic transmission through the channel wall of steel. The second is to obtain the acoustic coupling with the channel wall, and the next one is to wett of the inner surface of the wall by the melts.

The ultrasound Doppler velocimetry method with DOP3000 Velocimeter (Figure 1) was used in order to measure the acoustic flow investigation and flow velocities. The ultrasound Doppler velocimetry method has become an accepted method for obtaining acoustic flow investigation as shown for example in a reference [20].

With the DOP3000 there was a measurement of the speed of sound in melts by accurately measuring time, by means of an ultrasonic pulse measured over the measurement.

Before using the software, firstly, we install the probe as defined in the Figure 1. We placed the probe at a defined distance (Dmes) from a reflector on Figure 2. The reflector is a plan surface, placed perpendicularly to the US beam axis of the probe. The probe is completely immerged. The distance between the reflector and the probe surface (Dmes), which is named "Reference distance" in UDOP, must be in the range 15 to 50 mm and must be measured with precision as any error in the measured distance will be directly transferred to the sound speed measured value.

Figure 1 - The DOP3000 Velocimeter
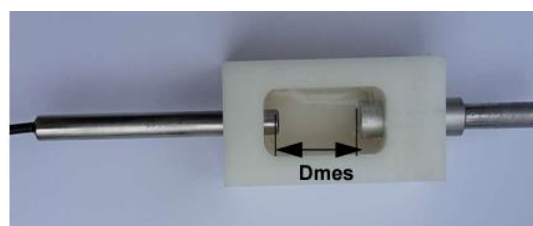
Figure 2 - The probe

The propagation of elastic waves is associated with the fundamental properties of material media, including the mass of particles, their space, and the bonds between particles of matter. These indicators, namely, the inertial factor (mass of particles), the spatial factor (volume per particle), and the stiffness factor between particles (compressibility) are sufficient for a general description of elastic waves absorption and propagation speed [13]. First of all, this is the relationship of the selected factors with the absorption coefficient of ultrasonic waves.

For the occurrence of such observations in the behavior of the melts' elastic properties, one can use the system analysis methods based on the D.I. Mendeleev Periodic phenomenon.

As is known, the absorption coefficient is determined by the Stokes-Kirchhoff formula in the general case [21]:

$$\beta = \frac{2\pi^2 f^2}{\rho v_s^3}\frac{4}{3}\eta + \chi\left(\frac{1}{C_V}-\frac{1}{C_P}\right),$$

χ - is the thermal conductivity coefficient, C_P and C_V equal the heat capacity at constant pressure and volume.

The Stokes-Kirchhoff formula will take the form after the replacement $\gamma = \dfrac{C_P}{C_V}$:

$$\beta\, V_A = \frac{2\pi^2 f^2}{\rho v_S^3}\left[\frac{4}{3}\eta + \frac{\chi}{C_P}(\gamma-1)\right] \qquad (1)$$

Formula (1) will be transformed to inertial, coupling and spatial factors based on the parameters $\eta = \rho\upsilon$, υ is the kinematic viscosity, $\dfrac{1}{\rho v_S^2} = \alpha_S$ is the adiabatic compressibility, $C_P = \dfrac{dQ}{dT}\dfrac{1}{m}$ is the melt heat capacity:

$$\frac{\beta v_S}{f^2} = 2\pi^2\alpha_S\left[\frac{4}{3}\rho\upsilon + \frac{\chi}{\left(\frac{dQ}{dT}\right)_P}m(\gamma-1)\right]. \qquad (2)$$

Let $\rho = \dfrac{m}{V} = \dfrac{N_A M_A}{N_A V_A}$ and $m = N_A M_A$, N_A is the

Avogadro number, M_A is the atomic mass, V_A is the atomic volume. Then we rewrite equality (2) in the form:

$$\frac{\beta v_S}{f^2} = \sigma M_A, \qquad (3)$$

$$\sigma = 2\pi^2\alpha_S\left[\frac{4}{3}\frac{\upsilon}{V_A} + \frac{\chi}{\left(\frac{dQ}{dT}\right)_P}N_A(\gamma-1)\right].$$

The obtained equation (3) makes acoustic parameters monitoring in simple substances melts more accessible. Experimental measurements monitoring by value using reference data [[22], [23], [24], [25], [26]] is shown in Figure 3.
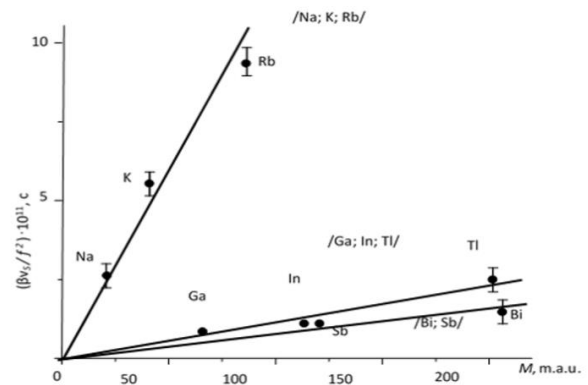
Figure 3 - Dependence at crystallization temperatures

We have established the correlation dependence between measurement results $\dfrac{\beta v_S}{f^2}$ and the parameter values M_A, where σ is a constant value for each group. Note: the bonding factors intragroup similarity is not only observed in condensed bodies but also in diatomic molecules.

The highest value of the dissociation energy is observed for five electrons in the outer shell, the most rigid bonds exist in diatomic molecules [27].

Local bonds become stronger (partial atomic association) with an increase in the number of external electrons in melts due to electron redistribution. There is no redistribution of electrons in diatomic molecules since they bond with a single direction from one atom to another. If the number of external electrons is more than five in diatomic molecules, then individual electrons are transformed into a non-bonding state. This situation is explained by a decrease in the dissociation energy of diatomic molecules, starting from the oxygen group [27]. The closest packing coordination number (the number of bonds realization directions) can reach twelve in condensed matter. If there are more electrons than necessary to implement a uniform bond, they are redistributed. As a result, bonds more rigid are formed between individual neighboring atoms, associations of atoms are created.

It should be noted that the weakening of bonds between associates leads to an increase in bonds in associates and a decrease in the overall rigidity of the melt macroscopic volume. This is confirmed by the sulfur group example. There is a high correlation between the parameter $\dfrac{\beta v_S}{f^2}$ and the atom associates in the liquids of this group. The experimental values will be equal for S, for Se, for Te:

$$\frac{\beta v_S}{f^2} = 19 \cdot 10^{-11}\,c\,, \quad \frac{\beta v_S}{f^2} = 6{,}7 \cdot 10^{-11}\,c, \quad \frac{\beta v_S}{f^2} = 1{,}34 \cdot 10^{-11}\,c$$

which indicates a decrease the atom associates in *S, Se, Te* melts.

Figure 3 showed that the parameter $\dfrac{\beta v_S}{f^2}$ increases from *Na* to *Rb* in the alkali metal series. This is confirmed by the fact that these groups of metals are prone to structure loosening with increasing atomic mass M_A.

The $\dfrac{\beta}{f^2}$ temperature dependence is quite complex. Immediately after melting, there is a decrease in the absorption coefficient of ultrasonic waves, which increases monotonically with increasing temperature. This includes the alkali metals and further all other simple metals that are densely packed in the solid state.

Two-component liquid-metal solutions with monotonically increasing ultrasound absorption polytherms should also be attributed to this class. The absorption coefficient of ultrasonic waves decreases immediately after melting. In addition, the absorption coefficient of ultrasonic waves increases monotonically with increasing temperature. This includes the alkali metals and further all other simple metals that are densely packed in the solid state. Melts, in which the absorption polytherms of ultrasonic waves do not increase monotonically with temperature, belong to the second class. This class includes semimetals and semiconductors, in which significant structural changes occur during melting. All melts with anomalous behavior of absorption polytherms and propagation rates (bismuth, antimony, tellurium, etc.) are characterized by the fact that their structural changes continue in a certain temperature range after melting.

This is especially pronounced in tellurium, antimony melts, etc.

The polytherm $\dfrac{\beta}{f^2}$ anomalous behavior temperature interval of these melts coincides with the "after-melting" temperature interval. The experimental results of equation (3) can be also used for compounds. For monitoring, let us consider *GaSb* and *InSb* compounds.
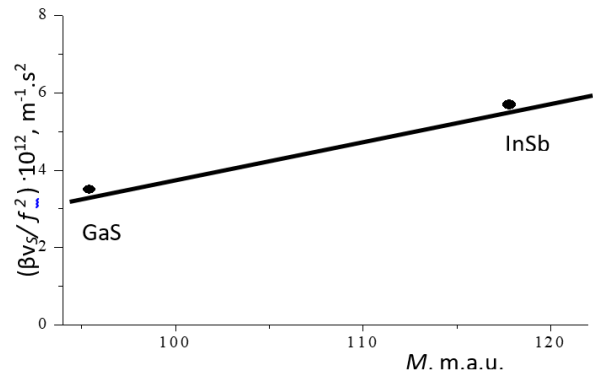
Figure 4 - Dependence   for *GaSb* and *InSb* systems

Dependence $\dfrac{\beta v_S}{f^2} - M$ is shown in Figure 4 for these compounds.

Thus, the acoustic analysis in electron melts experimental measurements shows that the absorption polytherms and the propagation velocity behavior of ultrasonic waves depend on the semimetals and semiconductors' acoustic properties. This was the reason for separating these melts into an electron melts separate class. A straight-line relationship between $\dfrac{\beta v_S}{f^2}$ and M_A inertial factor has been established.

For calculations, melt compounds were rotated by acoustically equivalent liquids from atoms of the same type by mass that satisfies the condition

$$M = M_1 X_1 + M_2 X_2, \qquad (4)$$

M_1, M_2 - atoms mass; X_1, X_2 - components atomic fractions.

The experimental results of equation (3) can be used for compounds, too. Let us consider *Bi-Sb* compound. Methods of descriptive statistics were used to systematize and describe the data. Experimental measurements monitoring by value using reference data [[22], [23], [24], [25], [26]] is shown in Figure 3. The experimental results are shown in Figure 4-14 for *GaSb* and *InSb*, $Bi_{0,25}Sb_{0,75}$, $Bi_{0,5}Sb_{0,5}$, $Bi_{0,75}Sb_{0,25}$, *Bi-Sb*, $Sn_{0,30}Te_{0,70}$, $Sn_{0,5}Te_{0,5}$, $Sn_{0,70}Te_{0,30}$, *Sn-Te* compounds. We used the Table 1 experimental measurements to build a Figure with markers in Excel.

Table 1 - Temperature dependence of Ultrasound absorption and propagation speed

T, К	$\frac{\beta}{f^2}\cdot 10^{15}$	ν_s	T, К	$\frac{\beta}{f^2}\cdot 10^{15}$	ν_s	T, К	$\frac{\beta}{f^2}\cdot 10^{15}$	ν_s
Ga			**Bi**			**Te**		
302	2.2	2866	526	9.2	1640	734	14.5	935
325	2.9	2868	545	9.3	1643	750	14.2	955
335	3.3	2870	565	9.5	1641	762	13.8	980
370	3.5	2865	599	9.8	1639	730	13.2	990
395	3.1	2860	610	9.9	1639	812	13	1015
405	3.4	2854	615	10	1638	830	12.9	1035
425	2.8	2853	630	10.3	1636	862	13	1045
450	2	2856	635	10.7	1636	883	13.1	1050
475	1.4	2858	660	10.8	1633	902	13.2	1060
500	1.2	2853	710	11.1	1630	912	13.3	1075
520	1.2	2847	730	11.3	1627	992	13.5	1090
545	1.22	2844	735	11.7	1621	974	14.1	1100
575	1.18	2848	740	12	1620	1006	15.1	1110
585	1.28	2849	755	12.4	1619	1051	17	1120
595	1.3	2841	770	12.9	1617	1078	17.5	1125
SnTe			**Se**			**Sb**		
1211	22.8	1533	520	725	1087	902	5.45	1902
1213	23.3	1531	526	635	1075	918	5.28	1911
1220	23.5	1528	544	630	1063	945	5.2	1915
1226	24	1526	560	665	1043	960	5.44	1914
1229	23.8	1522	574	565	1030	970	5.6	1913
1239	24.4	1523	620	610	1018	986	5.8	1917
1247	25.5	1520	624	680	1005	1000	5.83	1920
1254	27.9	1517	652	735	995	1020	6.4	1922
1262	29	1516	682	825	980	1035	6.5	1920
Bi₂Se₃			**Ga₂Te₃**			**Sb₂Te₃**		
1000	33	1398	1065	902	1156	902	24.4	1225
1005	32.01	1395	1075	909	1152	909	23.1	1230
1018	30.7	1390	1085	923	1151	923	22	1235
1025	30	1385	1097	933	1146	933	21	1238
1037	29.3	1368	1110	948	1142	948	18.5	1239
1045	28.8	1360	1112	969	1140	969	16.5	1244
1049	28.7	1358	1130	983	1141	983	15	1251
1060	28	1357	1148	1007	1174	1007	14.1	1251.5

Table 1 - continuation

1070	27.8	1350	1160	1030	1139	1030	13.8	1256
1074	27.7	1354	1185	1049	1156	1049	14	1258
InTe			**Sn**			**In**		
980	19.6	1156	500	4.8	2478	440	4.3	2307
990	19.01	1152	560	5.4	2472	462	4.4	2301
948	18.5	1151	584	5.1	2463	500	4.8	2295
1010	18	1146	619	5	2464	520	5	2290
1025	17.5	1142	680	6.5	2473	570	5.9	2278
1040	16.9	1140	740	9.5	2450	598	6.9	2264
1050	16.6	1141	820	10.5	2445	625	7.3	2250
1060	16.4	1174	880	12	2414	640	7.8	2242
1070	16.2	1139	940	12.4	2404	675	8.6	2232
Bi$_{0,75}$ Sb$_{0,25}$			**Sn$_{0,3}$ Te$_{0,7}$**			**Sn$_{0,7}$ Te$_{0,3}$**		
670	7.5	1698	868	18.5	1452	984	11.4	1929
690	9.5	1694	890	18.4	1449	995	11.7	1926
710	12.8	1690	910	19.5	1446	1020	12	1921
730	17	1688	938	20.6	1441	1045	12.2	1920
745	19.8	1687	980	21	1438	1050	12.7	1917
775	25.5	1684.5	1020	23	1428	1080	14	1912
800	30.1	1679	1060	24.8	1425	1087	14.5	1908

Dependence $\dfrac{\beta v_S}{f^2} - M_A$ is shown in Figure 5-7

for these $Bi_{0,25}Sb_{0,75}$, $Bi_{0,5}Sb_{0,5}$, $Bi_{0,75}Sb_{0,25}$ compounds.

$1 - \dfrac{\beta}{f^2}$, 2 - v_S T, K
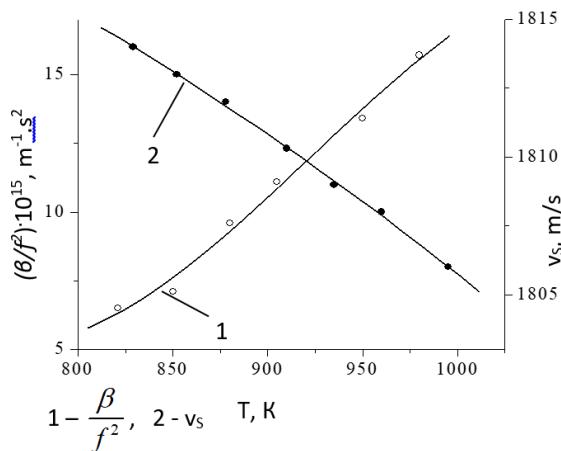
Figure 5 - Temperature dependence in the $Bi - Sb$ system (composition $Bi_{0,25}Sb_{0,75}$)

$1 - \dfrac{\beta}{f^2}$, 2 - v_S
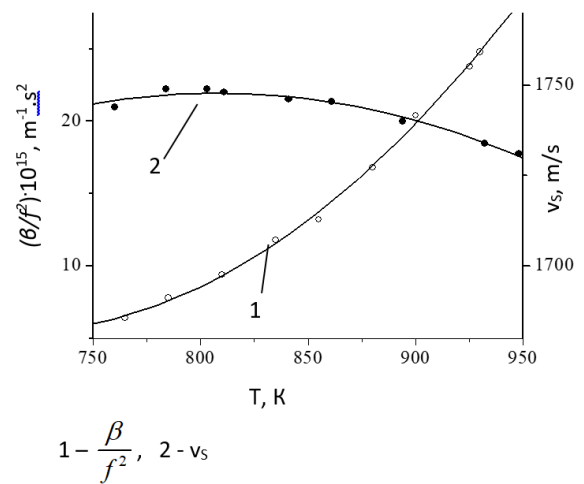
Figure 6 - Temperature dependence in the $Bi - Sb$ system (composition $Bi_{0,5}Sb_{0,5}$)

$1 - \dfrac{\beta}{f^2}$, $2 - v_S$
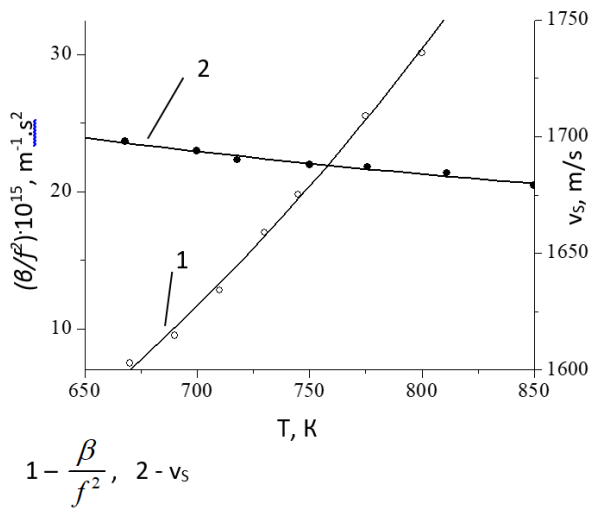
Figure 7 - Temperature dependence
in the $Bi - Sb$ system (composition $Bi_{0,75}Sb_{0,25}$)
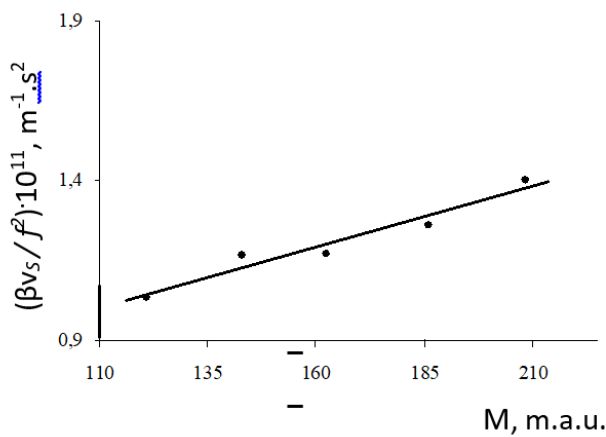
Figure 8 - Dependence for Bi-Sb system

The experimental data are practically placed on straight lines in Figure 8. This confirms the closeness of the calculated indicators to the ideal ones. Indeed, the authors of the references [[28], [29]] showed that the Bi-Sb system forms a regular solutions series with atoms' random arrangement.
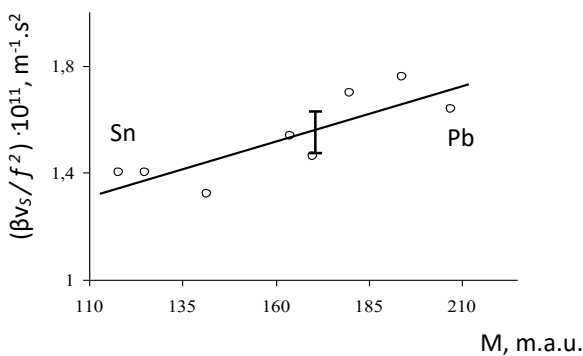
Figure 9 - Dependence for Sn-Pb system [17]

The results in the coordinates $\dfrac{\beta v_S}{f^2} - M_A$ are shown according to Pless's data [30] for the Sn-$Pв$ system in Figure 9. Authors of this study found that the $\dfrac{\beta v_S}{f^2}$ experimental measurements are practically placed on straight lines according to Pless's experiment.

Note that the indicated results are typical only for ideal systems, that is, for melts with an atoms random distribution. We have developed an algorithm for determining the ideality or non-ideality degree of an arbitrary binary system based on monitoring the ultrasonic absorption coefficient and propagation speed experimental measurements. These are $v_S^2 - \dfrac{1}{M_A}$ and $\dfrac{\beta v_S}{f^2} - M_A$ diagrams. We study the Sn-Te system, which forms a congruently melting semiconductor chemical $SnTe$ compound. The ultrasound speed and absorption experimental measurements in the compositions $Sn_{0,30}Te_{0,70}$, $Sn_{0,5}Te_{0,5}$, $Sn_{0,70}Te_{0,30}$ are shown in Figures 10, 11, 12. The ultrasound speed and absorption for liquid tin experimental measurements are shown graphically in Figure 12.

Authors did not show a diagram for the Sn-Te system, since it was previously studied by the references [[31], [32]] in Figure 13.

$1 - \dfrac{\beta}{f^2}$, $2 - v_S$, $3 - v_S$ [16] work data
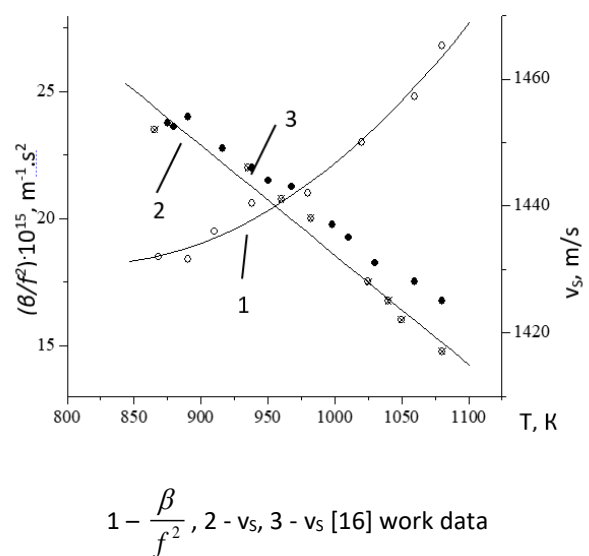
Figure 10 - Temperature dependence in $Sn_{0,30}Te_{0,70}$ melts

$$1 - \frac{\beta}{f^2}, \ 2 - v_s, \ 3 - v_s \ [16] \text{ work data}$$
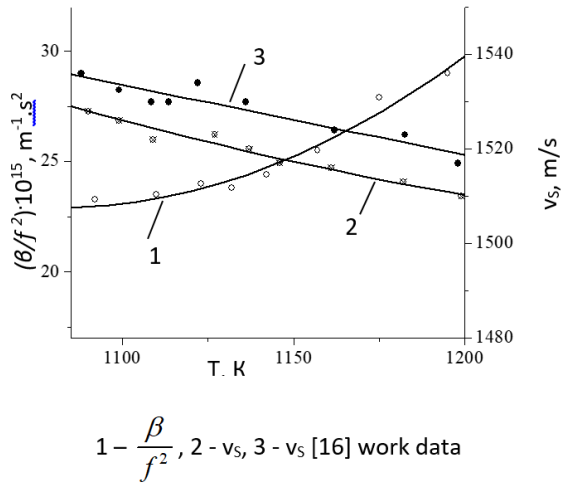
Figure 11 - Temperature dependence in $Sn_{0,5}Te_{0,5}$ melts

$$1 - \frac{\beta}{f^2}, \ 2 - v_s, \ 3 - v_s \ [16] \text{ work data}$$
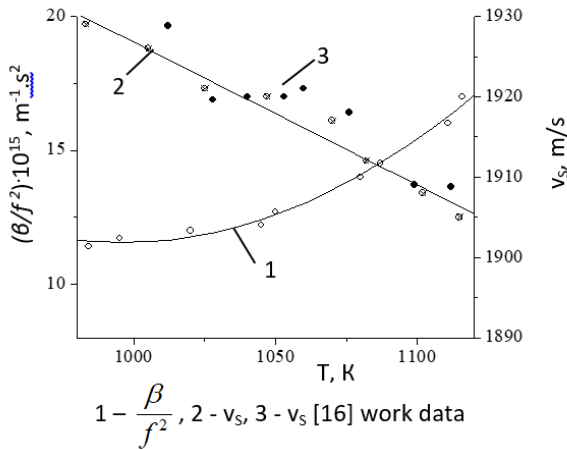
Figure 12 - Temperature dependence in $Sn_{0,70}Te_{0,30}$ melts

$$1 - \frac{\beta}{f^2}, \ 3 - v_s, \ 2 - \frac{\beta}{f^2} \ [8], \ 4 - v_s \ [16] \text{ work data}$$
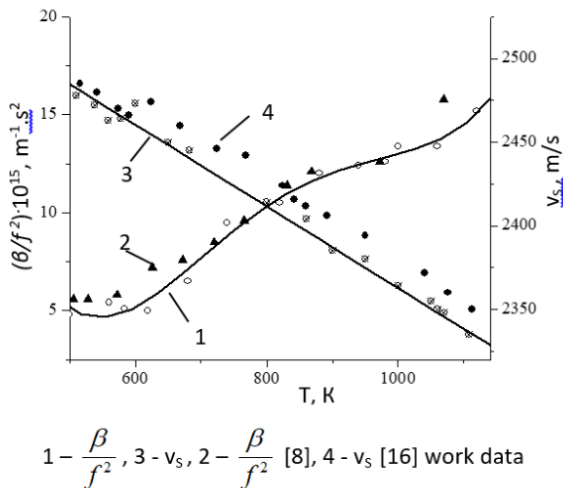
Figure 13 - Temperature dependence in liquid tin

$$1 - Sn_{0,30}Te_{0,70} \quad 2 - SnTe \quad 3 - Sn_{0,70}Te_{0,30}$$
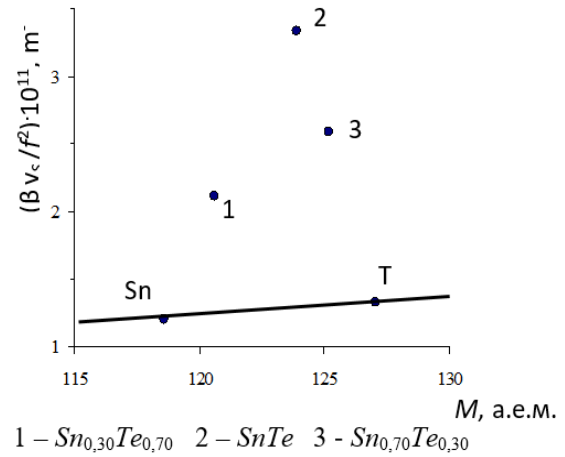
Figure 14 - Dependence for *Sn-Te* system

Calculations show that there are inconsistencies between the real isotherm and $\frac{\beta v_s}{f^2} - M_A$ linearity. Previously, for *Bi-Sb* and *Pв-Sn* systems, it was found that these deviations are associated with melt microheterogeneity of intermediate concentrations.

We have obtained a connection between the real isotherm $\frac{\beta v_s}{f^2} = f(M_A)$ and the corresponding linear diagram, which will allow us to evaluate the homogeneity or inhomogeneity of the melts and solutions.

Let us consider a melt of the *SnTe* compound stoichiometric composition. We calculate the *SnTe* experimental measurement $\frac{\beta v_s}{f^2}$ and represent it in Figure 13 with the number 2. Through this point we draw a straight line parallel to the *M* axis. Let us assume that the *SnTe* melt is atomic and calculate the average M_A atomic mass by formula (4).

An atomic *SnTe* melt corresponds to an extremely large M_A mass in an idealized system characterized by a linear dependence $\frac{\beta v_s}{f^2} - M_A$.

As a result, the atomic mass of a real melt largely exceeds the average value atomic mass of the components. This unambiguously takes place in a situation where a real *SnTe* melt consists not only atoms of tin and tellurium, but also larger particles, such as clusters or associates, whose masses exceed the component atoms masses.

System analysis based on the Periodic Law can also be applied to describe the behavior of the velocity of propagation of elastic waves in melts of simple substances. To establish such a pattern, we

analyze the Laplace equation of the following form where β_S is the adiabatic compressibility of the melt, ρ is the density.

$$v_S^2 = \frac{1}{\rho\beta_S}, \qquad (5)$$

In this case, the adiabatic compressibility of liquids from the thermodynamics point view can be represented as the reciprocal of the isothermal or adiabatic modulus of elasticity from formula where Ω is volume, P is pressure.

$$\beta_S = \frac{1}{\Omega}\frac{d\Omega}{dP}, \qquad (6)$$

Using the methods of the theory of similarity and dimension, authors of this study rewrite expression (5) in the following form:

$$\left[\frac{m^2}{s^2}\right] = \left[\frac{m^3}{kg}\right]\frac{\left[m^3\right]\cdot\left[\text{N/m}^2\right]}{\left[m^3\right]}, \qquad (7)$$

or

$$\left[\frac{m^2}{s^2}\right] = \left[\frac{m^3}{kg}\right]\frac{\left[\text{N}\cdot\text{m}^2\right]}{\left[m^3\right]}.$$

Finally

$$\left[\frac{m^2}{s^2}\right] = \frac{[J]}{[kg]}. \qquad (8)$$

From this relation, we can write the following empirical expression:

$$v_S^2 = b_1\frac{J}{M}, \qquad (9)$$

where J is the last valence electron ionization potential.

A relation like (9) makes it possible to use the ionization potentials of valence electrons to interpret the elastic properties of melts. In addition, it provides an opportunity to develop a new type diagram $v_S^2 - \frac{J}{M}$.

It should be emphasized that the use of the ionization potentials of atoms together with the Periodic Law was first applied to explain the chemical nature of substances.

In addition, the diagram $v_S^2 - \frac{J}{M}.,$ supplementing the diagram $\frac{\beta v_S}{f^2} - M$, can be used to identify the number of bonds of fractal-cluster formations in melts, but this requires special consideration.

In the light of the above, authors of this study analyzed relation (9) for the experimental data on the velocity v_S^2 of ultrasonic waves in the coordinates $v_S^2 - \frac{J}{M_A}$.

When processing the experimental data by the least squares method for the series Li+, Na+, K+, Rb+, Cs+, the first ionization potential was used, and for the third group Al³+, Ga³+, In³+, Tl³+, the third ionization potential was used. In this case, the following dependence was established (Figure 15)

$$v_S^2 = 5,7\cdot10^8\left(\frac{J}{M}\right).$$

The common rectilinear arrangement for both groups is due to the fact that the outer shells of the considered ions are closed, becoming in fact isoelectronic and characteristic of hard-to-deform shells of inert gases.

The generality of the coefficient b_1 requires disclosure of the nature of its origin.

In a more general form and for further analysis of experimental data, relation (9) can be represented as

$$v_S^2 = \gamma\frac{W}{M}, \qquad (10)$$

where γ is the similarity coefficient and W is the energy of the electronic subsystem from which the ionization energy J will then be extracted.

To clarify the nature of the coefficient b_1, we represent the energy of the state of the electronic subsystem as follows:

$$|W| = Rhc\frac{z^{*2}}{n^2}, \qquad (11)$$

where z* is the effective charge of the ion, R is the Rydberg constant.

To apply Bridgman's P-theorem, we represent (11) in the following form:

$$W = \text{const} \cdot R^d \cdot h^h \cdot z^k \cdot e^l \cdot r^m \cdot c^n.$$

After finding the power coefficients, authors of this study obtain the final version of formula (11):

$$|W| = \frac{2}{2} Rhc \frac{z^2}{n^2} \cdot \frac{hc}{2\pi e^2} \cdot \frac{2\pi e^2}{hc} \cdot \frac{r}{r} \cdot \frac{2\pi e^2}{2\pi e^2},$$

and taking into account $\alpha = \dfrac{2\pi e^2}{hc}$, it can be written

$$|W| = \frac{1}{2} \cdot \frac{Rr}{\alpha^2} \cdot F^{tr} \left[\frac{4\pi e^2}{r} \frac{z^{*2}}{n^2} \alpha \right],$$

where $F^{tr} \left[\dfrac{4\pi e^2}{r} \dfrac{z^{*2}}{n^2} \alpha \right] = J$.

The sign $F^{tr}[\ \ ]$ means the operator of functional transformation by the similarity method.

This expression denotes the ionization energy. Thus, the energy of the electronic subsystem $|W|$ expressed as:

$$|W| = \frac{1}{2} \cdot \frac{Rr}{\alpha^2} J, \qquad (12)$$

taking $r \approx a_0$, and also taking into account

$$R = \frac{me^4}{4\pi \hbar^3 e}, \qquad a_0 = \frac{\hbar^2}{me^2},$$

relation (12) can be simplified to the following form

$$W = \frac{1}{8\pi\alpha} J.$$

Substituting this into (10), we obtain

$$v_s^2 = \frac{\gamma}{8\pi\alpha} \frac{J}{M}. \qquad (13)$$

Comparing this expression with (9), we find

$$b_1 = \frac{\gamma}{8\pi\alpha}.$$

Comparing this ratio with the experimental values of b_1, we can establish that $\gamma = 10 + 8$.

In other words, we get

$$b_1 = \frac{1}{8\pi\alpha} \cdot 10^8.$$

Table 2 and Figure 15 present the combined experimental data for the Li+ and Al^{3+} series.

As can be seen, the experimental values can be approximated by the equation of a straight line emerging from the origin,

$$v_s^2 = b_1 \left(\frac{J}{M} \right),$$

where coefficient $b_1 = 5{,}7 \cdot 10^{+8}$.
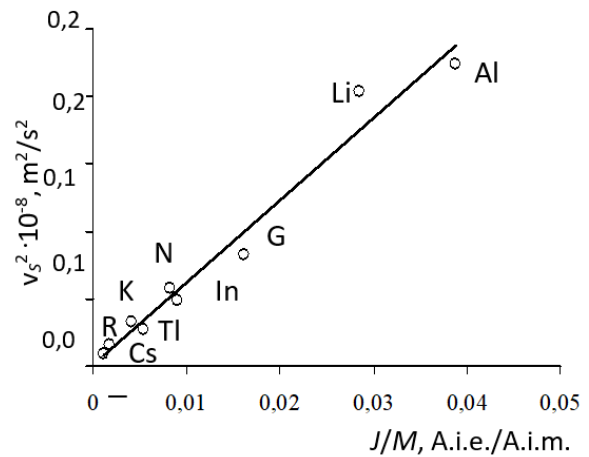
Figure 15 - Experimental dependence

The reliability of the coefficient b_1 obtained from the experiment, as well as its relation to the fine structure constant, can be established by the statistical method described in [[22], [23], [24], [25], [26]].

Following the logic of these works, we write the expression for the absolute confidence interval in the following form:

$$\delta = \frac{y_{max} - y_{min}}{t_R},$$

where y_{max} is the maximum value of v_s^2, y_{min} is the minimum value, t_R is the significance of the correlation coefficient determined by the formula

$$t_R = \frac{R\sqrt{n-k-1}}{1-R^2},$$

where k = 1 is the factors number, n is the points number, R is the correlation coefficient

$$R = \sqrt{1 - \frac{(n-1)\sum(y_э - y_T)^2}{(n-k-1)\sum(y_э - y_{cp})^2}}.$$

The relative confidence interval is defined as

$$\pm \frac{\delta}{y_{midl}}, \quad \text{or} \quad \frac{\delta}{y_{midl}} b_1 - b_1 < b_1 < b_1 + \frac{\delta}{y_{midl}} b_1. \quad (14)$$

When processing the experimental data, it was found that R = 0.97712 at the 95% confidence level. Coefficient t_R = 57,1699 >> 2.

Then, using the interval (14), we can write $5{,}43 \cdot 10^8 < b_1 < 5{,}97 \cdot 10^8$, whereas

$$b_T = \frac{1}{8\pi\alpha} \cdot 10^8 = 5{,}45 \cdot 10^8.$$

Table 2 - Experimental data on the series Li+ and Al³+

Ions of elements	$\dfrac{J}{M}$, $\dfrac{\text{A.i.e.}}{\text{A.i.m.}}$	v_S^2, m²/s², Experimental	v_S^2, m²/s² Theoretical
Al³⁺	0.038742994	22420000	2.21·10⁷
Li⁺	0.028552	20350000	1.63·10⁷
Ga³⁺	0.016186833	8213956	9.22·10⁶
In³⁺	0.008971086	4906225	5.11·10⁶
Na⁺	0.008213	5736025	4.68·10⁶
Tl³⁺	0.005358441	2608225	3.05·10⁶
K⁺	0.00408	3312400	2.33·10⁶
Rb⁺	0.001796	1587600	1.02·10⁶
Cs⁺	0.001076	935089	6.13·10⁵

This calculation shows that the found coefficient b_1 is within the confidence interval, which confirms the results obtained. Thus, the coefficient b_1 is also universal, as is α.

The experimental data analysis on the velocity of elastic waves based on ionization potentials and atomic mass leads to the following expression

$$v_s^2 = \gamma \frac{W}{M_A}$$

where γ = 10⁸, v_S is the ultrasonic waves speed, W is the electronic subsystem energy, equal to

$$W = \frac{1}{2} \frac{R a_0}{\alpha^2} F^{tr} \left[\frac{\alpha}{n^2} \frac{4\pi}{r} z^{*2} e^2 \right].$$

Here α is the fine structure constant, e is the charge, r is the interion distance, n is the effective quantum number, a_0 is the radius, z^* is the free electrons number per atom.

As noted earlier, sign $F^{tr}[\ \ ]$ means a functional transformation operator.

v_S^2 is represented in the form, according to the Laplace formula,

$$v_s^2 = \frac{1}{\beta_S \rho},$$

Or with $\rho = \dfrac{m}{V} = \dfrac{N_A M_A}{N_A V_A}$, $v_s^2 = \dfrac{V_A}{\beta_S} \dfrac{1}{M_A}$.

Let us designate as the connection factor

$$\frac{1}{b_S} = \frac{V_A}{\beta_S}.$$

On the other hand, heating leads to an increase in the number of free electrons, so to a change in the short-range order in the structure of the melt.

In other words, the elements of anisotropy in the short-range order are destroyed in the molten state, thereby an electronic and ionic subsystem rises. An increase in the number of free electrons, metallizing bonds, leads to a decrease in compressibility. Therefore, for the metals' compressibility, one can give the Ya.I. Frenkel formula:

$$\beta_S = \frac{18 r^4}{A z^{*2} e^2}, \qquad (15)$$

where r is the interion distance, A is the Madelung constant, z^* is the free electrons number per atom, and e is the electron charge.

The formula (15) taking into account the ionic volume can be represented as follows for the further analysis convenience

$$\beta_S = \frac{432 V' r}{4\pi A z^{*2} e^2}.$$

We can write passing from β_S to $\dfrac{1}{b_S}$

$$\frac{1}{b_S} = \frac{4\pi A z^{*2} e^2}{432 V' r}.$$

Because

$$\frac{1}{b_S} = \gamma W = \frac{1}{2} \frac{R a_0}{\alpha^2} F^{tr} \left[\frac{4\pi z^{*2} e^2}{r} \alpha \frac{1}{n^2} \right]$$

assuming the multiplicity of factors $F^{tr}[\ \ ]$ and equating

$$\frac{1}{b_S} = \frac{V_A}{V'} \frac{A}{432} \frac{4\pi}{r} z^{*2} e^2$$

and

$$\frac{1}{b_S} = \frac{1}{2} \frac{R a_0}{\alpha} \frac{4\pi}{r} z^{*2} e^2 F^{tr} \left[\frac{1}{n^2} \right],$$

can be installed

$$\frac{R a_0}{\alpha} F^{tr} \left[\frac{1}{n^2} \right] = \frac{A}{216} \frac{V_A}{V'}.$$

Thus, we can consider the connection between α and the Madelung constant to be established. This suggests that, at high densities of matter, elastic waves exhibit quantum properties, not to mention phonon-phonon interactions.

Conclusions

The practical value of direct acoustic measurements and feasibility in liquid metals in this work is demonstrated. These investigations can be used for ultrasonic melt processing optimization. The physical and chemical ultrasound effects on liquid melts structure were investigated. We determined that the chemical effect is an irreversible and permanent change in atom weight and the atom-weight distribution due to ultrasound in our study with specific components and ultrasound system. As the ultrasound intensity increases, the atom weight of liquid metals reduces and its atom-weight distribution becomes narrower; the liquid metals atom orientation along the flow direction reduces (in melt state). Ultrasound vibration increases the atom chains motion and makes them more disorder; it also affects the liquid metals relaxation process, leading to weakening the elastic effect.

The absorption, propagation speed temperature dependences, and compressibility of simple semimetals, semiconductors, and semiconductor compounds have been theoretically studied.

Experimental and theoretical results testify to the microheterogeneity of semimetals and semiconductors melts.

Generalization and analysis of experimental data on absorption and propagation speed on the Laplace equation basis and the D.I. Mendeleev periodic law unambiguously indicate the presence of microgroups of atoms (clusters) microheterogenizing semimetals and semiconductors melts.

The nature analysis of the v_s and α polytherms can be concluded from the literature data that a wide temperature range for the manifestation of anomalies in these properties is associated with the coexistence of metallic and interatomic bonds covalent types in the considered melts, which is inherent in clusters.

Semiconductor melts are separated into a separate class of electronic melts. The whole set of experimental data on viscosity, density, and electrical properties, as well as the results of structural studies show that this electron melts class exhibits changes in the short-range order structure upon heating. Therefore, anomalies and features of the melts of semimetals and semiconductors' acoustic properties should be considered manifestations of structural changes.

It is known that the fine structure constant α determines the relationship between electromagnetic and weak interactions, combining them into one theory. The results obtained above emphasize its connection with the elastic wave characteristics since the elastic properties of matter also have a wave nature, as well as electroweak interactions.

Сұйық металдардағы акустикалық өлшемдердің техникалық және практикалық мәнін көрсету

¹Қажыкенова С.Ш. , ¹Шайхова Г.С. , ¹Шалтақов С.Н. , ²Беломестный Д.

¹Абылқас Сағынов Қарағанды техникалық университеті, Қарағанды, Қазақстан
² Дуйсбург – Эссен университеті, Дуйсбург, Германия

ТҮЙІНДЕМЕ

Бұл жұмыста қарапайым жартылай металдардағы, жартылай өткізгіштердегі және жартылай өткізгіш қосылыстардағы ультрадыбыстың жұтылу және таралу жылдамдығының температураға тәуелділіктері зерттелген. Тәжірибелік және теориялық нәтижелер жартылай металдар мен жартылай өткізгіш балқымалардың микрогетерогенділігін дәлелдейді. Балқымалардағы ультрадыбыстың жұтылу және таралу жылдамдығы бойынша тәжірибелік деректерді Д.И. Менделеевтің периодтық заңы негізінде қорыту және талдау оларда жартылай металдар мен жартылай өткізгіштердің балқымаларын микрогетерогендейтін атомдар (кластерлер) микротоптарының болатындығын анық көрсетеді. Бұл мәселенің өзектілігі заттың сұйық күйі мәселесімен анықталады. Ультрадыбыстың сіңіру және таралу жылдамдығының температураға тәуелділігі осы жұмыстағы үлгілердің бірнеше тобын пайдаланып өлшенеді, әр топ әртүрлі температураға дейін қызады. Жартылай өткізгіштік қасиеті бар балқымалардың, олардың атомдық матрицасында шоғырлардың болуына байланысты, микробіртекті емес екендігі дәлелденді. Бұл нәтижелер жаңа құнды идеяларды, соның ішінде балқытуды ультрадыбыспен өнеркәсіптік масштабқа дейін масштабтау үшін қажет идеяларды тудырып отыр.

Авторлар туралы ақпарат:

Кажикенова Сауле Шарапатқызы
Техника ғылымдарының докторы, профессор, Абылқас Сағынов Қарағанды техникалық университетінің «Жоғары математика» кафедрасының меңгерушісі, Қарағанды, Қазақстан. Email: sauleshka555@mail.ru

Шаихова Гүлназира Серікқызы
Техника ғылымдарының кандидаты, Абылқас Сағынов Қарағанды техникалық университетінің «Жоғары математика» кафедрасының доцентінің м.а., Қарағанды, Қазақстан. Email: shaikxova_2011@mail.ru

Шалтаков Сағындық Нагашибайұлы
PhD, Абылқас Сағынов Қарағанды техникалық университетінің «Физика» кафедрасының аға оқытушысы, Қарағанды, Қазақстан. Email: sagyndyk613@mail.ru

Беломестный Денис
PhD, Дуйсбург-Эссен университетінің профессоры. Email: denis.belomestny@uni-due.de

Демонстрация возможности и практической ценности прямых акустических измерений в жидких металлах

¹Кажикенова С.Ш. , ¹Шаихова Г.С. , ¹Шалтаков С.Н. , ²Беломестный Д.

¹ Карагандинский технический университет имени Абылкаса Сагинова, Караганда, Казахстан
²Университет Дуйсбург – Эссена, Дуйсбург, Германия

АННОТАЦИЯ

В работе исследованы температурные зависимости поглощения и скорости распространения ультразвука в простых полуметаллах, полупроводниках и полупроводниковых соединениях. Экспериментальные и теоретические результаты свидетельствуют о микрогетерогенности расплавов полуметаллов и полупроводников. Обобщение и анализ экспериментальных данных по поглощению и скорости распространения ультразвука в расплавах на основе Периодического закона Д.И. Менделеева четко указывают на наличие в них микрогрупп атомов (кластеров), микрогетерогенизирующих расплавы полуметаллов и полупроводников. Актуальность этой проблемы предопределена проблемой жидкого состояния вещества. Зависимость поглощения и скорости распространения ультразвука от температуры измеряется с использованием нескольких групп образцов в настоящей работе, каждая группа нагревается до разной температуры. Доказано, что расплавы с полупроводниковыми свойствами являются микронеоднородными из-за наличия в их атомной матрице кластеров. Эти результаты дают ценные новые идеи и идеи, необходимые для масштабирования обработки расплава ультразвуком в промышленных масштабах.

Информация об авторах:

Кажикенова Сауле Шарапатовна
Доктор технических наук, профессор, заведующая кафедрой «Высшая математика», Карагандинский технический университет имени Абылкаса Сагинова, Карганда, Казахстан.
E-mail: sauleshka555@mail.ru

Шаихова Гульназира Сериковна
Кандидат технических наук, и.о.доцента кафедры «Высшая математика», Карагандинский технический университет имени Абылкаса Сагинова, Караганда, Казахстан.
E-mail: shaikxova_2011@mail.ru

Шалтаков Сагындык Нагашибаевич	PhD, старший преподаватель кафедры «Физика», Карагандинский технический университет имени Абылкаса Сагинова, Караганда, Казахстан. E-mail: sagyndyk613@mail.ru
Беломестный Денис	PhD, Профессор Университета Дуйсбург-Эссен, Дуйсбург, Германия. E-mail: denis.belomestny@uni-due.de

Reference

[1] YAO T, KONDIC V. Viscosity of Metallic Liquids. Nature. 1950; 166:483. https://doi.org/10.1038/166483a0

[2] Brenman M, Nuthinson P, Sandster ML, Schosieid P. Calculation of an effective pair interaction potential for Liquid neon from structure factor measuvements. J. Phys. C. Solid State Phys. 1974; 7(23):411-414.

[3] Havel J, Meloun M. Multiparametric curve fitting. Part. 9, Simultaneous regression estimation of stechiometry and stability constants of complexes. Talanta. 1986; 33(5):435-441. https://doi.org/10.1016/0039-9140(86)80111-4

[4] Mitra SK, Nuthinson P, Sandster ML, Schosieid PA. Pair interaction potential for rubidium calculated from thermodynamic and neutron diffraction data. Philos. 1976; 34(6):1087-1100.

[5] Bloek R, Sush IB, Blaser W, et. al. Measurement of the structure faeton of Liquid rubidium by neutron diffraction up to 1400 K and 200 bar. Ber. Bunsenges. Phys. Chem. 1976; 80(8):718-774.

[6] Regel AR, Glazov VM. Periodic law and physical properties of electronic melts. M.: Nauka. 1982, 296.

[7] Poltavtsev YuG. Struktura poluprovodnikovykh rasplavov [Structure of semiconductor melts]. Moscow: Metallurgy. 1984, 176. (in Russ.).

[8] Chinnam RK, Fauteux C, Neuenschwander J, Janczak-Rusch J. Evolution of the microstructure of Sn–Ag–Cu solder joints exposed to ultrasonic waves during solidification. Acta Materialia. 2011; 59(4):1474-1481. https://doi.org/10.1016/j.actamat.2010.11.011

[9] Kazhikenova SSh, Shaltakov SN, Nussupbekov B. Difference melt model. Archives of Control Sciences. 2021; 31(LXVII):607-627. https://doi.org/10.24425/acs.2021.138694

[10] Mesaros M, Martínez OE, Bilmes GM, Tocho JO. Acoustic detection of laser induced melting of metals. J. Appl. Phys. !997; 81(2):1014-1016. https://doi.org/10.1063/1.364196

[11] Hackett L, Miller M, Weatherred S. Non-reciprocal acoustoelectric microwave amplifiers with net gain and low noise in continuous operation. Nat Electron. 2023; 6:76-85. https://doi.org/10.1038/s41928-022-00908-6

[12] White DL. Amplification of ultrasonic waves in piezoelectric semiconductors. J. Appl. Phys. 1962; 33:2547-2554.

[13] Eskin DG, Tzanakis I, Wang F, Lebon GSB, Subroto T, Pericleous K, Mi J. Fundamental studies of ultrasonic melt processing. Ultrasonics Sonochemistry. 2019; 52:455-467. https://doi.org/10.1016/j.ultsonch.2018.12.028

[14] Kamioka H. Behavior of Tin-Bismuth alloys near melting point found by measurement of sound velocity. J. Phys. Soc. Jap. 1984; 53(4):1349-1355.

[15] Gitis MB, Mikhailov IG, Niyazov S. Sound absorption in liquid sulfur. Acoust. Journal. 1970; 16(3):472-473.

[16] Gallego LJ, Rey C, Crimson MJ. A Monte Carlo simulation study of the disjoining pressure in thin fluid films stercally stabilized by terminally attached chains. Mol. Phys. 1991; 74(2):383-395.

[17] Abowitz G, Gordon RB. Internal friction in metals: mercury and mercury-thallium Alloys. Acta metal. 1962; 10(7):671-679.

[18] Jarzynski L, Litovitz TA. Ultrasonic absorption in Liquid Sodium-Potassium alloys. J. Chem. Phys. 1964; 41(5):1290-1296.

[19] Reing EN, Beyer RT. Ultrasonic absorption in liquid selenium. J. Acoust. Soc. Amer. 1977; 62(3):582-588.

[20] Aider JL, Wesfreid JE. Characterisation of Longitudinal Görtler Vortices in a Curved Channel Using Ultrasonic Doppler Velocimetry and Visualizations. J. Phys. 1996; 6(7)893-906. https://doi.org/10.1051/jp3:1996162

[21] García-Colín LS, De La Selva SMT. The Stokes-Kirchhoff relation in chemically reacting fluids. Chemical Physics Letters. 1973; 23(4):611-613. https://doi.org/10.1016/0009-2614(73)89041-4

[22] Shekaari H, Golmohammadi B. Ultrasound-assisted of alkali chloride separation using bulk ionic liquid membrane. Ultrasonics Sonochemistry. 2021; 74:105549. https://doi.org/10.1016/j.ultsonch.2021.105549

[23] Liu Y, Yu W, Liu Y. Effect of ultrasound on dissolution of *Al* in *Sn*. Ultrasonics Sonochemistry. 2019; 50:67-73. https://doi.org/10.1016/j.ultsonch.2018.08.029

[24] Zheng Y, Yi Tan X, Xiaojuan Wan, Cheng X, Liu Zh, Yan Q. Thermal stability and mechanical response of Bi_2Te_3 - based materials for thermoelectric applications. ACS Applied energy materials. 2020; 3(3):2078-2089. https://doi.org/10.1021/acsaem.9b02093

[25] Chiba A, Ohmasa Y, Yao M. Vibrational, single-particle-like, and diffusive dynamics in liquid *Se, Te*, and $Te_{50}Se_{50}$. J. Chem. Phys. 2003; 119(17):9047-9062. https://doi.org/10.1063/1.1615234

[26] Inui M, Kajihara Y, Tsuchiya Y. Peculiar temperature dependence of dynamical sound speed in liquid $Se_{50}Te_{50}$ by inelastic x-ray scattering. Journal of Physics Condensed Matter. 2020; 32(21):214003. https://doi.org/10.1088/1361-648X/ab6d8e

[27] Shleifer F, Wilson JD, Loring R. Self-consistent theory of polymer dynamic in melts. J. Chem. Phys. 1991; 95:8474-8485. https://doi.org/10.1063/1.461277

[28] Liu JM, Wu WH, Zhai W, Wei B. Ultrasonic modulation of phase separation and corrosion resistance for ternary *Cu-Sn-Bi* immiscible alloy. Ultrasonics Sonochemistry. 2019; 54:281-289. https://doi.org/10.1016/j.ultsonch.2019.01.029

[29] Kuliev BB, Rustamov PG, Aliyanov MA, Kuliev EM. Ultrasonic studies on the interaction of SnTe-InTe systems. Physica Status Solidi (a). 1971; 4(2):127-130. https://doi.org/10.1002/pssa.2210040241

[30] Pless KG. Ultrasonic measurements in metals in the molten state and upon unsolidification [Ultraschallmessungen in metallen im Geschmolzenen zustand und Beim Enstarren]. Acustica. 1963; 3:240-244. (in Ger.).

[31] Inui M, Kajihara Y, Hosokawa Sh, Matsuda K, Tsuchiya Y. Dynamical sound speed and structural inhomogeneity in liquid *Te* studied by inelastic x-ray scattering. Journal of Non-Crystalline Solids. 2019; 1: 100006. https://doi.org/10.1016/j.nocx.2018.100006

[32] Yu W, Liu Y, Liu Y, Formation and Evolution of Cu-Sn Intermetallic Compounds in Ultrasonic-Assisted Soldering. J. Electron. Mater. 2019; 48:5595-5602. https://doi.org/10.1007/s11664-019-07405-1

Investigation of the beneficiation of refractory ferromanganese ores "Zhomart" deposits

[1]Dyussenova S.B., [1] Lukhmenov A.Yu., [2] Imekeshova M.A., [1*]Akimzhanov Z.A.

[1] *"Research and Engineering Center ERG" LLP, Astana, Kazakhstan*
[2] *JSC TNC "Kazchrome", Aktobe, Kazakhstan*

* Corresponding author e-mail: zhomart.akimzhanov@erg.kz

ABSTRACT

In order to provide ferroalloy production with high-quality raw materials, the need to develop technologies for processing of low-grade manganese and ferromanganese ores is becoming increasingly important. In view of the change in the quality characteristics of ores, the decrease in manganese content and the ability to beneficiation by traditional methods, it is necessary to consider new approaches and technological solutions. The article presents data from a study on the beneficiation of refractory iron-manganese ore from the Zhomart deposit. The mineralogy, physical and mechanical properties, and granulometric composition of the ore were determined. The results of a study on gravitational beneficiation using a laboratory pulsator with a pneumatic drive and a laboratory 2-chamber diaphragm jigging machine and magnetic beneficiation of ore with a high-intensity magnetic field are presented. Iron-containing concentrate (Fe-45% and Mn-6.5% is mainly represented by hematite mixed with non-metallic minerals quartz and calcite) and iron-manganese concentrate (Mn-21.7% and Fe-21.1% in the form of hematite, Brownite and pyrolusite, also mixed with quartz and calcite). The concentrates are not suitable for smelting manganese-containing ferroalloys but can be used in the process of electrothermal beneficiation with selective carbothermal reduction of iron in an ore-thermal furnace. The smelting products can be manganese cast iron and iron-free, low-phosphorus limiting manganese slag with a high ratio of manganese to iron.

	Information about authors:
Dyussenova Symbat Berikkalikyzy	*Ph.D., Mineral Processing Engineer «Research and Engineering Center ERG» LLP, D. Kunayev str. 2, 010000, Astana, Kazakhstan. E-mail: dusenova_s@mail.ru*
Lukhmenov Alexandr Yuryevich	*Mineral Processing Manager «Research and Engineering Center ERG» LLP, D. Kunayev str.2, 010000, Astana, Kazakhstan. E-mail: alexandr.lukhmenov@erg.kz*
Imekeshova Marina Anatolyevna	*Chief Mineral Processing Specialist JSC TNC "Kazchrome", M. Mametova str., 4A, 030008, Aktobe, Kazakhstan. E-mail: marina.imekesheva@erg.kz*
Akimzhanov Zhomart Akhmetsapayevich	*Ph.D., Mineral Processing Engineer «Research and Engineering Center ERG» LLP, D. Kunayev str.2, 010000, Astana, Kazakhstan. E-mail: zhomart.akimzhanov@erg.kz*

Introduction

Currently, ferroalloy production in Kazakhstan requires the provision of high-quality manganese concentrates in sufficient quantities with a manganese content of at least 35%. Along with the well-known manganese deposits of the Atasui and Ulytau ore districts: Zhairemskoye, Zhezdy, Kamys, Tur, Karazhal, etc., manganese-poor ores of the iron-manganese deposits Zhomart, Ushkatyn III, Kartobay and others, which are also concentrated in Central Kazakhstan.

A similar situation regarding the provision of ferroalloy production with manganese concentrates

is observed in Russia, where it also became necessary to develop technologies for the beneficiation of low-grade manganese ores.

Researchers of the Siberian State Industrial University note that in order to provide the Russian industry with its own raw materials [1], the use of Kuzbass manganese ores with high iron content is of greatest interest, and other studies provide data on the iron beneficiation of the manganese ore of the Kagaydatskoye deposit of Kuzbass [2]. During the study, the ore beneficiation has been performed by washing, gravitation, magnetic separation, and floatation. The sample contained 10.8% of manganese and 18.7% of iron. Positive results on the

beneficiation of the test samples were not obtained, since the ore is difficult to enrich, manganese-iron concentrate (19.9% Mn and 12.7% Fe) and iron-bearing concentrate (8.3% Mn and 31.3% Fe) were obtained. Therefore, hydrometallurgical methods of beneficiation of refractory iron-manganese ore were applied [3]. Autoclave stadial leaching was applied using calcium and iron chlorides as a solvent. After successive precipitation and calcination, high-quality manganese (58-60% Mn with a recovery of 90-92%) and iron (48-54% Fe with a recovery of 86-90%) concentrates were obtained.

The results of the hydrometallurgical scheme for processing poor iron-manganese ore are positive and very encouraging [[4], [5], [6]], but the implementation of this technology is difficult, due to the creation of a new hydrometallurgical production at the ore mining site.

Specialists studied alternative pyrometallurgical methods for the beneficiation and processing of ferromanganese ore [[7], [8]], in particular, interesting data are given in [9], where magnetizing roasting of ore crushed with a particle size of $-74\ \mu m$ (mass accounting for 80%) was combined in a fluidized bed at 600ºC followed by magnetic separation of the magnetizing roasting product at 1070 Oe. From the ore, 43.5% Fe and 11.4% Mn, iron concentrate 68.3%Fe (96.3% recovery), and manganese concentrate 33.7% Mn (86.8% recovery) were obtained. However, by analogy with hydrometallurgical methods, the implementation of beneficiation schemes with the inclusion of pyrometallurgical processes at the ore mining site is also difficult.

This article presents the results of a study on the beneficiation of iron-manganese ore from the Zhomart deposit, the study has been undertaken to obtain a large-lump concentrate for smelting furnaces, that is, in the so-called sparing beneficiation mode.

Experimental part and discussions of results

The study revealed the following:

- the ore mineralogy with the use of a polarizing microscope in reflected light with a combination X-ray diffraction and fluorescence analysis methods;

- the physical and mechanical properties and grain size distribution on methods described in reference [[10], [11]];

- the tests on the gravity dressing were conducted using the lab based pulsator with pneumatical drive and laboratory bicameral diaphragm jigging machine (more information will be described further in the article test);

- the tests on dry magnetic separation were conducted on a laboratory magnetic analyzer with a high-intensity magnetic field (more information will be described further in the relevant section of the article).

Iron-manganese ore of the "Zhomart" deposit according to X-ray diffraction analysis presented by the following base minerals: barren minerals – 28.9% of silica SiO_2; 17.8% of calcite $Ca(CO_3)$ – and ore minerals – 27.8% of hematite Fe_2O_3; 15.8% of braunite $(Mn_2O_3)_3 \cdot MnSiO_3$ and 9.6% of manganese superoxide MnO_2 –The diffraction pattern of the ore is demonstrated in Figure 1.
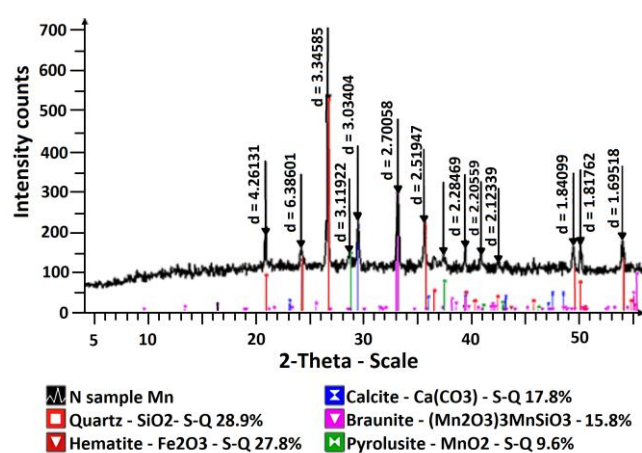
Figure 1 – The diffraction pattern of samples of starting iron-manganese ore

The photo of the exterior form of ore, size fraction from 0 to 50 mm is presented in Figure 2. The sample of iron-manganese ore with a reddish steel and black hue, mostly of a pricked pattern of the hematite and black iron finely banded ore, fine-grained manganese, and to a lesser extent, with a brownish-white color of silica and calcite.

According to the mineralogical analysis performed on Leica DM2500 M polarizing and stereoscopic microscope MBS-1 (MBS, Russia) binocular magnifying glass has been determined that the sample from the "Zhomart" deposit has two types of ores: silica-carbonatic iron oxide (concentrated in iron) and silica-carbonatic manganese oxide (concentrated in manganese):

1) *silica-carbonatic iron oxide* ore contains magnetite and hematite. The original groundmass of hematite is formed in the reduction and replacement processes of magnetite. Tabular grains of the hematite penetrate into magnetite through cracks, within defined areas from the periphery to

the center of magnetite crystals, or completely irregular. Hematite is characterized by small-scale clumps with the irregularly shaped grain size of less than 0.007 mm, sometimes finely dispersed, which form the finest twinning with silica or calcite. In addition to layer-by-layer clumps, string hematite is well-developed, most likely of the second phase, composing a network of coarse-scaled monomineral stringer selections, with a leafy-scaled, tabular grain shape of up to 0.035 mm. Magnetite is represented by irregular nested inclusions, of up to 0.06-0.035 mm, less frequently, idiomorphic crystals, intensely crook-veined with hematite. According to mineralogy, to release iron it is necessary to diminish the ore to fine dimensions of less than 0.071 mm.

Figure 2 – Iron-manganese ore of the "Zhomart" deposit

2) *silica-carbonatic manganese oxide* ore is a cycling between partings of silica-carbonatic composition and braunite- black manganese - pyrolusite aggregates, and also with grainy clumps of friedelite $(Mn,Fe)_8Si_6O_{15}(OH,Cl)_{10}$, red manganese $MnCO_3$, manganese calcite $(Mn,Ca)CO_3$, braunite and pyrolusite:

 - braunite is the primary ore mineral that forms close-grained aggregates to a greater extent idiomorphic grains of up to 0.09-0.18 mm. Fine-grained formations of black manganese-pyrolusite composition with power up to 0.014 mm thick develop along the cracks of grain cleavage;

 - the friedelite forms fine-grained formations with grain sizes up to 0.08 mm in a close twinning with the red manganese, silica, and calcite with dense insets in microscopic inclusions of the black manganese-pyrolusite composition with the size up to 0.007 mm. Against the background of fine-grained

fridelite, cleaved strings and nested clumps with power up to 0.07 mm have been observed, composed of black manganese - pyrolusite aggregates with an allotriomorphic-grained structure.

 - cleaved strings with power up to 0.8 mm, the black manganese - pyrolusite composition, performing the wall voids and cracks with the formation of leafy-scaled concretions of pyrolusite with the size up to 0.014 mm are characterized by a fairly wide development. According to mineralogy, in order to release manganese from the second type of ore, it is necessary to diminish the ore to fine dimensions of 0.1-0.5 mm.

The composition of ore according to X-ray fluorescence analysis is given in Figure 3.
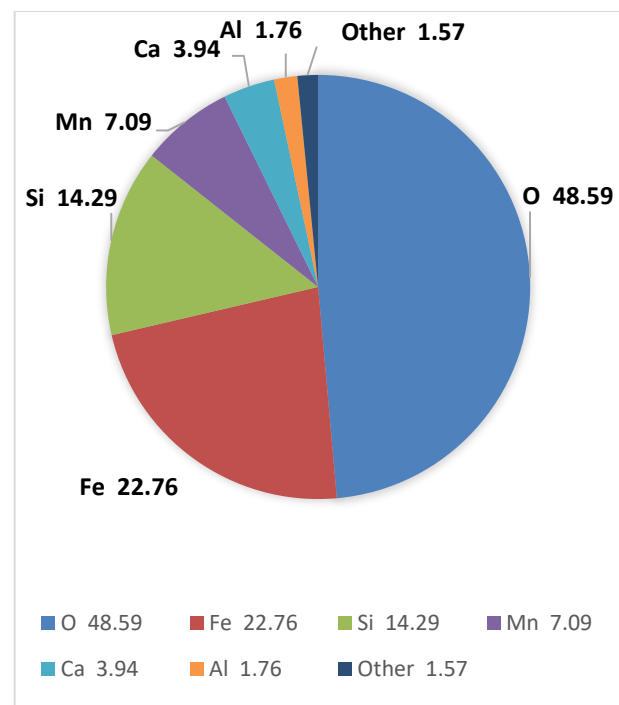
Figure 3 – The results of X-ray fluorescence analysis

According to Figure 3, the manganese, iron, and silicon content are at the level of 7.1%, 22.8%, and 14.3% respectively, in other words, the iron content in the ore is three times more than manganese.

In the process of studying the physical and mechanical properties of iron-manganese ore has been determined that: the true ore density is 3.57 g/cm^3; the bulk ore density (size -50+0.0 mm) is 2.01 g/cm^3; the bulk ore density (size -2.5+0.0 mm) is 1.73 g/cm^3; the ore hardness by M. Protodyakonov - 11.4 (medium hardness ore).

Table 1 – Granulometric analysis of ore sheared to 50 mm

Size, mm	Yield, %	Content, %			Recovery, %		
		Mn	Fe	SiO₂	Mn	Fe	SiO₂
- 50 + 40	8.92	3.03	34.57	27.27	2.80	11.14	8.56
- 40 + 20	28.56	7.91	32.63	22.75	23.42	33.67	22.85
- 20 + 10	14.46	11.41	28.80	27.27	17.11	15.04	13.87
- 10 + 5	10.53	12.34	28.23	27.71	13.47	10.74	10.26
- 5 + 2.5	6.34	13.29	24.44	26.61	8.73	5.60	5.93
- 2.5 + 1.25	4.49	14.11	23.97	26.54	6.57	3.89	4.19
- 1.25 + 0.63	3.66	14.26	23.93	28.11	5.41	3.17	3.62
- 0.63 + 0.315	2.38	10.01	24.25	34.96	2.47	2.09	2.93
- 0.315 + 0.1	4.44	13.81	24.72	29.75	6.35	3.97	4.65
- 0.1 + 0.071	1.12	7.24	21.95	48.30	0.84	0.89	1.90
- 0.071 + 0.0	15.10	8.20	17.96	39.99	12.83	9.80	21.24
Ore	**100.00**	**9.65**	**27.67**	**28.43**	**100.00**	**100.00**	**100.00**

In the course of the ore beneficiation study, a granulometric analysis was carried out (Table 1) to determine the size classes in which iron or manganese are mainly concentrated.

According to the results of granulometric analysis, the weighted average content of manganese and iron composed 9.65% and 27.67% respectively.

Based on the results presented in Table 2, the following may be noted:

- the largest ratio has large size classes -50+40 mm, -40+20 mm, and -20+10 mm, the total ratio consisted of 51.94% and the class -0.071+0.0 mm. The ratio of the subsequent size classes decreases from 10.53% in the -10+5 mm class and up to 1.12% in the -0.1+0.071 mm size class. The ratio of the size class -0.071+0.0 mm reached 15.10%;

- the distribution of manganese content by size classes has been unequal. The highest manganese contents in the range from 10.01% to 14.11% correspond to size classes in the range of -20+0.1 mm. The lowest manganese content in the large class is -50+40 mm and is composed of 3.03%. The content of manganese in the other size classes is in the range of 7.24-8.20%. The extraction of manganese into the size classes practically corresponds to their yields;

- the iron content by size classes is uneven. The highest iron content in the large class is -50+40 mm 34.57% and gradually decreases with decreasing size classes. The lowest iron content in the class with a size of -0.071 +0.0 mm consisted of 17.96%. The indicators of iron extraction in the size classes practically correspond to their yields.

It is known that modern methods of beneficiation of manganese ores are based on the difference in density [12], wettability, and magnetic characteristics of various chemical elements by which it is possible to purify ores from impurity elements. The paper provides data on the jigging of manganese ore in various size classes from 0.63 mm to 50 mm, while the combining concentrate of the jigging contained 40.2% manganese with the extraction of 71.4%.

The authors applied jigging of ore with desliming in the same apparatus as the proposed method a concentrate with a manganese content of 40% was prepared [13].

Based on the data of the granulometric analysis of the ore, as well as to obtain a large-lump concentrate, tests were carried out on the jigging of iron - manganese ore in the size classes of -50+13 mm; -13+2.5 mm and -2.5+0.5 mm.

A laboratory pulsator with a pneumatic drive was used to test the jigging of machine classes with a size of -50+13 mm, -13+2.5 mm. The frequency of pulsations equaled 50 – 70 oscillations per minute, the oscillation amplitude was 80 – 100 mm, the pulsation cycle was sinusoidal (50 – 0 – 50), the diameter of the chamber is 250 mm, the size of the sieve holes is 2.0 mm, the height of the alluvial jig is 250 mm, the flow rate of the screening underflow water is 4-6 m³/t and the specific load is 8 – 10 t/(h·m²).

The jigging of a size class of -2.5+0.5 mm was carried out in a laboratory bicameral diaphragm jigging machine of the OML TsNIGRI type with the following parameters: pulsation frequency 150 – 390 count/min, the height of the false-bed jig 40 mm prepared in the first camera from iron mineral grains with a density of more than 4000 kg/m³ and in the second camera from manganese minerals with a

Table 2 – The balance of metals gained from jigging of ore to obtain iron concentrate and middling

Title	Yield, %	Content, %		Recovery, %		Ratio Mn/Fe
		Mn	Fe	Mn	Fe	
Concentrate – chamber 1 - 50+13 mm	17.78	5.49	46.28	9.46	32.42	0.12
Concentrate – chamber 1 -13+2.5 mm	5.10	9.21	45.40	4.56	9.12	0.20
Total iron concentrate - 50+0.5 mm	**22.88**	**6.32**	**46.08**	**14.02**	**41.54**	**0.14**
Middling –chamber 2 -50+13 mm	15.82	16.19	27.36	24.83	17.06	0.59
Tails -13+2.5 mm	17.28	13.91	18.58	23.31	12.65	0.75
Size class -2.5+0.5 mm	8.98	14.77	23.11	12.86	8.18	0.64
Size class -0.5+0.0 mm	22.28	8.86	20.22	19.16	17.75	0.44
Total middlings -50+0.0 mm	**64.36**	**12.84**	**21.94**	**80.16**	**55.64**	**0.59**
Tails -50+13 mm	12.76	4.70	5.60	5.82	2.82	0.84
Ore -50+0.0 mm	**100.0**	**10.31**	**25.38**	**100.0**	**100.0**	**0.41**

density of more than 3000 kg/m^3 and a size class of 8-10 mm, pulsation amplitude of 6-8 mm, specific productivity of 5-6 t/(h/m^2), consumption of the screening underflow water of 3 m^3/t.

Consolidated indicators on the jigging for all size classes -50+13 mm; -13+2.5 mm and -2.5+0.5 mm with the production of iron concentrate and iron-manganese middling are shown in Table 2.

According to Table 2, it is clearly seen that a size class of less than 50 mm has been obtained after jigging:

- iron concentrate (yield 22.88%) with an iron content of 46.08% and manganese of 6.32% when extracting 41.51% and 14.02%, respectively, based on the mineralogy of the ore, iron is mainly represented by hematite.

- iron - manganese middling (yield 64.36%) with a manganese content of 12.84% and iron 21.94% with the manganese and iron extraction of 80.16%, 55.64% respectively, and which is not suitable for smelting ferroalloys, because a manganese content of at least 35% required.

The author [14] notes that various technological schemes could be applied for the beneficiation of manganese ores, including the combination of gravity and magnetic beneficiation techniques.

In articles [[15],[16],17]], a method for the beneficiation of manganese ore has been provided, which includes magnetic separation of a fine fraction of ore with a size class of less than 3 mm by known technology.

In order to increase the manganese content, tests were conducted on dry magnetic separation of

industrial products, which was carried out on a laboratory electromagnetic separator 138T-SEM with a high magnetic field intensity from 660 to 780 kA / m. Previously, the middling was diminish to dimensions of 2.5 mm, followed by classification by a size class of 0.1 mm (Figure 4).
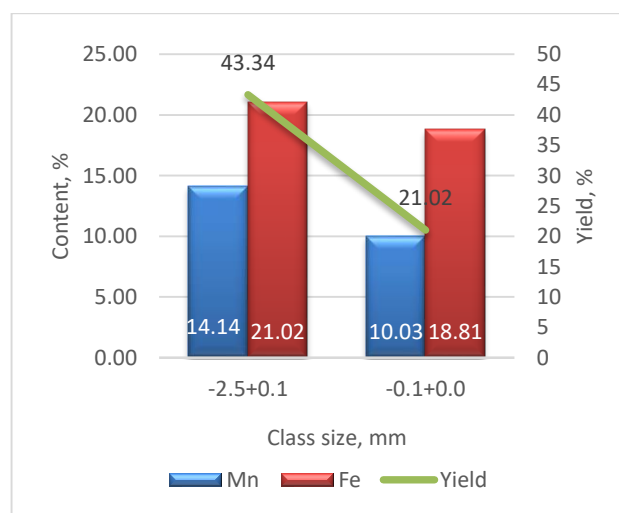
Figure 4 – Classification Results for the middling on jigging

The results for magnetic separation of size class -2.5+0.1 mm of the middling are shown in Table 3.

The total balance of ore processing of the "Zhomart" deposit with the use of jigging and magnetic separation processes to obtain additional iron and iron-manganese concentrate by magnetic separation is demonstrated in Table 4.

Table 3 – The balance of metals of magnetic separartion of the middling on the jigging to obtain iron and iron-manganese concentrate

Title	Yield, % from		Content, %		Recovery from process, %		Ratio Mn/Fe
	process	ore	Mn	Fe	Mn	Fe	
Iron concentrate, 660 kA/m	20.96	9.08	7.07	42.97	10.48	42.84	0.16
Iron-manganese concentrate, 780 kA/m	51.74	22.43	21.73	21.09	79.50	51.93	1.03
Tails, non-magnetic fraction 780 kA/m	27.30	11.83	5.19	4.03	10.02	5.23	1.29
Total middling -2.5+0.1 mm	**100.0**	**43.34**	**14.14**	**21.02**	**100.0**	**100.0**	**-**

Table 4 – The balance of metals of ore beneficiation of the "Zhomart" deposit with the use of jigging and magnetic separation

Title	Yield, %	Content, %		Recovery, %		Ratio Mn/Fe
		Mn	Fe	Mn	Fe	
Concentrate – chamber 1 -50+13 mm	17.78	5.49	46.28	9.49	33.83	0.12
Concentrate – chamber 1 -13+2.5 mm	5.10	9.21	45.40	4.57	9.52	0.20
Iron concentrate, magnetic fraction 660 kA/m -2.5+0.1 mm	9.08	7.07	42.97	6.24	16.04	0.16
Total iron concentrate -50+0.1 mm	**31.96**	**6.53**	**45.20**	**20.30**	**59.39**	**0.14**
Iron-manganese concentrate, magnetic fraction 780 kA/m -2.5+0.1 mm	**22.43**	**21.73**	**21.09**	**47.40**	**19.45**	**1.03**
Tails -50+13 mm	12.76	4.70	5.60	5.83	2.94	-
Tails, non-magnetic fraction 780 kA/m -2.5+0.1 mm	11.83	5.19	4.03	5.97	1.96	-
Size class -0.1+0.0 mm	21.02	10.03	18.81	20.50	16.26	-
Total tails -50+0.0 mm	**45.61**	**7.28**	**11.28**	**32.30**	**21.16**	**-**
Ore -50+0.0 mm	**100.0**	**10.28**	**24.32**	**100.0**	**100.0**	**-**

According to Table 4, it is seen that from the ore of the "Zhomart" deposit, according to the gravitational-magnetic scheme, could be obtained:

- iron concentrate (yield 31.96%) with an iron content of 45.2% and manganese content of 6.53% with the extraction of 59.39% and 20.3% respectively;

- iron - manganese concentrate (yield 22.43%) with the content of manganese 21.73% and iron 21.09% with the extraction of manganese 47.4% and iron 19.45%.

The study results showed that iron concentrate (Fe-45% and Mn-6,5% manganese are mainly represented by hematite mixed with non-metallic minerals, i.e silica and calcite) and iron-manganese concentrate (Mn-21,7% and Fe-21,1% iron presented by hematite, braunite and pyrrolusite also blend with silica and calcite).

Concentrates that could be obtained by ore beneficiation of the "Zhomart" deposit are not considered to be saleable for smelting manganese-containing ferroalloys. Potential use is in the process of electro-thermal phenomena with selective carbothermal reduction of iron in the ore-thermal furnace [[18], [19], [20]]. The smelting products will be manganese cast iron and ironless low-phosphorous marginal manganese slag with a high ratio of manganese to iron.

Conclusions

During the study, iron-manganese concentrate (Fe-45% and Mn-6.5%) and iron-manganese concentrate (Mn-21.7% and Fe-21.1%) were obtained from iron-manganese ore (Mn-10.3% and Fe-24.3%).

This type of ore is difficult to obtain concentrates. It can be seen from the data that in order to obtain concentrates with a sufficient

content of the target metal in the beneficiation process, it is necessary to include hydro- or pyrometallurgical processes.

The preference of this beneficiation scheme is determined by the need to reduce the mass of rock for further processing.

Concentrates obtained in the process of beneficiation by means of jigging and magnetic separation of Zhomart deposit ore are not conditioned for smelting manganese-containing ferroalloys, but can be used in the process of electrothermal beneficiation with selective carbothermal reduction of iron in the ore-thermal furnace. Smelting products can be manganese pig iron and iron-free low-phosphorus marginal manganese slag with high manganese to iron ratio.

«Жомарт» кен орнының қиын байытылатын темір-марганец кендерін байыту жұмыстарын зерттеу

¹ Дюсенова С.Б., ¹ Лухменов А.Ю., ²Имекешова М.А., ¹*Акимжанов Ж.А.

¹ «ERG ғылыми-зерттеу инжинирингтік орталығы» ЖШС, Астана, Қазақстан
²«Қазхром» ТҰК» АҚ Ақтобе, Қазақстан

ТҮЙІНДЕМЕ

Ферроқорытпа өндірісін жоғары сапалы шикізатпен қамтамасыз ету үшін төмен сапалы марганецті және темір-марганецті кендерді байыту технологияларын әзірлеу қажеттілігі күннен-күнге өзекті болуда. Кендердің сапалық сипаттамаларының, пайдалы зат үлесінің төмендеуін және дәстүрлі байыту әдістерімен байытудың өзгерулерін ескере отырып, жаңа тәсілдер мен технологиялық шешімдерді қарастыру қажет. Мақалада «Жомарт» кен орнындағы қиын байытылатын темір-марганец кенін байыту бойынша зерттеу деректері келтірілген. Кеннің минералогиясы, физикалық-механикалық қасиеттері және гранулометриялық құрамы анықталды. Пневматикалық жетегі бар зертханалық пульсаторды және зертханалық 2 камералы диафрагмалық тұндыру аппаратын қолдану арқылы гравитациялық байыту және жоғары қарқынды магнит өрісімен кенді магниттік байыту бойынша зерттеу нәтижелері берілген. Құрамында темір бар концентрат (Fe-45% және Mn-6,5% негізінен металл емес минералдар кварц және кальцит араласқан гематит түрінде) және темір-марганец концентраты (Mn-21,7% және Fe-21,1% гематит, броунит және пиролюзит, сонымен қатар кварц пен кальцитпен араласқан түрінде) алынды. Концентраттар құрамында марганеці бар ферроқорытпаларды балқыту үшін жарамсыз, бірақ оларды кен-термиялық пеште темірді селективті карботермиялық тотықсыздандыру арқылы электротермиялық байыту процесінде қолдануға болады. Балқыту өнімдері ретінде марганецтің темірге жоғары қатынасы бар марганецті шойын және темірсіз аз фосфорлы марганец шлактары болуы мүмкін.

Түйін сөздер: темір-марганецті кен, тұндыру, құрғақ магниттік сепарация, темір-марганецті концентрат

Авторлар туралы ақпарат:	
Дюсенова Сымбат Берікқалиқызы	*PhD, Байыту инженері, «ERG ғылыми-зерттеу инжинирингтік орталығы» ЖШС , Д. Қонаев к. 2, 010000, Астана қ., Қазақстан. E-mail: Dusenova_s@mail.ru*
Лухменов Александр Юрьевич	*Байыту менеджері, «ERG ғылыми-зерттеу инжинирингтік орталығы» ЖШС, Д. Қонаев к. 2, 010000, Астана қ., Қазақстан. E-mail: Alexandr.Lukhmenov@erg.kz*
Имекешова Марина Анатольевна	*Бас байтушы маман «Казхром» ТҰК» АҚ, М. Маметова к., 4А, 030008, Ақтөбе қ., Қазақстан. E-mail: Marina.Imekesheva@erg.kz*
Акимжанов Жомарт Ахметсапаевич	*PhD, Байыту инженері, «ERG ғылыми-зерттеу инжинирингтік орталығы» ЖШС, Д. Қонаев к. 2, 010000, Астана қ., Қазақстан. E-mail: Zhomart.Akimzhanov@erg.kz*

Исследование обогащения упорных железомарганцевых руд месторождения «Жомарт»

¹ Дюсенова С.Б., ¹ Лухменов А.Ю., ² Имекешова М.А., ¹*Акимжанов Ж.А.

¹ ТОО «Научно-исследовательский инжиниринговый центр ERG», Астана, Казахстан
² АО «ТНК «Казхром», Актобе, Казахстан

АННОТАЦИЯ

С целью обеспечения ферросплавное производство качественным сырьем все более актуальным становится необходимость разработки технологий обогащения бедных марганцевых и железомарганцевых руд. Ввиду изменения качественных характеристик руд, снижения содержания и обогатимости традиционными методами обогащения, необходимо рассматривать новые подходы и технологические решения. В статье приведены данные исследования по обогащению труднообогатимой железо-марганцевой руды месторождения «Жомарт». Определена минералогия, физико-механические свойства и гранулометрический состав руды. Приведены результаты исследования по гравитационному обогащению с использованием лабораторного пульсатора с пневматическим приводом и лабораторной 2-х камерной диафрагмовой отсадочной машины и магнитному обогащению руды с высокоинтенсивным магнитным полем. Получены железосодержащий концентрат (Fe-45% и Mn-6,5% в основном представлен гематитом в смеси с нерудными минералами кварцем и кальцитом) и железо – марганцевый концентрат (Mn-21,7% и Fe-21,1% в виде гематита, браунита и пирролюзита также в смеси с кварцем и кальцитом). Концентраты не являются кондиционными для выплавки марганец содержащих ферросплавов, но могут быть использованы в процессе электротермического обогащения с селективным карботермическим восстановлением железа в рудотермической печи. Продуктами плавки могут являться марганцовистый чугун и безжелезистый малофосфористый предельный марганцевый шлак с высоким отношением марганца к железу.

Ключевые слова: железомарганцевая руда, отсадка, сухая магнитная сепарация, железомарганцевый концентрат

Информация об авторах:	
Дюсенова Сымбат Берікқалиқызы	*PhD, Инженер по обогащению ТОО «Научно-исследовательский инжиниринговый центр ERG», ул. Д.Кунаева 2, 010000, г. Астана, Казахстан. E-mail: Dusenova_s@mail.ru*
Лухменов Александр Юрьевич	*Менеджер по обогащению, ТОО «Научно-исследовательский инжиниринговый центр ERG», ул. Д.Кунаева 2, 010000, г. Астана, Казахстан. E-mail: Alexandr.Lukhmenov@erg.kz*
Имекешова Марина Анатольевна	*Главный обогатитель АО «ТНК «Казхром», ул. М. Маметовой, 4А, 030008, г. Актобе, Казахстан. E-mail: Marina.Imekesheva@erg.kz*
Акимжанов Жомарт Ахметсапаевич	*PhD, инженер по обогащению, ТОО «Научно-исследовательский инжиниринговый центр ERG», ул. Д.Кунаева 2, 010000, г. Астана, Казахстан. E-mail: Zhomart.Akimzhanov@erg.kz*

References

[1] Nokhrina O, Gizatulin R, Golodova M, Proshunin I, Valuev D, Martyushev N, Karlina A. Alloying and Modification of Iron-Carbon Melts with Natural and Man-Made Materials. Metallurgist. 2022; 65:1429-1448. http://doi.org/10.1007/s11015-022-01289-z

[2] Nokhrina O, Gizatulin RA, Golodova MA, Proshunin IE, Valuev D, Martyushev N, Karlina AI. Alloying and Modification of Iron-Carbon Melts with Natural and Man-Made Materials. Metallurg. 2021; 12:65-79. http://doi.org/10.52351/00260827_2021_12_65

[3] Nohrina O, Rogihina I, Proshunin I, Valuev D. Preparation and Usage of High Quality Manganese-Containing Materials from Ferroalloy Production Waste. Key Engineering Materials. 2020; 839:106-113. http://doi.org/10.4028/www.scientific.net/KEM.839.106

[4] Hatk PK, Sukla LB, Das SC. Aqueous SO2 leaching studies on Nishikhal manganese ore through factorial experiment. Hydrometallurgy. 2000; 54(2):217-228. http://doi.org/10.1016/S0304-386X(99)00075-4

[5]   Veglio F, Trifoni M, Abbruzzese C, Toro L. Column leaching of a manganese dioxide ore: A study by using fractional factorial design. Hydrometallurgy. 2001; 59(1):31-44. http://doi.org/10.1016/S0304-386X(00)00139-0

[6]   Kang T, Liu Y, Huang Y, Dong J, Huang Q, Li Y. Synthesis and dephosphorization of iron manganese composite oxide by acid leaching on iron manganese ore. Advanced Materials Research. 2012; 554-556:489-493. http://doi.org/10.4028/www.scientific.net/AMR.554-556.489

[7]   Yang ZZ, Li GQ, Huang CH, Ding JF. Mn ore smelting reduction based on double slag operation in BOF. Applied Mechanics and Materials. 2013; 753-755:76-80. http://doi.org/10.4028/www.scientific.net/AMR.753-755.76

[8]   Pan MC, Liu XL, Zou R, Huang J, Han JC. Study of heat treatment technology on medium-carbon-low-alloy-steel large hammer formation of gradient performance. Advanced Materials Research. 2014, 881-883:1288-1292. http://doi.org/10.4028/www.scientific.net/AMR.881-883.1288

[9]   Shuai Yuan, Wentao Zhou , Yuexin Han, Yanjun Li. Individual beneficiation of manganese and iron from complex refractory ferromanganese ore by suspension magnetization roasting and magnetic separation. Powder Technology. 2020; 373:689-701. https://doi.org/10.1016/j.powtec.2020.07.005

[10] Otávio da Fonseca Martins Gomes, Julio Cesar Alvarez Iglesias, Sidnei Paciornik, Maria Beatriz Vieira. Classification of hematite types in iron ores through circularly polarized light microscopy and image analysis. Minerals Engineering. 2013; 52:191-197. https://doi.org/10.1016/j.mineng.2013.07.019

[11] Julio Cesar Alvarez Iglesias, Otávio da Fonseca Martins Gomes, Sidnei Paciornik. Automatic recognition of hematite grains under polarized reflected light microscopy through image analysis. Minerals Engineering. 2011; 24(12):1264-1270. https://doi.org/10.1016/j.mineng.2011.04.015

[12] Armando FdV Rodrigues, Homero Delboni Junior, Otavia MS Rodrigues, James Zhou, Kevin P Galvin. Gravity separation of fine itabirite iron ore using the Reflux Classifier – Part I – Investigation of continuous steady state separations across a wide range of parameters. Minerals Engineering. 2023; 201:108187. https://doi.org/10.1016/j.mineng.2023.108187

[13] Tukaram bai M, Pallam Srivani, Noothana P, Nageswara rao V. Beneficiation of Manganese Ore Using Froth Flotation Technique. Materials Today: Proceedings. 2019; 18(7):2279-2287. https://doi.org/10.1016/j.matpr.2019.07.010

[14] Jinjia Du, Yanqiong Zhang, Jiajia Lu, Jin Chen, Lei Gao, Shenghui Guo, Mamdouh Omran, Guo Chen. Mechanism of enhanced enrichment manganese from manganese ore-pyrite under microwave heating: Process optimization and kinetic studies. Colloids and Surfaces A: Physicochemical and Engineering Aspects. 2023; 656(B):130534. https://doi.org/10.1016/j.colsurfa.2022.130534

[15] Shuai Yuan, Wentao Zhou, Yuexin Han, Yanjun Li. Separation of manganese and iron for low-grade ferromanganese ore via fluidization magnetization roasting and magnetic separation technology. Minerals Engineering. 2020; 152:106359. https://doi.org/10.1016/j.mineng.2020.106359

[16] Abdykirova G, Toilanbay G, Dyussenova S, Kuldeyev E. The study of beneficiation of manganese-containing raw materials. International Multidisciplinary Scientific GeoConference Surveying Geology and Mining Ecology Management, SGEMthis link is disabled. 2017; 17(43):197-204.

[17] Abdykirova G Zh, Dyusenova SB, Toylanbay GA, Ramazanova ZhA. Magnetizing roasting of manganese-containing man-caused raw materials. Obogashchenie Rud. 2017; (5):54-58.

[18] Jianhua Chu, Yi Nian, Liqiang Zhang, Yanping Bao, Naqash Ali, Chaojie Zhang, Hongwei Zhou. Formation, evolution and remove behavior of manganese-containing inclusions in medium/high manganese steels. Journal of Materials Research and Technology. 2023; 22:1505-1521. https://doi.org/10.1016/j.jmrt.2022.12.023

[19] Biryukova A, Kuldeyev E, Dzhienaliyev T, Abdykirova G, Temirova S. Preparation of pellets from manganese concentrate for the production of ferromanganese. Croatica Chemica Actathis link is disabled. 2023; 62(1):135-138.

[20] Nokhrina OI, Rozhikhina ID, Rybenko IA, Golodova MA, Izrailsky AO. Hydrometallurgicheskoe obogachenie polymetallicheskich i zhelesomarganzevych rud [Hydrometallurgical enrichment of polymetallic and ferromanganese ores]. Izvestya vysshich uchebnych zavedeniy. Chernaya Metallurgiya [News of higher educational institutions. Ferrous metallurgy]. 2021; 64(4):273-281. https://doi.org/10.17073/0368-0797-2021-4-273-281 (in Russ.).

Mathematical model of the formation of barite-lead mineralization of the Ushkatyn III deposit (Central Kazakhstan)

[1] Askarova N.S., [1] Portnov V.S., [1]Rakhimova G.M., [2]Maussymbayeva A.D., [2]Madisheva R.K.

[1] Abylkas Saginov Karaganda Technical University NPJSC, Karaganda, Kazakhstan
[2] Kazakh multidisciplinary reconstruction and development institute (KazMRDI), Karaganda, Kazakhstan

[*]Corresponding author's email: srajadin-nazym@mail.ru

ABSTRACT

The genesis of stratiform deposits of lead and barite in sedimentary rocks is of great interest from the point of view of replenishing reserves of polymetallic ores. The aim of the work is to establish the regularity of the hydrogenic formation of ores in limestones, taking into account the influence of the nanosurface of pores and cracks based on a mathematical model of the movement and characteristics of ore-bearing solutions in the pores. The thicknesses of the surface layer of limestones and minerals included in the ore-containing strata and sulfide minerals are calculated. The results indicate that they are nanostructures with special physical properties different from the rest of the substance, which is confirmed by the regularity of the formation of a heavy sulfur isotope in ores of various textural types. The influence of hydrotherms with different densities, kinematic viscosity, and velocity on the intensity of mineralization formation in cracks and pores of limestone, as well as the occurrence of new feathering cracks around the fractures of dismemberment, is estimated. The dependence of the hydrothermal flow density on the diffusion of the liquid is established. The equation of kinematic viscosity is derived from the pressure in the solution flow, the velocity of its movement, the mass of particles of ore-forming elements, and sulfur isotopes under thermodynamic conditions of determined Gibbs energies. The relationship of the viscosity of the solution with the surface tension of the nanolayer of limestone particles in cracks and pores is shown, indicating that the greater this energy, the greater the velocity of movement of ore-forming solutions, the fewer branches of newly formed cracks around the dissection crack. The mathematical model is applicable for the numerical analysis of the regularity of mineralization in cracks, taking into account the influence of the nanostructural layer of cracks and pores of limestone in the thermodynamic conditions of the occurrence of an ore-bearing formation.

Keywords: Ushkatyn III, stratiform deposits, Atasu type, isotopic composition, mathematical model

	Information of the authors:
Askarova Nazym Srajadinkyzy	*Ph.D., senior lecturer of the Department of Geology and Exploration of Mineral Resources, Abylkas Saginov Karaganda Technical University NPJSC, 100027, Karaganda, Republic of Kazakhstan. E-mail: srajadin-nazym@mail.ru*
Portnov Vassiliy Sergeevich	*Doctor of Technical Sciences, Professor of the Department of Geology and Exploration of Mineral Deposits Abylkas Saginov Karaganda Technical University NPJSC, 100027, Karaganda, Kazakhstan. E-mail: vs_portnov@mail.ru*
Rakhimova G.M.	*Ph.D., Associate Professor of the Department of «Building Materials and Technologies» Abylkas Saginov Karaganda Technical University NPJSC, 100027, Karaganda, Kazakhstan. E-mail: galinrah@mail.ru*
Mausymbaeva Aliya Dumanovna	*Ph.D., Candidate of Technical Sciences, Researcher, Kazakh multidisciplinary reconstruction and development institute (KazMRDI), 100027, Karaganda, Kazakhstan. E-mail: aliya_maussym@mail.ru*
Madisheva Rima Kopbosynkyzy	*Ph.D., Researcher, Kazakh multidisciplinary reconstruction and development institute (KazMRDI), 100027, Karaganda, Kazakhstan. E-mail: rimma_kz@mail.ru*

Introduction

A large number of works have been dealing with the genesis of barite, lead, and zinc deposits in sedimentary complexes and areas, and the participation of generating hydrothermal systems in their formation (Kislyakov and Shchetochkin, 2000; Hanor, 2000; Robb, 2005; Hein et al., 2007; Wilkinson, 2014; Elswick and Maynard, 2014; Emsbo et al., 2016; Cansu and Ozturk, 2020; Smirnov, 1970; Baibatsha, 2012).

The main hypotheses regarding the genesis of barite lead-and-zinc deposits of the Atasu ore district and the Uspenskaya shear zone are described in a lot of works (Shcherba, 1964, 1967; Rozhnov, 1967, 1982; Kayupova, 1974; Buzmakov et al., 1975; Mitryaeva, 1979; Weimarn, 1982; Kalinin, 1982, 1985; Kalinin et al., 1984; Skripchenko, 1989; Varentsov et al., 1993).
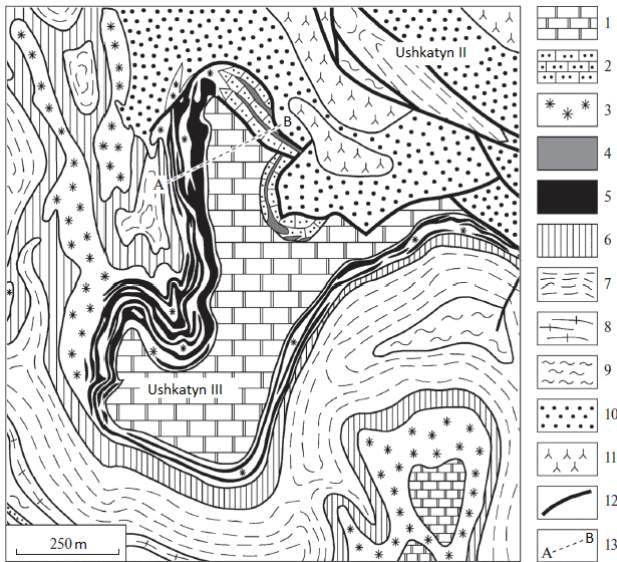

Figure 1 – Geological map of the Ushkatyn ore field (with simplifications).
1 – grey organogenic-detritus limestones, wavy-layered (C_1t_1); 2–5 – the pack is red-colored (D_3fm_2b):
2 – riphogenic organogenic-algal limestones,
3 – organogenic-detrital thin-layered limestones,
4 – barite-lead ores, 5 – ron and manganese ores;
6 – the pack is gray-colored (D_3fm_2a): organogenic-detrital lenticular-layered limestones;
7 – the pack is flishoid (D_3fm_1): rhythmic alternation of organogenic-detrital limestones, calcareous sandstones, and carbonaceous clay-siliceous-carbonate pelites;
8 – the pack is rhythmically layered (D_3fm_1): alternation of clay-siliceous-carbonate rocks with massive and ribbon-layered texture;
9 – the pack is intemperately layered (D_3fm_1): siliceous limestones, clay-carbonate rocks, shell rocks;
10 – The Darya formation (D_3fr): polymictic siltstones and sandstones;
11 – trachyriolites; 12 – faults.

The aim of this work is to study the regularities of the surface nanolayer of cracks and pores of ore-bearing limestones' effect on the formation of mineralization, taking into account textural factors and physical characteristics of aqueous solutions of hydrotherms.

The Ushkatyn III deposit was discovered in 1963 by V.Ya. Sereda when checking gravity anomalies identified by the Agadyr GRE.

Stratiform ore deposits are complex: iron-manganese and barite-lead bodies located on the wings of brachyform and box-like synclines lie in the section together with the enclosing deep-sea deposits of the Lower and Middle Famenian, participating in complex folding (Figure 1) [1].

They were formed in the active zone of seabed extension of the paleoriftogenic basin, along stepped normal faults and flexure-like bends, in the area of transition of deep-water Famennian facies to shallow-water facies.

A.N. Brusnitsyn [2] proposed a model of the formation of the Ushkatyn III deposit, in which barite-galena, iron, and manganese ores are the products of the development of a single hydrothermal system that developed in a thick sedimentary stratum. Barite-galena ores were formed near the surface of the seabed during the discharge of hydrothermal solutions in the inner zones of the still-forming reef. The ore matter deposited in the mixing area of hydrothermal solutions bearing Ba, Pb, Zn, Fe, Mn, and other elements filled the porous and fissure space of the reef, where the bacterial reduction of the sulfate ion of seawater to hydrogen sulfide took place. When hydrothermal fluid seeped through the reef, Ba and Pb deposited in it in the form of barite and galena, while Zn, Fe, and Mn remained in solution, which subsequently precipitated in the oxide form: Fe on the surface of the reef or at some distance from it, and Mn at a considerable distance. Zinc dissipated in the surrounding space without forming ore accumulations [3].

Iron and manganese, barite-galena ores of the Ushkatyn III ore deposit were formed as hydrothermal, superimposed on sedimentary rocks, simultaneously but in different parts of the sea basin [[4], [5]]. Thus, barite-galena ores are identified inside the carbonate structures of the coastal reef, while iron and manganese ores are identified on the bottom surface at some distance from the coast [6].

The difference between barite-galena ores of the Ushkatyn III deposit and other deposits is their low zinc content (Zn: Pb from 1:50 to 1:3000). The enclosing rocks of the barite-galena deposit are reef organogenic-algal limestones with the pronounced rhythmically banded structure, the average size of ore minerals is 20–30 μm, less often 100–500 μm [3].

Gray limestones are composed of a homogeneous mass of microgranular calcite (micrite), in which rounded or elongated lumpy-clotty segregations 0.1-0.2 mm in size are observed.

The texture of these limestones is massive, indistinctly layered, and lenticular-layered, caused by layers of siltstone [6]. Red and greenish-gray limestones contain tiny inclusions of hematite and siltstone with a large number of micropores.

The microgranular structure of limestones and good preservation of relics of microorganisms indicate the absence of the metamorphism effect.

The texture of ores is as follows: layered-banded, nest-like-latticed and continuous spotty, less often brecciated, breccia and vein textures. Barite, galena, and other minerals in banded textures develop along silty layers in limestones, filling the pore space. In the silty layers, there is a partial dissolution of calcite with rare formation of flattened-elongated caverns filled with ore minerals [7]. In all the textural varieties of ores, fine-grained structures predominate, with complex, not always unambiguously interpreted age relationships between minerals.

In works [[3], [6]], there are given the values of $\delta^{34}S$ in sulfide concentrate, which consists mainly of galena, the concentration of the "heavy" isotope varies from −25.7 to −12.6‰, and in barite, from 10.9 to 15.3‰ (Table 1). According to these data there has been built a dependency (Figure 2). Ore minerals are characterized by a very different isotopic comsposition of sulfur: galena is enriched in the light isotope ^{32}S, and barite is enriched by the heavy isotope ^{34}S. In the modern ocean, the value of $\delta^{34}S$ averages 21‰ [6]; in the water of the Late Devonian ocean, this value was 25–30‰. This indicates the formation of barite with participation of isotopically heavy sulfur dissolved in seawater sulfate ions. Sulfides were formed with participation of hydrogen sulfide enriched in the light isotope ^{32}S, which was formed at the stage of early diagenesis of sediments in the course of bacterial sulfate reduction [[7], [8]]. The processes of separation of sulfur isotopes in sediments containing organic matter are described in the work [9].

In work [3], the main signs of barite-galena ores formation in near-surface conditions during the formation of reef deposits are defined: a narrow stratigraphic range and stratiform type of ore-bearing deposit (as well as confinement); connection of ore bodies with consed mentation faults, which is confirmed by the absence of veinlet and other mineralization in the areas of late tectonic faults; the formation of textures and structures of ores is characteristic of incompletely consolidated ore-bearing carbonates; the isotopic composition of sulfur, carbon, and oxygen is characteristic of the joint participation in the formation of barite, sulfides, and carbonates.

A feature of the sedimentary stratum structure of the Ushkatyn III deposit is the transition of coastal facies to shelf facies, with lateral zonality of deposits of the same age with the replacement of the reef complex enclosing barite-galena ores with a bed of layered limestones containing layers of iron and manganese ores [[5], [6]].

The uniform distribution of trace elements (and accordingly a lot of accessory minerals) in the groundmass of the rocks indicates their simultaneous accumulation with the formation of ore-bearing deposits [3].

As a result of these processes, the newly formed hydrogen sulfide concentrates predominantly the light ^{32}S isotope, while the residual sulfate ion concentrates the heavy ^{34}S one. In a closed system with respect to the marine sulfate ion (that is, the access of SO_4^{2-} to the sediment is limited), as it is exhausted in the pore solution, the $\delta^{34}S$ values of both residual sulfate and hydrogen sulfide increase. If the system is open, then the concentration of $\delta^{34}S$ sulfate changes little compared to seawater and the concentration of hydrogen sulfide decreases markedly. The difference $\delta^{34} - \delta^{34}$ SHS can reach more than 40 ‰ [[9], [10], [11], [12]].

Experimental part

The results of determining the isotopic composition of sulfur in sulfides of ores, together with the isotope-geochemical characteristics of carbon and oxygen, made it possible for A.I. Brusnitsyn to develop models of the Ushkatyn III barite-galena deposit formation in the carbonate-reef structure [6]. Deposits of ore minerals occurred as a result of decreasing the temperature of hydrothermal solutions that entered the near-surface zones; increasing pH (due to oxygen dissolved in seawater); the appearance of SO^{2-} (in the composition of seawater); changes in the H_2S/HS^- ratio in pore water (during bacterial sulfate reduction). Barium and lead precipitated immediately upon the appearance of a sulfate ion in solutions and at very acidic concentrations of hydrogen sulfide and oxygen [[13], [14], [15]].

One of the additional reasons for the formation of mineralization in porous limestones, in the authors' opinion, is the nanostructure of the enclosing rock surface layer effect.

To study this, the results of studies are used that are reflected in the correlation field linking the concentration of $\delta^{34}S_{sulfide}$ with the ore textures of the Ushkatyn III deposit (Figure 2, Table 1), (the concentrations are given relative to the meteorite standard).

Table 1 – $\delta^{34}S_{sulfide}$ composition, %, in the galena of the Ushkatyn III deposit ores [2]

No.	layered-banded		nest-like-latticed		continuous spotty
	Ush 3-2	Ush 3-17	Ush 3-12	Ush 318-153	Ush 319-514
1	-16.7	-13.7	-22.5	-17.1	-25.7
2	-	-12.7	-16.1	-21.3	
3	-	-12.8	-17.4	-22.2	
4	-		-19.9	-20.8	
5			-19.0		
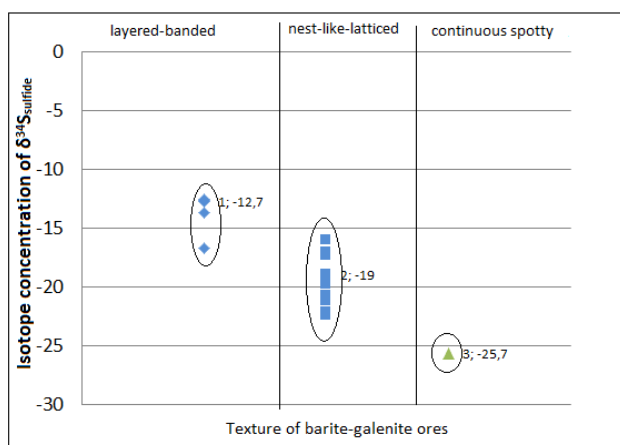
Figure 2 – Correlation fields of the $\delta^{34}S_{sulfide}$ concentration the texture of barite-galena ores of the Ushkatyn III deposit.

It can be seen in Table 1 that for the layered-banded texture, the values of $\delta^{34}S_{sulfide}$ range from -12.6 to -16.7; for nest-like-latticed texture from -16.2 to -22.2; and for continuous spotty it is -25.7.

Let us consider this pattern from the point of view of the nanostructured surface layer of porous and fractured limestones effect in which barite-lead mineralization is formed.

Classification of pores according to their radius is given in the work by M.N. Dubinin, 1980. These are macropores r > 100–200 nm; mesopores - 1.5-2.0 < r < 100-200 nm, micropores – r < 1.5-1.6. The latter are divided into ultramicropores r < 0.6-0.7 nm and supermicropores 0.6-0.7 < r < 1.5-1.6. Limestones are mainly represented by mesopores. Theoretically, in a layer consisting of one-

dimensional spherical particles, the average pore size will be equal to the size of the empty space formed with a single-layer staggered arrangement of three spheres. In this case, the pore radius is $r = 0{,}154 \cdot d(I)$ = 30.6 nm, which corresponds to mesopores. Non-metamorphosed limestones have the highest specific surface area, and limestones with a medium degree of metamorphism have the smallest specific surface area. For the ideal case, spherical particles of the same diameter $d(I)$, specific surface area S_{sp}, are given by the expression:

$$S_{sp} = 6/\rho \cdot d(I) \tag{1}$$

where ρ is the limestone density.

The concentrating of ore elements and $\delta^{34}S_{sulfide}$ in limestones is caused by the leading role of the hydrogenic mechanism. Regardless of the source of $\delta^{34}S_{sulfide}$ entering the basin, under conditions of the high specific surface area of limestones, ore elements, mainly lead and $\delta^{34}S_{sulfide}$, pass into the mobile form in the groundmass and eventually accumulate in the organic matter.

To assess the surface layer of limestones effect on the formation of mineralization, let us consider the mesostructures of this layer.

Mesoscopic physics or mesoscopics (MS) studies the physical properties of small size particles, the systems with sizes larger than atomic ones whose characteristics depend on the particle size, i.e. it is an intermediate layer between micro- and macrophysics. Characteristic of MS is the size and the number of particles in the sample. Mesoscopic bodies are those whose properties are determined by the behavior of one microscopic particle.

Let us consider the substance, including limestones, in the composition of the surface layer $d(I)$ and the $d(II)$ layer. To calculate the thickness of the surface layer $d(I)$ in work [15], for framework hydrocarbons, the relation is given:

$$d(I) = 0{,}17 \times 10^{-9} v \text{(m)} \tag{2}$$

It follows from equation (2) that the thickness of the surface layer $d(I)$ is determined by the molar (atomic) volume of the element (v = M/ρ, where M is the molar mass g/mol), ρ is density (g/cm^3)).

To determine the surface energy (σ) there is used the empirical dependence [13]:

$$\sigma = 0.7 \cdot 10^{-3} \cdot T_m, \qquad (3)$$

where T_m is the temperature of the massive sample melting without considering the surface and transition layers [16].

The surface layer $d(I)$ is a nanostructure (Table 2), where the first kind size effects are observed, determined by the entire group of atoms in the system, which are inherent only to nanoparticles and nanostructures [17]. In this $d(I)$ layer, there occurs reconstruction and relaxation with atoms associated with rearrangement of the surface layer [[18], [19]].

In the $d(I)$ layer, all physical parameters are subject to size effects, including the surface energy. A.I. Russanov, 1967, p. 190, shows that equation (VIII.55) is valid in the case of small radii of curvature, when $r \approx d(I)$), and that its value depends linearly on the h size:

$$\sigma = K \cdot d(I), \qquad (4)$$

where K is the coefficient of proportionality that depends on the temperature and the phase composition.

The $d(II)$ layer extends approximately to the size of $d(II) \approx 9d = d_\infty$ [[15], [16]]. From this size, dimensional properties begin that are called the second kind size effects. This size for nanostructures is associated with a certain critical parameter: the mean free path of carriers in transition phenomena, the dimensions of domain walls, the diameter of the Frank-Read loop for dislocation glide, and so on [19]. Some of the effects, such as the surface energy, are constant.

According to formulas (1) and (3), there is determined the thickness and the surface energy of a number of sulfides and oxides (Table 2).

Calcium oxide which is a part of limestone ($CaCO_3$), has the surface layer thickness $d(I)$ = 16.64 nm. The surface layer of limestones, in terms of particle size and distance between them, is included in the mesoscopic system of bodies (MS) and can be considered as a subsystem of a large closed system. These particles are characterized by the manifestation of quantum properties determined by the phase coherence length (h_φ)

that can vary over a wide range. In MS always $h_\varphi \leq$ 10^{-6} м = 1 micron.

Table 2 – The surface energy and the thickness of the Ba, Pb, Zn sulfides and Ca, Ba oxides surface

Compound	σ, J/m² (T-300K)	μ, (g/mol)	ρ, (g/cm³)	v, cm³/mol	The surface layer thickness, nm
sulfides					
BaS	0.385	169.40	4.25	39.86	39.86
PbS	0.195	239.96	7.60	31.49	31.48
ZnS	0.240	97.44	4.09	23.83	23.82
oxides					
CaO	0.436	56.08	3.37	16.64	16.64
BaO	0.389	153.34	5.72	26.81	28.81

It is known that the physical quantities characterizing the subsystem fluctuate, exchanging energy and particles with the environment [20].

In work [21], a model was proposed according to which the nano- and mesophases existing in the surface layers of crystals regulate the relationship between the crystal and the medium, selectively interacting with the substance-carrying complexes and reducing the probability of their "wrong" unloading. Continuously moving into the bulk of the crystal, by means of a solid-phase transformation, nano- and mesophases drop these elements into defective areas of mating with the matrix, where they form their own phases of micron or meso sizes. This fact is the reason for changing $\delta^{34}S_{sulfide}$ from the textural features of ores, the basis of which is their formation in limestone nanostructures, cracks, and pores.

It was shown in works [[15], [19]] that for nano- and mesostructures the size effects take the form:

$$A(r) = A_0(1 - d(I)/r), \; r >> d(I),$$
$$A(r) = A_0(1 - d(I)/d(I) + r), \; 0 < r < d(I). \qquad (5)$$

Here $A(r)$ is a variable physical property depending on the particle size (r) of the surface nanolayer with the thickness of $d(I)$, A_0 is the physical property of the massive sample.

In the layer $d(I)$, all elements are nanoluminophores [16], which can be considered as sensitive molecular probes for studying the

structure, including limestones. Small changes in the local structure in the layer $d(I)$ lead to significant changing the characteristics of the layer, which follows from formula (5); for this, instead of $A(r)$, it is necessary to use the amount of ore elements, including the sulfur isotope [[22], [23]].

The following models are used to describe the mesostructure of porous bodies: a lattice; a percolation; a capillary; fractal ones. Let us consider the relationship between fractality and the thickness of the surface layer of limestones.

It is known [24] that the sizes of geomaterials and elements blocks of the earth's crust are not arbitrary but make a certain discrete series in which the ratio of the block sizes of the n-th order to the size of neighboring blocks of the order (n+1) and (n–1) satisfies some fundamental ratio: the universal principle of material divisibility during destruction:

$$L_{(n-1)}/L_n = A = 2,618 \approx 3, \qquad (6)$$

where A is an ideal size ratio.

To determine the sides of the corresponding block sizes L_n in the hierarchy of scales, there is used the relationship [25]:

$$L_n = \begin{cases} (2-6)\cdot 10^{\left(\frac{n-11}{2}\right)} & \text{for } n = 2k\text{ - }1, \\ (1-2)\cdot 10^{\left(\frac{n-10}{2}\right)} & \text{for } n = 2k. \end{cases} \qquad (7)$$

Here k is an integer that changes from 1 to 9; L_n is a characteristic siz of the block of the n order.

The limestone surface layer thickness that mainly consists of CaO (Table 2), is 16.64 nm, which relates this layer to a nanostructure [24].

The established regularities that connect the difference in the concentration of $\delta^{34}S_{sulfide}$ with textural factors indicate that one of the influencing factors of the heavy sulfur isotope mineralization and concentration is the effect of nanostructures and of pores and cracks that arise during the division of geomaterials. These factors explain the formation of stratiform deposits of lead-and-zinc mineralization with carbonate orogenic structures.

It should be noted that the impurities adsorption (including $\delta^{34}S_{sulfide}$) is developed in the mesoporous structure of limestone due to the formation of adsorption layers on the surface of these mesopores, which lead to the volumetric

filling of these pores by the mechanism of capillary condensation that is described by the Kelvin equation [[25], [26]].

Let's consider the model of the hydro-therm movement in a fractured medium, in this case limestone, which is an aqueous solution with ore-forming elements, sulfur isotopes, and other components thereof.

To solve the problem, there is used the level of movement of an aqueous solution with the density $∫(r,z,t)$, which moves according to the $β(t)$ dependence in a crack of radius r, length L, in the direction z, with the use of the diffusion equation:

$$\frac{\partial f(r,z,t)}{\partial t} = a^2\left[\frac{\partial^2 f(r,z,t)}{\partial z^2} + \frac{1}{r}\cdot\frac{\partial}{\partial r}\left(r\frac{\partial f(r,z,t)}{\partial r}\right)\right], \qquad (8)$$

where $a^2 = D$ is the coefficient of the solution diffusion.

The solution of equation (8) is given in work [14]. Denoting the flow density $∫(r,z,t)$ by $\rho(r, z, t)$, at $z = \upsilon t$, where υ is the speed of the flow at the point z at the instant of time t and assuming the movement of the phase separation as automodel $β(t) = β0t$, there is used the asymptotic representation of Bessel functions and obtained:

$$\rho(r,z,t) = \frac{D^{3/2}}{\pi^{5/2}}\sqrt{\frac{L}{r}}\cdot\frac{1}{\upsilon\cdot\beta_0\cdot t}. \qquad (9)$$

Assuming that the speed of solution movement (z,t) depends only on the hydrothermal solution ρ density, and if the crack is not filled with solution ($\rho = 0$), then the solution moves in it with the maximum speed $\upsilon = \upsilon_{max}$, and when the crack is filled, the speed of solution movement in the crack falls to a complete stop ($\upsilon = 0$), when $\rho = \rho_{max}$.

$$\rho = \rho_{max}\left(1 - \frac{\upsilon}{\upsilon_{max}}\right), \quad 0 \leq \upsilon \leq \upsilon_{max}. \qquad (10)$$

If to assume in equation (10) that under the density of the liquid flow there is taken the degree of deposition of metals from the solution, the isotope of sulfur and other elements, and under the speed of the flow is taken as the speed of their deposition (that is proportional to the diffusion coefficient D), there are obtained the experimental regularities presented in work [27] that reflect

equations (9, 10) obtained in this work. Thus, formula (9) shows a significant dependence of the solution flow density on the diffusion coefficient, i.e. its rheology. According to the Newton's classical theory, it is equal to $D = \nu$, where ν is the kinematic coefficient of viscosity [19]. Let's consider the solution viscosity from the position of the thermodynamic approach, determine the kinematic viscosity ν using the response function [15], then the kinematic viscosity ν is determined as follows:

$$\nu = \frac{kT}{c} \cdot \frac{W}{G_{см}^0} \cdot \overline{N},\qquad(11)$$

where $\overline{N}kT = pV = (V = 1) = p$ is pressure in the solution flow; W is kinetic energy of the solution particles (molecules) ($W = m\upsilon^2/2$), $G_{см}^0$ is Gibbs energy of the solution; m is the particle mass, υ is their speed, c = const. Taking into account that $G_{см}^0 = \sigma S$, where S is the unit area of the nanolayer surface, there is obtained the equation of the relationship between the solution viscosity and the surface tension σ of the nanoparticles of the surface layer of the crack in limestone:

$$\nu = \frac{1}{c} \cdot \frac{p}{2\sigma S} \cdot m\upsilon^2.\qquad(12)$$

It follows from equation (12) that the hydrothermal flow in limestone cracks is proportional to its surface energy σ. The validity of the relation $D = \nu \sim 1/\sigma$ is obvious.

Let's consider a model of the crock formation in limestone. It should be noted that hydrothermal solutions that move along the existing cracks (open porosity of the layer, stress cracks, crack formation in a nanolayer of limestone, etc.) form new cracks under the action of pressure, temperature, capillary forces, dissolution of calcite, and at low values of the movement speed, the hydrothermal branching of small cracks, along the characteristic length of the cracks is maximal. With increasing pressure, one crack is practically formed with small branching of small feathering cracks having the critical radius r_k [21] that can be determined by the expression:

$$r_k = \frac{2\sigma V}{RT} = \frac{4\sigma \cdot V}{m\upsilon^2},\qquad(13)$$

where σ is the surface energy of the capillary material, in this case limestone, V is the molar volume, R is the universal gas constant, T is temperature.

Equation (13) makes it possible to estimate the critical hydrothermal flow velocity υ using the fracture and fluid characteristics. Using (13), a formula was obtained for calculating the number of cracks N per unit area of limestone:

$$N = \frac{1}{k_B \ln 2}\sqrt{\ln\left(1 - \frac{2\sigma}{\upsilon}\right)},\qquad(14)$$

where k_B is the Boltzmann constant. The product $k_B \ln 2$ is the energy equivalent of one unit of information.

The number of cracks per unit area of a limestone layer cannot be arbitrarily large and it is proportional to its porosity that is in turn determined by the principles of the closest packing of limestone particles.

Discussion of the results

The established pattern of changes in the heavy isotope of sulfur $\delta^{34}S_{sulfide}$ from the texture of barite-galena ores in limestones indicates a possible reason for the formation of mineralization in porous limestones due to the effect of their surface nanolayer. With the leading role of the heterogeneous mechanism of ore formation and heavy sulfur isotope formation in ores and their replenishment in the organic matter, an important role is played by a high specific surface of the nanolayer of ore-bearing limestones. It is shown that the thickness $d(I)$ of the surface layer is determined by one fundamental parameter: the molar (atomic) volume, and the surface energy of the limestone nanolayer is determined by the Tolman temperature. It determines the continuous transition into the bulk of the substance of the elements formed on the surface layer in its defective areas, forming the actual ore phases and the heavy isotope of sulfide sulfur associated with them, which is determined by equation (5).

The effect of pressure and temperature of hydrothermal ore-forming solutions in the mesostructures of porous limestones leads to the formation of crack development that obeys the principle of material divisibility and forms additional conditions for mineralization in these formed layer cracks.

The model of hydrothermal solution movement in a crack coincides quite well with the well-known

model presented in the work by V.S. Golubev (reports of the Academy of Sciences of the USSR, 1978, Vol. 238, No. 6. P. 1318-1320), taking into account the fact that in this case the velocity of the solution is associated with the density of the solution, and in the mentioned work, the liquid density is associated with the liquid filtration through a porous medium. The established relationship between the fluid flow density and the diffusion coefficient made it possible to establish the relationship between the kinematic viscosity of the hydro-therm and the surface tension of the crack surface layer along which the fluid moves. It is the higher, the lower the kinematic viscosity, all the other things being equal. The critical velocity of the hydro-therm movement through the crack is determined. Using this regularity, the regularity of the number of cracks per unit area of limestone is obtained. It is determined by the surface energy and kinematic viscosity of the solution. From this it follows that the number of cracks is related to the porosity of limestone through the surface energy of these pores.

Conclusions

There was established the dependence of the flux density of the hydrothermal solution on its diffusion; the relationship between kinematic viscosity and pressure in the solution flow, the velocity, the mass of particles, and the Gibbs energy of the mixture were obtained; the relationship between the viscosity of the solution and the surface tension of the limestone particles nanolayer was obtained; the critical radius of crack formation was determined. The resulting constraint equations are applicable for the numerical analysis in order to assess the effect of ore-bearing hydro-therms on ore deposition processes and to evaluate the efficiency of crack formation and their role in ore deposition, taking into account kinematic viscosity under thermodynamic conditions of the ore-bearing limestone horizon occurrence.

Conflict of interests. On behalf of all authors, the correspondent author declares that there is no conflict of interests.

Үшқатын III (Орталық Қазақстан) кен орнының барит-қорғасынды кенденуінің қалыптасуының математикалық моделі

[1*] Асқарова Н.С., [1] Портнов В.С., [1] Рахимова Г.М., [2] Маусымбаева А.Д., [2] Мадишева Р.М.

[1] «Әбілқас Сағынов атындағы Қарағанды техникалық университеті» КеАҚ, Қарағанды, Қазақстан
[2] Қазақстан көп бейінді қайта құру және дамыту институты (ҚазККДИ), Қарағанды, Қазақстан

ТҮЙІНДЕМЕ

Шөгінді жыныстардағы қорғасын, барит стратиформды кен орындарының генезисі полиметалл кендерінің қорын толықтыру тұрғысынан үлкен қызығушылық тудырады. Жұмыстың мақсаты-кеуектердегі кен ерітінділерінің қозғалысының математикалық моделі мен сипаттамаларына негізделген кеуектер мен жарықтардың нано бетінің әсерін ескере отырып, әктастарда кендердің гидрогендік түзілу заңдылығын анықтау. Кеннің қалыңдығы мен сульфидті минералдардың құрамына кіретін әктастар мен минералдардың беткі қабатының қалыңдығы есептелген. Нәтижелер олардың заттың қалған бөлігінен ерекше, физикалық қасиеттері бар наноқұрылымдар екенін көрсетеді, бұл әртүрлі текстуралық

типтегі кендерде ауыр күкірт изотопының түзілу заңдылығымен расталады. Әр түрлі тығыздығы, кинематикалық тұтқырлығы, жылдамдығы бар гидротермалардың әктастардың жарықтары мен тесіктерінде кенденудің пайда болу қарқындылығына, сондай-ақ бөлшектеу жарықтары айналасында жаңа жарықтардың пайда болуына әсері бағаланды. Гидротермалар ағынының тығыздығының сұйықтықтың диффузиясына тәуелділігі анықталды. Кинематикалық тұтқырлық теңдеуі ерітінді ағынындағы қысымнан, оның қозғалу жылдамдығынан, кенді құрайтын элементтер бөлшектерінің массасынан және Гиббс энергиясының термодинамикалық жағдайында күкірт изотоптарынан алынады. Ерітіндінің тұтқырлығының жарықтар мен кеуектердегі әктас бөлшектерінің наноқабатының беттік керілуімен байланысы көрсетілген, бұл энергия неғұрлым көп болса, кенді құрайтын ерітінділердің қозғалыс жылдамдығы соғұрлым көп болады, бөлшектене-ті н жарықшағының айналасында жаңадан пайда болған жарықтардың тармақтары азаяды. Математикалық модель кен қабатының термодинамикалық жағдайында әктастардың жарықтары мен кеуектерінің наноқұрылымдық қабатының әсерін ескере отырып, жарықтардың кендену заңдылығын сандық талдау үшін қолданылады.

Авторлар туралы ақпарат:

Асқарова Назым Сражадинқызы
PhD, «Әбілқас Сағынов атындағы Қарағанды техникалық университеті» КеАҚ «Геология және пайдалы қазбалар кен орындарын барлау» кафедрасының оқытушысы, 100027, Қарағанды, Қазақстан. E-mail: srajadin-nazym@mail.ru

Портнов Василий Сергеевич
«Әбілқас Сағынов атындағы Қарағанды техникалық университеті» КеАҚ «Геология және пайдалы қазбалар кен орындарын барлау» кафедрасының профессоры, техника ғылымдарының докторы, 100027, Қарағанды, Қазақстан. E-mail: vs_portnov@mail.ru

Рахимова Галия Мухамедиевна
PhD, «Әбілқас Сағынов атындағы Қарағанды техникалық университеті» КеАҚ «Құрылыс материалдары және технологиясы кафедрасының доценті, 100027, Қарағанды, Қазақстан. E-mail: galinrah@mail.ru

Маусымбаева Алия Думановна
PhD, т.ғ.к., Қазақстан көп бейінді қайта құру және дамыту институты (ҚазККДИ) ғылыми қызметкері, 100027, Қарағанды, Қазақстан. E-mail: aliya_maussym@mail.ru

Мадишева Рима Копбосынқызы
PhD, Қазақстан көп бейінді қайта құру және дамыту институты (ҚазККДИ) ғылыми қызметкері, 100027, Қарағанды, Қазақстан. E-mail: rimma_kz@mail.ru

Математическая модель формирования барит-свинцового оруденения месторождения Ушкатын III (Центральный Казахстан)

[1]*Асқарова Н.С., [1]Портнов В.С., [1]Рахимова Г.М., [2]Маусымбаева А.Д., [2] Мадишева Р.М.

[1] НАО «Карагандинский технический университет имени Абылкаса Сагинова», Караганда, Казахстан
[2]Казахстанский многопрофильный институт реконструкции и развития (КазМИРР)

АННОТАЦИЯ

Генезис стратиформных месторождений свинца, барита в осадочных породах представляет огромный интерес с точки зрения восполнения запасов полиметаллических руд. Целью работы является установление закономерности гидрогенного формирования руд в известняках с учётом влияния наноповерхности пор и трещин на основе математической модели движения и характеристик рудоносных растворов в порах. Рассчитаны толщины поверхностного слоя известняков и минералов входящих в состав рудовмещающей толщи и сульфидных минералов. Результаты свидетельствуют о том, что они являются наноструктурами обладающими особыми отличными от остальной части вещества, физическими свойствами, что подтверждается закономерностью формирования тяжелого изотопа серы в рудах различных текстурных типов. Оценено влияние гидротерм обладающих различными плотности, кинематической вязкости, скорости на интенсивность формирования оруденения в трещинах и порах известняков, а также возникновении новых оперяющих трещин вокруг трещин расчленения. Установлена зависимость плотности потока гидротерм от диффузии жидкости. Получено уравнение кинематической вязкости от давления в потоке раствора, скорости его движения, массы частиц рудообразующих элементов и изотопов серы в термодинамических условиях определяемых энергий Гиббса. Показано связь вязкости раствора　поверхностным натяжением нанослоя частиц известняка в трещинах и порах, свидетельствующая о том, что чем больше эта энергия, тем больше скорость движения рудообразующих растворов, тем меньше ветвлений вновь образованных трещин вокруг трещины расчленения. Математическая модель применима для численного анализа закономерности оруденения в трещинах с учетом влияния наноструктурного слоя трещин и пор известняков в термодинамических условиях залегания рудоносного пласта.

	Keywords: Ушкатын III, стратиформные месторождения, Атасуйский рудный район, изотопный состав, математическая модель
	Информация об авторах:
Асқарова Назым Сражадинқызы	*доктор PhD, преподаватель кафедры «Геология и разведка МПИ» НАО «Карагандинский технический университет имени Абылкаса Сагинова 100027, Караганда, Казахстан. E-mail: srajadin-nazym@mail.ru*
Портнов Василий Сергеевич	*доктор технических наук, профессор кафедры «Геология и разведка МПИ» НАО «Карагандинский технический университет имени Абылкаса Сагинова», 100027, Караганда, Казахстан. E-mail: vs_portnov@mail.ru*
Рахимова Галия Мухамедиевна	*доктор PhD, доцент кафедры «Строительные материалы и технологии» НАО «Карагандинский технический университет имени Абылкаса Сагинова», 100027, Караганда, Казахстан. E-mail: galinrah@mail.ru*
Маусымбаева Алия Думановна	*доктор PhD, к.т.н., научный сотрудник Казахстанский многопрофильный институт реконструкции и развития (КазМИРР), 100027, Караганда, Казахстан. E-mail: aliya_maussym@mail.ru*
Мадишева Рима Копбосынкызы	*научный сотрудник Казахстанский многопрофильный институт реконструкции и развития (КазМИРР), 100027, Караганда, Казахстан. E-mail: rimma_kz@mail.ru*

Reference

[1] Antonyuk RM, Ismailov HK. Promyshlennyye mestorozhdeniya metallicheskikh poleznykh iskopayemykh Tsentralnogo Kazakhstana. Geodinamicheskaya pozitsiya. stroyeniye. sostav rud [Industrial minerals minerals of Central Kazakhstan]. Karaganda. 2019, 85. (in Russ.).

[2] Brusnitsyn AI, Kuleshov VN, Sadykov SA, Perova EN, Vereshchagin OS. Izotopnyy sostav (δ^{13}C and δ^{13}O) i genezis margantsenosnykh otlozheniy mestorozhdeniya Ushkatyn-III. Tsentralnyy Kazakhstan [Isotopic composition (δ^{13}C and δ^{13}O) and genesis of manganese-bearing deposits of the Ushkatyn-III deposit, Central Kazakhstan]. Lithology and Minerals. 2020; 6:522-548. https://doi.org/10.31857/S0024497X20060026 (in Russ.).

[3] Brusnitsyn AI, Sadykov SA, Perova EN, Vereshchagin OS. Genezis barit-galenitovyh rud na primere kompleksnogo (Fe, Mn, Pb, BaSO$_4$) mestorozhdeniya Ushkatyn-III, Centralnyj Kazakhstan: analiz geologicheskih, mineralogicheskih i izotopnyh (d^{34}S,d^{13}C,d^{18}O) dannyh [Genesis of Barite–Galena Ores at the Ushkatyn-III Deposit, Central Kazakhstan: Analysis of Geological, Mineralogical, and Isotopic (δ^{34}S, δ^{13}C, δ^{18}O) Data. Geology of Ore Deposits. 2022; 64(3):247-275. https://doi.org/10.31857/S0016777022030029 (in Russ.).

[4] Askarova NS, Portnov VS, Kopobayeva AN, Roman AT. Feature space of the Atasu type deposits (Central Kazakhstan). Naukovyi Visnyk Natsionalnoho Hirnychoho Universytet. Dnipro: Dnipro University of Technology. 2021; 5:5-10. https://doi.org/10.33271/nvngu/2021-5/005

[5] Kurchavov AM, Hamzin BS. Glavnejshie rubezhi rudoobrazovaniya v orogennyh strukturah kaledonid Severnogo i Centralnogo Kazakhstana [The main boundaries of ore formation in the orogenic structures of the caledonides of Northern and Central Kazakhstan] Izvestiya NAS RK. Series of Geology and Technical Sciences. 2017; 3:24-34. (in Russ.)

[6] Brusnitsyn AI, Perova EN, Sadykov SA. Barit-svincovoe orudenenie v rifovyh izvestnyakah mestorozhdeniya Ushkatyn-III (Centralnyj Kazakhstan): usloviya lokalizacii, sostav, genesis [Barite-lead mineralization in reef limestones of the Ushkatyn-III deposit (Central Kazakhstan): localization conditions, composition, genesis]. Metallogeny of ancient and modern oceans. 2021; 27:44-46. (in Russ.).

[7] Wilkinson JJ. Sediment-hosted zinc-lead mineralization: processes and perspectives. Treatise on geochemistry. Second edition. Amsterdam, Elsevier. 2014; 13:219-250. https://doi.org/10.1016/B978-0-08-095975-7.01109-8

[8] Emsbo P, Seal RR, Breit GN, Diehl SF, Shah AK. Sedimentary exhalative (sedex) zinc-lead-silver deposit model. U.S. Geological Survey Scientific Investigations Report. 2016; 2010-5070:57. https://doi.org/10.3133/sir20105070N

[9] Vinogradov VI. Rol osadochnogo cikla v geohimii izotopov sery [The role of the sedimentary cycle in the geochemistry of sulfur isotopes]. M.: Science. 1980, 192. (in Russ.).

[10] Johnson CA, Emsbo P, Poolw FG, Rye PR. Sulfur-and oxygen-isptopes in sediment-hosyed stratiform barite deposits. Geochim Cosmochim Acta. 2009; 73:133-147. https://doi.org/10.1016/j.gca.2008.10.011

[11] Seal RR. Sulfur isotope geochemistry of sulside minerals. Reviews in mineralogy and geochemistry. 2006; 61:633-677. https://doi.org/10.2138/rmg.2006.61.12

[12] Vereshchagin OS, Britvin SN, Perova EN, Brusnitsyn AI, Polekhovsky YS, Shilovskikh VV, Bocharov VV, van der Burgt A, Cuchet S, Meisser N. Gasparite-(La), La(AsO$_4$), a new mineral from Mn ores of the Ushkatyn-III deposit, Central Kazakhstan, and metamorphic rocks of the Wanni glacier, Switzerland. American Mineralogist. 2019; 104:1469-1480. https://doi.org/10.2138/am-2019-7028

[13] Griffith EM, Paytan A. Barite in the ocean – occurence, geochemistry and palaeoceanographic applixations. Sedimentology. 2012; 59:1817-1835. https://doi.org/10.1111/j.1365-3091.2012.01327.x

[14] Hoefs J. Stable isotope geochemistry. Berlin Heidelberg: Springer-Verlag. 2018, 437.

[15] Cansu Z, Ozturk H. Formation and genesis of Paleozoic sediment-hosted barite deposiys in Turkey. Ore Geology Reviews. 2020; 125:1-16. https://doi.org/10.1016/j.oregeorev.2020.103700

[16] Rekhviashvili SSh, Kishtikova EV, Karmokova Ryu, and etc. K raschetu postoyannoj Tolmena [To calculate the Tolman constant]. Letters to the Journal of Technical Physics. 2007; 33(2):1-7. (in Russ.)

[17] Portnov VS, Yurov V, Reva M, Mausymbaeva A, Imanbaeva S. Nanostructures in surface layers of coal matter. Visnyk of Taras Shevchenko National University of Kyiv, Geology. 2021; 4(95):54-62. https://doi.org/10.17771/1728-2713.95.07

[18] Oura K, Lifshits VG, Saranin AA, et al. Vvedenie v fiziku poverhnosti [Introduction to Surface physics]. M.: Science. 2006,

490. (in Russ.).

[19] Yurov VM, Guchenko SA, Laurinas VCh. Tolshina poverhnostnogo sloya, poverhnostnaya energiya i atomnyj obem elementa [Surface layer thickness, surface energy and atomic volume of the element]. Physico-chemical aspects of studying clusters, nanostructures and nanomaterials. 2018; 10:691-699. https://doi.org/10.26456/pcascnn/2018.10.691 (in Russ.).

[20] Andrievskij RA, Ragulya AV. Nanostrukturnye materialy [Nanostructured materials]. M.: Academy. 2005, 192. (in Russ.).

[21] Suzdalev IP. Nanotehnologiya: fiziko-himiyananoklasterov, nanostruktur i nanomaterialov [Nanotechnology: physico-chemistry of nanoclusters, nanostructures and nanomaterials]. M.: KomKniga. 2006, 592. (in Russ.).

[22] Kutolin SA. Fizicheskaya himiya mezostruktury [Physical chemistry of mesostructure]. Novosibirsk: Publishing House Chem. Lab. NCD. 2015, 104. (in Russ.).

[23] Tauson VL, Babkin DN, Pastushkova TM, Smagunov NV, Voronova IYu, Menshikov VI, Bryanskij NV, Lipko SV, Arsentev KYu. Dvojstvennye koefficienty raspredeleniya mikroelementov v sisteme «mineral-gidrotermalnyj rastvor» [Dual distribution coefficients of trace elements in the mineral-hydrothermal solution system]. Geochemistry. 2016; 2:165-181. https://doi.org/10.7868/s0016752516020060 (in Russ.).

[24] Mullagaliyeva LF, Baimukhametov SK, Portnov VS, Yurov VM, Ibragimova DA. Nanostructures of coal beds in the Sherubaynurinsky section of the Karaganda basin. Naukovyi Visnyk Natsionalnoho Universytetu. 2022; 4(190):17-22. https://doi.org/10.33271/nvngu/2022-4/017

[25] Yurov VM, Ibraev NH, Guchenko SA. Eksperimentalnoe opredelenie poverhnostnogo natyazheniya nanochastic i nanoplenok [Experimental determination of the surface tension of nanoparticles and nanofilms]. News of Universities. Physics. 2011; 54(1/3):335-340. (in Russ.).

[26] Bazhukova IN, Pustovarov VA, Myshkina AV, Ulitko MV. Lyuminescentnye nanomaterialy, dopirovannye redkozemelnymi ionami, i perspektivy ih biomedicinskogo primeneniya (obzor) [Luminescent nanomaterials doped with rare earth ions and prospects for their biomedical application (review)]. Optics and spectroscopy. 2020; 128(12):1938-1957. https://doi.org/10.21883/OS.2020.12.50334.146-20 (in Russ.).

[27] Bogdankevich IL, Litvin VO, Loza OT. O sozdanii plazmennogo relyativistskogo svch-generatora bez silnogo magnitnogo polya [On the creation of a plasma relativistic microwave generator without a strong magnetic field]. Brief reports on Physics of the Lebedev P.N. Physical Institute of the Russian Academy of Sciences. 2016; 2:19-24. (in Russ.).

The method of non-stationary flooding and the conditions for its effective use in the operation of an oil field

[1]Effendiyev G.M., *[2]Moldabayeva G.Zh., [2]Tuzelbayeva Sh.R., [2]Imansakipova Z.B.,[3]Hongjun Wu

[1]Azerbaijan National Academy of Sciences, Baku, Azerbaijan
[2]Satbayev University, Almaty, Kazakhstan
[3]LLP "DPS Kyzylorda", Kyzylorda, Kazakhstan

*Corresponding author email: g.moldabayeva@satbayev.university

ABSTRACT

The article describes the essence of unsteady waterflooding, which is one of the most effective methods of increasing the oil recovery factor, used to change the direction of filtration flows, which makes it possible to engage in the development of undeveloped oil reserves and reduce the rate of watering of the deposit in productive reservoirs. A common technological method of unsteady water flooding is the use of cyclic modes of operation of injection wells. The essence of this method is that at an unsteady state in the oil deposit, there are conditions for the continuous manifestation of elastic forces of the reservoir system. In a heterogeneous reservoir between different zones, channels, and fluid flows there are gradients of hydrodynamic pressures, due to which there can be fluid flows from one layer to another, from fractures to blocks, as well as changes in flow directions. During unsteady flooding of heterogeneous formations, a part of oil reserves in low-permeability layers or zones remains uncovered by injected water. The waterflooded reservoir appears as an unsystematic alternation of watered and oil-saturated microflows. While creating in such reservoirs alternately changing in value and direction of pressure gradients, conditions for injection water penetration into stagnant oil-saturated low-permeable zones and channels appear in the oil reservoir and oil movement from them to active drainage zones. As a result of the analysis, the positive effect of the implementation of unsteady waterflooding technology was revealed, and recommendations for improving its application at other operational facilities of oil fields were given.

Keywords: non-stationary flooding, injection well, cyclic injection, oil recovery, filtration, heterogeneity.

Efendiev Galib Mammadovich	Doctor of Technical Sciences, Professor. Institute of Oil and Gas of the National Academy of Sciences of Azerbaijan, Baku, Azerbaijan. Email: galib_2000@yahoo.com
Moldabayeva Gulnaz Zhaksylykovna	Doctor of Technical Sciences, Professor, Satpayev University, st. Satpaeva 22, 050000, Almaty, Kazakhstan. Email:g.moldabayeva@@satbayev.university
Tuzelbayeva Sholpan Ryskulbekkyzy	Master of technical sciences, doctoral student, Satpayev University, st. Satpaeva 22, 050000, Almaty, Kazakhstan. Email: s.tuzelbayeva@satbayev.university
Imansakipova Zemfira Beketovna	Master of technical sciences, doctoral student, Satpayev University, st. Satpaeva 22, 050000, Almaty, Kazakhstan. Email: z.imansakipova@satbayev.university
Hongjun Wu	Master of technical sciences, LLP "DPS Kyzylorda", Amangeldy Imanov street, 112A, Kyzylorda, Kazakhstan. Email: wus520@mail.ru

Introduction

Non-stationary flooding (NC) is applicable both at an early and late stage of development. It is also possible to use it in highly watered fields developed by the method of conventional stationary flooding, even after reaching the maximum cost-effective flow rate of producing wells. Methods of non-stationary flooding are widely used in oil fields, however, they are not always effective due to insufficient strict compliance with the recommendations [1].

Since there is a high water content in them, scientific and technical solutions for blocking permeable areas of the reservoir become crucial. In this regard, ways to use effective water insulation compositions are being investigated [[2], [3]]. A considerable number of compositions are known and great experience of their application in various geological and physical conditions has been accumulated. However, their technological efficiency is low and does not exceed 40–50 % [4].

The effectiveness of this method is influenced by the geological structure of the deposit, the current state of development (the flooding system, the working stock of wells, the level of waterlogging, the proportion and nature of the production of geological reserves), heterogeneity in permeability, etc [5]. Therefore, the need to predict the effectiveness of the cyclic impact process is an urgent task. The problem of water inflows has always remained at the center of attention, and in recent years, especially more often began to attract the attention of researchers [[6], [7]]. Theoretical and experimental studies aimed at studying on mechanism of origin of water inflows, reasons for their origin, and also search for methods of struggle against this phenomenon, were carried out.

The purpose of this work was to increase the elastic reserve of the reservoir system by periodically changing the water injection pressure. The analysis of geological field data carried out by the author showed that the traditionally considered geological factors and the filtration capacity properties of rocks do not exhaust all the factors affecting the flow rate of the well. The complex nature of the distribution of reservoirs and the high heterogeneity of the section were also taken into account, which resulted in a wide variety of deposits by types of natural reservoirs and the nature of saturation. The use of non-stationary flooding made it possible to reduce unproductive injection and reduce possible losses of mobile oil reserves [8].

The main part. Selection of a potential site for non-stationary flooding It is carried out taking into account the following circumstances, depending on the systems of development and organization of the cyclic process of injection and selection of liquid. When choosing options, it is necessary to take into account the location of injection and production wells by area, to prevent language water breakthroughs by changing the operating modes of wells, to pump water through nearby wells in opposite modes.

The stronger the heterogeneity of the formation, the higher the amplitude of pressure fluctuations should be, since with its growth the amount of pulsating energy introduced into the formation to overcome filtration resistances to the oscillatory in the fluid flow increases [9].

The choice of the optimal injection pressure should be carried out by taking into account the geological and physical characteristics of the formations, the analysis of field development data, the results of well research, and data on hydraulic fracturing. In nonlinear filtration, when the reservoir pressure increases, the permeability of the reservoir increases, and when it decreases, the periodic (cyclic) pressure change will lead to an additional increase in the average reservoir pick–up during the cycle, depending on the nonlinearity parameter and the amplitude of the oscillations [10].
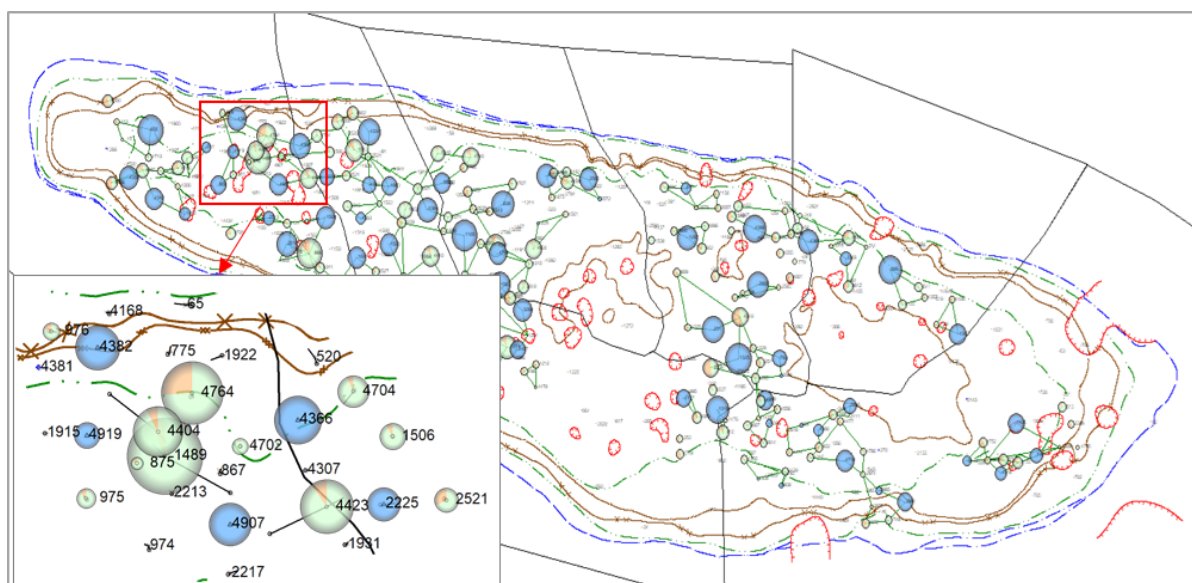

Figure 1 - Selected Yu-2+3 for experimental work
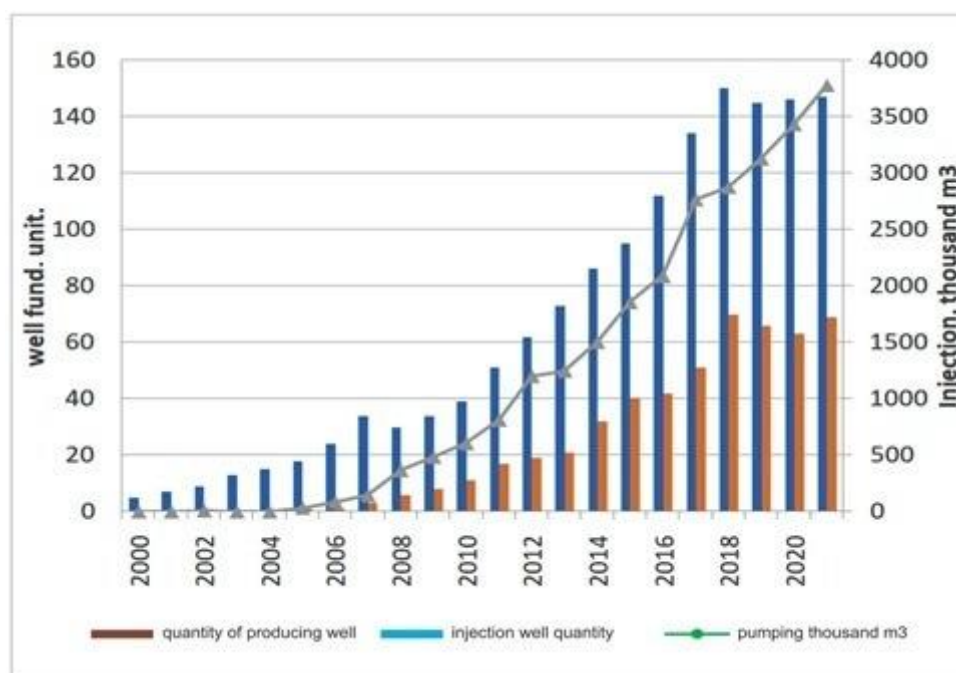
Figure 2 - Schedule of field development for the Yu-2+3 facility

The distribution of the average pressures over the cycle along the length of the formation will differ more strongly from the linear one, the higher the amplitude of the oscillations. Thus, the cyclical effect on an inhomogeneous reservoir in the presence of a dependence of permeability on pressure will give additional intensification and additional coverage of flooding due to the interaction of the nonlinearity of the process with its periodicity. Based on the review and practical application, the following conditions were formed [[11], [12]]:

• an existing development system with an organized PPD system;

• production of reserves significantly lags behind waterlogging;

• presence of significant residual recoverable oil reserves;

• significant heterogeneity of the interlayers within the layers, in terms of permeability;

• maximum full opening of the effective oil-saturated thickness in production and injection wells;

• Reservoir pressure at the initial level;

• technical serviceability of wells;

• hydrodynamic connection of wells (tracer studies). According to the above criteria, a site was selected at the Yu-2+3 facility in the field Figure 1.

Experimental studies of non-stationary flooding

The geological structure, reservoir permeability heterogeneities, and their relationship to each other have been studied for this site. Maps of losses (liquid, oil, Keksp), sedimentary microfacies, RMS attributes, electrofacies, lithotypes, total thicknesses, and isobars were constructed, and reports of JSC "NIPIneftegaz" and LLP "ALSTRON" on tracer studies (wells) were analyzed №№4309, 4366) [[13], [14]]. As of 01.01.2022, geological reserves for the Yu-2+3 facility amount to 36,360 thousand tons, initial recoverable reserves – 9,332 thousand tons, OIZ – 3,493 thousand tons, production from the bottom – 63%, accumulated oil production – 5839 thousand tons. 147 producing and 67 injection wells are located at this facility. The accumulated water injection is 27,413 thousand m3, and the current compensation for the selection by injection is 107% (Figure 2).

According to geological and physical criteria, the most suitable is site No. 1. Plot No. 1. 4 injection wells No.4382, 4919, 4366, 4907 are operating in the selected area in the area of BCNS 1.

The intake capacity of injection wells averages 188 m3/day, the average annual water content of the site is 90%, the current compensation is 165%. Maintenance of reservoir pressure at the site is carried out by pumping Alb Cenomanian water [15].

Figure 3 - Indicator output from reacting wells

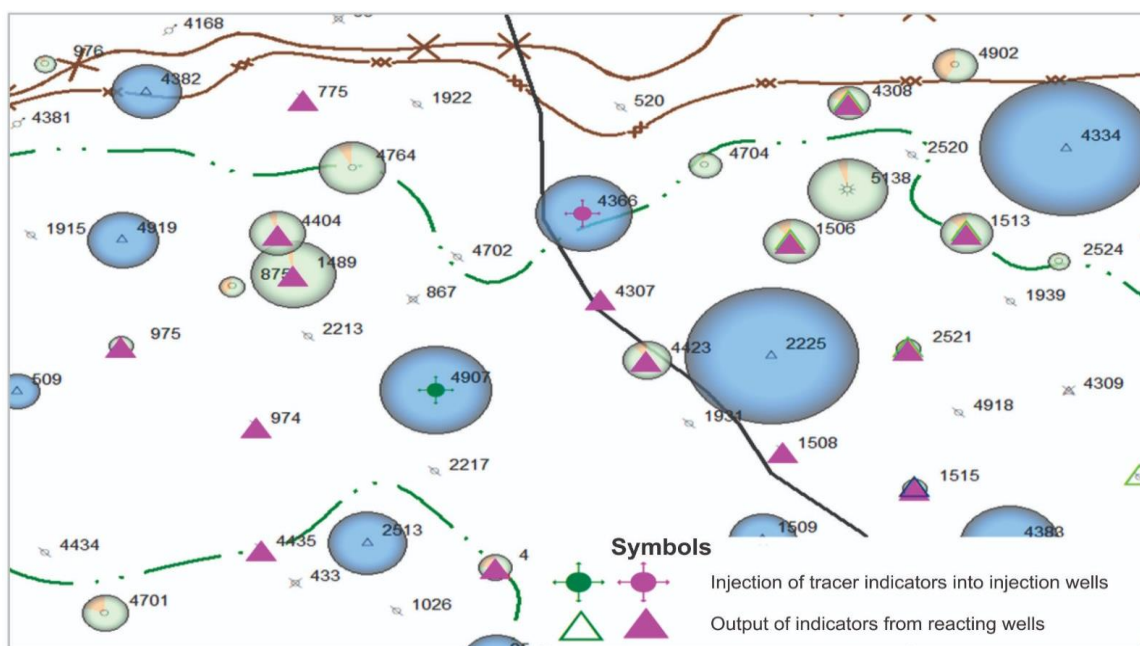To determine the direction of filtration flows, carbamide (2020) and disodium phosphate (2014) were injected in 2014 and 2020.

In 2020, a tracer study was conducted in the injection well No. 4907 (injection of carbamide). According to the results of laboratory studies, the output of the indicator was recorded for 14 wells (№№875, 975, 1489, 1506, 2517, 4404, 4421, 4423, 4435, 4702, 4704, 4764, 4824, 4881). In 4 wells (№№2213, 3213, 4307, 4965) no samples were taken because the wells were in conservation.

Disodium phosphate was injected into well No. 4366 in order to determine the distribution of hydrodynamic flows in the formation. The output of the indicator is fixed for all 16 wells (№№775, 974, 975, 1489, 1502, 1506, 1508, 1513, 1515, 2521, 4307, 4308, 4404, 4421, 4423, 4435). It can be noted that the indicator was traced in reacting production wells No. 4907 and No. 4366 (Figure. 3), which was the rationale for choosing this site.

Further, the time of operation and shutdown of wells during cyclic injection is determined, which is determined by the formula of M.L.

Surguchev using the reservoir parameters:

$\omega = 2p/L2$

$T = L2/2\rho$ where $p = K/\mu\varepsilon$ is the average piezo conductivity of low-permeable interlayers; K- permeability μ -viscosity ε is the compressibility coefficient of the rock Calculated, the average duration of cycles (stop/work) was 7 days, further durations up to 14 days.

This made it possible, by increasing the period of cyclic exposure, to shift the area of maximum intensity of fluid exchange between layers of different permeability into the inter-well space in the direction of the selection area. The cycle begins with the shutdown of the injection wells of the western group No. 4382 and 4919.

Wells of the eastern group No.4366, 4907 have been operating for 7 days. After 7 days, the wells of the western group are working and the wells of the eastern part of the group are shut down. At the end of 7 days, wells in the southern part No. 4919, 4907 are working, and wells No. 4366, 4382 are shut down in the northern part [[16], [17], [18]]. Wells No. 4366, and 4382 in the northern part are operating for 7 days, and wells No. 4919, and 4907 in the southern part are shut down. At the end of 7 days, wells No. 4919, and 4382 in the western part are turned off for 14 days, and wells No. 4366, and 4907 in the eastern part work for 14 days. Then the cycle repeats. Non-stationary flooding in 2022 at this site of the first operational facility began in March. Symmetrical cycles with the duration of the work period (downtime) of 7 and 14 days were used. Prior to the start of the experimental work, an audit and verification of the tightness and serviceability of the shut-off valves were carried out, the current state of the faces of injection wells involved in the process was determined, and a hydrodynamic study was carried out by the efficiency method for injection wells. It is recommended to conduct a GDIS to determine dynamic levels and to take control

samples to determine water availability in all 9 reacting wells [[19], [20]].

The effect of cyclic injection was monitored for 9 wells. Production well No. 4702 did not participate in the analysis due to high water availability. Accumulated oil production is shown in Figure 4. that before the cyclical flooding in February, oil production was 438.3 tons, after the completion of the cycle, oil production was 895.5 tons, respectively.

At the start date of the application of non-stationary flooding, the water content of the wells of the site was 88%, with an average monthly oil flow rate of 5.4 t/day. In the first cycle of application of the NC, the water content decreases by (1%) with a significant increase in the oil flow rate to 7.3 t/day (Figure 5) [21]. A month after the start of non-stationary flooding, the water content decreases to 77% with an increase in the average monthly oil flow rate to 12.8 t/day.
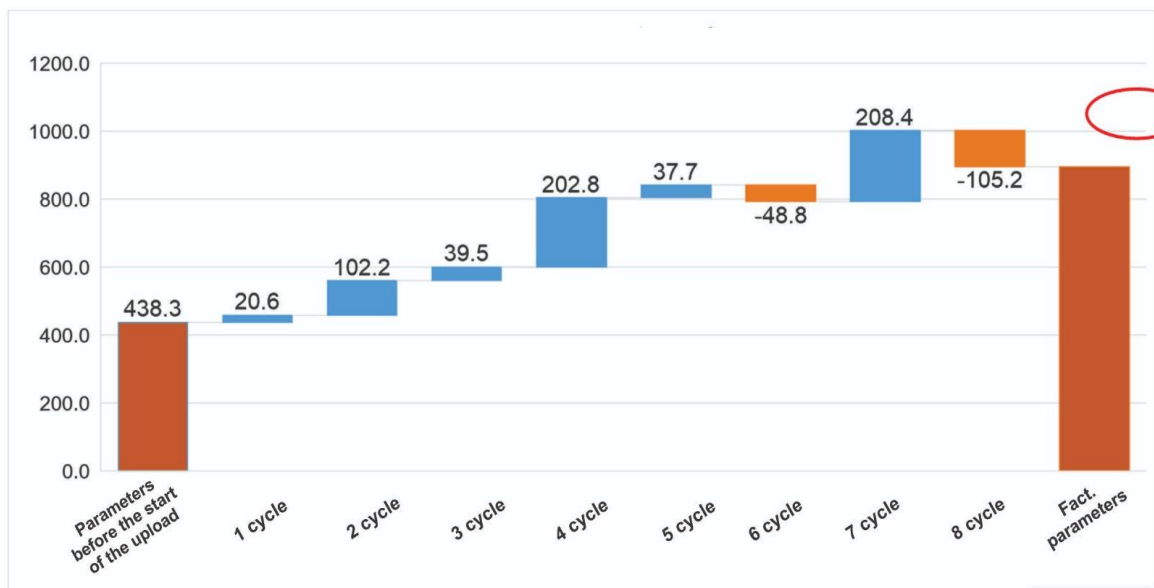

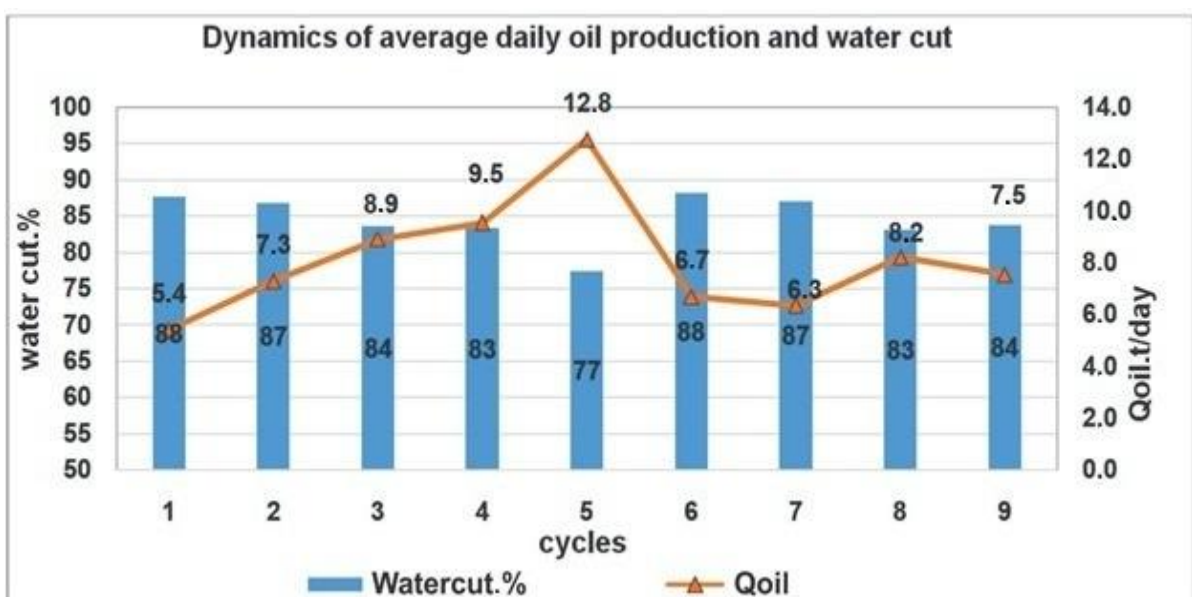**Figure 4 -** Accumulated oil production by cycles

Figure 5 - Dynamics of average daily oil production and water availability

Results and discussion

Thus, the non-stationary flooding program was implemented in full and confirmed its technological effectiveness. The duration of the OPI for non-stationary flooding was 84 days, during this period 8 cycles were carried out. Due to the impact of non-stationary flooding, an increase of 457.2 tons of additional oil production was obtained.

The water content of reacting wells has decreased №№4764, 875, 1489, 4764, 4704, 4423, and in the whole area from 88% to 78%. During the analyzed period, 50% less water was pumped into the reservoir than before the event, and compensation for selection by injection decreased by 65%. At the same time, the reservoir pressure rose from 193 to 234 kg/cm^2.

The results of experimental studies allowed obtaining the dependence of the resistance factor on the permeability of the medium and the concentration of the solution, which will make it possible to create conditions for the isolation of water inflows using a non-stationary flooding program in the considered medium. The application of the methodology of rational planning of experiments allows one to get maximum information during the realization of the experiment plan. Reduction in water mobility can be achieved even at minimum concentrations. In this regard, the expression for determining the necessary concentration depending on the permeability of the medium is obtained. The application of appropriate methods of data processing and information analysis makes it possible to justify the choice of polymer solution.

Conclusion

In most fields, after almost complete production, the residual oil is in a capillary-pinched form or in the form of separate oil columns. To increase the completeness of its extraction, the method of non-standard flooding is widely used, the effectiveness of which has been proven during pilot work at the Yu-2+3 field facility.

Analysis of geological and physical characteristics of objects and the existing development system, it can be noted that this method is applicable almost everywhere. In order to achieve the greatest efficiency from the introduction of cyclic impact, it is recommended to use the criteria proposed in this paper for the selection of sites and the technology of work.

The results obtained and the workflow presented in this paper provide a better understanding of the mechanism of polymer solutions in waterflooding. In addition, the definition of optimized workflows to evaluate any solutions in porous media and changes in permeability is supported.

Тұрақталмаған (стационарлы емес) су жіберу әдісі және оны мұнай кен орнын игеру кезінде тиімді пайдалану шарттары

[1]Эфендиев Г.М., *[2]Молдабаева Г.Ж., [2]Түзелбаева Ш.Р., [2]Имансакипова З.Б.,[3]У ХунЦзюнь

[1] Әзірбайжан Ұлттық Ғылым академиясы, Баку, Әзірбайжан
[2] Сәтбаев университеті, Алматы, Қазақстан
[3] ЖШС "DPS Қызылорда", Қызылорда, Қазақстан

ТҮЙІНДЕМЕ

Мақалада стационарлы емес су жіберудің мәні көрсетілген, бұл сүзгі ағындарының бағытын өзгерту үшін қолданылатын мұнай өндіру коэффициентін арттырудың тиімді әдістерінің бірі болып табылады. Бұл әдіс өндірілмеген мұнай қорларын игеруге және өнімді коллекторлардағы кен орындарының сулану қарқынын төмендетуге мүмкіндік береді. Тұрақталмаған су жіберудің кең таралған технологиялық әдісі ретінде айдау ұңғымаларының циклдік жұмыс режимдері қолданылады. Бұл әдістің мәні мынада: мұнай кен орнында тұрақталмаған жағдайда қабат жүйесінің серпімді күштерінің үздіксіз болатын жағдайлар туындайды. Әр түрлі аймақтар, арналар мен сұйықтық ағындары арасындағы біріңғай емес қабатта гидродинамикалық қысым градиенттері пайда болады, соның арқасында сұйықтықтың кейбір қабаттардан екіншісіне, жарықтардан блоктарға ағуы мүмкін. Сонымен қатар ағындардың бағыттары өзгереді. Тұрақталмаған су жіберу кезінде біріңғай емес қабаттардың төмен өткізгіш қабаттардағы немесе аймақтардағы мұнай қорларының бір бөлігі айдалатын сумен қамтылмаған күйінде қалады. Су басқан қабат суланған және мұнаймен қаныққан микроағзалардың жүйесіз ауысқан түрінде болады. Мұндай коллекторларда көлемі мен бағыты бойынша кезектесіп өзгеретін қысым градиенттерін құру кезінде мұнай қабатында қысымды суды мұнаймен қаныққан өткізгіштігі төмен аймақтар мен арналарға енгізу және олардан мұнайды белсенді дренаждық аймақтарға ауыстыру үшін жағдайлар туындайды. Талдау нәтижесінде стационарлық емес су жіберу технологиясын іске асырудың оң әсері анықталды, сондай-ақ оны мұнай кен орындарының басқа объектілерінде қолдануды жетілдіру бойынша ұсыныстар берілді.

Түйін сөздер: Стационарлық емес су айдау, айдау ұңғымасы, циклдік айдау, мұнай беру, сүзу, гетерогенділік.

Авторлар туралы ақпарат:

Эфендиев Галиб Мамедович
Техника ғылымдарының докторы, профессор, Әзірбайжан Ұлттық Ғылым академиясының Мұнай және газ институты, Баку, Әзірбайжан. Email: galib_2000@yahoo.com

Молдабаева Гульназ Жаксылыковна
Техника ғылымдарының докторы, профессор, Сәтбаев Университеті, Алматы, Қазақстан. Email: g.moldabayeva@satbayev.university

Түзелбаева Шолпан Рысқұлбекқызы
Техника ғылымдарының магистрі, докторант, Сәтбаев Университеті, Алматы, Қазақстан. Email: s.tuzelbayeva@satbayev.university

Имансакипова Земфира Бекетовна
Техника ғылымдарының магистрі, докторант, Сәтбаев Университеті, Алматы, Қазақстан. Email: z.imansakipova@satbayev.university

У ХунЦзюнь
Техника ғылымдарының магистрі, ЖШС «DPS Қызылорда», Қызылорда, Амангелді Иманов көшесі, 112А. Email: wus520@mail.ru

Метод нестационарного заводнения и условия его эффективного применения при эксплуатации нефтяных месторождении

¹Эфендиев Г.М., *²Молдабаева Г.Ж., ²Тузельбаева Ш.Р., ²Имансакипова З.Б., ³У ХунЦзюнь

¹Национальная академия наук Азербайджана, Баку, Азербайджан
²Satbayev University, Алматы, Казахстан
³ТОО "DPS Кызылорда", Кызылорда, Казахстан

АННОТАЦИЯ

В статье изложена сущность нестационарного заводнения, которое является одним из достаточно эффективных методов увеличения коэффициента извлечения нефти, применяемого для изменения направления фильтрационных потоков, что позволяет вовлечь в разработку невыработанные запасы нефти и снизить темпы обводнения залежи в продуктивных коллекторах. Распространенным технологическим методом нестационарного заводнения является использование циклических режимов работы нагнетательных скважин. Сущность такого метода заключается в том, что при неустановившемся состоянии в нефтяной залежи возникают условия для непрерывного проявления упругих сил пластовой системы. В неоднородном пласте между различными зонами, каналами и потоками жидкостей возникают градиенты гидродинамических давлений, за счет которых могут происходить перетоки флюида из одних слоев в другие, из трещин в блоки, а также изменяются направления потоков. При нестационарном заводнении неоднородных пластов часть запасов нефти в низкопроницаемых прослоях или зонах остается неохваченной закачиваемой водой. Заводняемый пласт представляется как бессистемное чередование обводненных и нефтенасыщенныхмикропотоков. При создании в таких коллекторах попеременно изменяющихся по величине и направлению градиентов давления, в нефтяном пласте возникают условия для внедрения нагнетаемой воды в застойные нефтенасыщенные малопроницаемые зоны и каналы, и перемещения из них нефти в зоны активного дренирования. В результате анализа выявлен положительный эффект от реализации технологии нестационарного заводнения, а также даны рекомендации по совершенствованию ее применения на других эксплуатационных объектах нефтяных месторождений.

Ключевые слова: нестационарное заводнение, нагнетательная скважина, циклическая закачка,нефтеотдача, фильтрация, неоднородность.

Эфендиев Галиб Мамедович	*Информация об авторах:*
	Доктор технических наук,профессор. Институт Нефти и газа Национальной академии наук Азербайджана, Баку, Азербайджан. Email: galib_2000@yahoo.com
Молдабаева Гульназ Жаксылыковна	*Доктор технических наук,профессор. Satbayev University, Алматы, Казахстан. Email: g.moldabayeva@satbayev.university*
Тузельбаева Шолпан Рыскулбековна	*Магистр технических наук, докторант, Satbayev University, Алматы, Казахстан. Email: s.tuzelbayeva@satbayev.university*
Имансакипова Земфира Бекетовна	*Магистр технических наук, докторант, Satbayev University, Алматы, Казахстан. Email: z.imansakipova@satbayev.university*
У ХунЦзюнь	*Магистр технических наук, ³ТОО "DPS Кызылорда", Кызылорда, ул.Амангельды Иманов, дом 112А. Email: wus520@mail.ru*

References

1. Liu Wenzheng, He Hong, Yuan, Fuqing, Liu Haocheng, Zhao Fangjian, Liu, Huan, Luo, Guangjie. Influence of the Injection Scheme on the Enhanced Oil Recovery Ability of Heterogeneous Phase Combination Flooding in Mature Waterflooded Reservoirs. ACS OMEGA. 2022; 7(27):23511–23520 https://doi.org/10.1021/acsomega.2c02007

2. Leng, Jianqiao, Sun, Xindi, Wei, Mingzhen, Bai, Baojun. A Novel Numerical Model of Gelant Inaccessible Pore Volume for In Situ Gel Treatment. GELS. 2022;8(6), 375 https://doi.org/10.3390/gels8060375

3. Bai Baojun, Zhou Jia, Yin, Yin Mingfei. A comprehensive review of polyacrylamide polymer gels for conformance control. PETROLEUM EXPLORATION AND DEVELOPMENT. 2015; 42(4):525-532. https://doi.org/10.1016/S1876-3804(15)30045-8

4. Zhang Guoyin, Yu Jianjia. Effect of commonly used EOR polymers on low concentration surfactant phase behaviors. FUEL. 2021; 2:286. https://doi.org/10.1016/j.fuel.2020.119465

5. Wang Dongmei, Namie Shane, Seright Randall. Pressure Modification or Barrier Issues during Polymer Flooding Enhanced Oil Recovery. GEOFLUIDS. 2022. https://doi.org/10.1155/2022/6740531

6. Peter Mora, Gabriele Morra, Dave Yuen, Ruben Juanes. Study of the Effect of Wetting on Viscous Fingering Before and After Breakthrough by Lattice Boltzmann Simulations. SPE Middle East Oil & Gas Show and Conference. 2021. https://doi.org/10.2118/204536-MS

7. Ximena Guerrero, Daniel Ricardo Medina, Alberto Munoz, Jhon Rubiano, Alied Bejarano, Hernando Trujillo, Nicolas Saltel, Julian Trillos, Jerson Becerra, Diego Castellanos, Cesar Coronado. Water Isolation and Sand Control: Breaking Barriers with Expandable Steel Patch Technology. Society of Petroleum Engineers (SPE). 2020. https://doi.org/10.2118/201432-MS

8. Ximena Guerrero, Daniel Ricardo Medina, Alberto Munoz, Jhon Rubiano, Alied Bejarano, Hernando Trujillo, Nicolas Saltel, Julian Trillos, Jerson Becerra, Diego Castellanos, Cesar Coronado. Water Isolation and Sand Control: Breaking Barriers with Expandable Steel Patch Technology. SPE Annual Technical Conference and Exhibition. 2020.

9. Ali Al-Azmi, Hassan Al-Qattan, Mohamad Al-Do. An Effective Solution for Unwanted Water Production Obtained from Water Coning Mechanism: Field Application" International Petroleum Technology Conference. 2022. https://doi.org/10.2523/IPTC-22371-MS

10. Tariq K Khamees, Ralph E Flori. Can the Viscoelasticity of HPAM Polymer Solution Make the Polymer Flooding Compete with Gel Treatment to Improve Sweep Efficiency? A Comparison with Different Polymer Gel Systems" SPE International Conference on Oilfield Chemistry. 2022. (https://doi.org/10.2118/193592-MS

11. R. S. Seright, Dongmei Wang. Polymer Retention "Tailing. Phenomenon Associated with the Milne Point Polymer Flood. SPE Journal. 2022; 27(05):2863-2881. https://doi.org/10.2118/209354-PA

12. Miguel Gonzalez, Tim Thiel, Nathan St. Michel, Jonathan Harrist, Erjola Buzi, Huseyin Seren, Subhash Ayirala, Lyla Maskeen, Abdulkarim Sofi. A New Viscosity Sensing Platform for the Assessment of Polymer Degradation in EOR Polymer Fluids. SPE Annual Technical Conference and Exhibition. 2022; SPE-210014-MS. https://doi.org/10.2118/210014-MS

13. Jiaming Li, Guang Zhao, Ning Sun, Lihao Liang, Ning Yang, Caili Dai. Construction and evaluation of a graphite oxide Nanoparticle-Reinforced polymer flooding system for enhanced oil recovery. Journal of Molecular Liquids. 2022; 367(B). https://doi.org/10.1016/j.molliq.2022.120546

14. Javad Razavinezhad, Arezou Jafari, Seyed Masoud, Ghalamizade Elyaderani. Experimental investigation of multi-walled carbon nanotubes assisted surfactant/polymer flooding for enhanced oil recovery. Journal of Petroleum Science and Engineering. 2022; 214. https://doi.org/10.1016/j.petrol.2022.110370

15. Moldabayeva G ZH, Agzamov AKh, Suleimenova RT, Elefteriadi DK, Abileva SZh, Baluanov B.A. Hydrodynamic modeling of field development using enhanced oil recovery methods. Kompleksnoe Ispolzovanie Mineralnogo Syra = Complex Use of Mineral Resources. 2021; 317(2):14-22. https://doi.org/10.31643/2021/6445.13

16. Abhijit Chaudhuri, R Vishnudas. A systematic numerical modeling study of various polymer injection conditions on immiscible and miscible viscous fingering and oil recovery in a five-spot setup. FUEL. 2022; 232:431-443. https://doi.org/10.1016/j.fuel.2018.05.115

17.   Moldabayeva GZh, Suleimenova RT, Agzamov AKh, Abileva SZh, Baluanov BA. The effectiveness of the use of physical impact on the reservoir to reduce the viscosity and increase oil recovery, Kompleksnoe Ispolzovanie Mineralnogo Syra = Complex Use of Mineral Resources. 2021; 316(1):53-61 https://doi.org/10.31643/2021/6445.07

18.   AL-Obaidi SH, Smirnov VI, Khalaf FH. New Technologies to Improve the Performance of High Water Cut Wells Equipped With ESP. Technium. 2021; 3(1):104-113.

19.   Wojtanowicz AK, and et al. A New Completion Method to Minimize Oil Well Production Water cut in Bottom-water-drive Reservoirs. The Journal of Canadian Petroleum Technology. 1995; 34(8):56-62.

20.   Lon A. Stuebinger and Gerald M. Elphingston. New opportunities offered by downhole oil/water separation. Word Oil. 1998; 219(12):71-78.

21.   Bowlin KR, and et al. Field application of in-situ gravity segregation to remediate prior waterconing. Journal of Petroleum Technology. 1997; 49(10):1117-1120.

Research and development of gold ore processing technology

¹Kenzhaliyev B.K.,¹*Koizhanova A.K., ¹Atanova O.V., ¹Magomedov D.R., ²Nurdin H.

¹Institute of Metallurgy and Ore Beneficiation JSC, Satbayev University, Almaty, Kazakhstan

²Universitas Negeri Padang, Padang 25131, Indonesia

*Corresponding author email: a.koizhanova@satbayev.university

ABSTRACT

This paper presents the results of technological studies of two samples of gold-bearing ore from the gold-bearing deposit of Kazakhstan deposits 1 and 2. A comprehensive analysis of ore samples by X-ray fluorescence, X-ray phase, chemical, and mineralogical methods was carried out. The calculated initial gold content was determined, and X-ray fluorescence analysis showed that the main elements that make up the ore are oxygen up to 51% and silicon up to 33%. X-ray phase analysis showed the presence of more than 95% quartz and muscovite in the samples. The form of finding gold in the ore, according to the results of mineralogical analysis, is defined as free gold and gold in iron hydroxide. Silver is present in the studied samples in the form of various types of halides. An ore beneficiation scheme has been developed and presented, including gravity and flotation. Gravity enrichment was carried out in two stages, with the production of concentrate and tailings, with the maximum recovery of gold in concentrate up to 91%, flotation enrichment using butyl xanthate reagents and a blowing agent, was carried out in two stages with the production of main and control concentrates and final flotation tailings. The subsequent hydrometallurgical study of the ore was carried out to assess the effect of sodium cyanide on the extraction of gold, tests were performed on the leaching of the initial samples of the ore and the obtained flotation and gravity concentrates in the agitation mode, it was found that cyanide leaching is an effective method for processing the mineral raw materials of the gold-bearing deposit of Kazakhstan, and the obtained flotation concentrates, with the recovery of gold into solution under optimal conditions up to 98%. The results obtained make it possible to predict the effectiveness of the main technological stages in the ore processing scheme, technology optimization, and maximum gold recovery.

Keywords: mineralogical analysis, gold, ore, concentrate, gravity, flotation, cyanidation.

	Information about authors:
Kenzhaliyev Bagdaulet Kenzhaliyevich	Doctor of Technical Sciences, Professor, General Director-Chairman of the Management Board of the JSC "Institute of Metallurgy and Ore Beneficiation", Satbayev University, Almaty, Shevchenko srt., 29/133, Kazakhstan. Email: bagdaulet_k@satbayev.university
Koizhanova Aigul Kairgeldyevna	Candidate of technical sciences, head of the laboratory of special methods of hydrometallurgy, JSC "Institute of Metallurgy and Ore Beneficiation", Satbayev University, Almaty, Shevchenko srt., 29/133, Kazakhstan. Email: aigul_koizhan@mail.ru, a.koizhanova@satbayev.university
Atanova Olga Viacheslavovna	Candidate of technical sciences, leading researcher, JSC "Institute of Metallurgy and Ore Beneficiation", Satbayev University, Almaty, Shevchenko srt., 29/133, Kazakhstan. Email: ovatanova@gmail.com
Magomedov David Rasimovich	Researcher, master, JSC "Institute of Metallurgy and Ore Beneficiation", Satbayev University, Almaty, Shevchenko srt., 29/133, Kazakhstan. E-mail: davidmag16@mail.ru
Hendri Nurdin	Department of Mechanical Engineering, Faculty of Engineering, Universitas Negeri Padang, Padang 25131, Indonesia. E-mail: hens2tm@ft.unp.ac.id

Introduction

Enhanced environmental requirements and the task of increasing the complexity of the use of raw materials modify the assessment and reassessment of new gold fields and operated ones, respectively. Gold ores are usually characterized by a significant variety of material composition, which implies the use of a larger number of processes, schemes, and options to process them. The technology for processing of gold ores is complex and specific, and differences in the material composition, processing properties, and technological category of ores determine the methods of concentration and

extraction, as well as the possibility of processing according to a single process scheme.

In connection with the depletion of reserves of free-milling and high-grade ores, new deposits with a low content of valuable components, a complex or variable mineral composition, and technologically refractory ores are put into operation. The complex, heterogeneous, and variable composition of ores within a single deposit complicates the processing scheme and causes the need to adjust technological modes, and sometimes it requires processing ores according to various process schemes [[1], [2], [3], [4], [5]]. Depending on enrichability, gold fields are classified as: - placer; - silica gold vein; - primary quartz carbonate-sulphide; - sulfide; - carbonaceous shales. Placer and silica gold vein fields are free-milling. Gold is extracted from solid sulfide ores as a by-product. When producing concentrates of non-ferrous metals such as copper, zinc, lead, and molybdenum, the technology for the concentration of gold-bearing carbonaceous shales has not been developed [[6], [7], [8], [9], [10]].

Primary quartz-sulfide deposits are the most common deposits of gold-bearing ores. These ores are divided into free-milling and refractory ones. When processing refractory ores by direct cyanidation or a combined method, including the stage of ore pretreatment and concentration by flotation, less than 60-75% of gold is extracted, while when enriching free-milling ores, more than 90% is extracted [[11], [12], [13], [14]].

Moreover, the qualitative and quantitative composition differs within the perimeter of one deposit; therefore, research on improving the efficiency of gold extraction, flotation concentration of crude minerals containing fine gold, and the use of gravity concentration methods are relevant.

Features of refractory ores are the presence of fine gold which is usually embedded in pyrite or other sulfides and is found in an unreleased form inside mineral particles of sulfides. The particle size of gold in such ores is usually less than 20 μm [[15], [16], [17], [18], [19], [20], [21], [22]].

Experimental part

Materials and basic methods. In this research, we used modern research and analytical equipment such as Optima 2000 DV atomic emission spectrometer (United States); D8 ADVANCE X-ray diffractometer; Thermo Nicolet Avatar 370 FTIR spectrometer; Venus 200 X-ray fluorescence spectrometer (PA Nalyical B.V., Holland), and AxioScope A1 optical microscope. MShL-22k ball mill (Russia) was also used;

Main results and analysis. The material composition of the base ore was studied and technological regimes were worked out for dressing and hydrometallurgical processing by cyanidation in order to extract gold into a productive solution.

To determine the material composition of the ore for the content of S_{total}, $S_{sulfate}$, $S_{sulfide}$, Au, Ag, CaO, and SiO_2 and for further research, ore pretreatment was carried out. The samples received were subjected to pretreatment operations such as averaging and quartering. The selected averaged samples were received for chemical, fluorescent, phase, and mineralogical analyses. The sample processing scheme is compiled for each deposit and each type of ore, taking into account the characteristics of the mineral and the size of the initial samples.

Table 1 – Results of X-ray fluorescence analysis of ore samples of gold-bearing deposits of Kazakhstan 1 and 2

Element	Content, %	Element	Content, %	Element	Content, %	Element	Content, %
Dep 1 (Deposit 1)							
O	51.59	S	0.357	Cu	0.023	P	0.031
Na	0.022	K	0.405	Zn	0.005	Fe	1.969
Mg	0.151	Ca	0.056	Rb	0.007	Pb	0.092
Al	1.658	Ti	0.082	Zr	0.002	Bi	0.003
Si	33.557	Mn	0.010	Mo	0.011		
Dep 2 (deposit 2)							
O	49.344	P	0.037	Mn	0.031	Zr	0.05
Na	0.087	S	**0.295**	Fe	**4.715**	Mo	0.009
Mg	0.270	K	0.494	Cu	0.079	Pb	0.092
Al	2.591	Ca	0.192	Zn	0.007	Ni	0.007
Si	29.566	Ti	0.117	Rb	0.010	Sr	0.004

In preparation for the research, the sample were mixed and reduced in accordance with the standard procedure with the allocation of weighed quantities for technological research and the study of the material composition.

Technological experiments including various methods of studying the material composition of the feedstock and microscopic studies provide data for characterizing the morphology of gold and the degree of its association with ore components. The detailed elemental composition of the base ore samples of gold-bearing deposits of Kazakhstan 1 and 2 (Table 1) was determined by fluorescence analysis which allows to capture of the spectra of elements from beryllium to uranium. The results are shown in Table 1.

According to the results of the analysis, we can conclude that the studied samples contain oxygen (O) at 51.59% for Dep 1 and 49.34% for Dep 2, and silicon (Si) at 33.55% for PK1 and 29.56% for Dep 2. The sulfur content (S) is low and amounts to 0.36% for Dep 1 and 0.29% for Dep 2. The content of Al is 1.65 and 2.59%, respectively.

The main composition of the rock-forming components was determined by X-ray phase analysis. The survey was carried out using the D8 Advance (Bruker) apparatus (α-Cu, tube voltage 40 kV, current 40 mA). Processing of the obtained data of diffraction patterns and calculation of interplanar distances were carried out using the EVA software. Sample decoding and phase search were performed using the Search/match program with the use of the 2020 PDF-2 powder diffractometric database. The results of the X-ray phase analysis are shown in Table 2.

According to the research results, the crystalline part of the image studied consists of quartz (Dep 1 97.3% and Dep 2 95.9%) and muscovite. The research data give grounds to assume that the technological type of ore under study is silica gold.

The subsequent mineralogical analysis made it possible to establish the main forms of finding gold in the rocks of mineral raw materials.

To establish forms of gold deportment, ore samples of gold-bearing deposits of Kazakhstan 1 and 2 were mineralogically analyzed. A polished section ($\varnothing$ = 25 mm, weight = 10-15 grams) formed from this material was studied under an optical microscope AxioScope A1.

Mineralogical analysis of ore samples with a size of up to 0.1 mm in order to study the ore mineral composition and forms of gold deportment. The study was carried out using an OLYMPUS-BX 51m microscope in reflected light, and mineralogical analysis was carried out using an electron probe microanalyzer.

To perform the analysis, the sample was divided into heavy and light fractions. According to the method, heavy fractions were isolated in a heavy liquid with a specific gravity of 2.9 g/cm^3 with the subsequent production of polished artificial briquettes.

Mineralogical analysis in reflected light. Examination of Dep 1 sample. According to the results of the study, non-metallic minerals that make up more than 95% of the area of the polished section 1 were determined as quartz grains of grayish-milky-white color and mica, which was confirmed by X-ray analysis (quartz 97.3% and muscovite 2.7%). The copper mineralization of the secondary sulfide enrichment zone is represented by pyrite. In this sample, iron-containing minerals and oxidized minerals account for about 2-3% of the area of the polished section. Under the reflected light microscope, pyrite occurs in the oxidation zone of iron oxides. The inclusion of large sizes up to 2 mm is shown in Figure 3. Pyrite is white with a brass-yellow tinge and shows high reflectivity. Iron hydroxides are often found to be light gray, have brown internal reflexes, and be isotropic (Figure 1).

Table 2 – Results of X-ray phase analysis of the initial sample of gold-bearing deposits of Kazakhstan 1 and 2

Range	Name	Formula	Content, %
Dep 1			
PDF 01-085-0865	Quartz	SiO_2	97.3%
PDF 00-003-0849	Muscovite	H4K2(Al,Fe)6Si6O24	2.7%
Dep 2			
PDF 01-085-0865	Quartz	SiO_2	95.9 %
PDF 00-003-0849	Muscovite	H4K2(Al,Fe)6Si6O24	4.1 %

This figure shows the collomorphic structure of limonite. The size reaches up to 1.5-2 mm. There are also grains that are non-metallic and impregnated with iron oxides. Perhaps this is a clayey substance or fine sedimentary rocks (Figure 1). 1000x magnification found no visible gold grains.
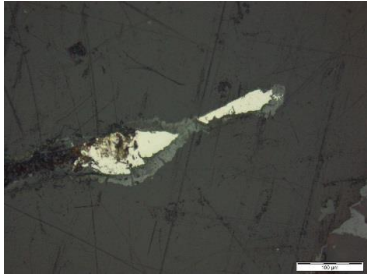
Relic of pyrite in iron hydroxides. 200x magnification

Figure 1 – Mineralogical analysis in reflected light

Examination of Dep 2 sample. X-ray phase analysis showed the content of the crystalline phase: quartz 95.9% and muscovite 4.1%. The sample is similar to the Dep 1 one. In this polished section, the grains are larger and have a collomorphic structure, iron hydroxides are larger in % content, and the grain size reaches up to 3 mm. Both free single grains of pyrite and iron hydroxides were found (Figure 2).

Relic of pyrite in iron hydroxides.200x magnification

Figure 2 – Mineralogical analysis in reflected light

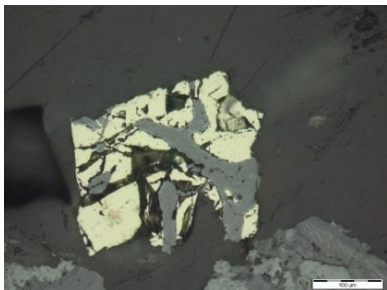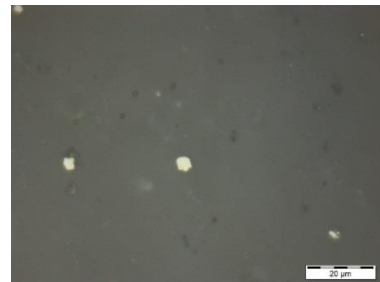***Mineralogical analysis using an electron probe microanalyzer.*** The polished section is made of heavy fractions. The sample mainly consists of fragments of iron hydroxides such as goethite, limonite, and rarely hematite. There are single grains of pyrite which are usually found in the form of relics in iron oxides and hydroxides, less often in the form of free grains (Figure 3). Thorough scanning of the briquettes under a conventional microscope at 200x magnification revealed no gold; at 1000x magnification, gold was found. To confirm the presence of gold in the sample, the surface of the briquette was studied by X-ray spectral microanalysis using the Superprobe 733electron probe microanalyzer (JEOL, Japan). Analyses of the elemental composition of minerals (microinclusions) and photographs of various types of radiation were performed using an energy-dispersion spectrometer manufactured by OXFORD INSTRUMENTS (England).

Scanning the briquette found two grains of gold in iron hydroxides (Figure 4) with a % content of Fe 3.98; Ag 0.15; Au 95.87, and the second point with a content of Fe 11.61; Ag 0.08; Au 88.31.

Free grain of pyrite. 1000x magnification

Figure 3 – Mineralogical analysis using an electron probe microanalyzer.

The gold-bearing deposit of Kazakhstan 2 (Dep 2) sample is similar in mineral composition to the Dep 1 sample. The inclusions are dominated by hydroxides and iron oxides. Free grains of pyrite are also present in a small amount (Figure 4); it is mainly found as relics in iron hydroxides.
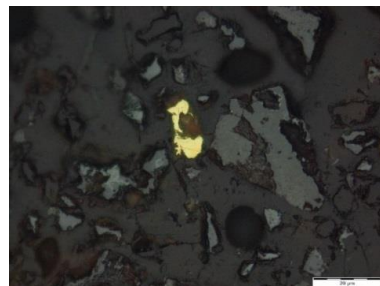
Pyrite in iron hydroxide. 1000x magnification

Figure 4 – Mineralogical analysis using an electron probe microanalyzer

Study of the material composition of the initial samples (Dep 1 and Dep 2). The ground material of two initial samples of gold-bearing deposits of Kazakhstan 1 and 2 was received for the study of the material composition. In order to concentrate useful and accompanying ore minerals from samples in a heavy liquid with a specific gravity of 2.9g/cm³, heavy fractions were isolated with subsequent production of polished artificial sections

(briquettes). The briquettes were scanned, and hydroxides and oxides of iron predominated therein. Free grains of pyrite were found in a small amount, mainly as relics in iron hydroxides (Table 3).

Table 3 – Gold deportment in the initial samples of gold-bearing deposits of Kazakhstan 1 and 2

Deportment and content of Au, g/t					
Au_{free}, oxidized minerals.	Au is bound by a crystal lattice of minerals (iron oxides and hydroxides)*	Au with sulfide minerals	Au in quartz veins	ΣAu	Au_{total}
Base ore of gold-bearing deposit of Kazakhstan 1					
ND	3.15	<0.1	<0.01	3.25	3.25
Base ore of gold-bearing deposit of Kazakhstan 2					
<0.1	4.0	<0.05	<0.01	4.15	4.15

* Almost all of the gold in Dep 1 and Dep 2 is located in the nodes of the crystal lattices of minerals, represented mainly by oxide and hydroxide compounds of iron.

Gold-bearing deposit of Kazakhstan 1 sample. Scanning the briquette surface by X-ray spectral microanalysis found two gold crystals in iron hydroxides. Grain sizes are 0.003-0.005 mm. The first gold grain point contains Au 95.87%, and the second gold grain point contains Au 88.31%. Along with gold, several grains of silver halides such as Ag, Br, Ag, and J were found (Figure 5). All grains are in the form of inclusions in iron hydroxides.
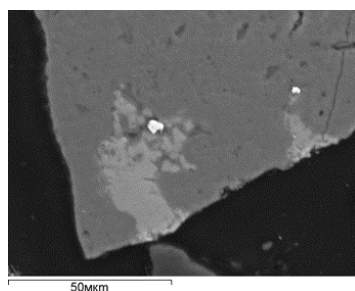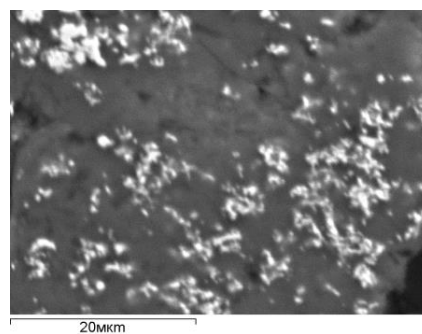

Figure 5 – X-ray spectral microanalysis of the Prirechnoye 1 sample. Gold grains in iron hydroxides

At the same time, silver which is part of the Dep 1 and Dep 2 samples, was found in compounds represented by various types of halides. Deportment of silver compounds, %: Cl 11.86; Br 9.94; Ag 76.79; I 1.42.

Gold-bearing deposit of Kazakhstan 2 sample. The mineral composition of the sample is close to the one described above. The briquette was scanned, and grains of iron hydroxides with fine dispersion inclusiveness were found therein, which, according to the analysis, is represented by gold

(Figure 6). Gold is found in iron oxides in the form of tiny grains with a size of less than 1 μ.

Inclusions of the smallest grains of gold in iron hydroxide

Figure 6 – X-ray spectral microanalysis of the gold-bearing deposit of Kazakhstan 2 sample

Thus, Figure 6 shows the facts of the occurrence of inclusions of gold particles with thin inclusions in iron hydroxides. The shape of the goldenrods is diverse and can be spherical, rounded, monolithic, hooked, elongated, or incorrect. The surface of Au grains is both smooth with clear contours, and rough, relief.

Discussion of the results

Gravity concentration was studied using the base ore ground to 98% content of 0-0.071 mm fraction on a 3-inch Knelson KC-MD3 3 centrifugal concentrator with continuous unloading. This concentrator contains a rotating cone-shaped rotor with two grooves in the upper part with clamping valves installed along the circumference. At the bottom of the grooves, there are holes for fluidizing water. During operation, the heavy fraction accumulates in the grooves, and the valves are periodically opened to discharge the accumulated concentrate. The concentrate output varies depending on the frequency and duration of opening of the clamping valves.

The raw material in the form of pulp is fed into the rotor through a feeding pipe on the bottom of the cone. Under the action of centrifugal forces, the pulp is thrown against the wall of the cone and, moving to the threshold, stratified. Heavy minerals settle on the inner surface of the cone, slide to the gap and get inside the shell. Under the action of water supplied from the pipe, they are washed out through the threshold into the heavy fraction collector. The light fraction goes through the threshold into the receiver. The inner diameter of the threshold may be equal to, or less than, the inner

diameter of the threshold. It depends on the location of the rotor axis, the magnitude of centrifugal forces, as well as on the mineral composition of the raw material. The output of the heavy fraction at a fixed value of the internal diameter of the threshold is controlled by the supply of water through the channels.

Research conditions: The diameter of the concentrator cone is 7.5 cm, the water flow is 3.5 L/min, the pressure is 25 kPa, and the acceleration of the gravitational fall is 60 g. Table 4 presents the results of gravity concentration.

Table 4 – Results of two-stage gravity concentration of Dep 1 and Dep 2 samples of the gold-bearing deposit of Kazakhstan

Product	Weight, g	Weight output, %	Au, g/t	E_{Au}, %
Dep-1				
Rougher concentrate	158.3	5.3	23.5	44.16
Scavenger concentrate 1	155.9	5.2	14.6	27.02
Scavenger concentrate 2	144.9	4.8	11.5	19.78
Final concentrate	**459.1**	**15.3**	**16.7**	**91.0**
Tailings	2540.9	84.7	0.3	9.0
Total	3000.0	100.00	2.81	100.00
Dep-2				
Rougher concentrate	144.8	4.8	39.25	47.61
Scavenger concentrate 1	142.3	4.7	19.7	23.48
Scavenger concentrate 2	141.5	4.7	15.3	18.14
Final concentrate	428.6	14.3	24.9	89.2
Tailings	2571.4	85.7	0.5	10.8
Total	3000.0	100.00	3.98	100.00

Before gravity concentration, Dep 1, and Dep 2 samples were ground in a ball mill to 90 % content of 0-0.071 mm fraction. The enrichment was carried out in one stage with the production of two main products, gravity concentrate and tailings. The obtained concentrates and tailings after drying were analyzed for the content of valuable components, and the concentrates of Dep 1 and Dep 2 samples were also used in further leaching experiments. The concentrates of the two stages were combined. The calculation of the balance of gravity concentration products showed that the estimated initial gold

content in Dep 1 and Dep 2 is 2.81 g/t and 3.98 g/t, respectively. Thus, the discrepancy with the results of the analysis of the gold content in the initial PK 1 sample (3.21 g/t) is 12.5% (Discrepancy = (2.81/3.21 – 1.0) ×100%). In the Dep 2 sample with a gold content of 4.12 g/t, the difference in the enrichment balance was 3.4%.

Technological studies of flotation concentration were carried out with ground base ore of gold-bearing deposits of Kazakhstan 1 and 2. For flotation concentration experiments, Dep 1 and Dep 2 samples were ground in a ball mill to 90 % content of 0-0.071 mm fraction. Laboratory studies were carried out on standard laboratory flotation machines of the Mechanobr type with a chamber volume of 3.0 L. Flotation was performed at a ratio of solid particles in the pulp equal to 33%. Flotation concentration was carried out in two stages with the production of the main and Scavenger concentrates, as well as the final tailings of flotation.

During flotation studies, reagent regimes were carried out using the following reagents: For rougher flotation: pH 9.0; butyl xanthogenate 120 g/t; foamer C7 60 g/t; duration 10 min; for scavenger flotation: pH 9.0, butyl xanthogenate 60 g/t; foamer C7 30 g/t; duration 5 min. All the obtained concentrates and flotation tailings were dried for further analysis. Dep 1 and Dep 2 concentrates were used in subsequent gold leaching experiments.
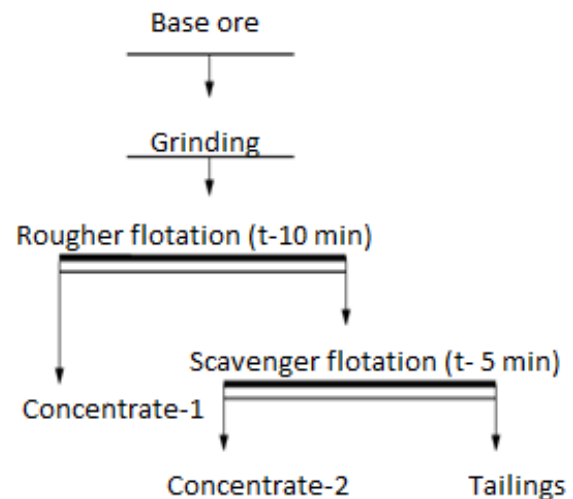

Figure 7 – Studies of flotation concentration; flotation scheme (gold-bearing deposit of Kazakhstan (1 and 2 deposits)

Figure 7 shows an experimental scheme for determining the optimal fineness of the floated material. The results of flotation concentration experiments are presented in Table 5.

Table 5 – Results of flotation of Dep 1 and Dep 2 samples ground to 90 % content of 0-0.071 mm fraction

Product	Weight, g	Weight output, %	Au, g/t	E_{Au}, %
Dep-1				
Rougher concentrate	215.6	10.8	29.0	83.64
Scavenger concentrate 1	139.7	7.0	4.2	7.85
Scavenger concentrate 2	75.4	3.8	2.2	2.22
Final concentrate	**430.7**	**21.5**	**16.3**	**93.7**
Tailings	1569.3	78.5	0.3	6.30
Total	2000.0	100.00	3.74	100.00
Dep-2				
Rougher concentrate	291.0	14.6	13.32	49.96
Scavenger concentrate 1	235.0	11.8	11.5	34.83
Scavenger concentrate 2	112.4	5.6	5.65	8.19
Final concentrate	**638.4**	**31.9**	**11.3**	**93.0**
Tailings	1361.6	68.1	0.4	7.0
Total	2000.0	100.00	3.88	100.00

The calculation of the balance of flotation concentration products showed that the estimated initial gold content in Dep 1 and Dep 2 is 3.74 g/t and 3.88 g/t, respectively.

Thus, the discrepancy with the results of the analysis of the gold content in the initial Dep 1 sample (3.21 g/t) is +16.5% When calculating the experimental error and estimated data, the discrepancy was $(3.74/3.21 – 1.0) \times 100\%$). In the Dep 2 sample with a gold content of 4.12 g/t, the difference in the enrichment balance was 5.83 %.

Hydrometallurgical studies of ore samples from the gold-bearing deposit of Kazakhstan (Dep1 and Dep 2) were carried out using samples ground to 80 % content of 0-0.071 mm fraction.

To assess the effectiveness of cyanide leaching for extracting gold from the raw materials of the Prirechnoye deposit, tests were performed on the leaching of base ore samples, gravity, and flotation concentrates. The study of the leaching process was carried out by tank leaching method with stirring activation [[18], [19]]. The data is presented in Table 6.

Leaching process mode. Cyanide (NaCN) concentration is 0.2%; duration of cyanidation is 24 h; pulp density during cyanidation is 30% solid; pH 10.5. The test sample was ground to 80 % content of 0-0.071 mm fraction, then pulped and tested in agitation mode, while controlling the alkalinity pH at 10.5. To ensure an initial pH value of 10.5, alkali NaOH was added to the sodium cyanide solution. Upon completion of cyanide leaching, the pulp was filtered, and the solid precipitate (cake) was analyzed for gold content.

Table 6 – Results of agitated cyanide leaching of gold-bearing deposit of Kazakhstan 1 and 2 samples

Option/conditions	Initial Au, g/t	Cake$_{Au}$, g/t	E_{Au}, %
Dep 1 base ore	3.21	0.08	97.51
Dep 2 base ore	4.12	0.13	96.84
Dep 1 rougher concentrate, gravity	23.5	3.83	83.70
Dep 2 rougher concentrate, gravity	39.25	20.0	49.04
Dep 1 rougher concentrate, flotation	29.0	0.54	98.14
Dep 2 rougher concentrate, flotation	13.32	0.61	95.42

The results of the studies show that during cyanide leaching of ground base ore of gold-bearing deposits of Kazakhstan 1 and 2, gold extraction in optimal modes is 97.51% and 96.84%, respectively. Gold extraction was calculated by the residual content in the cake.

Thus, the extraction of gold in optimal modes is in %:

- gravity concentration of gold-bearing deposit of Kazakhstan 1 and 2 ore: 91.0 and 89.2, respectively;

- gravity concentration of Dep 1 and Dep 2 ore followed by cyanidation of gravity concentrate: 83.70 and 49.04;

- flotation concentration of Dep 1 and Dep 2 ore: 93.7 and 93.0;

- flotation concentration of Dep 1 and Dep 2 ore followed by cyanidation of flotation concentrate: 98.14 and 95.42, respectively.

It follows from the data in Table 6 that the base ore of the gold-bearing deposit of Kazakhstan 1 and 2 and the flotation concentrates of the gold-bearing deposit of Kazakhstan 1 and 2 are well cyanized. Gravity concentrate of Dep 1 and Dep 2 is cyanidated slightly worse.

Conclusions

The technology for processing gold ores is specific and complex. For the complete recovery of the precious metal, a combination of various processing methods such as concentration and hydrometallurgical wats is used. The complex material composition, the scale of deposits, and environmental requirements require a comprehensive study of raw materials, analyses, and technological experiments. The ultimate goal of the research is to develop a technology with maximum recovery of the target metal. We carried out a technological assessment of ore from the gold-bearing deposit of Kazakhstan deposit (Dep 1 and Dep 2 samples), studied the material composition, and tested ore for the enrichment and efficiency of hydrometallurgical recovery of gold by agitated cyanide leaching. It has been confirmed that silica gold vein is the technological type of ore. Based on the study of the material composition and deportment of gold and associated minerals, it was proposed to conduct technological studies on gravity and flotation concentration, where greater efficiency and selectivity were shown in the flotation cycle; according to the results of the analysis, 93.7 % and 93.0 % passed into the scavenger concentrate for Dep 1 and Dep 2 samples, respectively. Gravity concentration has a lower efficiency in relation to this ore (91.0 % and 89.2 %) due to the loss of fine gold during the release of mineral grains. The proposed technology of ore processing of the gold-bearing deposit of Kazakhstan includes ore preparation (grinding to 80 % content of 0-0.071 mm fraction, flotation with a reagent composition: pH 9.0; butyl xanthogenate 120 g/t; foamer C7 60 g/t, with further agitated cyanide leaching by tank leaching method at a concentration of cyanide (NaCN) of 0.2; pulp density of 30% solid and alkalinity pH of 10.5). Further recovery of gold from the productive solution is possible by electrolysis after concentration by the ion exchange method.

Алтын кенін өңдеу технологиясын зерттеу және дамыту

¹Кенжалиев Б.К.,¹Койжанова А.К., ¹Атанова О.В., ¹Магомедов Д.Р., ²Nurdin H.

¹ Металлургия және кен байыту институты, Сәтбаев Университеті, Алматы, Қазақстан
²Мемлекеттік Паданг Университеті, Паданг 25131, Индонезия

ТҮЙІНДЕМЕ

Бұл жұмыста Қазақстандағы құрамында алтыны бар кен орындарының екі үлгісін –Кенорын 1 және Кенорын 2 үлгілерінің технологиялық зерттеулерінің нәтижелері берілген. Рентгендік флуоресценция, рентгендік фазалық, химиялық және минералогиялық әдістермен кен үлгілерін кешенді талдау жүзеге асырылды. Есептелген бастапқы алтын құрамы анықталып, рентгендік флуоресценциялық талдау кенді құрайтын негізгі элементтер ретінде 51%-ға дейін оттегі және 33%-ға дейін кремний болатынын көрсетті. Рентгендік фазалық талдау үлгілерде 95%-дан астам кварц пен мусковиттің барын көрсетті. Минералогиялық талдау нәтижелері бойынша кендегі алтын бос алтын және теміргидроксидіндегі алтын түрінде болатыны анықталды. Зерттелетін үлгілерде күміс әр түрлі галогенидтер түрінде кездеседі. Гравитациядан және флотациядан тұратын кенді байыту схемасы әзірленді және ұсынылды. Гравитациялық байыту концентратпен қалды өндірумен, концентраттағы алтынның максималды алынуы 91%-ға дейін, бутилксантогенатыре агентін және көбіктендіргішті пайдалана отырып флотациялық байытумен, негізгі және бақылау концентраттары және соңғы флотациялық қалдықтар алынатын, екі кезеңде жүзеге асырылды. Натрий цианидінің алтынды өндіруге әсерін бағалау үшін кеннің гидрометаллургиялық зерттеулері жүргізілді. Кеннің бастапқы үлгілерін және алынған флотациялық және гравитациялық концентраттарды араластыру режимінде шаймалау бойынша сынақтар жүргізілді. Цианидті шаймалау Қазақстандағы құрамында алтыны бар кен орнының минералдық шикізатын және одан алынатын флотациялық концентраттарды өңдеудің тиімді әдісі болып табылатынын және оңтайлы жағдайда 98%-ға дейін алтынды ерітіндіге қайтару мүмкін болатыны анықталды. Алынған нәтижелер кенді өңдеусіз басындағы негізгі технологиялық кезеңдердің тиімділігін, технологияны оңтайландыруды және алтынның максималды алынуын болжауға мүмкіндік береді.

Авторлар туралы ақпарат:

Кенжалиев Багдаулет Кенжалиевич	Техника ғылымдарының докторы, профессор, бас директор "Металлургия және кен байыту институты" АҚ; Сәтбаев Университеті, Шевченко к-сі, 29/133, 050013, Алматы, Қазақстан. Email: bagdaulet_k@satbayev.university
Койжанова Айгуль Кайргельдыевна	Техника ғылымдарының кандидаты, гидрометаллургияның арнайы әдістері зертханасының меңгерушісі, "Металлургия және кен байыту институты" АҚ; Сәтбаев Университеті, Шевченко к-сі, 29/133, 050013, Алматы, Қазақстан. Email:aigul_koizhan@mail.ru, a.koizhanova@satbayev.university
Атанова Ольга Вячеславовна	Техника ғылымдарының кандидаты, жетекші ғылыми қызметкер, "Металлургия және кен байыту институты" АҚ; Сәтбаев Университеті, Шевченко к-сі, 29/133, 050013, Алматы, Қазақстан. Email:ovatanova@gmail.com
Магомедов Давид Расимович	ғылыми қызметкер, магистр, "Металлургия және кен байыту институты" АҚ; Сәтбаев Университеті, Шевченко к-сі, 29/133, 050013, Алматы, Қазақстан. E-mail: davidmag16@mail.ru
Hendri Nurdin	Машина жасау кафедрасы, Инженерлік факультет, Мемлекеттік Паданг Университеті, Паданг 25131, Индонезия. E-mail: hens2tm@ft.unp.ac.id

Исследование и разработка технологии переработки золотосодержащей руды

[1]Кенжалиев Б.К., [1]Койжанова А.К., [1]Атанова О.В., [1]Магомедов Д.Р., [2]Nurdin H.

[1]АО «Институт металлургии и обогащения», Satbayev University, Алматы, Казахстан
[2]Государственный Университет Паданга, Паданг 25131, Индонезия

АННОТАЦИЯ

В данной работе представлены результаты технологических исследований двух образцов проб золотосодержащей руды месторождения Казахстана– месторождения 1 и 2. Проведен комплексный анализ образцов руды рентгенофлуоресцентным, рентгенофазовым, химическим и минералогическим методами. Определено расчетное исходное содержание золота, так же, рентгенофлуоресцентныманализом показано, что основными элементами, составляющими руду, являются кислород до 51% и кремний до 33%. Рентгенофазовый анализ показал присутствие в пробах кварца, более, чем 95% и мусковита. Форма нахождения золота в руде, по результатам минералогического анализа, определена, как свободное золото и золото в гидроокисле железа. Серебро присутствует в исследуемых образцах в форме галогенидов различного типа. Разработана и представлена схема обогащения руды, включающая гравитацию и флотацию. Гравитационное обогащение проводилось в две стадии, с получением концентрата и хвостов, максимальное извлечение золота в концентрат до 91%, флотационное обогащение с использованием реагентов бутилового ксантогената и вспенивателя, проводилось в две стадии с получением основного и контрольного концентратов и итоговых хвостов флотации. Последующее гидрометаллургическое исследование руды проводилось для оценки влияния цианида натрия на извлечение золота, выполнены тесты по выщелачиванию исходных проб руды и полученных флотационных и гравитационных концентратов в агитационном режиме, установлено, что цианидное выщелачивание является эффективным способом для переработки минерального сырья золотосодержащего месторождения Казахстана, и полученных флотационных концентратов, с извлечением золота в раствор при оптимальных условиях до 98%. Полученные результаты позволяют прогнозировать эффективность основных технологических этапов в схеме переработки руды, оптимизации технологии и максимального извлечения золота.

Ключевые слова: минералогический анализ, золото, руда, концентрат, гравитация, флотация, цианирование.

Информация об авторах:

Кенжалиев Багдаулет Кенжалиевич	Доктор технических наук, профессор, генеральный директор АО «Институт металлургии и обогащения»; Сатпаев Университет, 050013, ул. Шевченко, 29/133, Алматы, Казахстан. Email: bagdaulet_k@satbayev.university
Койжанова Айгуль Кайргельдыевна	Кандидат технических наук, заведующая лабораторией спецметодов гидрометаллургии, АО «Институт металлургии и обогащения»; Satbayev University, 050013, ул. Шевченко, 29/133, Алматы, Казахстан. Email: aigul_koizhan@mail.ru, a.koizhanova@satbayev.university
Атанова Ольга Вячеславовна	Кандидат технических наук, ведущий научный сотрудник, АО «Институт металлургии и обогащения»; Satbayev University, 050013, ул. Шевченко, 29/133, Алматы, Казахстан. Email:: ovatanova@gmail.com
Магомедов Давид Расимович	Научный сотрудник, магистр, АО «Институт металлургии и обогащения»; Satbayev University, 050013, ул. Шевченко, 29/133, Алматы, Казахстан. E-mail: davidmag16@mail.ru
Hendri Nurdin	Кафедра машиностроения, инженерный факультет, Государственный Университет Паданга, Паданг 25131, Индонезия. E-mail: hens2tm@ft.unp.ac.id

References

[1]   Liu W, Deng X, Han S, Chen X, Li X, Aibai A, Wu Y, Wang Y, Shan W, Li Z, et al. Pyrite Textures and Compositions in the Dunbasitao Gold Deposit, NW China: Implications for Ore Genesis and Gold Mineralization Processes. Minerals. 2023; 13(4):534. https://doi.org/10.3390/min13040534

[2]   Adamov EV. Tekhnologiya rud tsvetnykh metallov [Technology of non-ferrous metal ores]. M: MISIS. 2007, 470. (in Russ).

[3]   Bocharov VA, Ignatkina VA, Lapshina GA, Khachatryan LS. Osobennosti izvlecheniya zolota iz zolotosoderzhashchikh sul'fidnykh rud [Features of extracting gold from gold-bearing sulfide ores]. Gorno-informatsionnyyi analiticheskiy byulleten' [Mining information and analytical bulletin]. 2004; 12S:297-301. (in Russ).

[4]   Mhandu TJ, Park I, Jeon S, Hamatsu S, Elakneswaran Y, Ito M, Hiroyoshi N. A Pretreatment of Refractory Gold Ores Containing Sulfide Minerals to Improve Gold Leaching by Ammonium Thiosulfate: A Model Experiment Using Gold Powder and Arsenic-Bearing Sulfide Minerals. Metals. 2023; 13(8):1357. https://doi.org/10.3390/met13081357

[5]   Kotova OB, Ozhogina EG, Rogozhin AA. Innovatsionnyye podkhody k otsenke kachestva mineral'nogo syr'ya [Innovative approaches to assessing the quality of mineral raw materials]. Plaksinskiye chteniya [Plaksinsky readings]. 2012. (in Russ).

[6]   Komogortsev BV, Varenichev AA. Problemy pererabotki bednykh I upornykh zolotosoderzhashchikh rud [Problems of processing poor and refractory gold-bearing ores]. Gornyy informatsionno-analiticheskiybyulleten' [Mining information and analytical bulletin]. 2016, 204-218. (in Russ).

[7]   Abdyldayev NN, Usenov NA, Koizhanova AK, YessimovaDM, Akchulakova ST. Determination of substantial composition of gold-bearing raw material and development of technology for its processing. Complex Use of Mineral Resources. 2017; 3:11.

[8]   Koizhanova A, Sedelnikova G, Erdenova M, Berkinbaeva A, Kamalov E. Study of biohydrometallurgical technology used to recover gold from ore at a gold-recovery plant. Kompleksnoe Ispolzovanie Mineralnogo Syra = Complex Use of Mineral Resources. 2021; 316(1):24-31. https://doi.org/10.31643/2021/6445.03

[9]   Mamayeva A, Kenzhegulov A, Panichkin A, Kshibekova B, Bakhytuly N. Deposition of carbonitride titanium coatings by magnetron sputtering and its effect on tribo-mechanical properties. Kompleksnoe Ispolzovanie Mineralnogo Syra = Complex Use of Mineral Resources. 2022; 321(2):65-78. https://doi.org/10.31643/2022/6445.19

[10] Sedelnikova GV. Mirovoy opyt pererabotki zoloto sul'fidnykh rud i kontsentratov [World practice of processing gold sulfide ores and concentrates]. Bulletin of the Kazakhstan National Academy of Natural Sciences. 2014; S:42-44. (in Russ).

[11] International Mineralogical Association Commission on new minerals, nomenclature and classification The IMA List of Minerals. 2019.

[12] Zhang Y, Cui M, Wang J, Liu X, Lyu X. A review of gold extraction using alternatives to cyanide: Focus on current status and future prospects of the novel eco-friendly synthetic gold lixiviants. Miner. Eng. 2022; 176:107336.

[13] Zelenov VI. Metodika izucheniya zolotosoderzhashchikh I serebrosoderzhashchikh rud [Methodology for the study of gold and silver-bearing ores]. M.: Nedra. 1989, 302. (in Russ).

[14] Koizhanova AK, Kenzhaliev BK, Bisengalieva MR, Mukusheva AS, Gogol DB, Abdyldaev NN, Magomedov DR. Calculation of Thermodynamic and Structural Characteristics of Gold and Silver Solvate Complexes Russian Journal of Inorganic Chemistry.2020; 65(7):1051-1060. ISSN 0036-0236.

[15] Sedelnikova GV. Mirovoy opyt pererabotki zolotosul'fidnykh rud I kontsentratov [World practice of processing gold sulfide ores and concentrates]. Vestnik Kazakhstanskoy natsional'noy akademiy estestvennykh nauk [Bulletin of the Kazakhstan National Academy of Natural Sciences]. 2014; 3S:42-44. (in Russ).

[16] Xie F, Chen J, Wang J. Review of gold leaching in thiosulfate-based solutions. Trans. Nonferrous Met. Soc. China. 2021; 31:3506-3529.

[17] Jeon S, Ito M, Tabelin CB, Pongsmrankul R, Kitajima N, Park I, Hiroyoshi N. Gold recovery from shredder light fraction of E-waste recycling plant by flotation-ammonium thiosulfate leaching. Waste Manag. 2018; 77:195-202.

[18] Mineev GG, Panchenko AF. Rastvoriteli zolota I serebra v gidrometallurgii [Solvents of gold and silver in hydrometallurgy]. M.: Metallurgy. 1994, 241. (in Russ).

[19] Koizhanova AK, Toktar G, Craig E Banks, Magomedov DR, Kubaizhanov AA. Research of hydrometallurgical method of leaching gold from flotation tails with using bio-oxidation. Kompleksnoe Ispolzovanie Mineralnogo Syra = Complex Use of Mineral Resources. 2020; 314(3):28-39. https://doi.org/10.31643/2020/6445.24

[20] Boduen AYa, Fokina SB, Petrov GV, Serebryakov MA. Modern hydrometallurgical technologies for processing refractory gold-bearing raw materials. Sovremennye Problemy Naukii Obrazovaniya. 2014; 6:63.

[21] Yusupkhodjayev AA, Berdiyarov BT, Matkarimov ST, Radjabov AI, Radjabova GI. Improvement of technology of processing of persistent gold-bearing ores and concentrates using oxidative burning. International Journal of Engineering and Advanced Technology. 2019; 9(2):4793-4796. https://doi.org/10.35940/ijeat.b3935.129219

Research of the production of iron ore sinter from bauxite processing waste

Zhunussova A.K., Bykov P.O., Zhunusov A.K., *Kenzhebekova A.Ye.

Torayghirov University, Pavlodar, Kazakhstan

*Corresponding author email: kenzhebekova_psu@mail.ru

ABSTRACT

This article presents the results of a study of the agglomeration of waste alumina ferrous sands and the use of sinter as a substitute for metal charge in steelmaking. At this time, in the process of processing bauxite, JSC "Aluminium of Kazakhstan" produces a large number of fines, which is of great interest to ferrous metallurgy. Wastes from alumina production include a variety of waste sludge, including red, gray sludge, and ferrous sands. According to the chemical composition, ferrous sands can be attributed to iron ore material with a high content of alumina. Most of these problems are eliminated by preliminary agglomeration of fines. In this work, agglomeration studies made it possible to establish the optimal parameters for sintering ferrous sands. When using 10% fuel, the best sintering performance is achieved. The optimal parameters for sintering ferrous sands mixed with other metallurgical wastes are such as productivity - 0.92 t / m^2 h, mechanical strength - 80.0%, sintering speed - 19.3 mm/min, yield - 82.0%, the maximum temperature in the layer is 1340 °C. The results of laboratory melt carried out in an induction melting furnace indicate the possibility of using a sinter as a substitute for metal charge in iron and steel smelting. The conducted melting confirms the fundamental possibility of using a sinter, made from waste products of alumina production of ferrous sands, is a man-made charge material that is suitable for use as a 5% additive to the metal charge in the smelting of iron-carbon alloys similar in composition to cast irons.

Keywords: Ferrous sand, agglomerate, sintering, charge gas permeability, sintering rate, metal charge, smelting.

	Information about authors:
Zhunussova Aygul Kairgeldinovna	*Student Ph.D., Department of "Metallurgy", Torayghirov University, 140008, Lomova Street 64, Pavlodar, Kazakhstan. Email: zhunusova.aig@mail.ru*
Bykov Petr Olegovich	*Candidate of Technical Sciences, Professor, Department of "Metallurgy", Torayghirov University, 140008, Lomova Street 64, Pavlodar, Kazakhstan. Email: bykov_petr@mail.ru*
Zhunusov Ablay Kairtassovich	*Candidate of Technical Sciences. Professor, Department of "Metallurgy". Torayghirov University, 140008, Lomova Street 64, Pavlodar, Kazakhstan. Email: zhunusov_ab@mail.ru*
Kenzhebekova Anar Yerbolatovna	*Student Ph.D., Department of "Metallurgy", Torayghirov University, 140008, Lomova Street 64, Pavlodar, Kazakhstan. Email: kenzhebekova_psu@mail.ru*

Introduction

At this time, in the process of processing bauxite, JSC "Aluminium of Kazakhstan" produces a large number of fines, which is of great interest to ferrous metallurgy. Wastes from alumina production include a variety of waste sludge, including red, gray sludge, and ferrous sands. Iron sands are formed as a result of the leaching of bauxites according to the Bayer scheme. When bauxite is leached at JSC "AK", a scheme has been developed for removing the iron component of bauxite (ferrous sands) [1]. The formed ferrous sands contain over 50% Fe$_2$O$_3$, which, by their chemical composition, are suitable for use in the production of ferrous metals. According to

preliminary estimates, more than 500 thousand tons of such waste are generated per year. This is only in Kazakhstan. And according to [2], more than 2.7 billion tons of bauxite waste have accumulated in the world, and annually its amount only increases by 120 million tons.

Currently, the world has a wide variety of works on the processing of bauxite waste from alumina production. However, the ongoing research is not all of the interest from the side of metallurgy. Many technologies for processing wastes from alumina production are expensive for the implementation of the presented studies, and most of them are accompanied by complexity and multi-stage processing processes. According to its composition,

bauxite waste can be used in various industries [[3], [4], [5], [6], [7]].

At present, a large number of different methods for processing sludge waste from alumina production have been developed in the world [[8], [9]]. In the works [[10], [11], [12], [13]], the technologies for extracting valuable rare earth metals and components from alumina production sludge are considered.

In [[14], [15]], the technology of processing wastes from alumina production (red mud) by agglomeration was studied. In this direction, many years of great work have been done on the processing of red mud by agglomeration, and positive results have been obtained. It follows that ferrous metallurgy seems to be the most promising for the processing of ferrous sludge (ferrous sands).

In Kazakhstan, the research, presented in [16], is devoted to the study of ferrous sands. The analysis of the physicochemical data on the composition of ferrous sands shows that they can be considered a potential raw material for the production of pigments and cast iron. In [[17], [18]], a method was developed for the processing of alumina production waste - red mud by reduction smelting to produce cast iron and slag containing rare earth elements and titanium dioxide. The work [[19]. [20]] shows the possibility of hydrochemical enrichment of ferrous sands by leaching with alkali-aluminate solutions of alumina production.

Industrial waste is often used in metallurgy as cheap substitutes for iron ores. As a rule, technogenic wastes have a fractional composition of less than 5 mm. When working on a fine charge in a blast furnace, the blast pressure on the tuyeres and the loss of blast pressure in the charge column increase significantly. All this leads to the hanging of the mixture, and gas permeability deteriorates. There is a deterioration in the degree of use of chemical and thermal energy. Under such conditions, it is not necessary to operate the furnaces normally and achieve the productivity of the workshops. It is obvious that most of these difficulties are eliminated by preliminary agglomeration of fines.

The agglomeration of ore materials makes it possible to involve various technogenic wastes in metallurgical processing [20], such as screenings of ores, sludge, mill scale, flue, and aspiration specks of dust [21], and pyrite cinders. The agglomerated high-quality charge prepared for smelting will make it possible to utilize existing waste, improve the operation of furnaces, reduce dust removal, reduce the specific consumption of coke, and increase metal smelting.

Experimental part

Ferrous sands were used as the material under study. Ferrous sands are waste products of alumina production, as are waste sludges, including red, gray sludge, and ferrous sands. According to the chemical composition of the studied material presented in Table 1, ferrous sands can be attributed to iron ore material with a high content of alumina.

When conducting experiments on the agglomeration of alumina production waste, iron sands of a fraction of 0-5 mm were used as a charge in a mixture with mill scale, in a ratio of 70:30. Screenings of coke were used as fuel. The fraction 0.1–1.6 mm has the most unfavorable effect on pelletization [20]. It is in this fineness range that many man-made wastes and the material under study (iron sands) fall, the granulometric composition of ferrous sands is presented in Table 2. The aspiration dust of steelmaking was used as a clay component to improve the compressibility of the charge [21]. The use of aspiration dust had a favorable effect on pelletization, which accelerates with an increase in the number of nuclei in the charge. Pelletization was also facilitated by the use of return in the charge, in which the bulk has the presence of the smallest particles [[20], [21], [22]].

Table 1 – Chemical composition of materials

Materials	Fe_{gen}	SiO_2	MnO	Al_2O_3	MgO	CaO	S	P	C
Ferrous sand - waste of alumina production	61.0	7.8	-	19.0	0.5	5.7	0.2	-	-
Rolled scale from mill	76.8	0.8	1.7	-	-	-	-	-	0.10
Aspiration dust	50.9	1.7	2.0	3.5	2.0	3.0	0.021	0.002	3.2

Table 2 - Granulometric composition of iron sands

Fraction, mm	-0.06	-0.2-0.06	-0.5-0.2	-1-0.5	-3-1	-5-3
Unit. %	2.0	14.7	43.2	20.5	6.8	12.8

Table 3 - The chemical composition of the ash and the technical composition of screening coke fraction 0-10 mm, %

SiO_2	CaO	MgO	Al_2O_3	Fe_2O_3	A	V	W
47.2	10.9	7.0	10.2	11.6	23.0	4.8	6.2

Mixing of the mixture was carried out in a drum mixer. The optimal moisture content of the charge was selected empirically, by a gradual increase from 5 to 10%. The use of clay components contributed to the improvement of the properties of the mixture during its preparation before sintering, it turned out to be friable, and the improvement in gas permeability reduced the sintering time. The experiments were carried out on a laboratory sintering plant, according to the established methodology in the laboratory of the Department of Metallurgy, Toraighyrov University (Pavlodar).

Before pelletizing, iron sand was subjected to pre-drying at 100-150 °C in a drying oven, since after leaching evaporators, iron sands have a high humidity (70-80%). The moisture content of the material was reduced to 5-15%.

The following seeds were used as sintering charge: iron sand, scale (20%), coke breeze (5-10%), return (20%), and aspiration dust. Mixing and pelletizing was carried out in a drum mixer. For better pelletization of iron sand in the mixture, aspiration dust of a fraction of 0-5 mm was used, since this material in the composition has a finely dispersed clay part. Due to the use of waste sludge as part of the sintering charge, the degree of pelletization of the material under research is improved. Screenings of PRC Coke were used as fuel (Table 3). The return was used from the previous sinter. Agglomerate was used as a bed. The incendiary mixture consisted of a mixture of sawdust and coke breeze, lightly moistened with water. Ignition mixture - wood shavings moistened with kerosene.

Bowl parameters: diameter 100 mm, bowl height allows sintering charge up to 500 mm. The sinter plant is equipped with a VVN-1.5 vacuum pump, a TXA, BP thermocouple, and a multi-channel automatic temperature recorder (ART-2) of the sintering process (fixing the temperature of the gas outlet, charge layer at different heights).

The charge was loaded using a special device, which makes it possible to significantly reduce the segregation and compaction of the charge. Ignition was carried out for one minute at a rarefaction of 300-350 mm wg. incendiary and ignition mixture. Sintering was carried out at a constant vacuum under a grate of 1000 mm of water column. The thermocouple readings - the temperature in the bed, and the temperature of the exhaust gases, were recorded on ART-2. The start of sintering was determined by the moment of ignition of the coke, and the end of the process was determined by the time of reaching the maximum temperature of the exhaust gases. The flue gas temperature was measured with a thermocouple (TCA) installed on the gas outlet pipeline. After the end of sintering, the cake was unloaded from the bowl, cooled for 10 minutes in the air, weighed on a laboratory balance, then dropped from a height of 2 m onto a steel plate according to GOST 25471 - 82, after which the yield of classes was determined (including the good fraction +8 mm). Further samples of the agglomerate fraction +5 - 40 mm were subjected to the determination of mechanical strength according to GOST 15137 - 77.

The discussion of the results

During the research, the amount of coke was changed from 5 to 10%. Figures 1, 2, and Table 4 present the results of laboratory studies. From the figures and tabular data (table 4), it can be seen that the amount of fuel has a positive effect on the sintering performance. At 3–5%, the sintering rates are quite low. Changes are observed with an increase in the amount of fuel from 6%. At 7 - 8% fuel, the sintering speed increases slightly to 16.3 – 16mm/min, the plant productivity increases to 0.69 - 0.70 t / m2 h, mechanical strength 75.0 - 77.3%, the yield of suitable sinter is 66.9 - 70%.

A noticeable change is observed with an increase in the amount of fuel in the sinter charge by 9–10%. Changes are visible in the sintering speed, there is an increase from 18.4 to 19.3 mm/min, the productivity of the plant increases from 0.86 to 0.92 t/m^2 h, mechanical strength is 79.0 - 80.0%, and yield 79 - 82%.

The best results in terms of strength and yield of suitable sinter were obtained with an increase in the amount of fuel by up to 11%. However, there is a slight decrease in the sintering speed and productivity of the sinter plant. This is obvious since the carbon of the fuel during combustion releases the heat necessary for the sintering of the charge. If there is not enough fuel in the charge, then the temperature required for sintering (at which liquid phases begin to form) will not be reached and physicochemical transformations in the charge will be poorly developed. The mixture with insufficient fuel will not sinter to the end (a sufficient amount of bonding of all particles among themselves is not formed throughout the entire layer), which will lead to a weak strength of the resulting sinter, which is demonstrated by the data in Figures 1 and 2.
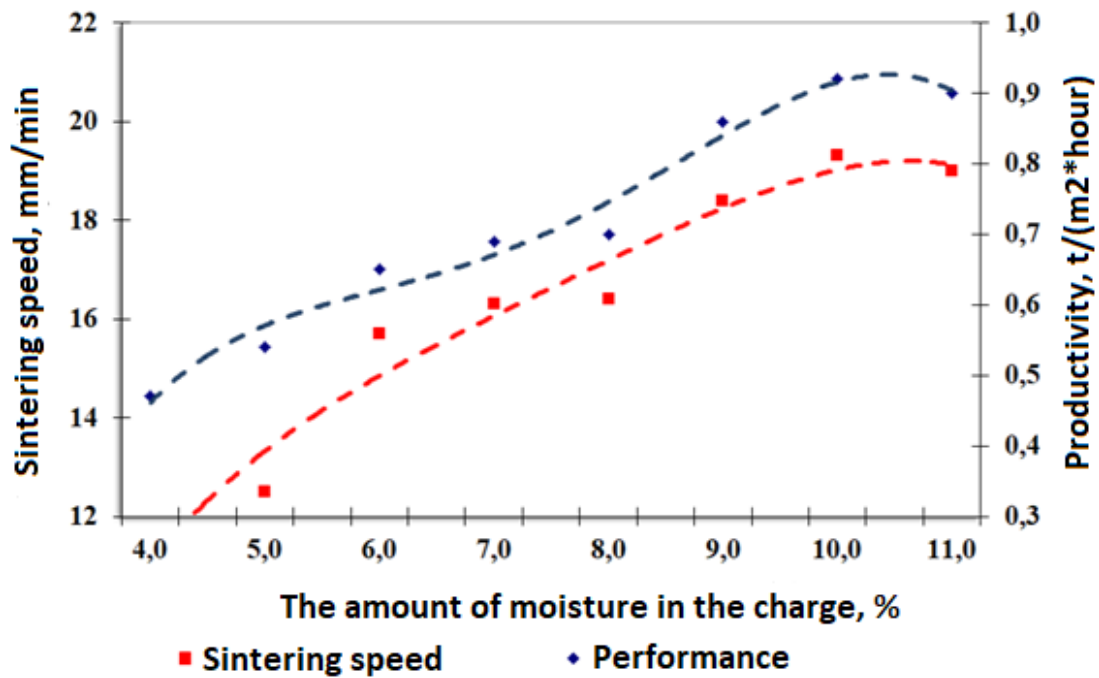

Figure 1 – Influence of the amount of fuel on the sintering performance in terms of productivity and sintering speed
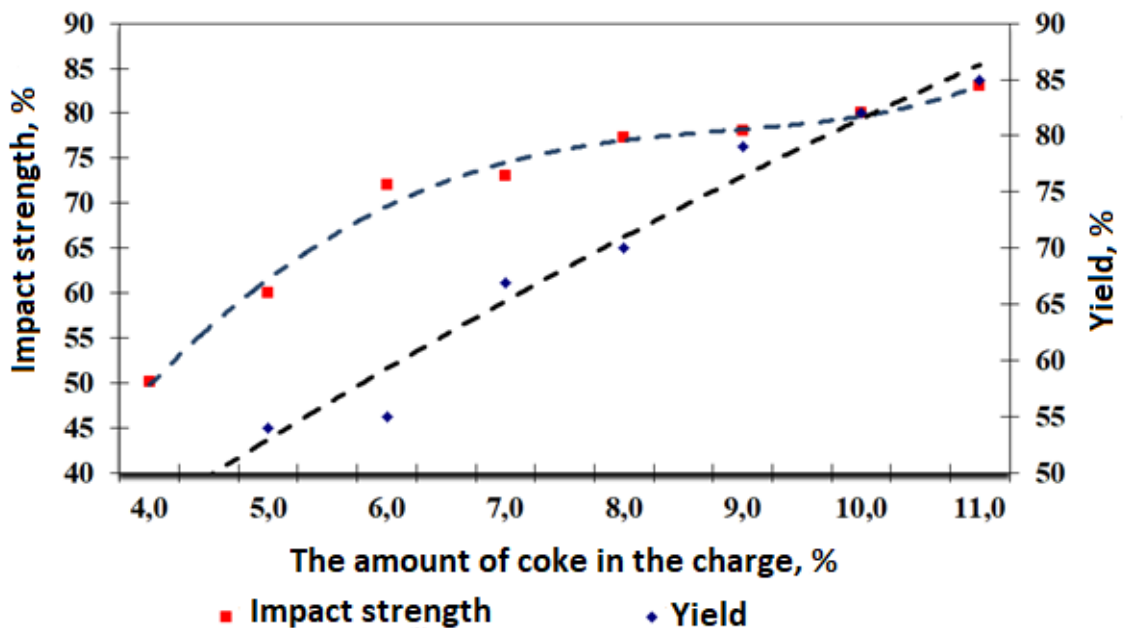

Figure 2 – Influence of the amount of fuel on the sintering performance in terms of strength and yield of suitable sinter

On the other hand, excessive consumption of fuel causes the development of high temperatures, which will cause excessive melting of the sinter and a decrease in mechanical strength, such as with an increase in fuel up to 11%. It is necessary to have such a fuel consumption at which the agglomerate would have good mechanical strength and would not be strongly melted [[21], [22]]. These studies were carried out in order to determine the appropriate fuel consumption for such a sinter.

Thus, the use of 10% fuel should be considered the optimal parameter for sintering iron sands in a mixture with other metallurgical waste, since the best indicators of the sintering process were achieved: productivity - 0.92 t/m^2 h, mechanical strength - 80.0%, speed sintering - 19.3 mm/min, good yield - 82.0%, maximum temperature in the layer - 1340 °C. Figure 3 shows photographs of iron sand (a) and iron ore sinter (b).

The chemical composition of the produced iron ore sinter is shown in table 5.

Further research work was carried out to assess the possibility of using iron ore sinter as a substitute for metal charge in steelmaking. For this purpose, induction melting was carried out in an ITP-0.005 furnace. The agglomerate was loaded into pre-molten metal. The melting of the metal was carried out according to the basic technology of melting steel grade St40. The average specific power consumption in melts using a sinter is higher by 0.52 kW/t than in base melts, which is 0.2%, i.e. the average specific power consumption is practically at the same level. The outlet metal temperature was 1450–1500°C. The temperature was measured using a tungsten-rhenium thermocouple (VR) and an MRT-6 multichannel temperature recorder. The average duration of the melts was 1 hour 30 minutes. Data on the chemical composition of the metal are presented in Table 6.

Table 4 – Sintering performance with changes in fuel consumption

№ of Experiment	The amount of coke in the charge, %	Sintering speed, mm/min	Productivity, t/m^2 hour	Strength according to GOST - 15137-87	Yield, %
1	3	10.4	0.38	-	-
2	4	11.3	0.47	50.1	47.2
3	5	12.5	0.54	68.0	54.0
4	6	15.7	0.65	72.0	55.0
5	7	16.3	0.69	75.0	66.9
6	8	16.4	0.70	77.3	70.0
7	9	18.4	0.86	78.0	79.0
8	10	19.3	0.92	80.0	82.0
9	11	19.0	0.90	83.0	85.0

Table 5 – Chemical composition of iron ore sinter.

Material name	Chemical composition, %						
	Fe$_{gen}$	Al$_2$O$_3$	SiO$_2$	CaO	MgO	S	P
Iron ore sinter	53.0	15.82	11.36	4.96	4.86	0.59	0.066

Figure 3 – Iron sand (a) and iron ore sinter (b)

Table 6 – The chemical composition of the metal

№ of smelting	Content of elements, %				
	C	Si	Mn	S	P
1	4.70	0.200	0.250	0.020	0.020
2	3.20	0.004	0.015	0.008	0.020
3	0.20	0.009	0.010	0.009	0.008

Table 7 – Chemical composition of the metal part of the charge, %

C	Mn	Si	S	P	Cu	Al
0.40	0.45	0.25	0.020	0.015	0.10	0.020

Table 8 - Chemical composition of the resulting ingots, %

C	Mn	Si	S	P	Cu	Al
0.45	0.20	0.15	0.020	0.015	0.08	0.08

The analysis showed that the obtained alloys have a low content of harmful impurities: the content of sulfur and phosphorus is not more than 0.02%. When conducting experimental heats, steel scrap of steel grade St-40 was used as the metal part of the charge and iron ore agglomerate in the amount of 0.80 kg.

The chemical composition of the metal part of the charge is presented in Table 7.

The total weight of the mixture was 5.8 kg. The average duration of heat is 1 hour 30 minutes, and the temperature of the metal at the outlet is 1600 °C. During melting, slag was induced by the following composition of materials:

- quicklime (CaO) - 45%;
- silica (SiO_2) - 25%;
- metallurgical alumina + fluorspar (CaF_2) - the rest.

During the melting process, the formation of foamy slags was observed. Foamy slags affect the process of oxidation of solid carbon particles in the sinter with the formation of carbon dioxide. Under production conditions, when using agglomerate, it will allow obtaining a reduction in the specific consumption of electricity and reducing agents. This statement is confirmed by individual heats, where the specific consumption was 480–510 kW in terms of a ton of good products.

The resulting iron-carbon alloy was deoxidized with aluminum and cast into cast iron molds. As a result of experimental melting in an induction furnace, 5 ingots of 5 kg each were obtained, the chemical composition of which is presented in Table 8.

The yield of suitable metal was 95.0%. Estimating the content of permanent impurities in obtained samples, the following conclusions can be drawn:

- low content of sulfur and phosphorus due to the use of iron ore sinter containing a minimum amount of harmful impurities;

- the use of iron ore sinter as part of the charge leads to an increase in the carbon content in excess of the calculated amount. This means a higher degree of carbon uptake when using iron ore sinter compared to using carbonaceous materials added during carburization smelting.

The results of melting with the use of iron ore sinter obtained in this work indicate their successful application as a substitute for the metal part of the charge for steel melting. In the process of research in laboratory conditions, 20 kg of steel and iron-carbon alloys were smelted using a sinter of various compositions.

Thus, the fundamental possibility of steel smelting using a sinter is shown. A carbonaceous reducing agent, which is part of the sinter, has a positive effect on the reduction process of steelmaking. It should also be noted that the most important thing is that the agglomerate allows you to partially replace cast iron and steel scrap, significantly reducing the cost of metal.

Conclusions

1 Agglomeration makes it possible to involve in the metallurgical process of various production wastes, such as ferrous sands, sludge, mill scale, flue, and aspiration dust. The high-quality agglomerate charge prepared for smelting in the form of iron ore will make it possible to dispose of existing waste, improve the operation of furnaces, reduce dust removal, reduce the specific consumption of coke, and increase metal smelting;

2 Sintering studies made it possible to establish the optimal parameters for the sintering of ferrous sands. When using 10% fuel, the best sintering performance is achieved. The optimal parameters for sintering iron sands mixed with other metallurgical wastes are: productivity - 0.92 t / m^2 h, mechanical strength - 80.0%, sintering speed - 19.3 mm/min, yield - 82.0%, the maximum temperature in the layer is 1340 °C;

3 The results of laboratory melts carried out in an induction melting furnace indicate the possibility of using a sinter as a substitute for metal charge in steelmaking;

4 The results of the melts carried out in the ITP-0.005 induction furnace in order to assess the effectiveness of replacing scrap iron showed that the resulting iron-carbon alloy is similar in chemical composition to gray cast iron SCH15 GOST 1412-85;

5 Conducted smelting confirms the fundamental possibility of using an iron ore sinter, made from waste products of alumina production of iron sand, is a man-made charge material that is suitable for use as a 5% additive to a metal charge in the smelting of iron-carbon alloys similar in composition to cast iron. The content of harmful impurities in the resulting alloys is minimal and is: 0.009-0.026% sulfur and 0.008-0.022% phosphorus. Yield of suitable metal during melting in an induction furnace is 95.0%.

Conflict of interest. On behalf of all authors, the correspondent author declares that there is no conflict of interest.

Бокситтерді қайта өңдеу қалдықтарынан темір кені агломератын алуды зерттеу

Жүнісова А.Қ., Быков П.О., Жүнісов А.Қ., Кенжебекова А.Е.

Торайғыров университеті, Павлодар, Қазақстан

ТҮЙІНДЕМЕ

Бұл мақалада темірлі құм алюминий қалдықтарының агломерациясын зерттеу және болат балқыту кезінде агломератты металл шикіқұрамының орнына қолдану нәтижелері келтірілген. Қазіргі уақытта "Қазақстан алюминийі" АҚ-да бокситтерді қайта өңдеу процесінде көп мөлшерде ұсақ-түйектер түзіледі, олар қара металлургия үшін үлкен қызығушылық тудырады. Химиялық құрамы бойынша темірлі құмдарды, құрамында алюминий мөлшері жоғары темір кенді материалға жатқызуға болады. Аталған мәселелер ұсақ-түйекті алдын ала кесектеу – агломерациялау арқылы шешіледі. Бұл жұмыста агломерациялық зерттеулер темірлі құмдардың күйежентектеудің оңтайлы параметрлерін анықтауға мүмкіндік берді. Отынның 10 % пайдаланған кезде, агломерацияның ең жақсы көрсеткіштеріне қол жеткізілді. Басқа металлургиялық қалдықтармен қоспада темірлі құмдардың күйежентектеудің оңтайлы параметрлері келесідей болды: өнімділік - 0,92 т/ м2·сағ., механикалық беріктігі – 80,0 %, күйежентектеу жылдамдығы-19,3 мм/мин., жарамдылық түсімі – 82,0 %, қабаттағы максималды температура - 1340 °C. Индукциялық балқыту пешінде жүргізілген зертханалық балқытулардың нәтижелері шойын мен болатты балқыту кезінде металл шикіқұрамының орнына агломератты қолдану мүмкіндігін көрсетті. Жүргізілген балқытулар техногендік шикіқұрам материалы болып табылатын темір құмының алюминий өндірісінің қалдықтарынан жасалған агломератты пайдаланудың мүмкіндігін растайды, құрамы бойынша шойынға жақын темір-көміртекті қорытпаларды балқыту кезінде металл шикіқұрамға 5% қоспа ретінде пайдалануға жарамды.

	Авторлар туралы ақпарат:
Жүнісова Айгүл Қайыргелдықызы	*Докторант, Металлургия кафедрасы, Торайғыров университеті, Павлодар, Қазақстан. Email: zhunusova.aig@mail.ru*
Быков Пётр Олегович	*Техника ғылымдарының кандидаты, профессор, «Металлургия» кафедрасы, Торайғыров университеті, Павлодар, Қазақстан. Email: bykov_petr@mail.ru*
Жүнісов Абылай Қайыртасұлы	*Техника ғылымдарының кандидаты, профессор, «Металлургия» кафедрасы, Торайғыров университеті, Павлодар, Қазақстан. Email: zhunusov_ab@mail.ru*
Кенжебекова Анар Ерболатқызы	*Докторант, Металлургия кафедрасы, Торайғыров университеті, Павлодар, Қазақстан. Email: kenzhebekova_psu@mail.ru*

Исследование получения железорудного агломерата из отходов переработки бокситов

Жунусова А.К., Быков П.О., Жунусов А.К., Кенжебекова А.Е.

Торайгыров университет, Павлодар, Казахстан

АННОТАЦИЯ

В данной статье приводятся результаты исследования агломерации отходов глиноземного железистых песков и использовании агломерата в качестве заменителя металлошихты при выплавке стали. В данное время в АО «Алюминий Казахстана» в процессе переработки бокситов образуется большое количество мелочи, представляющий для черной металлургии большой интерес. К отходам глиноземного производства относятся разнообразные отвальные шламы, среди которых красные, серые шламы и железистые пески. По химическому составу, железистые пески можно отнести железорудному материалу с повышенным содержанием глинозема. Большая часть перечисленных проблем устраняется предварительным окускованием мелочи - агломерацией. В данной работе агломерационные исследования позволили установить оптимальные параметры спекания железистых песков. При использовании 10 % топлива достигнуты наилучшие показатели спекания. Оптимальными параметрами спекания железистых песков в смеси с другими металлургическими отходами являются: производительность - 0,92 т/м^2·час, механическая прочность – 80,0 %, скорость спекания – 19,3 мм/мин, выход годного – 82,0 %, максимальная температура в слое – 1340 °C. Результаты лабораторных плавок, проведенных в индукционной плавильной печи, свидетельствуют о возможности применения агломерата в качестве заменителя металлошихты при выплавке чугуна и стали. Проведенные плавки подтверждают принципиальную возможность использования агломерата, изготовленных из отходов глиноземного производства железистого песка, является техногенным шихтовым материалом, который пригоден к использованию в качестве 5 %-ной добавки к металлической шихте при выплавке железоуглеродистых сплавов, близких по составу к чугунам.

Ключевые слова: Железистый песок, агломерат, спекание, газопроницаемость шихты, скорость спекания, металлошихта, плавка

	Информация об авторах:
Жунусова АйгульКаиргельдиновна	*Докторант. Кафедра «Металлургия», Torayghirov University, Павлодар, Казахстан. Email: zhunusova.aig@mail.ru*
Быков Петр Олегович	*Кандидат технических наук, профессор. Кафедра «Металлургия», Torayghirov University, Павлодар, Казахстан. Email: bykov_petr@mail.ru*
Жунусов АблайКаиртасович	*Кандидат технических наук, профессор. Кафедра «Металлургия», Torayghirov University, Павлодар, Казахстан. Email: zhunusov_ab@mail.ru*
КенжебековаАнарЕрболатовна	*Докторант. Кафедра «Металлургия», Torayghirov University, Павлодар, Казахстан. Email: kenzhebekova_psu@mail.ru*

References

[1]   Ibragimov AT, Budon SV. Razvitie tekhnologii proizvodstva glinozema iz boksitov Kazahstana. Pavlodar.: TOO «Dom pechati». 2010, 304.

[2]   Power G, Grafe M, Klauber C. Bauxite residue issues: I. Current management, disposal and storage practices. Hydrometallurgy. 2011; 108(1,2):33-45. https://doi.org/10.1016/j.hydromet.2011.02.006

[3]   Klauber C, Grafe M, Power G. Bauxite residue issues: II. Options for residue utilization. Hydrometallurgy. 2011; 108(1,2):11-32. https://doi.org/10.1016/j.hydromet.2011.02.007

[4]   Grafe M, Power G, Klauber C. Bauxite residue issues: III. Alkalinity and associated chemistry. Hydrometallurgy. 2011; 108(1-2):60-79. https://doi.org/10.1016/j.hydromet.2011.02.004

[5]   Grafe M, Klauber C. Bauxite residue issues: IV. Old obstacles and new pathways for in situ residue bioremediation. Hydrometallurgy. 2011; 108(1,2):46-59. https://doi.org/10.1016/j.hydromet.2011.02.005

[6]   Bakirov A, Abdullina S, Zhunusov A, Oleynikova N. Preliminary Chemical Activation of Ash Waste with Release of Carbon

Concentrate. Chemical Engineering Transactions. 2021; 8:973-978. https://doi.org/10.3303/CET2188162

[7] Bykov P, Kuandykov A, Zhunusov A. Refining of Primary Aluminum from Vanadium. Defect and Diffusion Forum. 2021; 410:405-410. https://doi.org/10.4028/www.scientific.net/DDF.410.405

[8] Taneez M, & Hurel C. A review on the potential uses of red mud as amendment for pollution control in environmental media. Environmental Science and Pollution Research. 2019; 26:22106-22125. https://doi.org/10.1007/s11356-019-05576-2

[9] Ujaczki É, Feigl V, Molnár M, Cusack P, Curtin T, Courtney R, & Lenz M. Re-using bauxite residues: benefits beyond (critical raw) material recovery. Journal of Chemical Technology & Biotechnology. 2018; 93(9):2498-2510. https://doi.org/10.1002/jctb.5687

[10] Zeng H, Lyu F, Sun W, Zhang H, Wang L, Wang Y. Progress on the industrial applications of red mud with a focus on China. Minerals. 2020; 10:773. https://doi.org/10.3390/min10090773

[11] Xue S, Wu Y, Li Y, Kong X, Zhu F, Hartley W, Li X, and Ye Y. Industrial wastes applications for alkalinity regulation in bauxite residue: a comprehensive review. Journal of Central South University; 2010; 26(2):268-288.

[12] Akcil A, Akhmadiyeva N, Abdulvaliyev R, Abhilash, & Meshram P. Overview on extraction and separation of rare earth elements from red mud: focus on scandium. Mineral Processing and Extractive metallurgy review. 2018; 39(3):145-151. https://doi.org/10.1080/08827508.2017.1288116

[13] Hertel T, & Pontikes Y. Geopolymers, inorganic polymers, alkali-activated materials and hybrid binders from bauxite residue (red mud)–Putting things in perspective. Journal of Cleaner Production. 2020; 258:120610. https://doi.org/10.1016/j.jclepro.2020.120610

[14] Yu F, Huangfu L, Wang C, Li C, Yu J, Li W, & Gao S. Recovery of Fe and Al from red mud by a novel fractional precipitation process. Environmental Science and Pollution Research. 2020; 27:14642-14653. https://doi.org/10.1007/s11356-020-07970-7

[15] Mukiza E, Ling Ling Zhang, Xiaoming Liu, Na Zhang. Utilization of red mud in road base and subgrade materials: A review. Resources, Conservation and Recycling. 2019; 141:187-199. https://doi.org/ 10.1016/j.resconrec.2018.10.031

[16] Khalifa AA, Bazhin VY, Ustinova YV, & Shalabi ME. Study of the kinetics of the process of producing pellets from red mud in a hydrogen flow. Journal of Mining Institute. 2022; 254:261-270. https://doi.org/10.31897/PMI.2022.18

[17] Pozmogov VA, Kulbdeev EI, Dorofeev DV, Imangalieva LM, Kvyatkovskaya MN. Opredelenie sostava i svojstv zhelezistyh peskov glinozemnogo proizvodstva dlya poiska putej ih pererabotki. Kompleksnoe Ispolzovanie Mineralnogo Syra = Complex Use of Mineral Resources. 2018; 3:69-77. https://doi.org/10.31643/2018/6445.19

[18] Abdulvaliev RA, Akhmadieva NK, Gladyshev CV, Imangalieva LM, Manapova AИ. The modified red mud reduction smelting. Kompleksnoe Ispolzovanie Mineralnogo Syra = Complex Use of Mineral Resources. 2018; 306(3):15-20. https://doi.org/10.31643/2018/6445.12

[19] Ahmadieva NK, Abdulvaliev RA, Akchil A, Gladyshev SV, Kul'deev EI. Krasnyj shlam glinozemnogo proizvodstva kak potencial'nyj istochnik dlya polucheniya redkozemel'nyh elementov. Obzor. Kompleksnoe Ispolzovanie Mineralnogo Syra = Complex Use of Mineral Resources. 2016; 4:98-104

[20] Zhunusov A, Tolymbekova L, Abdulabekov Ye, Zholdubayeva Zh, Bykov P. Agglomeration of manganese ores and manganese containing wastes of Kazakhstan. Metallurgija. 2021; 60: (1-2):101-103.

[21] Zhunusov AK, Bykov PO, Kenzhebekova AE, Zhunussova AK, Rahmat Azis Nabawi. Study of the isothermal kinetics of reduction of sinter from mill scale. Kompleksnoe Ispolzovanie Mineralnogo Syra = Complex Use of Mineral Resources. 2024; 328(1):59-67. https://doi.org/10.31643/2024/6445.07

Analysis of the thermal regime of converting of copper-lead matte with high-sulfur copper concentrate

Zoldasbay E.E., *Argyn A.A., Dosmukhamedov N.K.

Satbayev University, Almaty, Kazakhstan

* Corresponding author email: aidarargyn@gmail.com

ABSTRACT

According to the earlier conclusions about the possibility of direct processing of high-sulfur copper concentrates with copper-lead matte, analysis of the thermal regime of converting was carried out. It is shown that the traditional calculation methods used to calculate autogenous smelting are not entirely correct and require taking into account the effect of excess sulfur on the temperature regime of the process. It has been established that in the process of converting copper-lead mattes, a wide range of temperature variation is observed - from 1027 ^{0}C to 1300 ^{0}C. When the concentrate is combined with the matte, the temperature regime of the process is stabilized, which ensures the optimal level of SO_2 concentration in the gases required for the production of sulfuric acid. Based on the calculation of the material balance of converting copper-lead mattes using the existing technology and with the addition of a concentrate, the structure of the heat balance of the converting process was established. A strong change in the structure of the heat balance is shown, which is explained by the reduction of magnetite with excess sulfur and an increase in heat due to the oxidation of an additional amount of iron sulfide introduced with the concentrate. A comparative analysis of the technological parameters of the 1st converting period of copper-lead mattes calculated by the proposed method with the practical data of a specific metallurgical unit allows assessing the degree of approximation of the processes occurring in the unit until the thermodynamic equilibrium.

Key words: copper-lead matte, high sulfur copper concentrate, converting, material balance, thermal regime, sulfur, sulfiding.

	Information about authors:
Zoldasbay Erzhan Esenbaiuly	*PhD, Satbayev University, 050013, Almaty, 22 Satbayev st., Kazakhstan. E-mail: zhte@mail.ru*
Argyn Aidar Abdilmalikuly	*PhD, Satbayev University, 050013, Almaty, 22 Satbayev st., Kazakhstan. E-mail: aidarargyn@gmail.com*
Dosmukhamedov Nurlan Kalievich	*Candidate of Technical Sciences, Professor, Satbayev University, 050013, Almaty, 22 Satbayev st., Kazakhstan. E-mail: nurdos@bk.ru*

Introduction

The deterioration in the quality of primary sulfide raw materials due to the increased content of impurities in them led to the complication of the composition of the products obtained during matte smelting. This problem acquires particular relevance for the conditions of converting copper-lead mattes produced by Kazzinc LLP, which are characterized by an increased content of metal impurities: up to 25% lead, up to 4% arsenic and up to 1.0% antimony. When converting such mattes, poor quality blister copper (96-98% Cu) is obtained. Recycled converter slags contain up to 35% lead, ~3% copper and up to 1.5% of arsenic and antimony. Despite the low technological performance of the process, converting remains the main process of blister copper production in the technological scheme of the lead

production of Kazzinc LLP, due to the lack of an alternative method for processing copper-lead mattes.

The results of extensive studies of foreign experience in the processing of copper concentrates in converters [[1], [2], [3]] showed wide opportunities for using the converter as a smelting unit, especially in the first period of converting copper matte. However, despite the achieved positive results, the introduction of the developed methods into production has a restriction due to the lack of effective devices for loading a fine concentrate into the converter. Known installations for loading the concentrate into the converter require specific preparation (drying, grinding, using a complex loading installation) and do not provide a minimum dust removal when loading fine material [[4], [5], [6], [7], [8], [9]].

Many foreign researchers express an opinion about the effectiveness of using a converter exclusively as a melting unit for direct smelting of sulfide copper concentrates with copper extraction in one stage. On this principle, the processes of continuous converting and obtaining blister copper in one stage using autogenous processes are built. However, as the analysis shows, this approach is not entirely effective, due to the large yield of copper-rich slags, which require additional processing to extract valuable metals from them. In addition, the obtained converter slags are characterized by an increased content of lead, arsenic and antimony, the presence of which significantly reduces the quality of the products obtained and the extraction of copper into blister copper.

In the well-known works devoted to the direct smelting of concentrates in converters, the issues of the simultaneous use of high-sulfur components of the concentrate (pyrite, chalcopyrite, etc.) as a sulfiding agent to improve the quality of converter slag and blister copper are practically not considered. The solution of this issue will improve the efficiency of direct smelting of concentrates in converters, and improve the technological performance of the converting process as a whole.

The results of systematic studies of the theoretical features of the interaction of non-stoichiometric higher sulfides with the components of the slag melt, conducted by the Scientific Center named after I.A. Onaev [[10], [11]] showed that excess sulfur formed as a result of dissociation of higher sulfides is completely spent on magnetite reduction and slag sulfiding. Perhaps, these are single studies, where the possibility of simultaneous use of high-sulphur copper concentrate as a sulfidizing agent to improve the quality of converting products has been proved. It has been established that when the concentrate is blown into the converter slag bath at the initial moment, its chemical composition practically does not change. Higher sulfides (pyrite, chalcopyrite) are mixed in the slag bath, without dissociation to their stable sulfides. With further bubbling of the melt, excess sulfur released as a result of the dissociation of higher sulfides is completely absorbed by the slag melt and provides deep reduction of magnetite and sulfidation of oxides of non-ferrous and associated (Pb, As, Zn, Sb) metals, with their deep sublimation into dust in the form of their non-toxic sulfides [[12], [13]].

Based on the results of theoretical and experimental studies, a method was developed for depleting converter slag with high-sulfur copper concentrate, which formed the core of the technology for direct smelting of high-sulphur copper concentrates in converters together with copper matte. The developed technology has been introduced at the Balkhash, Zhezkazgan and Irtysh copper smelters. The obtained positive results of the industrial operation of the technology provide great opportunities for its use in the conditions of converting copper-lead mattes at Kazzinc LLP.

The purpose of this work is to predict the technological modes of the converting process based on the calculation of material and heat balances for converting copper-lead mattes with high-sulfur copper concentrate.

Research methods

The main methodological principle of the developed technology of direct smelting of concentrates in converters is a thermodynamic approach to describing the bubbling process of converting mattes. This way provides a reliable determination of the qualitative and quantitative characteristics of the formed complex condensed (liquid) and vapor-gas phases for given input converting parameters: compositions and quantities of initial materials, temperature conditions, redox potentials, etc.

The thermodynamic approach is based on the idea of achieving thermodynamic equilibrium (or a state close to it) between the smelting products (matte-slag), which makes it possible to use the laws of chemical thermodynamics to establish the behavior of non-ferrous and related impurity metals during the converting of copper-lead mattes together with a concentrate.

As the basic core of research, the results of works on the study of the forms of presence of metals in converting products [10], data on the behavior of compounds of non-ferrous and related metals under the conditions of converting copper-lead mattes with high-sulfur copper concentrate [13] were used.

The structuring of the obtained results with a large array of industrial data (65 points of product compositions) was carried out based on a multivariate rectilinear analysis of statistical dependencies, which provided the way to establish the optimal technological parameters and modes of the converting process. To solve such problems in metallurgical practice, mathematical models [[13], [14], [15], [16], [17], [18], [19], [20]] are widely used,

which describe with sufficient accuracy the calculation of the equilibrium yield of smelting products and the composition of chemically reacting systems. This approach leads to carry out a complex procedure for describing the converting of copper-lead mattes using a well-developed technique for constructing algorithms and programs designed to obtain reliable data.

The paper uses an iterative algorithm for modeling the converting process, which describes the existing process of converting copper-lead mattes with a sufficiently high accuracy and allows predicting the optimal parameters and thermal conditions for converting copper-lead matte together with high-sulfur copper concentrate.

To supply a finely dispersed concentrate, an ejection device can be used, which is connected to the loading pipe without any special costs and technical complications. The scheme of concentrate supply to the converter is shown in Figure 1.
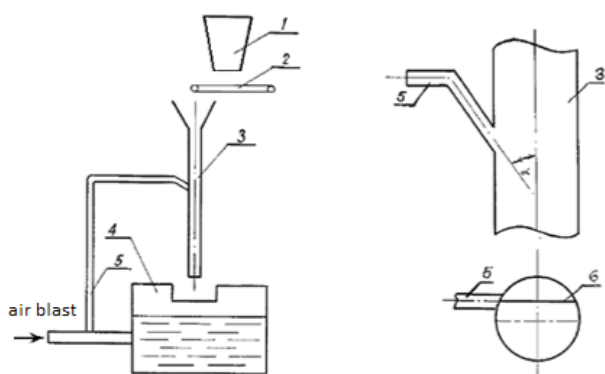

Figure 1 - Scheme of supplying fine materials to the converter
1 - bunker; 2 - conveyor; 3 - loading pipe; 4 - converter; 5 - air duct; 6 - axis of the air flow inlet pipe, α - nozzle inlet angle, 22-30º.

The device and method of operation of the ejection device for supplying finely dispersed materials to the converter are described in detail in [21].

Results and discussion

Autogenous smelting of sulfide raw materials of non-ferrous metals is characterized by a complex mechanism for the formation of the final products of the process. The prediction of the technological modes of operation of furnaces, including converters, is carried out on the basis of the calculation of the material and heat balances of the smelting. When determining the thermal effect from the interaction of the initial charge and oxidizing blast at a given amount of oxygen, the following main processes are taken into account:
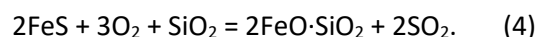
1. Dissociation of higher sulfides:

$$FeS_2 = FeS + 1/2S_2 \qquad (1)$$

$$2CuFeS_2 = Cu_2S + 2FeS + 1/2S_2. \qquad (2)$$
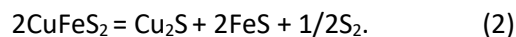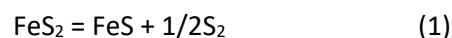
2. Oxidation of elemental sulfur released by reactions (1) and (2):

$$S_2 + 2O_2 = 2SO_2. \qquad (3)$$

3. Oxidation of iron sulfide:

$$2FeS + 3O_2 + SiO_2 = 2FeO \cdot SiO_2 + 2SO_2. \qquad (4)$$

The amount of iron sulfide oxidized by reaction (4) is calculated from the oxygen balance. In this case, it is assumed that elemental sulfur is the first to interact with oxygen and the degree of reaction (3) is equal to unity.

The heat released during the course of reactions (3) and (4) forms the main income items of the heat balance of smelting.

Let us consider the traditional problem of simplified calculation of heat release during autogenous smelting of sulfide raw materials under conditions of equilibrium between matte, slag and gas phase. In this case, it is necessary to take into account not only SO_2, but also S_2 in the composition of the gas phase, due to the equilibrium of the reaction:

$$2(FeO) + 3/2S_2 = 2[FeS] + SO_2. \qquad (5)$$

The achievement of equilibrium in this case is explained by the fact that the oxidation of sulfur to SO_2 proceeds until an equilibrium ratio between them is established in accordance with reaction (5). In this case, the ratio between the values of the partial pressures P_{SO2} and P_{S2} is determined by the activities of FeS and FeO, which depend on the composition of the matte and slag.

If we accept that the partial pressure of sulfur in the gas phase is determined by equilibrium (5), then it can be found from the expression:

$$P_{S_2} = K \cdot P_{SO2}^{2/3} \left(\frac{a_{FeS}}{a_{FeO}}\right)^{4/3}; \qquad (6)$$

$$K = \exp\left(\frac{1,906 - 9219,26}{T}\right) \quad [14],$$

where: K – reaction equilibrium constant (5);
a_{FeS}, a_{FeO} – activity [FeS], (FeO);
P_{S2}, P_{SO2} – partial pressures of S_2 and SO_2 in the gas phase.

The calculation method is narrowed to determining the values of a_{FeS}, generating the material and heat balances of the process. Accounting for the presence of elemental sulfur in the gas phase leads to the need to reconsider the material and heat balances. Therefore, the calculations are carried out taking into account the introduction of the iteration for the partial pressure of sulfur.

For industrial iron silicate slags, the value of a_{FeO} is in a rather narrow range (from 0.35 to 0.45), therefore, in calculations, its value is usually taken equal to $a_{FeO}=0.4$, which corresponds to real industrial slags. When carrying out specific calculations for multicomponent slags, experimental data [22] can be used. Taking into account the assumption of the constancy of a_{FeO}, according to the data of [23], it is possible to determine the value of a_{FeS} depending on the copper content in the matte, similarly to how it was done in [[24], [25], [26]]. After that, using expression (6), the equilibrium partial pressure of elemental sulfur in the gas phase is determined.

As initial data for the calculation, the following are usually chosen: the composition of the concentrate and quartz flux, the copper content in the matte, the Fe/SiO2 ratio in the slag, the degree of enrichment of the blast with oxygen, and the operating temperature of the process.

The underburning of sulfur in the gas phase and the corresponding adjustment of the oxygen consumption for smelting, due to their influence on the heat balance, are important for the correct choice of the technological regime of the autogenous process. These circumstances should strongly affect the melting of high-sulfur copper concentrate with copper-lead matte, which has an interest from the point of view of extracting copper and associated metals into targeted products. Note that the proposed calculation method is applicable for autogenous smelting of sulfide raw materials and the process of converting pure copper mattes together with high-sulfur copper concentrate.

Mentioned traditional method for calculating autogenous melts does not take into account the interaction between the components of the products formed during the smelting process - matte, slag and the gas phase, which can change the amount of heat release and the structure of the heat balance. This condition has direct relevance when performing calculations for the conditions of converting complex composition copper-lead mattes with high-sulfur copper concentrate. In this case, calculations have to consider that due to the existence of equilibrium according to reaction (5), part of the elemental sulfur formed as a result of the dissociation of higher sulfides does not burn out, but it is almost completely absorbed by the melt and is spent on slag sulfiding. Along with this, in the calculations it is also necessary to take into account the contribution to the heat balance of the 1st converting period, heat release from the oxidation reactions of PbS and ZnS, which are present in a significant amount in the matte. Thus, the complication of the mechanism of phase formation makes it necessary to consider, along with the main processes 1-3 considered above, the occurrence of additional processes 4, 5 in the slag melt:

4. Sulfidation of oxides of non-ferrous metals, iron and associated metal impurities with elemental sulfur released by reactions (1) and (2):

$$2MeO + 3/2S_2 = 2MeS + SO_2, \quad (7)$$
$$(Me - Cu, Pb, Zn, As, Sb, Fe).$$
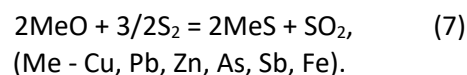
5. Interactions between oxides and sulfides of non-ferrous metals and iron according to exchange reactions:

$$Me^1O + Me^2S = Me^1S + Me^2O. \quad (8)$$
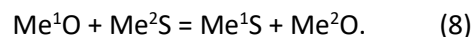
The interaction of sulfur with magnetite cannot be neglected either:

$$2Fe_3O_4 + 1/2S_2 = 6FeO + SO_2, \quad (9)$$

as a result of which the equilibrium content of magnetite in the slag is established.

The reliability of the assumptions was verified by a comparative analysis of the results of temperature fluctuations and the composition of the converting products (matte, slag), obtained by calculation and direct measurements of the technological

parameters of converting copper-lead mattes in the industrial scale.

For technological calculations, an iterative algorithm for modeling the process of converting copper-lead mattes was used, which allows predicting the optimal parameters and thermal conditions of the converting process with a sufficiently high accuracy.

Temperature measurements of converter slags during their discharge and melts during each loading of a new portion of matte in the plant were carried out using an HD 1150A optical pyrometer. The results of measurements of the temperature and compositions of the converting products, obtained by calculation and direct measurements in the factory, showed their good consistency.

The developed modeling algorithm was used to estimate the heat balance of converting copper-lead mattes together with high-sulfur copper concentrate.

The reliability of the model was checked based on a comparative analysis of the predicted temperature and compositions of slag and matte with those measured in an industrial scale. Temperature variations observed in the conditions of converting copper-lead mattes for four charges of the converter with matte, obtained in the plant, and during the joint smelting of high-sulfur copper concentrate with copper-lead matte, are shown in Fig.2.

It can be seen that with the existing technology for converting copper-lead mattes, strong temperature fluctuations are observed - from 1027 ^{0}C to 1300 ^{0}C (Fig. 2(A)). This indicates that the converter is operated in the intense thermal load mode. Fluctuations in the temperature regime reduce the stability of the converter, and, as a result, lead to a reduction in its service life.

During the joint processing of the concentrate with the matte, the temperature variation is insignificant, which is between 1120 ^{0}C and 1270 ^{0}C (Fig. 2(B)). Process temperature equalization ensures converter stability, performance and extended converter life.

Despite the small number of measured temperatures, it can be seen that the model prediction is justified for the composition of the slag. The predicted temperatures of matte and slag, according to existing technology, are usually subject to significant fluctuations, which is in good agreement with the measured temperatures. Comparative analysis of the predicted composition of the slag and the content of silica in it (Table 1), taking into account the uncertainty in the weight of added materials at the plant allows to conclude that the developed model predicts the iron content well in the slag. However, the tendency to underestimate the silica content and overestimate the iron content suggests that more material flows are being added to the converter than expected during operation.

Table 1 shows the comparative results of the measured and predicted technological indicators for the content of iron and silica in white matte and converter slags selected during the research.
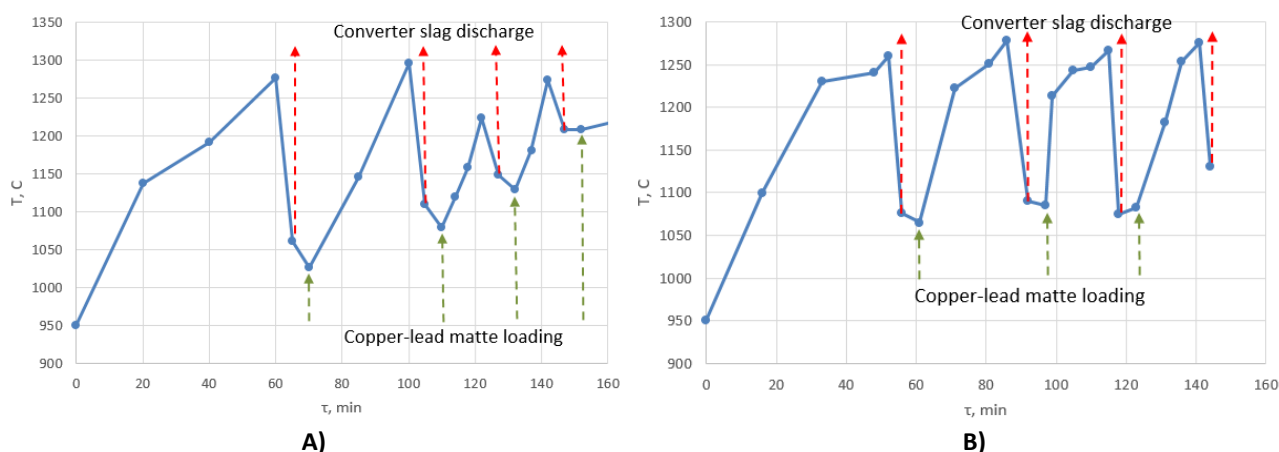

Figure 2 - Dynamics of changes in the temperature regime of the 1st period
of copper-lead matte converting:

A) - according to the existing technology;
B) - with the addition of high-sulfur copper concentrate.

Table 1 - Comparative analysis of the compositions of the products of converting of copper-lead mattes of the 1st period

Products	Chemical composition, wt. %							
	Cu	Pb	Zn	Fe	As	Sb	S	SiO$_2$
Copper lead matte	35.5	26.0	1.4	15.1	2.8	0.7	15.0	
Quartz flux	-	-	-	-	-	-	-	85.0
Copper concentrate	24.5	2.5	3.4	28.6	0.1	0.2	35	3.6
White matte	56.4	20.9	0.2	3.5	3.6	1.0	13.5	-
	70.6	4.0	0.2	2.9	0.6	0.6	18.2	
Converter slag	7.9	22.3	2.1	24.7	2.4	0.6	-	22.3
	1.2	0.7	0.2	47.8	0.3	0.2		26.8
Converter dust	1.1	55.7	0.8	2.6	5.2	0.8	5.9	1.1
	0.8	58.9	8.7	0.4	5.3	1.3	10.0	0.3

The numerator is existing technology;   **The denominator** is new technology.

Table 2 - Dynamics of changes in the content of SO$_2$ in waste gases

№	Discharge #	Existing technology		New technology	
		(Cu), %	SO$_2$, %	(Cu), %	SO$_2$, %
1	Discharge #1	4.07	5.07	1.09	8.35
2	Discharge #2	3.91	6.5	0.58	9.02
3	Discharge #3	4.34	6.08	1.47	11.26
4	Discharge #4	11.94	7.5	0.39	12.95

Table 3 - Material balance of the 1st converting period of copper-lead matte according to the existing technology

Name	Products output		Cu		Pb		Zn		Fe		As		Sb		S		SiO$_2$	
	%	t	%	t	%	t	%	t	%	t	%	t	%	t	%	t	%	t
Matte	57.4	100	35.5	35.5	26	26	1.4	1.42	15.2	15.2	2.8	2.8	0.7	0.7	15.1	15.1		
Blowing	36.0	62.7																
Quartz flux	6.58	11.5															85	9.7
Total:	**100**	**174.2**		**35.5**		**26.0**		**1.42**		**15.2**		**2.8**		**0.7**		**15.1**		**9.7**
White matte	29.8	51.8	66.5	34.5	4.5	2.34	0.1	0.07	6.02	3.1	3.8	1.9	0.3	0.1	14.6	7.6		
Converter slag	25.7	44.7	2.23	1.0	32.0	14.3	0.9	0.40	26.6	11.9	0.7	0.4	0.6	0.3			20.7	9.3
Dust	8.23	14.3	0.12	0.02	65.1	9.3	6.6	0.94	0.92	0.1	3.7	0.5	2.2	0.3	5.26	0.7	3.40	0.4
Exhaust gases	36.3	63.2													10.7	6.8		
Total:	**100**	**174.2**		**35.5**		**26.0**		**1.42**		**15.1**		**2.8**		**0.7**		**15.1**		**9.7**

It can be seen that after sulfiding converter slag with high-sulphur copper concentrate, its quality is significantly improved compared to converter slag obtained by the existing technology. The content of copper in the slag is reduced by more than 6 times. The lead content is significantly reduced: from 22% to 0.72%, which indicates the almost complete sublimation of lead into dust. The content of zinc and arsenic is reduced by 10 times, antimony - by 3 times. Deep sublimation of impurities into dust removes them from the general technological chain, which as a result will significantly improve the quality of the resulting targeted products.

The results of calculations of the gas phase, obtained by the model, showed that under the conditions of converting the concentrate with the matte, the stabilization of the temperature regime in the converter allows increasing the SO$_2$ content in gases by more than 1.5 times (Table 2), and maintain

Table 4 - Material balance of the 1st converting period of copper-lead mattes together with high-sulphur copper concentrate

Name	Products output		Cu		Pb		Zn		Fe		As		Sb		S		SiO$_2$	
	%	t	%	t	%	t	%	t	%	t	%	t	%	t	%	t	%	t
Matte	56.9	100.0	35.5	35.5	26.0	26.0	1.4	1.42	15.2	15.2	2.8	2.8	0.7	0.7	15.1	15.1		
Blowing	31.3	54.9																
Quartz flux	5.57	9.8															85	8.3
Cu concentrate	6.20	10.9	23.6	2.6	2.5	0.3	3.4	0.37	28.6	3.1	0.1	0.01	0.2	0.02	31.9	3.5	3.6	0.4
Total:	**100**	**175.6**		**38.1**		**26.3**		**1.79**		**18.3**		**2.8**		**0.7**		**18.6**		**8.7**
White matte	36.3	63.8	59.5	37.9	14.2	9.1	0.1	0.08	5.47	3.5	5.2	1.9	0.4	0.1	13.6	8.8		
Converter slag	18.9	33.2	0.2	0.07	18.6	6.2			38.1	12.7	0.2		1.3	0.3			24.1	8.0
Dust	11.0	19.4	0.1	0.02	57.0	11.0	8.8	1.71	10.9	2.1	8.0	0.9	3.1	0.3	4.80	0.9	3.5	0.7
Exhaust gases	33.7	59.2													15.1	8.9		
Total:	**100**	**175.6**		**38.1**		**26.3**		**1.79**		**18.3**		**2.8**		**0.7**		**18.6**		**8.7**

Figure 3 - The structure of the heat balance of converting copper-lead mattes:
A) - according to the existing technology;
B) - with the addition of high-sulfur copper concentrate

the optimal level throughout 1st converting period. This ensures the stability of the sulfuric acid plant.

Tables 3 and 4 show the material balances of the 1st converting period of copper-lead mattes according to the existing technology and in their joint processing with high-sulfur concentrate, calculated according to practical plant data: ratio (Fe)/(SiO$_2$)=1.3, the degree of enrichment of the blast with oxygen is 23%, the operating temperature is 1523 K. Zyryanovsky high-sulfur copper concentrate was used as a sulfiding agent.

Figure 3 shows the structures of the heat balances of the 1st period of converting copper-lead matte according to the existing technology and the

joint smelting of matte with high-sulfur copper concentrate, calculated on the basis of the corresponding material balances (Tables 3, 4).

It is easy to see that the total heat per 100 kg of charge (matte + concentrate), equal to 259221.56 kJ, only slightly exceeds the value of the total heat of converting copper-lead mattes using the existing technology, which is 239551.45 kJ. At the same time, a significant change in the structure of the heat balance of converting during the joint smelting of the concentrate together with the matte looks very attractive (Fig. 3 (B)). The change in the ratio of the articles of heat input can be interpreted by the complete assimilation of elemental sulfur by the melt and sulfidation of the slag. A significant contribution to the change in the structure of the total heat balance during the joint converting of the concentrate with matte is made by an additional amount of iron sulfide introduced with the concentrate, the oxidation of which "closes" the heat balance of converting.

Thus, the calculation method proposed in this paper, which takes into account the presence and behavior of elemental sulfur and the additional amount of iron sulfide introduced with high-sulfur copper concentrate, can be used to refine the material and heat balances of converting during the joint processing of high-sulfur copper-containing concentrates and products with copper-lead mattes.

Conclusions

1. When calculating the conversion of copper-lead mattes together with a high-sulfur concentrate, it is necessary to take into account the presence of elemental sulfur, which is almost completely consumed for the sulfiding of slag metal oxides.

2. On the example of direct processing of concentrate in converters, a comparative analysis of the heat balances of two oxidizing melts was carried out: converting copper-lead matte according to the existing technology, and joint melting of Zyryanovsky high-sulfur copper concentrate with copper-lead matte. It is shown that in the second case there is a strong change in the structure of the heat balance towards improvement due to the process of sulfiding of the slag and oxidation of an additional amount of FeS introduced with the concentrate.

3. Comparative analysis of the technological parameters of the 1st converting period of copper-lead mattes calculated by the proposed method with the practical data of a particular metallurgical unit allows to assess the degree of approximation of the processes occurring in the unit until the thermodynamic equilibrium.

4. For a more accurate prediction of the heat balance of converting copper-lead mattes together with high-sulfur copper concentrate, it is necessary to know the activity values of magnetite, sulfides and oxides of non-ferrous metals in complex multicomponent sulfide melts.

Мыс-қорғасын штейнін жоғары күкіртті мыс концентратымен бірге конвертерлеудің жылу режимін талдау

Жолдасбай Е.Е., Арғын А.Ә., Досмұхамедов Н.Қ.

Сәтбаев университеті, Алматы, Қазақстан

ТҮЙІНДЕМЕ

Жұмыста бұрын жасалған жоғары күкіртті мыс концентраттарын мыс-қорғасын штейнімен бірлесіп тікелей өңдеу мүмкіндігі туралы қорытындылар негізінде конвертерлеудің жылу режиміне талдау жүргізілді. Автогенді балқымаларды есептеу үшін қолданылатын дәстүрлі есептеу әдістері толығымен дұрыс емес және артық күкірттің процестің температуралық режиміне әсерін ескеруді қажет етеді. Мыс-қорғасын штейндерін конвертерлеу процесінде температураның өзгеруінің кең диапазоны бар екендігі анықталды – 1027 ⁰C-тан 1300 ⁰C-қа дейін. Концентратты штейнмен бірге конвертерлеу кезінде процестің температуралық режимі тұрақтандырылады, бұл күкірт қышқылын өндіруге қажетті газдардағы SO_2 концентрациясының оңтайлы деңгейін қамтамасыз етеді. Қолданыстағы технология бойынша және концентратты қосып мыс-қорғасын штейндерін конвертерлеудің материалдық балансын есептеу негізінде конвертерлеу процесінің жылу балансының құрылымы белгіленді. Жылу балансының құрылымының едәуір өзгерісі көрсетілген, бұл магнетиттің артық күкіртпен ыдырауымен және концентратпен енгізілген темір сульфидінің қосымша мөлшерінің тотығуымен жылудың жоғарылауымен түсіндіріледі. Нақты металлургиялық агрегаттың практикалық деректерімен мыс-қорғасын штейндерін конвертерлеудің 1-ші кезеңін ұсынылған әдістеме бойынша есептелген технологиялық параметрлерін салыстырмалы талдауы ондағы процестердің термодинамикалық тепе-теңдікке жақындау дәрежесін бағалауға мүмкіндік береді.

Түйін сөздер: мыс-қорғасын штейні, жоғары күкіртті мыс концентраты, конвертерлеу, материалдық баланс, жылу режимі, күкірт, сульфидтеу.

Жолдасбай Ержан Есенбайұлы	*Авторлар туралы ақпарат:* *PhD, Satbayev University, 050013, Алматы, Сатпаев көш. 22, Қазақстан. E-mail: zhte@mail.ru*
Арғын Айдар Әбділмәлікұлы	*PhD, Satbayev University, 050013, Алматы, Сатпаев көш. 22, Қазақстан. E-mail: aidarargyn@gmail.com*
Досмухамедов Нурлан Калиевич	*Т.ғ.к., Профессор. Satbayev University, 050013, Алматы, Сатпаев көш. 22, Қазақстан. E-mail: nurdos@bk.ru*

Анализ теплового режима конвертирования медно-свинцового штейна совместно с высокосернистым медным концентратом

Жолдасбай Е.Е., Аргын А.А., Досмухамедов Н.К.

Satbayev University, Алматы, Казахстан

АННОТАЦИЯ

В работе на основании ранее сделанных выводов о возможности прямой переработки высокосернистых медных концентратов совместно с медно-свинцовым штейном проведен анализ теплового режима конвертирования. Показано, что традиционные методы расчета, применяемые для расчета автогенных плавок не совсем корректны, и требуют учета влияния избыточной серы на температурный режим процесса. Установлено, что в процессе конвертирования медно-свинцовых штейнов наблюдается широкий диапазон варьирования температуры – от 1027 ⁰C до 1300 ⁰C. При совместном конвертировании концентрата со штейном температурный режим процесса стабилизируется, что обеспечивает оптимальный уровень концентрации SO_2 в газах, необходимый для производства серной кислоты. На основании расчета материального баланса конвертирования медно-свинцовых штейнов по существующей технологии и с добавлением концентрата установлена структура теплового баланса процесса конвертирования. Показано сильное изменение структуры теплового баланса, который объясняется восстановлением магнетита избыточной серой и увеличением тепла за счет окисления дополнительного количества сульфида железа, вводимого с концентратом. Сравнительный анализ рассчитанных по предлагаемой методике технологических параметров 1-го периода конвертирования медно-свинцовых штейнов с практическими данными конкретного металлургического агрегата позволяет оценить степень приближения протекающих в нем процессов к термодинамическому равновесию.

Ключевые слова: медно-свинцовый штейн, высокосернистый медный концентрат, конвертирование, материальный баланс, тепловой режим, сера, сульфидирование.

Жолдасбай Ержан Есенбайулы	*Информация об авторах:* *PhD, Satbayev University, 050013, Алматы, ул. Сатпаева 22, Казахстан. E-mail: zhte@mail.ru*
Аргын Айдар Абдилмаликулы	*PhD. Satbayev University, 050013, Алматы, ул. Сатпаева 22, Казахстан. E-mail: aidarargyn@gmail.com*
Досмухамедов Нурлан Калиевич	*К.т.н., Профессор. Satbayev University, 050013, Алматы, ул. Сатпаева 22, Казахстан. E-mail: nurdos@bk.ru*

References

[1]   Rosello A, Martinez J, Barrios P, Carrillo F. Desulfurization rate during the copper blow in a Peirce-Smith converter. Metallurgical and Materials Transactions. 2008; 39B:16-22.

[2]   Vieira L, Guzzo M, Bittencourt Marques M, de Souza M, Merdjani R, Kongoli F. Optimization and Control of Hoboken Converter Operations With FLOGEN CONTOP Control Expert System. Sustainable Industrial Processing Summit SIPS. Barrios Intl. Symp. Non-ferrous Smelting & Hydro/Electrochemical Processing. Montreal, Canada. 2017; 1:91-92.

[3]   Schlesinger ME, King MJ, Sole KC, Davenport WG. Extractive Metallurgy of Copper. 2011.

[4]   Bulatov KV, Skopov GV, Skopin DYu, Yakornov SA. Processing of Polymetallic Concentrates in Melting Facility "Pobeda" (LLC "Mednogorsk Copper-Sulfur Combine"). Non-ferrous Metals. 2014; 10:39-44.

[5]   Orlov AK, Konovalov GV, Boduen AYa. Pyrometallurgical Selection of Copper-Zinc Materials. Journal of Mining Institute. 2011; 192:65-68.

[6]   Wang, S, Davenport W. World copper smelter data. In Copper 2019, Paper no 595947. Vancouver, BC: CIM, Montreal. 2019.

[7]   Taskinen P, Akdogan G, Kojo I, Lahtinen M, Jokilaakso A. Matte converting in copper smelting. Mineral Processing and Extractive Metallurgy. 2019; 128(1-2):58-73. https://doi.org/10.1080/25726641.2018.1514774

[8]   Liu Z, Xia L. The practice of copper matte converting in China. Mineral Processing and Extractive Metallurgy. 2019; 128:117–124. https://doi.org/10.1080/25726641.2018.1543147

[9]   Zhai X, Li N, Zhang X, Fu Y, Jiang L. Recovery of cobalt from converter slag of Chambishi copper smelter using reduction smelting process. Trans Nonferrous Met Soc. China. 2011; 21(10):2117-2121.

[10] Dosmukhamedov N, Egizekov M, Zholdasbay E, Kaplan V. Metals Recovery from Converter Slags Using a Sulfiding Agent. JOM. 2018; 70(10):2400-2406.

[11] Dosmukhamedov NK, Fedorov AN, Zholdasbay EE, Argyn AA. Investigation of Cu, Pb, Zn, As, Sb Distribution during the lead semiproducts and copper-zinc concentrate comelting. Non-ferrous Metals. 2020; 1:8-14. https://doi.org/10.17580/nfm.2020.01.02

[12] Dosmukhamedov NK, Argyn AA, Zholdasbay EE, Kurmanseitov MB. Behavior of Cu, Zn, Pb, As compounds during copper-zinc concentrate and matte comelting in converters. Non-Ferrous Metals. 2020; 2(49):11-18.

[13] Dosmukhamedov NK, Argyn AA, Zholdasbay EE. Behavior of copper compounds and associated metal impurities in the process of converting copper-lead mattes. Collection of scientific articles of the Interuniversity Scientific Congress "Higher School: Scientific Research". Moscow, Russia. 2020, 127-139.

[14] Sohn HS, Fukunaka Y, Oishi T. Yazawa Int. Symp.: Metallurgical and Materials Processing. Principles and Technologies (I), Kongoli F, Itagaki K, Yamauchi C, and Sohn HY, eds., TMS, Warrendale, PA. 2003, 131-146.

[15] Demetrio S, Ahumada J, Durán MA, Mast E, Rojas U, Sanhueza J. Slag Cleaning: The Chilean Copper Smelter Experience. JOM. 2000, 20-25.

[16] Cardona N, Mackey PJ, Coursol P, Parada R, Parra R. Optimizing Peirce–Smith Converters Using Thermodynamic Modeling and Plant Sampling. JOM. 2012; 64(5).

[17] Coursol P, Tripathi N, Mackey P, Leggett T. Can. Met. Quart. 2010; 49(3):255-262.

[18] Montenegro V, Sano H, Fujisawa T. Recirculation of high arsenic content copper smelting dust to smelting and converting processes. Minerals Engineering. 2013; 49:184-189.

[19] Swinbourne DR, Kho TS. Computational Thermodynamics Modeling of Minor Element Distributions During Copper Flash Converting. Metallurgical and Materials Transactions. 2012; 43B:823-829.

[20] Kubashevsky O, Alcock SV. Metallurgical thermochemistry. M.: Metallurgy. 1982.

[21] A.S. USSR 1534081. Device for supplying fine materials to a converter with a lateral gas outlet / Dosmukhamedov NK, Egizekov MG, Spitchenko VS et al. Opubl. 1990, 1.

[22] Bagrova TA, Vaskevich AD, Zaitsev VYa, Kukoev VA. Homogeneity range and activity of the components of iron-silicate melts containing CaO and Al_2O_3. Nonferrous metals. 1985; 2:7-10.

[23] Yazawa A. Can. Metal. Quart. Thermodynamic considerations of Copper smelting. 1974; 13:443-453.

[24] Vaskevich AD, Sorokin ML, Kaplan VA. General thermodynamic model of copper solubility in slags. Nonferrous metals. 1982; 10:22-26.

[25] Bellemans I, De Wilde E, Moelans N, Verbeken K. Metal losses in pyrometallurgical operations - A review. Advances in Colloid and Interface Science. 2018; 255:47-63. https://doi.org/10.1016/j.cis.2017.08.001

[26] Guntoro PI, Jokilaakso A, Hellstén N, Taskinen P. Copper matte-slag reaction sequences and separation processes in matte smelting. Journal of Mining and Metallurgy, Section B: Metallurgy. 2008; 54B:(3):301-11. https://doi.org/10.2298/JMMB180214021G

Analytical Review of Conductive Coatings, Cathodic Protection, and Concrete

[1*]Ainakulova D.T., [1]Muradova S.R., [2]Khaldun M. Al Azzam, [3]Bekbayeva L.K., [4]Megat-Yusoff P.S.M, [5]Mukatayeva Z.S., [6]Ganjian E., [1,7]El-Sayed Negim

[1] School of Materials Science and Green Technologies, Kazakh-British Technical University, Almaty, Kazakhstan
[2] Pharmacological and Diagnostic Research Centre (PDRC), Faculty of Pharmacy, Al-Ahliyya Amman University, Amman 19328, Jordan
[3] National Nanotechnology Open Laboratory, Al-Faraby Kazakh National University, Almaty, Kazakhstan
[4] Universiti Teknologi Petronas, Bandar Seri Iskandar 31750, Perak, Malaysia
[5]Institute of Natural Science and Geography of KazNPU named after Abai, Almaty, Kazakhstan
[6]Concrete Corrosion Tech LTD, 12 Humphrey Middlemore Drive, Birmingham, England B17 0JN
[7]School of Petroleum Engineering, Satbayev University, Almaty, Kazakhstan

* Corresponding author email: da_ainakulova@kbtu.kz

ABSTRACT

The principal and most expensive type of degradation that currently affects the performance of reinforced concrete bridge constructions is the corrosion of steel reinforcement. Strong financial losses result from the corrosion of reinforced concrete structures. One popular technique for preventing corrosion in reinforced concrete structures is cathodic protection. Since it can give necessary current in a situation where reinforced concrete buildings have high resistance, impressed present cathodic protection (ICCP) provides strength and adaptability. Conductive coatings, discrete anode systems, titanium-based mesh in cementitious overlay, conductive overlay with carbon fibers, and flame-sprayed zinc are examples of anode materials that are often used for impressed current cathodic (ICC). Chloride ions, in particular, are exceedingly difficult to permeate through a continuous epoxy coating on steel, making an epoxy coating a very effective barrier to these hostile chemicals. Epoxy resins are a great option for shielding metal surfaces from the environment and hostile environments because of their outstanding anti-corrosion qualities, good adherence to a variety of surfaces, and chemical resistance. In this work, the cathodic protection, ICCP, various conductive coatings, and epoxy coating as anode material are reviewed.

Keywords: protection, impressed current, reinforced concrete corrosion, epoxy coatings.

Information about authors:

Ainakulova Dana Tulegenkyzy	*Ph.D. student at Materials Science and Technology of New Materials, School of Materials Science and Green Technologies, Kazakh-British Technical University, st. Tole bi 59, 050000, Almaty, Kazakhstan. Email: da_ainakulova@kbtu.kz*
Muradova Sabina Rustamkyzy	*Master's Degree in Materials Science and Technology of New Materials, School of Materials Science and Green Technologies, Kazakh-British Technical University, st. Tole bi 59, 050000, Almaty, Kazakhstan. Email: sab.muradova.01@mail.r*
Khaldun M. Al Azzam	*Ph.D., Associate Professor Department of Pharmaceutical Sciences, Pharmacological and Diagnostic Research Center (PDRC), Faculty of Pharmacy, Al-Ahliyya Amman University, Amman 19328, Jordan. Email: azzamkha@yahoo.com*
Bekbayeva Lyazzat Kairatovna	*Ph.D., Lecturer at National Nanotechnology Open Laboratory, Al-Faraby Kazakh National University, 71, Al-Faraby av., 050040, Almaty, Kazakhstan, Almaty, Kazakhstan. Email: lyazzat_bk2019@mail.ru*
Puteri Sri Melor Megat-Yusoff	*Ph.D., Assistant professor at Mechanical Engineering Department, Universiti Teknologi Petronas, Bandar Seri Iskandar 31750, Perak, Malaysia. Email: puteris@petronas.com.my*
Mukatayeva Zhazira Sagatbekovna	*Candidate of Chemical Sciences, Associate Professor of the Institute of Natural Sciences and Geography of Abai KazNPU. Email: jazira-1974@mail.ru*
Ganjian Eshmaiel	*Ph.D., Professor, Concrete Corrosion Tech LTD, 12 Humphrey Middlemore Drive, Birmingham, England B17 0JN. Email: concorrosion@gmail.com*
Negim Attia El-Sayed	*Ph.D., Professor at School of Materials Science and Green Technologies, Kazakh-British Technical University, st. Tole bi 59, 050000, Almaty, Kazakhstan. Professor at Geology and Oil-gas Business Institute named after K. Turyssov, Department of Petroleum Engineering, Satbayev University, Almaty, Kazakhstan. Email: a.negim@kbtu.kz*

Introduction

One of the major issues contributing to significant economic losses worldwide is metal corrosion. Due to the early collapse of structural elements, corrosion of metals in engineering equipment might result in accidents [1]. Concrete structures, like all building materials, are gradually and irreversibly destroyed. This happens not only under the yoke of time but also because of many factors. Corrosion destruction is one of the

significant reasons for the decrease in durability and damage to reinforced concrete structures. External and internal influences on concrete lead to the destruction of the structure of the hardened mixture and the loss of quality characteristics such as strength, density, and so on. In simpler terms, they lead to the corrosion of concrete. Corrosion of concrete is the process of destruction of the structure of concrete and its embrittlement under the influence of environmental factors. It occurs under the influence of some aggressive substance, and the penetration of this substance into the concrete structure through the pores or cracks of the concrete structure. An adverse setting refers to the consequences of water and cold temperatures, the process of dampening and subsequent drying of concrete, as well as the effects of both clean and mineral-laden waters [[1], [2]].

Since it might eventually affect structural performance and integrity, steel corrosion in concrete structures is still considered the major obstacle in the construction industry. When steel in a concrete building deteriorates as a result of exposure to a corrosive environment, corrosion takes place [2]. Corrosion is an electrochemical process. Steel's mechanical qualities, specifically its bond strength, deteriorate due to rust. The most significant issue is how to prevent corrosion in structures made of concrete and reinforced concrete, and finding a solution will help structures, buildings, and structures used for a variety of functions last longer. For diverse technological domains, there are numerous strategies to stop metals from corroding [3].

One popular technique for preventing corrosion in reinforced concrete structures is cathodic protection. Cathodic protection is considered a technique used to stop corrosion occurring in metal surfaces, which involves making a metal surface the cathode of an electrochemical cell. Bridges and jetties are two reinforced concrete constructions that may be repaired using the embedded cathodic steel reinforcement from this process. Nonetheless, of the amount of chloride present in the concrete, it has been demonstrated that this approach prevents corrosion from occurring in reinforced concrete structures [3]. By cathodic polarizing a metal surface that has rusted, cathodic protection (CP) slows down corrosion [4].

Anodes connected to a power source that continually produces electrical flow make up systems for influenced current cathodic protection. In the sacrificial anode method of protection, active metals other than the base metal are utilized to "sacrifice" ions. These "sacrificial anodes" have a higher electrochemical potential than typical alloys like magnesium, aluminum, or zinc. When compared to a sacrificial anode, this technique frequently presents substantially longer protection. An endless power source powers the anode [4].

The ICCP consists of a monitoring system, an anode system that corrodes slowly, and an outer current power source that pushes a small amount of electric current during the reinforcing steel to balance the current flow from the effect of corrosion. Although RC structures may be repaired using any of the two CP systems, the ICCP system offers more adaptability and durability due to its current output's ability to be changed to generate the required current in situations of high concrete structure resistivity [5].

Conducive coatings, independent anode systems, titanium-based mesh in cementitious overlay, conductive overlay with carbon fibers, and flame-sprayed zinc are some examples of anode components for the ICCP system [5]. The selection of anode materials, which is largely based on the life cycle of the structures, the kinds of corrosion and structure, anode installation techniques, operation, the requirement for routine maintenance, and the life cycle price of the CP system, has not yet been proven to be efficient and appropriate for the majority of anodes currently in use [6]. Epoxy-based materials are considered one of the best in the line of anti-corrosion materials. They have excellent adhesion to ferrous metals, many types of plastics, and glass [7].

Coatings are traditionally distinguished by high protective properties, hardness, chemical resistance, excellent water resistance, and resistance to oil products. Materials of this group of chemical curing, as a result of which they are resistant to solvents and petroleum products, the coating film does not soften under the influence of high temperatures [8].

Epoxy resins have high adherence to metals and are resistant to halogens, and some acids (strong acids, particularly oxidizing acids, have poor resistance). Various types of glue, plastics, electrical insulating varnishes, and textolite (glass and carbon fiber plastics) are prepared from epoxy resins. Epoxy resins are promising products for the production of anti-corrosion coatings. Coatings based on them are characterized by high hardness, abrasion, and chemical resistance, and excellent adhesion to various substrates [9].

Corrosion process in Reinforced Concrete Structures

Typically, the alkaline concrete environment passivates the reinforcing steel in concrete, shielding it from corrosion. Environmental factors, however, have the potential to eliminate the passivating layer from the surface of steel, cause substantial corrosion in reinforced concrete structures, and take away the passivating layer from the surfaces of steel [10].

There are some main reasons why steel in concrete passivates and corrodes. First of all, the pH of the concrete where the rebars are inserted is decreased by atmospheric carbon dioxide consumption. If the pH drops below 11, corrosion might begin. This process is known as the carbonation of the concrete overlay.

Secondly, chloride infiltration of the concrete overlay, such as that caused by exposure to seawater or deicing salts. Chloride intrusion can be brought on by direct contact with de-icing salts on surfaces like bridge decks, balconies, and pavement as well as by aerosols from bridge decks and roadways on nearby civil buildings [10].

Depassivation of the reinforcing steel causes the establishment of a local corrosion cell that works similarly to the battery (Figure 1). Local areas that have been depassivated serve as anodes and passive areas serve as cathodes. Rust is produced when oxygen is reduced to hydroxyl ions at the cathodic sites and iron is oxidized at the anodic sites. Chlorides cause pitting corrosion, which can cause the rebars to deteriorate quickly and lose their integrity in localized areas. Carbonation causes regular corrosion on the steel surface, but this process is rather slow. Particularly, corrosion brought on by carbonation results in the production of several corrosion products, which weaken and break the concrete overlay [10].
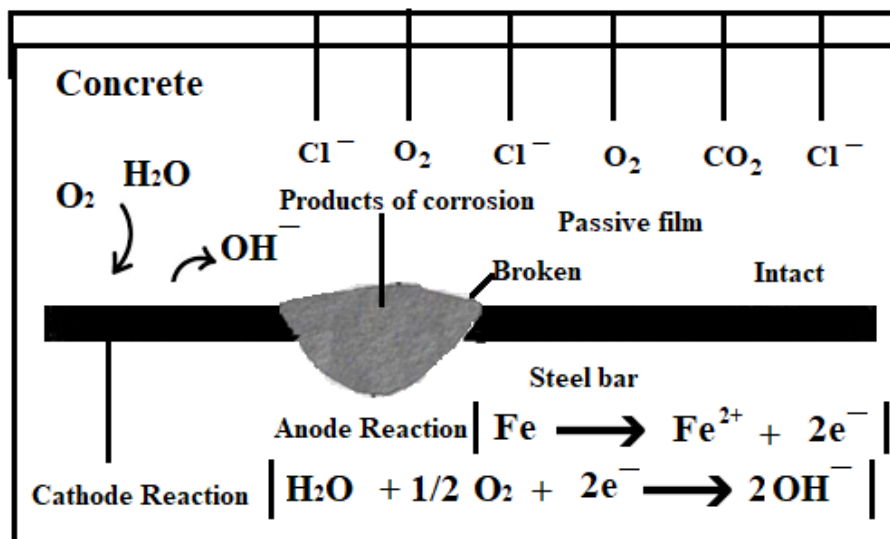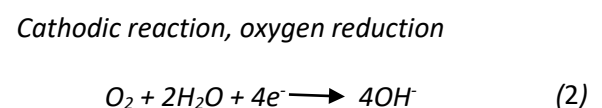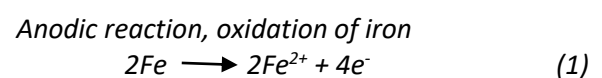

Figure 1 - Schematic image of a corrosion cell

Steel corrodes in concrete structures when it starts to degrade after being exposed to an environment that can do so [11]. When a structure is subjected to corrosion, current leaves it at the anode site, moves across an electrolyte, and then returns to it at the cathode site. The electrolyte, a liquid that conducts electricity, is utilized to transfer electrons from the anode to the cathode [12]. Figure 2 shows a visual representation of the corrosion that occurs in the steel process at the anode and cathode.

Electrochemical reactions, such as the oxidation of iron, can be used to characterize corrosion. These electrochemical reactions are anodic (produce electrons). The electrolyte's characteristics influence the cathodic process, which consumes electrons.

The oxygen reduction cathodic reaction is what causes corrosion in concrete. Steel corrosion in concrete has the following reactions as
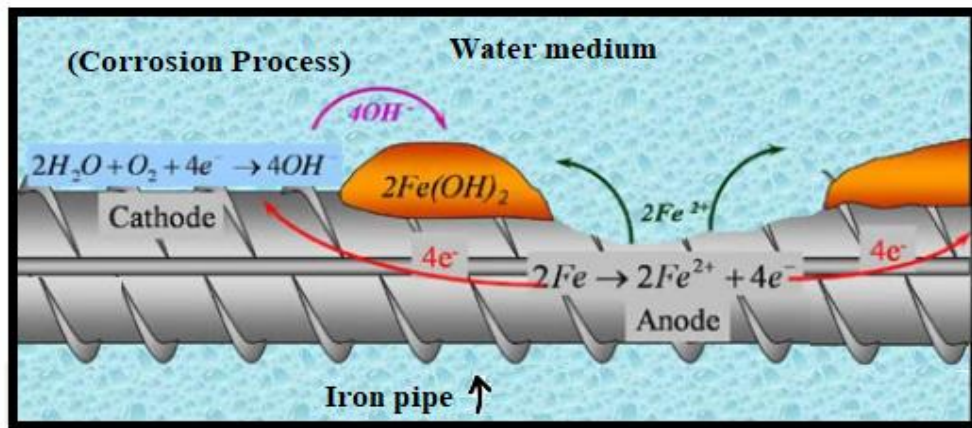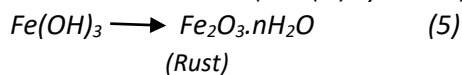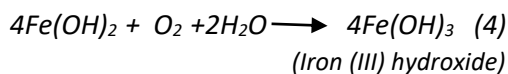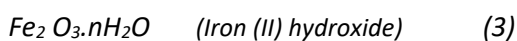
Anodic reaction, oxidation of iron
$$2Fe \longrightarrow 2Fe^{2+} + 4e^{-} \qquad (1)$$

Cathodic reaction, oxygen reduction

$$O_2 + 2H_2O + 4e^{-} \longrightarrow 4OH^{-} \qquad (2)$$

Figure 2- Diagram of the corrosion occurring in the corrosion process

Simultaneous reactions occur in the cathodic and anodic zones on the surface of steel. An exposed steel surface in concrete that forms an electrochemical cell is referred to as a corrosion system. A cathodic and anodic region, an electron conductor (rebar), an ion conductor (electrolyte), and a conductor for ions make up an electrochemical cell. Concrete pore water serves as an electrolyte [13].

Iron (II) hydroxide is created by combining two distinct processes, as shown in equation (3), while iron (III) hydroxide is created by additional oxidation, as shown in equation (4). Iron (III) hydroxide is shown to dehydrate in equation (5) to generate $Fe_2O_3 \cdot nH_2O$, also known as rust. These are the equations written as,

$$Fe_2 O_3 \cdot nH_2O \qquad (Iron\ (II)\ hydroxide) \qquad (3)$$

$$4Fe(OH)_2 + O_2 + 2H_2O \longrightarrow 4Fe(OH)_3 \quad (4)$$
$$(Iron\ (III)\ hydroxide)$$
$$Fe(OH)_3 \longrightarrow Fe_2O_3 \cdot nH_2O \qquad (5)$$
$$(Rust)$$

Cathodic Protection
Impressed Current Cathodic Protection (ICCP)

In protected concrete constructions, a passive oxide coating stops steel from corroding. However, the oxide coating may become less effective or even disappear due to corrosion brought on by chloride- or carbonation-induced contamination of the concrete around the steel bar. Concrete cracking and spalling may result from additional corrosion

[14]. Corrosion is typically prevented by corrosion-product- or oxygen-adsorbed film (or protective layer), and the rate of corrosion that occurs on steel surfaces can be slowed down by highly alkaline water. Utilizing an existing repair technique, such as cathodic protection, can stop or reduce steel corrosion in RC structures [15].

Cathodic protection offers greater benefits than other methods for restoring RC structures since it requires less time for monitoring and inspections, a wider range of anode systems, and less time for removing concrete and repairing it [16].

The key advantages of cathodic protection over the other anti-corrosion treatment techniques are that it may be used by simply maintaining a dc circuit and that its effectiveness can be monitored continually. A coated structure is frequently treated with cathodic protection to prevent corrosion in potential coating-damaged areas. It can be used to extend the life of existing constructions [17].

By using galvanic (sacrificial) anodes or "impressed" current, cathodic protection can be provided in one of two methods.

Sacrificial Anode Cathodic Protection (SACP)

As displaced in Figure 3, the SACP system is composed of an outside sacrificial anode, such as a metal having a greater potential for the electrode than steel reinforcement, that is electrically linked to another metal that acts as the anode.

However, due to the high concrete resistivity, galvanic anodes typically are unable to economically produce sufficient current. Therefore, the RC

structures are repaired using current cathodic protection (ICCP) [18]. This strategy is thought to be more costly and requires a reliable source of low direct current (DC) power to provide the system with current.

Impressed Current Cathodic Protection (ICCP)

In the situation of ICCP, an external power source is used to initiate a modest amount of current via the reinforcing steel to reverse the flow of the metal, which commonly employs platinum used as a node because of the slow rate of corrosion, as seen in Figure 3. Steel reinforcement in RC structures will accept electrons from the external anode, causing it to become cathodic and so prevent more corrosion [19]. A true system in practical applications often includes a DC power supply, monitoring devices, and cabling [18].

The optimum use for ICCP is in large buildings in which galvanic CP would not create enough current to guarantee total protection. The ICCP is widely utilized in concrete projects due to its improved capacity to deliver high voltages when compared to the SACP. A 1-5A and 2-24V DC power source will normally power each separately controlled anode zone [18]. To permit current to pass and flow through the ICCP, the shielding metal, and anode must be in contact with an electrolytic medium (concrete). Although concrete has a high electrical impedance, the presence of the pore solution, which behaves as an electrolyte, allows current to pass through.

Although it is significant to consider hydrogen embrittlement in steel, alkali-silica reaction in aggregates, and interactions with nearby structures when utilizing the technique, ICCP outperforms the SACP system in terms of flexibility and durability [18].

The ICCP system needs a constant direct current (DC) power supply despite being more effective, in particular, for concrete in high-resistance environments. Furthermore, it is critical to ensure that the anode material used in the ICCP system is a good electrical conductor with a low corrosion rate and mechanical properties, is affordable, is easily produced in a range of shapes, is simple to install, and can handle large current densities [15]. The advantages of ICCP are depicted in Figure 3.
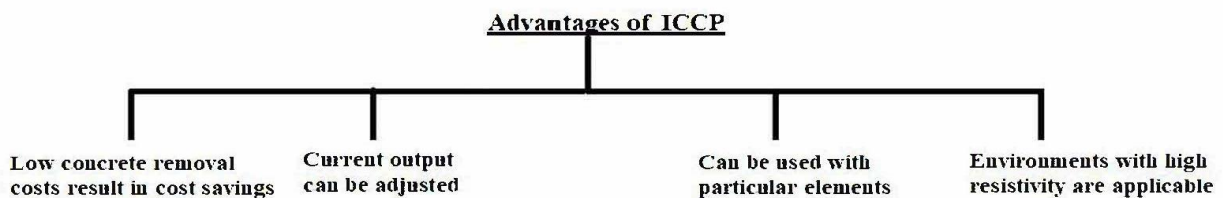

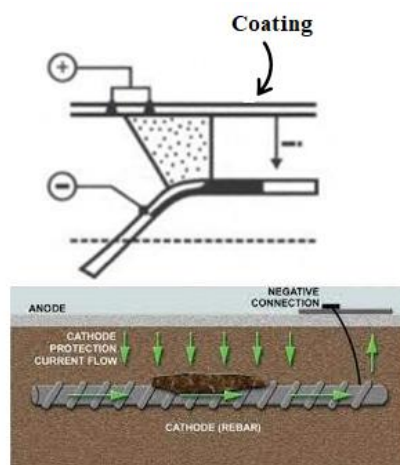**Figure 3** - Advantages of Impressed Current Cathodic Protection (ICCP)

Figure 4 - A schematic diagram of cathodic protection used for the corrosion prevention of rebars steel in concrete: conductive coating

The principle of protection of cathodic using conductive coating is shown schematically in Figure 4.

Applying the polymer/graphite dispersion to the concrete surface will install the anode. The conductive coating is devoted to a secondary anode. The secondary anode's current distribution is controlled by a "primary anode" that is embedded into it at a distance of one to two meters apart and made of materials that can withstand anodic reactions, like platinum-clad titanium, copper-cored niobium, or MMO-titanium. Applying conductive coatings is simple and less expensive [[20], [21], [22], [23]]. Additionally, coatings that conduct conductive can be utilized on any structure of concrete structures.

Conductive Coatings

One of the most popular and well-known anode technologies for the protection of the cathodic of reinforced concrete structures is the conductive-coated anode. It is reasonably simple to maintain and affordable. The installation of anodes at certain locations is necessary for the majority of used systems for the current protection of the cathode. The fundamental drawback of such a solution is poor protective current distribution, which is mostly caused by the anodes' constrained surface area. Additionally, cutting apertures and removing the external concrete layer are relatively expensive construction tasks associated with anode installation. Another issue is the potential harm to anodes during assembly. The majority of issues can be resolved by using conductive coatings as anodes.

The alternative method of solving this issue makes it possible to implement coating and cathodic protection simultaneously, hence enhancing the efficiency of protection. The following benefits come with this solution, such as installation simplicity, the ability to guard difficult-to-reach areas, and the assurance of a sizable anodic system surface permitting similar spreading of the protective current. Additionally, there is a significant decrease in the cost of installing cathodic protection systems (applying coatings is far less expensive than installing anodes in points) [[24], [25]].

The industry is encouraged by the speed of technological advancement to look for improved anode materials for CP systems. Anode materials that are typically utilized for ICCP consist of coatings that are conductive, titanium-based mesh used in cementitious overlays, discrete anode systems, and conductive overlay with carbon fibers [26].

There are two types of coatings as inorganic and organic coatings. The dispersion of zinc dust in an inorganic or organic binder might be spherical, lamellar, or a combination of both [27]. The binder is used to separate organic coatings from inorganic ones, which is frequently epoxy for organic coatings and silicate for inorganic coatings. The most popular technique for preventing the corrosion of metallic elements in transportation and infrastructure is the use of organic coatings [28].

Roller, Brush, or air spray methods are used to apply organic anode coatings to thicknesses of 0.25 to 0.50 mm [29]. Disbandment is a common failure mode that can be brought on by-products obtained from the anodic reaction that may be acidic to the alkaline concrete, causing the coating to lose adhesion [30]. Although wet adhesion and cathodic disbonding resistance can be improved by applying an epoxy coating to a substrate that has already had 3-glycidoxyy propyl silane treatment, Sofian and Noda disagree [31].

Based on the inclusion of pigmentary carbon in a coated polymer matrix, Darowicki *et al.* [32] were given electrochemical tests for conducting coatings. Impedance measurements have been used to calculate the electrochemical characteristics of conducting coatings. Using data from coatings' electric and electrochemical investigations, the following result has been reached. The amount of graphite in coatings affects their electric and electrochemical characteristics. Over 50% of graphite content coatings are distinguished by minimal resistances and potential stability under prolonged anodic polarization.

Nevertheless, they also have worse mechanical qualities, and after 12 days of exposure, they start to become porous. Due to this, high graphite content coatings despite having outstanding electric properties cannot be used to cover concrete. Low barrier qualities and quick increases in resistance and potential during prolonged anodic polarization are characteristics of coatings with tiny graphite concentrations (35% and less). The development of the steel-graphite cell can significantly reduce the electrode potential, indicating the porosity of these coatings [32].

Epoxy Coating as Anode Material

Corrosive substances, especially chloride ions, are effectively blocked by an epoxy coating on steel because the latter will not easily diffuse through a solid epoxy covering. Consequently, the steel surface is shielded.

There are two hypotheses have evolved regarding the protective potential of epoxy-coated reinforcement.

Firstly, acording to the physical barrier theory, the epoxy coating serves as a barrier to keep chloride ions and other abrasive materials from coming into touch with the steel surface.

Secondly, the epoxy coating functions as a high-resistance coating, decreasing corrosion by raising electrical resistance between nearby coated steel sites where cathodic reactions can occur [33].

These two hypotheses provide a convincing justification for the usage of epoxy-coated reinforcement as a safety measure for structures found in marine settings.

The application, however, hasn't received adequate research. Epoxy coating is a top base of concrete, particularly when used as anode material for an ICCP system.

ERs as Anti-Corrosive Coating

The qualities of epoxy resin rely on factors such as resin quality, hardener, and curing circumstances. Figure 5 displays the primary characteristics of epoxy resins.   - High strength. It is this property that has provided a stable demand for epoxy resins for many years. The tensile and compressive strength of the hardened mixture is comparable to the strength of typical grades of heavy concrete.

- Excellent adhesive properties: Epoxy resins have excellent adhesive properties, which, combined with strength, made them an excellent adhesive.

- Good waterproof properties: cured epoxy resin is practically waterproof.

- Resistant to a wide range of aggressive chemicals

- Physical and mechanical parameters at a higher level.

Gujjar SV et al. [33] looked into the best resin coating among the ones currently in use for mild steel surfaces. The resins such as polyurethane, epoxy, phenolic, and polyester) were applied to the mild steel surface using pneumatic spray coating. The corrosion rate and mechanical characteristics of mild steel covered with various resins were also evaluated and compared to a bare steel surface through the execution of numerous experiments (including an immersion test, a salt spray test, a test of tensile strength, and a test of scratch hardness).

It was found that mild steel samples coated using epoxy resin got good corrosion resistance. Epoxy resin-coated mild steel specimens had a considerably higher tensile strength. The surface morphology of the surface of the mild steel specimens covered with epoxy resin exhibits minute rust particles when compared to other resins and plain mild steel. FESEM analysis showed that samples coated with epoxy resin had the least damaged surfaces when compared to other resin-covered surfaces. Epoxy resins were used to create the coated samples, which outperformed samples composed of polyurethane, phenolic, and polyester resins. A polyamide hardener is used to cure the two-component epoxy clear lacquer known as FINECOAT-EP 200. Epoxy resin is considered the ideal resin used for coating mild steel surfaces to block corrosion and improve mechanical properties [33].
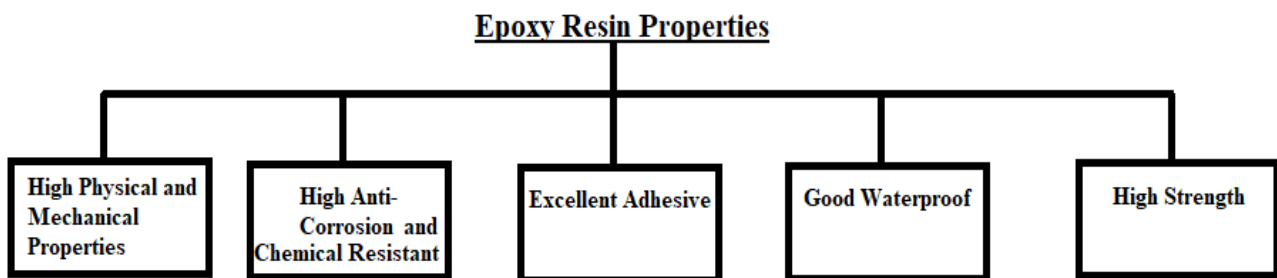

Figure 5 - The main properties of epoxy resins

Conclusions

It is clear from the review that corrosion of concrete reinforcing is a significant problem and must be considered when constructing concrete structures exposed to harsh conditions. One of the main factors harming reinforced concrete (RC) constructions is corrosion of the steel reinforcing the concrete. Designing an effective protection plan requires an understanding of the corrosion process, including its thermodynamic and kinetic characteristics.

One of the most broadly applicable and economically advantageous methods for preventing steel corrosion in reinforced concrete has been demonstrated to be cathodic protection. Conduit coatings can protect difficult-to-reach areas and provide a broad surface area for the anode system to ensure regular distribution of the protective current. They are also simple to install. The cost of installing a cathodic protection system is also significantly reduced since the coating is far less expensive than installing spot anodes. Epoxy coating can be employed as an anode material in an ICCP system owing to its outstanding anti-corrosion and mechanical qualities.

Conflicts of interest. The authors declare no conflicts of interest, financial or otherwise.

Өткізгіш бояуларға, катодты қорғауға және бетонға аналитикалық шолу

[1*]Айнакулова Д.Т., [1]Мурадова С.Р., [2]Халдун М. Аль Аззам, [3]Бекбаева Л.К., [4]Мегат-Юсуф П.Ш.М., [5]Мукатаева Ж.С., [6]Ганжиан Э., [1,7]Негим Эльсайд

[1] Материалтану және жасыл технологиялар мектебі, Қазақ-Британ техникалық университеті, Алматы, Қазақстан
[2] Фармакологиялық және диагностикалық зерттеу орталығы (PDRC), Фармацевтикалық ғылымдар бөлімі, Фармацевтика факультеті, Амман университеті Әл Ахлия, Амман, 19328, Иордания
[3] Нанотехнологиялардың ұлттық ашық зертханасы, Әл-Фараби Қазақ ұлттық университеті, Алматы, Қазақстан
[4] Петронас технологиялық университеті, Бандар-Сери-Искандар 31750, Перак, Малайзия
[5] Абай атындағы ҚазҰПУ, Жаратылыстану және география институты
[6] ЖШҚ «Concrete Corrosion Tech», Хамфри Миддлмор Драйв, 12, Бирмингем, Англия B17 0JN
[7] Қ.Тұрысов атындағы Геология және мұнай-газ ісі институты, Сәтбаев Университеті, Алматы, Қазақстан

ТҮЙІНДЕМЕ

Қазіргі уақытта темірбетон көпір құрылымдарының жұмысына әсер ететін бұзылудың негізгі және ең қымбат түрі-болат арматураның коррозиясы. Темірбетон конструкцияларының коррозиясы айтарлықтай қаржылық шығындарға әкеледі. Темірбетон конструкцияларында коррозияны болдырмаудың қажетті әдістерінің бірі-катодты қорғаныс. Катодты қорғаныс (ICCP) беріктік пен бейімделуді қамтамасыз етеді, өйткені ол темірбетон ғимараттары жоғары қарсылыққа ие болған жағдайда қажетті ток бере алады. ICCP үшін әртүрлі өткізгіш жабындар мен анодты материалдар, мысалы, көміртекті талшықты өткізгіш жабындар мен мырыш, сондай-ақ дискретті анодтар түріндегі анодтық жүйелер және цементтеу жабынындағы титан негізіндегі торлар жиі қолданылады. Хлорид иондары, әсіресе, болатқа қатты эпоксидті жабын арқылы ену қиын, бұл оны қатты химиялық заттардан қорғау үшін өте тиімді тосқауыл етеді. Эпоксидті шайырлар металл беттерін коррозияға қарсы қасиеттерінің, әртүрлі беттерге жақсы адгезиясының және химиялық төзімділігінің арқасында қоршаған орта мен коррозиялық ортаның әсерінен қорғаудың тамаша нұсқасы болып табылады. Осылайша, бұл жұмыс анод материалы ретінде катодты қорғауды, ICCP, әртүрлі өткізгіш жабындарды және эпоксидті жабындарды қарастырады. Бұл әдістер мен материалдар темірбетон конструкцияларын коррозиядан қорғау және жұмыс жағдайында олардың беріктігі мен сенімділігін жақсарту үшін үлкен маңызға ие.

Түйін сөздер: қорғаныс, келтірілген ток, темірбетон коррозиясы, эпоксидті жабындар.

Айнакулова Дана Тулегенқызы	Ph.D. докторант Материалтану және жаңа материалдар технологиясы, Материалтану және жасыл технологиялар мектебі, Қазақ-Британ Техникалық Университеті, Төле би көш., 59, 050000, Алматы, Қазақстан. Email: da_ainakulova@kbtu.kz
Мурадова Сабина Рустамқызы	Магистр, Материалтану және жаңа материалдар технологиясы, Материалтану және жасыл технологиялар мектебі, Қазақ-Британ Техникалық Университеті, Төле би көш., 59, 050000, Алматы, Қазақстан. Email: sab.muradova.01@mail.ru
Халдун М. Аль Аззам	Ph.D., доцент, Фармацевтикалық ғылымдар кафедрасы, Фармакологиялық және диагностикалық зерттеу орталығы (PDRC), Фармация факультеті, Амман Эл-Ахлия университеті, Амман, 19328, Иордания. Email: azzamkha@yahoo.com
Бекбаева Ляззат Кайратовна	Ph.D., Лектор, Нанотехнологиялардың ұлттық ашық зертханасы, Әл-Фараби Қазақ ұлттық университеті,71, Әл-Фараби көшесі а. в., 050040, Алматы, Қазақстан. Email: lyazzat_bk2019@mail.ru
Путери Шри Мелор Мегат-Юсуф	Ph.D., доцент, Механикалық инженерия кафедрасы, Петронас технологиялық университеті, Бандар-Сери-Искандар 31750, Перак, Малайзия. Email: puteris@petronas.com.my
Мукатаева Жазира Сагатбековна	Химия ғылымдарының кандидаты, Абай атындағы ҚазҰПУ, Жаратылыстану және география институтының қауымдастырылған профессоры. Email: jazira-1974@mail.ru
Ганжиан Эшмайл	Ph.D., Профессор, ЖЩК «Concrete Corrosion Tech», Хамфри Миддлмор Драйв, 12, Бирмингем, Англия B17 0JN. Email: concorrosion@gmail.com
Негим Аттиа Эльсайд	Ph.D., Материалтану және жасыл технологиялар мектебінің профессоры, Қазақ-Британ Техникалық Университеті, Төле би көш., 59, 050000, Алматы, Қазақстан; Профессор Қ. Тұрысов атындағы Геология және мұнай-газ ісі институты, Мұнай Инженериясы Кафедрасы, Сәтбаев Университеті, Сәтбаев көш. 22а, 050013, Алматы, Қазақстан. Email: a.negim@kbtu.kz

Аналитический обзор проводящих красок, катодной защиты и бетона

1* Айнакулова Д.Т., 1 Мурадова С.Р., 2 Халдун М. Аль Аззам, 3 Бекбаева Л.К., 4 Мегат-Юсуф П.Ш.М., 5 Мукатаева Ж.С., 6 Ганжиан Э., 1,7 Негим Эльсайд

1 Школа материаловедения и зеленых технологий, Казахстанско-Британский Технический Университет, г. Алматы, Казахстан

2 Центр фармакологических и диагностических исследований (PDRC), отделение фармацевтических наук, фармацевтический факультет, Амманский университет Аль-Ахлия, Амман 19328, Иордания

3 Национальная открытая лаборатория нанотехнологий, Казахский национальный университет им. Аль-Фараби, Алматы, Казахстан

4 Технологический университет Петронас, Бандар-Сери-Искандар 31750, Перак, Малайзия

5 Институт Естествознания и географии КазНПУ имени Абая, г. Алматы, Казахстан

6 ООО«Concrete Corrosion Tech», Хамфри Миддлмор Драйв, 12, Бирмингем, Англия B17 0JN

7 Институт геологии и нефтегазового дела им. К. Турысова, Сатбаев Университет, г. Алматы, Казахстан

АННОТАЦИЯ

Основным и наиболее дорогостоящим видом разрушения, который в настоящее время влияет на эксплуатационные характеристики железобетонных мостовых конструкций, является коррозия стальной арматуры. Коррозия железобетонных конструкций приводит к значительным финансовым потерям. Одним из востребованных методов предотвращения коррозии в железобетонных конструкциях является катодная защита. Катодная защита (ICCP) обеспечивает прочность и адаптивность, так как может выдавать необходимый ток в ситуации, когда железобетонные здания обладают высоким сопротивлением. Для ICCP часто используются различные токопроводящие покрытия и анодные материалы, такие как токопроводящие покрытия с углеродными волокнами и цинк, а также анодные системы в виде дискретных анодов и сетки на основе титана в цементирующем покрытии. Ионы хлорида, особенно, трудно проникают через сплошное эпоксидное покрытие на стали, что делает его очень эффективным барьером для защиты от агрессивных химических веществ. Эпоксидные смолы представляют собой отличный вариант для защиты металлических поверхностей от воздействия окружающей среды и агрессивных сред благодаря их выдающимся антикоррозийным свойствам, хорошей адгезии к различным поверхностям и химической стойкости. Таким образом, в данной работе рассматриваются катодная защита, ICCP, различные токопроводящие покрытия и эпоксидное покрытие в качестве материала анода. Эти методы и материалы имеют большое значение для защиты железобетонных конструкций от коррозии и улучшения их долговечности и надежности в условиях эксплуатации.

Ключевые слова: защита, наложенный ток, коррозии железобетона, эпоксидные покрытия.

Информация об авторах:

Айнакулова Дана Тулегенқызы	Ph.D. докторант Материаловедения и Технологии Новых Материалов, Школы материаловедения и зеленых технологий, Казахстанско-Британский технический университет, ул. Толе би, 59, 050000, Алматы, Казахстан. Email: da_ainakulova@kbtu.kz
Мурадова Сабина Рустамқызы	Магистр, Материаловедения и Технологии Новых Материалов, Школы материаловедения и зеленых технологий, Казахстанско-Британский технический университет, ул. Толе би, 59, 050000, Алматы, Казахстан. Email: sab.muradova.01@mail.ru

Халдун М. Аль Аззам	*Ph.D., Ассоциированный профессор кафедры фармацевтических наук, Центр фармакологических и диагностических исследований (PDRC), фармацевтический факультет, Амманский университет Аль-Ахлия, Амман 19328, Иордания. Email: azzamkha@yahoo.com*
Бекбаева Ляззат Кайратовна	*Ph.D., Лектор Национальная открытая лаборатория нанотехнологий, Казахский национальный университет им. Аль-Фараби, 71, ул. Аль-Фараби А.В., 050040, Алматы, Казахстан. Email: lyazzat_bk2019@mail.ru*
Путери Шри Мелор Мегат-Юсуф	*Ph.D., Ассоциированный профессор кафедры Механической Инженерии, Технологический университет Петронас, Бандар-Сери-Искандар 31750, Перак, Малайзия. Email: puteris@petronas.com.my*
Мукатаева Жазира Сагатбековна	*Кандидат химических наук, Ассоциированный профессор Института Естествознания и географии КазНПУ имени Абая. Email: jazira-1974@mail.ru*
Ганжиан Эшмайл	*Ph.D., Профессор, ООО «Concrete Corrosion Tech», Хамфри Миддлмор Драйв, 12, Бирмингем, Англия B17 0JN. Email: concorrosion@gmail.com*
Негим Аттиа Эльсайд	*Ph.D., Профессор Школы материаловедения и зеленых технологий, Казахстанско-Британский технический университет, ул. Толе би, 59, 050000, Алматы, Казахстан. Профессор Института геологии и нефтегазового дела им. К. Турысова, Кафедра Нефтяной Инженерии, Сатбаев Университет, ул. Сатбаева 22а, 050013, г. Алматы, Казахстан. Email: a.negim@kbtu.kz*

References

[1] Sun P, Wang Z, Lu Y, Shen S, Yang R, Xue A, Parker T, Wang J, Wang Q. Analysis of the corrosion failure of a semiconductor polycrystalline distillation column. Process Safety and Environmental Protection. 2020; 135(12):244-256. https://doi.org10.1016/j.psep.2020.01.007

[2] Bertolini L, Carsana M, Gastaldi M, Lollini F, Redaelli E. Corrosion of steel in concrete and its prevention in aggressive chloride-bearing environments, 5th International Conference on Durability of Concrete Structures, Shenzhen, Guangdong Province, China, Jun 30–Jul 1 2016. Shenzhen University. 2016, 13-26.

[3] Callon R, Daily SF, Funahashi M: Selection Guidelines for Using Cathodic Protection Systems for Reinforced and Prestressed Concrete Structures, In Corrosion 2004, NACE International. 2004.

[4] Mosaieb MFH, Monfaredi K. Novel Cathodic Protection System based on Photovoltaic Cells. Transaction of Electrical and Electronic Circuits and Systems. Materials Science. 2014; 4(20):117-123.

[5] Wilson K, Jawed M, Ngala V. The selection and use of cathodic protection systems for the repair of reinforced concrete structures. Construction and Building Materials. 2013; 39:19-22. https://doi.org/10.1016/j.conbuildmat.2012.05.037

[6] Das SC. Zinc rich paint as anode system for cathodic protection (CP) of reinforced concrete structures and development of corrosion. CP monitoring probes. Unpublished PhD thesis. Coventry University. 2012.

[7] Makhmetova A, Negim ES, Ainakulova D, Yeligbayeva G, Khatib J. An Overview of Epoxy Resins as coating to protect metals from corrosion. Kompleksnoe Ispolzovanie Mineralnogo Syra = Complex use of mineral resources. 2024; 328(1):20-32. https://doi.org/10.31643/2024/6445.03

[8] Syrmanova K, Negim E, Kaldybekova J, Tuleuov AM. Epoxylitane Compositions Modification with Using Thermoplastic Polyurethane. Oriental Journal of Chemistry. 2016; 32(1):1.

[9] Syrmanova K, Negim E, Kaldybekova J, Suleimenova M, Baizhanova S. Study of modification process of the epoxylitane composites. Industrial Technology and Engineering. 2015; (3):75-83.

[10] Schwarz W. Cathodic Corrosion Protection of Steel Reinforced Concrete Structures with a New Conductive Composite Paint System, Bauinstandsetzen und Baudenkmalpflege 6. Jahrgang. 2000; 6:597-618.

[11] Raupach M. History of EFC-WP11, "Corrosion in Concrete". Institute for Building Materials Research of Aachen University, Aachen, Germany. 2014.

[12] Zaki A. Principles of Corrosion Engineering and Corrosion Control, Butterworth-Heinemann. 9th ed. Elsevier. 2006.

[13] Bhuiyan S. Effectiveness of impressed current cathodic protection systems in concrete following current interruption. Thesis. Master of Engineering. School of Civil, Environmental and Chemical Engineering. RMIT University. 2015.

[14] Johan A. Corrosion of steel in concrete at various moisture and chloride levels, Lund University and Swerea/Kimab, ISBN 978-91-7673-[133-8]. 2015.

[15] Nadzri NIM, Amin NM. A Review of Cathodic Protection in Repairing Reinforced Concrete Structures, Journal of Mechanical Engineering. 2019; 16(2):183-198.

[16] Design Manual for Roads and Bridges, Cathodic Protection for Use in Reinforced Concrete Highway Structures, 3, Highways Agency, London, UK. 2002.

[17] Eur Ing RL. Kean of ARK Corrosion Services, NPL for the Department of Trade and Industry. 1981.

[18] Wilson K, Jawed M, Ngala V. The selection and use of cathodic protection systems for the repair of reinforced concrete structures. Construction and Building Materials. 2013; 39:22-25. https://doi.org/10.1016/j.conbuildmat.2012.05.037

[19] Broomfield JP. The Principles and Practice of Galvanic Cathodic Protection for Reinforced Concrete Structures. Technical Note 6. Corrosion Prevention Association, Bordon, UK. 2000.

[20] Broomfield JR. Corrosion of Steel in Concrete, E&FN Spon, London; 1997 615 W. Schwarz 5W.F. Perenchio, U.R. Landgren, R.E. West and K.C. Clear, Cathodic Protection of Concrete Bridge Substructures, NCHRP Report 278. 1985, 61.

[21] Davies K. Impressed current cathodic protection systems for reinforced concrete, in Cathodic Protection of Steel in Concrete, ed. P.M. Chess: E&FN Spon, London. 1998, 59-91.

[22] Lambert P. Economic aspects, in Cathodic Protection of Steel in Concrete, ed. P.M. Chess, E&FN Spon, London. 1998, 177-184.

[23] Society for the Cathodic Protection of Reinforced Concrete (SCPRC), Cathodic Protection of Steel in Concrete - Status Report, Report No SCPRC/001.95, SCPRC, PO Box 72, Leighton Buzzard, Bedfordshire, LU7 7EU, UK. 1995.

[24] Muradova SR, Negim El-Sayed, Makhmetova AR, Ainakulova DT, Mohamad NMI. An Overview of the Current State and the Advantages of using acrylic resins as anticorrosive coatings. Kompleksnoe Ispolzovanie Mineralnogo Syra = Complex use of mineral resources. 2023; 327(4):90-98. https://doi.org/10.31643/2023/6445.44

[25] Goyal A, Pouya HS, Ganjian E. A Review of Corrosion and Protection of Steel in Concrete. Arab J Sci Eng. 2018; 43:5035-5055. https://doi.org/10.1007/s13369-018-3303-2

[26] Wilson K, Jawed M, Ngala V. The selection and use of cathodic protection systems for the repair of reinforced concrete structures. Construction and Building Materials. 2013; 39:19-20. https://doi.org/10.1016/j.conbuildmat.2012.05.037

[27] Lyon SB, Bingham R, Mills DJ. Advances in corrosion protection by organic coatings: What we know and what we would like to know. Progress in Organic Coatings. 2016; 102:2-7.

[28] BSI. ISO 12696:2012: Cathodic protection of steel in concrete. BSI, London, UK. 2012.

[29] Wicks ZW, Jones FN, Pappas SP. Organic Coatings: Science and Technology. 2nd ed. John Wiley and Sons, New York. 1994.

[30] Sofian AHB, Noda K. The Investigation of Zinc-Rich Paint (ZRP) Behavior in NaCl Solution by Electrochemical Methods. In The Malaysia-Japan Model on Technology Partnership, Springer Japan. 2015; 3-7.

[31] Epoxy Coated Reinforcement: Part One. 2008. (Accessed 25 July 2023). https://www.totalmateria.com/page.aspx?ID=CheckArticle&site=kts&NM=227

[32] Darowicki K. Conducting coatings as anodes in cathodic protection. Progress in organic coatings 2003; 46(3):191-196. https://doi.org/10.1016/S0300-9440(03)00003-1

[33] Gujjar SV, Nadar N, Choudhary K, Hunashyal AM, Shahapurkar K, Mujtaba MA, Asadullah M, Soudagar MEM, YunusKhan TM, Ismail KA, Elfasakhany A. Investigation of Various Coating Resins for Optimal Anticorrosion and Mechanical Properties of Mild Steel Surface in NaCl Solution. Advances in Materials Science and Engineering. 2022; 2:9(2203717). https://doi.org/10.1155/2022/2203717

Study of the structure and electrical properties of graphene oxide (GO) and graphene oxide+nanocellulose (GO+NC)

**[1] Almasov N.Zh., [1] Kurbanova B. A., [2] Kuanyshbekov T.K., [2] Akatan K.,
[3] Kabdrakhmanova S. K., [1*]Aimaganbetov K.P.**

[1] International Science Complex ASTANA, Astana, Kazakhstan
[2] Sarsen Amanzholov East Kazakhstan State University, Ust-Kamenogorsk, Kazakhstan
[3] Satbayev University, Almaty, Kazakhstan

* Corresponding author email: kazybek012@gmail.com

ABSTRACT

Proton exchange membranes (PEMs) that function at elevated temperatures surpassing 100°C and exhibit exceptional mechanical, chemical, and thermochemical stability have garnered significant interest. This is primarily due to their practical utility in proton exchange membrane fuel cells (PEMFCs). In the present era, an extensive array of polymers and polymer-blended membranes have been scrutinized for their applicability in this domain. Each of these materials presents a set of advantages and disadvantages. However, the realm of PEMFCs is still in search of the perfect membrane endowed with distinct properties. Graphene oxide, a two-dimensional substance arising from the oxidation of graphite, has manifested itself as a promising candidate. Oxygen (O) functional groups are incorporated within the sp^2 carbon (C) plane of the oxidized graphite, forming graphene oxide. This material can be synthesized by exfoliating graphite oxide, a three-dimensional carbon-based compound, into layered sheets using ultrasonic or mechanical agitation. The presence of multiple reactive oxygen functional groups renders graphene oxide suitable for a diverse array of applications, such as composite polymers, energy conversion materials, environmental safeguards, sensors, transistors, and optical components. This versatility is attributable to its outstanding electrical, mechanical, and thermal properties. Among the various methodologies for graphene oxide synthesis, the modified Hammer method stands out for its simplicity, cost-effectiveness, and high yield. This research delves into the structural analysis of graphene oxide obtained through the Hammer method, utilizing commercially available graphite. The study involves the creation of membranes based on carboxymethylcellulose (NC) that integrate dispersed graphene oxide (GO) sheets. These novel membranes, as well as pristine graphene oxide, were subjected to a comprehensive array of analytical techniques including XRD, XPS, Raman, FTIR, and SEM microscopy. Additionally, electrophysical characterizations were undertaken employing electrochemical impedance spectroscopy (EIS) measurements. The investigation uncovered that the introduction of NC into the graphene oxide matrix significantly enhances the electron conductivity of the composite membrane. Simultaneously, the presence of graphene oxide contributes to the mechanical robustness and thermomechanical stability of the membrane structure. The principal impetus behind this article lies in furnishing vital insights into the physical and structural attributes of graphene oxide membranes relevant to their deployment in hydrogen energy applications.

Keywords: Hammers method, graphene oxide, nanocellulose, XRD, XPS, IR Fourier spectroscopy, impedance spectroscopy (EIS)

	Information about authors:
Almasov Nurlan Zhumabekovich	*PhD, International Science Complex ASTANA, 010000, Astana, Kazakhstan. Email: nurlanalmasov@gmail.com*
Kurbanova Bayan Amzekyzy	*Master, International Science Complex ASTANA, 010000, Astana, Kazakhstan. Email: bayan.kurbanova@nu.edu.kz*
Kuanyshbekov Tilek Kuanyshbekuly	*PhD, Sarsen Amanzholov East Kazakhstan State University, Ust-Kamenogorsk, Kazakhstan. Email: kuanyshbekov_17@mail.ru*
Akatan Kydirmolla	*PhD, Sarsen Amanzholov East Kazakhstan State University, Ust-Kamenogorsk, Kazakhstan. Email: ahnur.hj@mail.ru*
Kabdrakhmanova Sana Kanatbekovna	*PhD, Satbayev University, 050040 Almaty, Kazakhstan. Email: Sanaly33@mail.ru*
Aimaganbetov Kazybek Pirzhanuly	*PhD student, International Science Complex ASTANA, 010000, Astana, Kazakhstan. Email: kazybek012@gmail.com*

Introduction

Graphene oxide (GO) originates from the exfoliation of graphite oxide, resulting in a layered structure containing one or multiple carbon atom layers, accomplished through ultrasonic or mechanical processes [1]. These GO sheets are mainly classified as chemically generated graphene, displaying analogous characteristics to pristine graphene. However, a fundamental distinction exists between graphene and GO: while graphene solely comprises sp^2 hybridized carbon atoms, GO encompasses a carbon framework featuring diverse oxygen based functional groups.

Back in 1859, Brodie labeled graphene oxide as either graphite oxide or graphitic acid [2]. This was achieved through the chemical treatment of graphite using $KClO_3$ and HNO_3. The subsequent step involves the transformation of graphite oxide into monolayer sheets of GO, a process that can be accomplished using various thermal and mechanical techniques [3]. In the current context, the monatomic carbon stratum within graphite oxide is recognized as graphene oxide (GO).

Four methods of GO synthesis are well known, such as Brody's method [2], Staudenmaier's method [4], Hammer and their modifications [[5], [6]], and Tur's method [7]. At present, the synthesis of GO by the modified Hammer method is considered to be the most common method.

GO contains various functional groups of active oxygen, and its polymer composites enable the development of materials for energy conversion and environmental protection [8].

In addition, GO can be used to produce membranes for obtaining pure water. In recent years, multilayer two-dimensional films for purification and chemical separation of water have been obtained from bilayer hydroxides (LDHs), transition metal dichalcogenides (MoS_2, WS_2), transition metal carbides (MXene), and many other materials based on graphene [[9], [10], [11], [12]].

Compared with other 2D membranes, graphene oxide (GO) membranes have better sheet structure, efficient separation, and flexible fabrication methods. Studies have shown that GO multilayer membranes can effectively trap water contaminants, and water molecules can quickly flow between layers with virtually no friction [[12], [13]].

Because cellulose is partially crystalline, it comprises regions that are both crystalline and non-crystalline [14]. The polymer's molecular and intermolecular chemical constituents possess distinctive characteristics, including hydrophilicity, limited solubility in certain aqueous environments, and a capacity for straightforward chemical modification. Cellulose can be categorized into different structural arrangements and transformed from one configuration to another through either chemical or thermal processes [15].

Nanocellulose (NC) exhibits superior physical, chemical, biological, magnetic, electrical and optical characteristics compared to some materials in their nanoscale form [16]. Conceptually, NCs can be obtained at different stages using hydrolysis technique, i.e. (1) extraction of extractives/hemicellulose using physicochemical, biological or a combination of two or more treatments, (3) separation of cellulose unit fibrils or microfibrils to obtain nanofibers using different substances and (4) solvent removal, ultrasonic treatment, centrifugation, stabilization and drying [[17], [18], [19], [20]].

As a natural nanomaterial, plant-derived nanocellulose and natural cellulose have the same properties as graphene, such as large size, specific surface area, mechanical and chemical properties, high crystallinity, biodegradability, and renewable resource intensity [21]. Recently, many researchers have been working on combining NCs with graphene to create functional hybrid composites of nanocellulose and graphene [[22], [23], [24]].

Experimental part

Two different graphene oxide (GO, GO+NC) based samples were fabricated by the Hammers method (Table 1) [[25], [26]].

Table 1 - Samples of graphene oxide

Name	Thickness
1. GO	18.03 – 23.5 micron
2. GO+NC(1/1)	12.36 micron

The morphological structure of the samples was determined using the SEM Crossbeam 540 research instrument. The results obtained are shown in Figure 1.
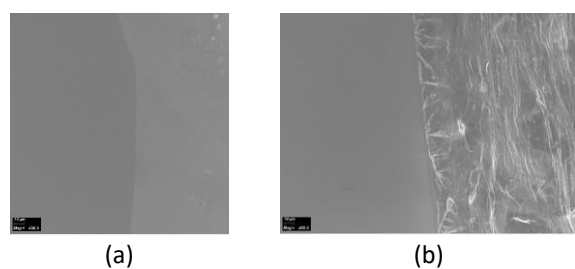
(a)   (b)

Figure 1 - SEM images of samples of graphene oxide a) (GO) and b) GO + nanocellulose (NC)

The spectra of GO, GO+NC were studied by X-ray photoelectron spectroscopy. The results obtained are presented in fig. 2. The spectra of the two samples in the figure show the difference in binding energy (GO = 280-290 eV, GO+NC = 290-300 eV).

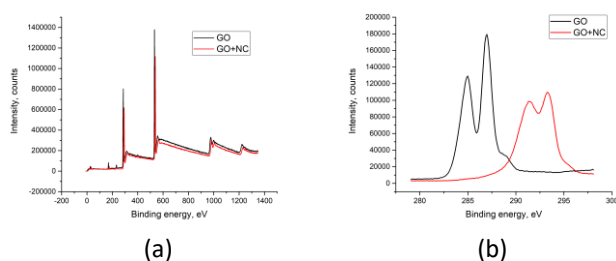IR spectra were determined using a Nicolet iS10 IR Fourier spectrometer (Fig. 3-a) and the Raman spectra were studied (Fig. 3-b).

(a)   (b)

Figure 2 - X-ray photoelectron spectrum (XPS) of GO + NC samples

(a)   (b)
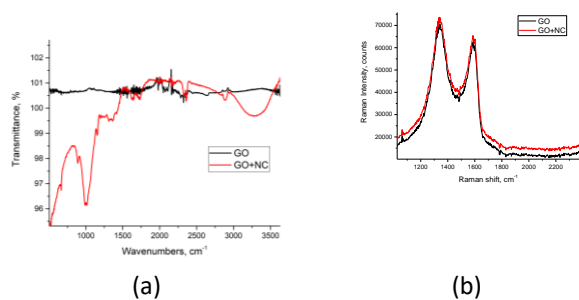
Figure 3 - a) FTIR spectra and

b) Raman spectra of GO and GO + NC samples

The electrical characteristics of the samples were studied in various temperature ranges by the method of impedance spectroscopy (HF2 Impedance spectroscopy, Zurich). The copper element was deposited on the surface of the sample by magnetron sputtering to create an electrical ohmic contact. Plasma power 40 W, deposition time 30 min.

(a)   (b)
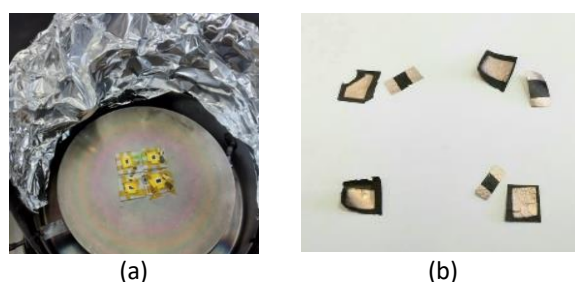
Figure 4 - a) the process of magnetron deposition and b) the type of samples obtained

Impedance measurements were carried out at a sinusoidal voltage amplitude of 50 mV in the frequency range from 10 Hz to 1 MHz. On fig. 5 shows the measurement results.

Results and Discussion

As can be seen from the SEM images (Fig. 1), the addition of nanocellulose to graphene oxide leads to the formation of a composite material with pores and folds.

On fig. 2 shows the C 1s XPS spectra for GO and GO + NC. It can be seen that the spectrum of C 1s GO has two peaks at 284.6 and 286.6 eV, corresponding to the sp^2 and C-O carbon functional groups, respectively. However, the addition of nanocellulose led to an upward shift in the binding energy and a twofold decrease in the overall intensity. The peak shift is related to a change of oxidation state of GO after adding NC, where the higher binding energy shows higher oxidation state [27]. The intensity is directly connected to the number of atoms with respective oxidation state. Thus, there is a certain degree on the amount of oxidized atoms in GO+NC composite which is less than the amount of non-oxidized atoms in pristine GO without any addition. Also, the XPS spectrum of graphen oxide showed there isn't any elements other than C and O, indicating the absence of foreign impurities.

A typical Raman spectrum (Fig. 3b) of GO is characterized by an approximate G band. The Raman spectrum has a 1605 cm^{-1} band corresponding to the E2g phonon of the sp^2 C atoms and a 1353 cm^{-1} D band corresponding to the point phonon K absorption mode of A1g symmetry. Here, the graphene G band was observed at 1600 cm^{-1}, which was slightly shifted from the GO position. There was no difference in the Raman spectra of GO and GO + NC models.

In the FTIR GO spectrum (Fig. 3a), there is a strong and broad elongated O-H vibrational band

which occurs at 3410 cm^{-1} from - due to oxidation. In addition, the carboxyl at 1721 cm^{-1} has a C = O stretching band, an O-H deformation vibrational band at 1404 cm^{-1} and a C - O stretching band at 1087 cm^{-1}. The addition of nanocellulose resulted in an increase in the total FTIR conductivity signal and additional peaks.
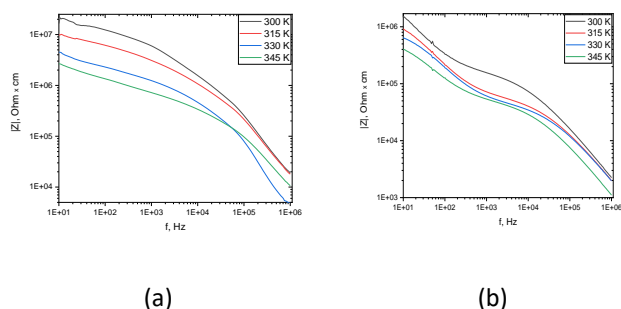

Figure 5 - frequency dependence of electrical resistance with temperature change,
a) GO, B) GO + NC

In Figure 5, it can be seen the difference in the electrical resistance of graphene oxide and GO + NC samples. Temperature dependences of the research samples were also revealed. The obtained results show that at room temperature the electrical resistance of graphene oxide is one order of magnitude higher than GO+NC. As the temperature increases, the resistance of both samples decreases and the conductive property increases. Whether these materials can be used as a fuel cell is evidenced by actual studies.

Conclusions

Graphene oxide and GO + NC results obtained by simple chemical wet process, XRD, FTIR, Raman, SEM showed successful results. It was investigated that the conductivity of the samples increased with increasing temperature during operation using electrochemical impedance spectroscopy (EIS) measurements. XPS results showed that the addition of NC to the GO leads to the increase of oxidation degree of the whole membrane. GO with elevated levels of oxygen content could make the membrane significantly more hydrophilic. This enhancement in hydrophilicity would lead to improved membrane properties, such as a decrease in biofouling processes and an increase in water flux. Also, GO can be easily dispersed in water and exfoliated in a wide range of solvents due to the hydrophilicity. Graphene oxide plays an important role in the development of science and technology today. Studies show that graphene oxide can be used for not only making battery and supercapacitor cathodes, electrical sensors, photovoltaic devices, electrochromic devices and optical devices, but also for making membranes in hydrogen energy. Many studies provide evidence for the future utilization of graphene oxide, which is an advanced technology based on graphene oxide.

Conflicts of interest. There is no conflict of interest between the authors.

Графен оксиді (GO) және графен оксиді + наноцеллюлоза (GO+NC) құрылымын және электрлік қасиеттерін зерттеу

¹ Алмасов Н.Ж., ¹ Курбанова Б.Ә., ² Қуанышбеков Т.Қ., ² Ақатан Қ., ³ Кабдрахманова С.К., ¹ Аймаганбетов К.П.

¹ «АСТАНА» Халықаралық Ғылыми Кешені, Астана, Қазақстан
² Сәрсен Аманжолов атындағы Шығыс Қазақстан мемлекеттік университеті, Өскемен, Қазақстан
³ Сәтбаев университеті, Алматы, Қазақстан

ТҮЙІНДЕМЕ

Жоғары температурада жұмыс істейтін және тамаша механикалық, химиялық және термохимиялық тұрақтылыққа ие протон алмасу мембраналары (PEM) протонды мембраналық отын элементтерінде (PEMFC) практикалық қолданылуына байланысты көп назар аударуда. Қазіргі уақытта осы мақсаттар үшін полимерлермен араласқан көптеген полимерлі және әртүрлі мембраналар зерттелуде, олардың барлығында артықшылығы және кемшіліктері бар. Дегенмен, PEMFC бірегей қасиеттері бар идеалды мембраналар әлі де жоқ. Графен оксидінің құрамында әртүрлі реактивті оттегі функционалдық топтары бар, бұл оның тамаша қасиеттеріне байланысты оны полимер композиттері, энергияны түрлендіруге арналған материалдар, қоршаған ортаны қорғау қолданбалары, сенсорлар, транзисторлары және оптикалық қолданбалар сияқты көптеген қолданбаларда электрлік, механикалық және жылулық қасиеттері негіз ретінде қолданылады. Графен оксидін синтездеу үшін кеңінен қолданылатын әдіс қарапайым процесс, құны төмен және жоғары кірістілігіне байланысты модификацияланған Хаммер әдісі болып табылады. Бұл жұмыста біз коммерциялық графитін пайдалану арқылы Хаммерс әдісімен алынған графен оксидінің құрылымдық зерттеулері туралы баяндаймыз. Бұл графен оксидінің құрылымдық сипаттамаларын беретін өлшеу құрылғыларымен әр түрлі спектрометрлердің көмегімен қарастырылады. Дисперсті графен оксиді (GO) парақтары бар карбоксиметилцеллюлоза (NC) негізіндегі мембраналар PEMFC қолданбалары үшін жасалып, зерттелді. Бұл мембраналар мен графен оксиді XRD, XPS, Raman, FTIR және SEM микроскопиясының комбинациясы арқылы зерттелді, ал электрофизикалық сипаттау электрохимиялық импеданс спектроскопиясы (EIS) өлшемдері арқылы орындалды. GO-ға CMC қосу бүкіл мембрананың электр өткізгіштігін жоғарылататыны, ал GO мембрананың жақсы механикалық және термомеханикалық тұрақтылығын қамтамасыз ететіні анықталды. Бұл мақаланы жазудың негізгі мотивациясы графен оксидінің сутегі энергетикасында қолданылатын мембраналар үшін қажетті физикалық құрылымдық сипаттамалар беру болып табылады.

Түйін сөздер: Хаммерс әдісі, графен оксиді, наноцеллюлоза, XRD, XPS, ИК Фурье-спектроскопия, импеданс спектроскопия (EIS)

Авторлар туралы ақпарат:

Алмасов Нурлан Жумабекович — *PhD, «АСТАНА» Халықаралық Ғылыми Кешені, Астана, Қазақстан, 010000. Email: nurlanalmasov@gmail.com*

Курбанова Баян Әмзеқызы — *Магистр., «АСТАНА» Халықаралық Ғылыми Кешені, 010000, Астана, Қазақстан. Email: bayan.kurbanova@nu.edu.kz*

Куанышбеков Тилек Куанышбекулы — *PhD, Сәрсен Аманжолов атындағы Шығыс Қазақстан мемлекеттік университеті, Өскемен, Қазақстан. Email: kuanyshbekov_17@mail.ru*

Ақатан Қыдырмолла — *PhD, Сәрсен Аманжолов атындағы Шығыс Қазақстан мемлекеттік университеті, Өскемен, Қазақстан. Email: ahnur.hj@mail.ru*

Кабдрахманова Сана Канатбековна — *PhD, Сәтбаев Университеті, 050040 Алматы, Қазақстан. Email: Sanaly33@mail.ru*

Аймаганбетов Казыбек Пиржанулы — *PhD докторант, «АСТАНА» Халықаралық Ғылыми Кешені, Астана, Қазақстан. Email: kazybek012@gmail.com*

Исследование структуры и электрических свойств оксида графена (GO) и оксид графен+наноцеллюлоза (GO+NC)

[1] Алмасов Н.Ж., [1] Курбанова Б.А., [2] Қуанышбеков Т.К., [2] Ақатан Қ., [3] Кабдрахманова С.К., [1] Аймаганбетов К.П.

[1] Международный научный комплекс "Астана", Астана, Казахстан
[2] Восточно-Казахстанский университет имени Сарсена Аманжолова, Усть-Каменогорск, Казахстан
[3] Satbayev University, Алматы, Казахстан

АННОТАЦИЯ

Протонообменные мембраны (PEM), работающие при высоких температурах выше 100 °C, с превосходной механической, химической и термохимической стабильностью, привлекли большое внимание в связи с их практическим применением в топливных элементах с протонообменными мембранами (PEMFC). В настоящее время для этого применения исследовано огромное количество полимеров и различных полимерных мембран, все из которых имеют как плюсы, так и минусы. Однако идеальных мембран с уникальными свойствами для PEMFC все еще нет. Оксид графена представляет собой двумерный материал, образованный из окисленного графита с функциональными группами кислорода (O), занимающими плоскость sp^2 углерода (C). Оксид графена можно получить путем

расслаивания оксида графита (окисленного трехмерного материала на основе углерода) на ламинированные листы с использованием ультразвукового или механического перемешивания. Оксид графена содержит различные функциональные группы активного кислорода, что делает его основой для многих приложений, таких как полимерные композиты, материалы для преобразования энергии, приложения для защиты окружающей среды, датчики, транзисторы и оптические приложения благодаря его превосходным электрическим, механическим и термическим свойствам. Широко используемым методом синтеза оксида графена является модифицированный метод Хаммерса из-за его простого процесса, низкой стоимости и высокого выхода. В этой работе мы сообщаем о структурных исследованиях оксида графена, полученного методом Хаммерса с использованием технического графита. Мембраны на основе карбоксиметилцеллюлозы (NC) с листами дисперсионного оксида графена (GO) были изготовлены и исследованы для применения PEMFC. Эти мембраны и первичный GO были изучены с помощью комбинации XRD, XPS, Raman, FTIR и SEM-микроскопии, в то время как электрофизические характеристики были выполнены с использованием измерений электрохимической импедансной спектроскопии (EIS). Выявлено, что добавление NC к GO повышает электрическую проводимость всей мембраны, а GO обеспечивает хорошую механическую и термомеханическую стабильность мембраны. Основной мотивации написания этой статьи является обеспечение необходимых физических структурных характеристик для мембран из оксида графена, используемых в водородной энергетике.

Ключевые слова: метод Хаммерса, оксид графена, наноцеллюлоза, XRD, XPS, ИК Фурье-спектроскопия, импедансной спектроскопии (EIS)

Алмасов Нурлан Жумабекович	*PhD, Международный научный комплекс "Астана", 010000, Астана, Казахстан. Email: nurlanalmasov@gmail.com*
Курбанова Баян Әмзеқызы	*Магистр., Международный научный комплекс "Астана", 010000, Астана, Казахстан. Email: bayan.kurbanova@nu.edu.kz*
Куанышбеков Тилек Куанышбекулы	*PhD, Восточно-Казахстанский университет имени Сарсена Аманжолова, Усть-Каменогорск, Казахстан. Email: kuanyshbekov_17@mail.ru*
Ақатан Қыдырмолла	*PhD, Восточно-Казахстанский университет имени Сарсена Аманжолова, Усть-Каменогорск, Казахстан. Email: ahnur.hj@mail.ru*
Кабдрахманова Сана Канатбековна	*PhD, Satbayev University, 050040 Алматы, Казахстан. Email: Sanaly33@mail.ru*
Аймаганбетов Казыбек Пиржанулы	*PhD докторант, Международный научный комплекс "Астана", 010000, Астана, Казахстан. Email: kazybek012@gmail.com*

References

[1] Zhao J, Liu L, Li F. Graphene Oxide: Physics and Applications. New York: Springer; 2015, 3. https://doi.org/10.1007/978-3-662-44829-8

[2] Brodie B.C. On the atomic weight of graphite. Philos. Trans. R. Soc. London, Ser. B. Series B, Biol. Sci. 1859; 149:249-259. https://doi.org/10.1098/rstl.1859.0013

[3] Dreyer DR, Park S, Bielawski CW, Ruoff RS. The chemistry of graphene oxide. Chem. Soc. Rev. 2010; 39:228-240. https://doi.org/10.1039/B917103G

[4] Staudenmaier L. Verfahren zur Darstellung der Graphitsäure (Method for the preparation of graphitic acid). Berichte der Deutschen Chemischen Gesellschaft. 1898; 31:1481-1487. https://doi.org/10.1002/cber.18980310237

[5] Hummers WS, Offeman RE. Preparation of graphitic oxide. J. Amer. Chem. Soc. 1958; 80:1339. https://doi.org/10.1021/ja01539a017

[6] Ranjan P, Agrawal S, Sinha A, Rao TR, Balakrishnan J, Thakur AD. A low cost non-explosive synthesis of graphene oxide for scalable applications. Sci. Reports. 2018; 8:12007. https://doi.org/10.1038/s41598-018-30613-4

[7] Marcano DC, Kosynkin DV, Berlin JM, Sinitskii A, Sun Z, Slesarev A, et al. Improved synthesis of graphene oxide. ACS Nano. 2010; 4:4806-4814. https://doi.org/10.1021/nn1006368

[8] Sierra U, Álvarez P, Blanco C, Granda M, Santamaría R, Menéndez R. Cokes of different origin as precursors of graphene oxide. Fuel. 2016; 166:400-403. https://doi.org/10.1016/j.fuel.2015.10.112

[9] Yang YB, Yang XD, Liang L, et al. Large-area graphene nanomesh/carbon-nanotube hybrid membranes for ionic and molecular nanofiltration[J]. Science. 2019; 364(6445):1057-1062. https://doi.org/10.1126/science. aau5321

[10] Gao Ke, Xu Zhonghuang, Hong Yubin, et al. Graphene oxide-ceramic composite nanofiltration membrane Preparation and Properties of Layer-by-Layer Assembly[J]. Acta Chemie Sinica. 2017; 68(5):2177-2185.

[11] Yang Q, Su Y, Chi C, et al. Ultrathin graphene-based membrane with precise molecular sieving and ultrafast solvent permeation[J]. Nat. Mater. 2017; 16(12):1198-1202. https://doi.org/10.1038/nmat5025

[12] Zhang MC, Guan KC, Ji YF, et al. Controllable ion transport by surface-charged graphene oxide membrane[J]. Nat. Commun. 2019; 10(1):1253. https://doi.org/10.1038/s41467-019-09286-8

[13] Xie Q, Alibakhshi MA, Jiao SP, et al. Fast water transport in graphene nanofluidic channels[J]. Nat. Nanotechnology. 2018; 13(3):238-245. https://doi.org/10.1038/s41565-017-0031-9

[14] Tarchoun AF, Trache D, Klapötke TM, Derradji M, Bessa W. Ecofriendly isolation and characterization of microcrystalline cellulose from giant reed using various acidic media. Cellulose. 2019; 26:7635-7651. https://doi.org/10.1007/s10570-019-02672-x

[15] Tshikovhi A, Mishra SB, Mishra AK. Nanocellulose-based composites for the removal of contaminants from wastewater. Int. J. Biol. Macromol. 2020; 152:616-632. https://doi.org/10.1016/j.ijbiomac.2020.02.221

[16] Trache D. Nanocellulose as a promising sustainable material for biomedical applications. AIMS Mater. Sci. 2018; 5:201-205. https://doi.org/10.1016/j.ijbiomac.2020.02.221

[17] Vineeth S, Gadhave RV, Gadekar PT. Chemical modification of nanocellulose in wood adhesive. Open J. Polym. Chem. 2019; 9:86. https://doi.org/10.4236/ojpchem.2019.94008

[18] Pires JR, Souza VG, Fernando AL. Valorization of energy crops as a source for nanocellulose production–current knowledge and future prospects. Ind. Crop. Prod. 2019; 140:111642. https://doi.org/10.1016/j.indcrop.2019.111642

[19] Phanthong P, Reubroycharoen P, Hao X, Xu G, Abudula A, Guan G. Nanocellulose: Extraction and application. Carbon Resour. Convers. 2018; 1:32-43. https://doi.org/10.1016/j.crcon.2018.05.004

[20] Chen W, Yu H, Lee S-Y, Wei T, Li J, Fan Z. Nanocellulose: A promising nanomaterial for advanced electrochemical energy storage. Chem. Soc. Rev. 2018; 47:2837-2872. https://doi.org/10.1039/C7CS00790F

[21] Lin N, Dufresne A. Nanocellulose in biomedicine: Current status and future prospect, Eur. Polym. J. 2014; 59:302-325. https://doi.org/10.1016/j.eurpolymj.2014.07.025

[22] Xing J, Tao P, Wu Z, Xing C, Liao X, Nie S. Nanocellulose-graphene composites: A promising nanomaterial for flexible supercapacitors, Carbohyd Polym. 2019; 207:447-459. https://doi.org/10.1016/j.carbpol.2018.12.010

[23] Du X, Zhang Z, Liu W, Deng Y. Nanocellulose-based conductive materials and their emerging applications in energy devices - A review, Nano Energy. 2017; 35:299-320.

[24] Xiong R, Kim HS, Zhang L, Korolovych VF, Zhang S, Yingling YG, Tsukruk VV. Wrapping Nanocellulose Nets around Graphene Oxide Sheets, Angew. Chem. 2018; 130(28):8644-8649. https://doi.org/10.1002/ange.201803076

[25] Kuanyshbekov TK, Akatan K, Kabdrakhmanova SK, Nemkaeva R, et al. Synthesis of Graphene Oxide from Graphite by the Hummers Method. Oxid Commun. 2021; 44(2):356.

[26] Akatan K, Kuanyshbekov TK, Kabdrakhmanova SK, Imasheva AA, Battalova AK, Abylkalykova RB, Nasyrova AK, Ibraeva ZhE. Synthesis of nanocomposite material through modification of graphene oxide by nanocellulose, Chem Bull Kaz Nat Univ. 2021; 3:14-20. https://doi.org/10.15328/cb1238

[27] Al-Gaashania R, Najjar A, Zakaria Y, Mansour S, Atieh MA. XPS and structural studies of high quality graphene oxide and reduced graphene oxide prepared by different chemical oxidation methods. Ceramics International. 2019; 45:14439-14448. https://doi.org/10.1016/j.ceramint.2019.04.165

Synthesis of Biodegradable Polymer-Based on Starch for Packaging Films: A Review

1*Iskalieva A., 2Orazalin Zh., 2Yeligbayeva G., 3Irmukhametova G., 4Taburova S., 4Toktar T.

1School of Chemical Engineering, Kazakh-British Technical University, Almaty, Kazakhstan
2School of Petroleum Engineering, Satbayev University, Almaty, Kazakhstan
3Department of Chemistry & Technology of Organic Substances, al-Farabi Kazakh National University, Almaty, Kazakhstan
4School of Energy and Petroleum Industry, Kazakh-British Technical University, Almaty, Kazakhstan

* Corresponding author email: asylzat@bk.ru

ABSTRACT

Due to their crucial qualities and functionalities, polymers have received a lot of attention in recent years as food packaging materials. These characteristics include non-toxicity, ease of availability, biocompatibility, and biodegradability, showing their promise as an alternative to traditional plastic packaging, which has long been under investigation for its environmental impact. Given the present emphasis on sustainable development, research into biopolymers as eco-friendly and sustainable food packaging materials is critical. The synthesis of biodegradable polymers-based on starch represents a significant stride towards sustainable packaging solutions. As the global demand for eco-friendly materials continues to grow, ongoing research and innovation in this field are poised to lead to the development of starch-based packaging films with improved properties and widespread commercial applications. As a result, the primary goal of this review is to create a biodegradable polymer based on corn-starch and PVA with strong physicomechanical characteristics for usage in plastic bags.

Keywords: Polymers, biodegradability, packaging, plastic bags.

	Information about authors:
Iskalieva Asylzat Zhambulovna	*Ph.D. student at School of Chemical Engineering, Kazakh-British Technical University, Str. Tole bi, 59, 050000, Almaty, Kazakhstan. Email: asylzat@bk.ru*
Orazalin Zhandos Kairatuly	*School of Petroleum Engineering, Satbayev University, 22 Satpayev Street, 050013, Almaty, Kazakhstan. Email: zhandos1403@bk.ru*
Yeligbayeva Gulzhakhan Zhakparovna	*School of Petroleum Engineering, Satbayev University, 22 Satpayev Street, 050013, Almaty, Kazakhstan. Email g.yeligbayeva@satbayev.university*
Irmukhametova Galiya	*Department of Chemistry & Technology of Organic Substances, Natural Compounds & Polymers Faculty of Chemistry and Chemical Technology al-Farabi Kazakh National University 71, al-Farabi av., 050040, Almaty, Kazakhstan. Email: Galiya.Irmukhametova@kaznu.kz*
Taburova Sitora Nematovna	*Bachelor's student at School of Energy and Petroleum Industry, Kazakh-British Technical University, st. Tole bi 59, 050000, Almaty, Kazakhstan. Email: s_taburova@kbtu.com*
Toktar Tomiris Altaykyzy	*Bachelor's student at the School of Energy and Petroleum Industry, Kazakh-British Technical University, St. Tole bi 59, 050000, Almaty, Kazakhstan. Email: t_toktar@kbtu.com*

Introduction

Synthetic polymers and products made from them have a high demand for attributes of human life, but their use creates a lot of problems. Synthetic polymer materials are yielded from non-renewable raw materials, and their accumulation and problematic disposal lead to a deterioration of the environmental situation and the creation of a global problem. The volume of production of synthetic plastic materials, mainly polyolefin, is more than 300 million tons per year. Polyolefin is polyethylene and polypropylene, which can be obtained by petroleum organic synthesis. It is worth emphasizing that up to 98% of the world's plastics are produced from non-renewable raw materials such as oil, gas, and coal processing products. Their stocks are limited [1]. Nowadays, the scope of use of plastic materials is extensive and is used in almost all areas of human activity. The largest share of processing of synthetic polymers falls on the manufacture of containers and packaging. The volume of this sector is approximately 60% of the total volume of plastics processing. About 40% of plastic is used for food packaging and the bottling of drinks. A large mass of used goods is made of synthetic polymers, and only about 20% are recycled [[2], [3], [4]]. According to data from the World Bank organization, about 2.01 billion tons of solid

household waste are generated annually in the world, and around 242 million tons (12%) of the total amount of solid waste is related to plastic materials [5]. The problem of solid waste management is relevant in the world and the Republic of Kazakhstan is not excluded. In 2021 the amount of solid household waste in Kazakhstan was estimated at 125 million tons for what we used 3 200 official landfills and only 18.3% of solid household waste is recycled [6].

Utilization is a possible solution to reduce the volume of waste of artificial plastics. The utilization process can include recycling, combustion, pyrolysis, and recirculation. Combustion and pyrolysis can contribute to the reduction of waste but worsen the environmental situation. In addition, highly toxic compounds such as furans and dioxins are formed during combustion [7].

Plastic considerably pollutes the air, water, and soil because it contains harmful compounds (lead and cadmium pigments, which are frequently used as additives in low-density polyethylene, high-density polyethylene, and polypropylene), and because it is not biodegradable. Plastic bags have the potential to harm the environment in three different ways. Firstly, natural resources that need to be protected are mainly used for the manufacture of plastic bags: oil, natural gas, or coal. Secondly, during the production of plastic, many harmful pollutants are formed, which production companies need to properly deal with. According to market research, the plastic bags of Kazakhstani manufacturers, which produce them mainly based on petrochemical products, do not decompose quickly because of mineralization and can remain in microscopic form indefinitely [8]. Numerous illnesses, including blood and renal ailments, immunological and brain system abnormalities, and birth defects in children, can be brought on by these compounds [9]. In addition to being extremely poisonous, the primary chemicals utilized in the production of plastic bags include certain carcinogens including benzene and vinyl chloride, as well as gaseous and liquid hydrocarbons that harm the environment. It was found that some synthetic plastics used for the manufacture of plastic containers increase the risk of cancer. Since a moderately dangerous substance for the human body is used for their production - bisphenol A (diphenyl propane A). Bisphenol A dissolves well in an aqueous medium; therefore, it can get into food and directly into the human body through the blood [1].

A more effective and popular way to accelerate the biological degradation of the polymer matrix of synthetic polymers is to add various natural additives to the polymer structure that serve as a nutrient medium for microorganisms and accelerate the destruction of the polymer composition. Polysaccharides (starch, dextrin, chitosan, cellulose, wood processing waste) have become the most widespread in the production of biodegradable packaging [[10], [11]]. Despite a significant amount of work devoted to the production of biopolymer materials, their characteristics, and applications, the issue of creating biodegradable systems to reduce the time of biological decomposition has not been fully resolved [12]. The development of new plastic polymer materials that decompose due to microorganisms in soil and water is one of the urgent and priority directions of science development [13]. Polymer degradation can also be caused by exposure to ultraviolet and thermal radiation, sunlight, hydrolysis, and oxidation of air [14].

The addition of poly (ethylene glycol) methyl ester methacrylate [PEGMA] to polymer compositions filled with natural fillers to create biodegradable compositions has not been previously carried out, which is a novelty of this work. In this regard, studies on the effect of poly (ethylene glycol) methyl ether methacrylate in polymer compositions based on polyvinyl alcohol and natural starch filler for the creation of biodegradable polymers are of both scientific and practical interest.

To achieve this goal, the following scientific tasks were set:

1) Selection of certain components and their ratio.

2) Study technological parameters in the production of materials with high-performance characteristics, such as physical, mechanical, and technological properties.

3) Observe the ability to rapidly biodegrade, considering the regulation of degradation processes.

4) Study the solubility of [PVA-b-S]-g-PEGMA biofilms in water, tea, coke, and soil.

Consequently, PEGMA was grafted onto a PVA/S mix copolymer with potassium persulfate acting as the initiator. By using elongation and tensile strength tests, the impact of the blend ratio ([PVA]:[S]:[PEGMA]) and the molecular weight (300, 500, and 950 g/mol) of PEGMA on the physicomechanical characteristics of PVA/S blends

was investigated. It was discovered that the water phase is the best environment for the biodegradability of the produced PVA/S/PEGMA mix films. Additionally, the study aims to offer a quick and affordable way to create biodegradable starch/PVA/PEGMA mix films with better physical qualities, which may find potential uses in the disposable packaging industries [15].

Biodegradable Polymers

The biodegradability of polymers is the ability of a material to decompose without residue under the influence of bacteria, fungi, UV radiation, light, solar radiation, and other natural factors in natural conditions on environmentally friendly substances [16]. The main concept of biopolymer production is to create methods close to the natural cycles of nature. To obtain them, renewable raw materials are used, containing in their composition substances that arise in plants during photosynthesis. Biopolymers are being developed, which are later used as fertilizers, and thanks to microbes and hornbeams, water and carbon dioxide are converted in natural conditions.

Biodegradation is a chemical process caused by biological activity that changes the chemical structure of a material and contributes to the production of natural end products of metabolism.

Synthesis of Biopolymers

Currently, there are three possible directions to produce biopolymers:

1. Synthesis of plastics based on renewable polymers. The synthesis of biodegradable plastics based on natural high-molecular polymers, such as starch, cellulose, chitosan, protein, etc. is used to create composite materials with a variety of natural fillers. Today, biodegradable materials based on cellulose and its derivatives are the most common source of raw materials to produce disposable tableware, packaging material, and other products.

2. Giving the ability to biodegradate plastic materials popular today from petrochemical raw materials. To give biodegradation to plastics, molecules with certain functional groups are introduced into the structure of the main polymer, accelerating its photo-destruction. Composite materials with biodegradable additives that initiate the decomposition of the initial polymer are also

obtained. Or purposefully synthesize biodegradable plastics based on petrochemical polymers. For example, a mixture of cellulose, alkyl ketones or compounds containing carbonyl groups accelerates the photodecomposition and biodegradation of polyethylene, polypropylene, or polyethylene terephthalate.

3. Production of biodegradable polyesters by chemical or biological methods. According to literary sources, this direction has been actively developing recently. The direction is based on the biotechnological or chemical synthesis of biopolymers based on hydroxycarboxylic acids, such as glycolic, lactic, valerian, and others [1].

The biodegradability and non-toxicity of bioplastics are the fundamental requirements for purchasing them. Standards for polymaterials are used for this purpose, and they provide for testing of all additives and polymers to prevent environmental harm [17].

The biodegradation of polymer materials is significantly influenced by the size and chemical structure of the molecule, the presence and type of replacements, and supramolecular micro- and macrostructure [18].

There are certain fragments in the structure which enhance the biodegradation of plastic [18]:

1) heteroatoms;

2) double bonds R = CH2; R = CH–R1; hydroxyl groups R–CH2–OH; R–CH(OH)–R; ether bonds R–CO–H; R–CO–R1, etc.;

3) less than five CH2 groups;

4) volumetric substituents;

5) Natural products of microorganisms, such as starch, cellulose, lactose, magnesium, and urea.

The main mechanisms of polymer biodegradation are biological hydrolysis, which begins with the adsorption of microorganisms on the surface and biological oxidation depends on the chemical composition of the monomer link [18].

Types of Bioplastic Materials

The two categories of raw materials used to create bioplastics are renewable and non-renewable raw materials. Polymer materials are also distinguished by spontaneous decomposition in the natural environment, that is, by biodegradation: biodegradable and non-biodegradable [18]. Based on the above characteristics, all plastics are divided into the following groups as shown in Table 1.

Table 1 - Classification of plastics by raw materials

The raw material	Type of plastic
Non-biodegradable plastics from non-renewable raw materials.	Some examples of these include polyethylene, polypropylene, polyvinyl chloride, polyethylene terephthalate, polystyrene, polybutylene terephthalate, polycarbonate, and polyurethane.
Biodegradable plastics from non-renewable raw materials.	These are synthetic, non-natural materials derived from petrochemical hydrocarbon raw materials; yet, due to specific structural properties, they are biodegradable. Polybutyrates (adipic acid, dimethyl terephthalate, and 1,4-butanediol copolymers (PBAT), polybutylene succinates (PBS), polyvinyl alcohol (PVA), polycaprolactones (PCL), and polyglycolic acid (PGA) are examples of this category.
Non-biodegradable plastics are based on natural raw materials.	These include biopolyethylene, biopolyvinyl chloride, terephthalic PET biopolyesters, etc.
Biodegradable plastics from natural raw materials:	- with the formation of a polymer chain in a natural way. These are biopolymers based on starch, cellulose, etc. - with the formation of a polymer chain with the help of microorganisms in a certain environment. These are polyhydroxyalkanoates; - with the formation of a polymer chain, during the synthesis of a monomer due to a biological process. This is polylactic acid. In this work, the type of biodegradable plastics from natural raw materials prepared by a new biopolymer is examined and studied for degradability.

Natural Biopolymers
Bioplastics from Biomass

Polysaccharides are the most famous natural macromolecules. These are high-molecular carbohydrates consisting of glycoside bonds. They are often one of the important structural elements of the framework of plants and animals. Plants such as potatoes, wheat, legumes, sunflowers, beets, and a variety of wood serve as raw materials to produce a variety of biodegradable polymer products. Now, natural polymers such as polysaccharides, cellulose, rubber, polypeptides, chitin, epoxidized oil, lignin, pullulan, polyesters, etc. are used. The most popular is starch because it is less expensive and obtained from potatoes, wheat, corn, and rice [19].

Starch is a white amorphous powder, tasteless and odorless. Starch does not dissolve in cold water but swells in hot water and forms a paste. In industry, starch is obtained from potatoes (starch content - up to 24%) or corn kernels (57-72%).

Amylopectin (Figure 1), is a highly branching polymer composed of short chains of -1,4 linked by -1,6-links. Connections, and amylose, an essentially linear polysaccharide comprised of -1,4-anhydroglucose units, make up starch. Due to the valence angles between the glucose atoms, amylose molecules have between 200 and 20,000 glucose units and are made up of them in a spiral shape. The polymer amylopectin contains a significant amount of branching. Thirty glucose units are connected along the length of a short-side chain. The starch source affects the relative ratio of the two elements. The usual concentration of amylose is between 15 and 25 percent and is often present as a secondary component. As a raw material for biodegradable goods, starch is currently readily accessible at a cost that is far lower than that paid even for commercial polymers. However, because pure starch has an excessive amount of hydroxyl groups that may absorb water, items created from it have two severe drawbacks: fragility and susceptibility to moisture. The economic potential of starch-based polymers is considerably reduced by these two characteristics; however, research is already underway to enhance starch-based materials. Starch-based materials' rather low mechanical qualities were traditionally overlooked by combining them with other
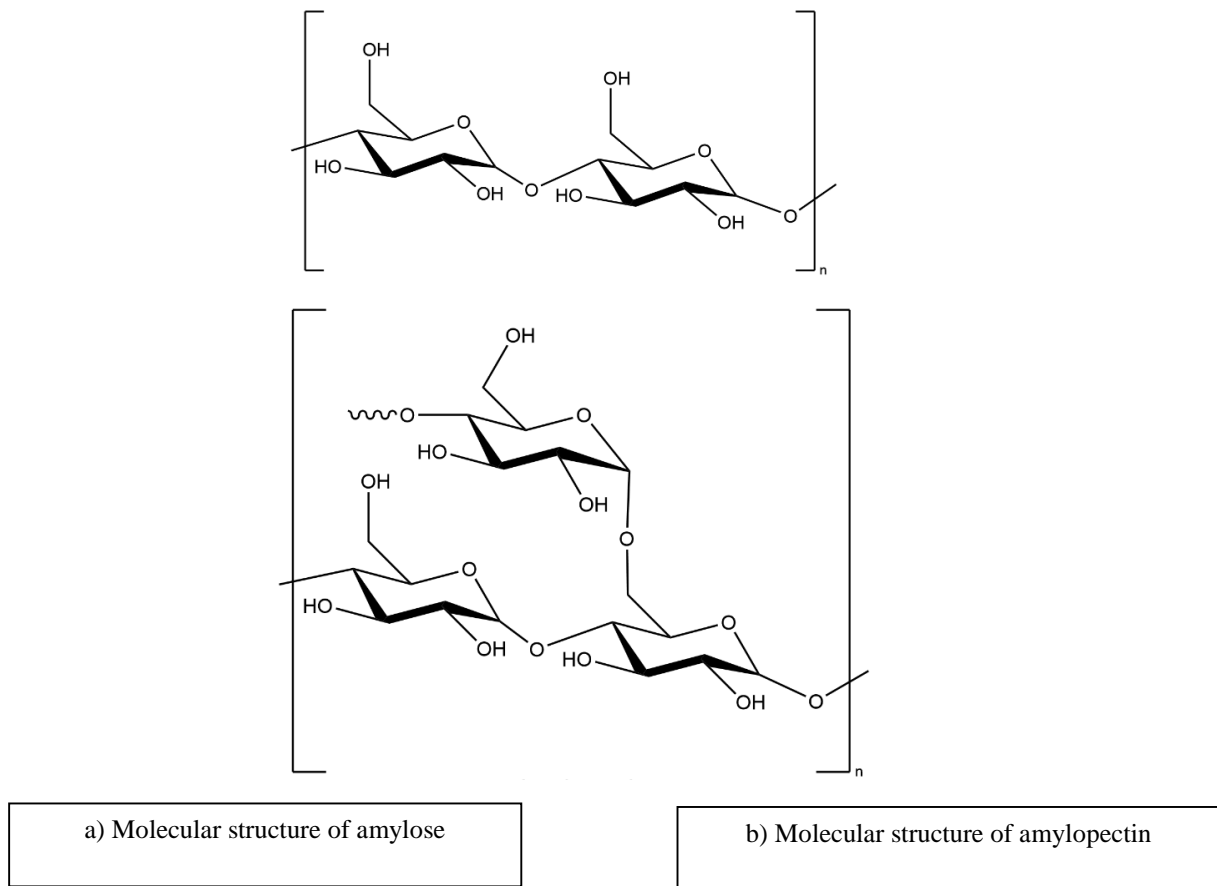
a) Molecular structure of amylose	b) Molecular structure of amylopectin

Figure 1 - Chemical structure of amylose (a) and amylopectin (b)

biopolymers, adding a lot of plasticizers like glycerin or ethylene glycol, or altering the chemical makeup of starch itself. The ratio of amylose to amylopectin, the ability of the starch to form films, the size and shape of the grain, and the temperature at which the starch becomes gelatinous are all influenced by the source of the starch. The overall structure, shape, and thermal properties of starch are influenced by the ratio of amylose and amylopectin [18].

The decomposition of biopolymers is facilitated by hydroxyl groups that bind water. Starch is a polymer with functional (-OH) hydroxyl groups in the structure, which consist of D-glucose. When a small amount of acid is added to the starch solution as a catalyst, its hydrolysis occurs. Macromolecules break down into smaller molecules (dextrin, maltose), and the final product of the hydrolysis reaction is alpha glucose. The reaction mechanism proceeds as follows: a positively charged ion is attracted to an oxygen bridge between two alpha-glucose residues, and connects with an oxygen atom, thereby breaking the connection. On the atom of the second fragment of the starch molecule, it forms a positive charge, which attracts the water molecule to itself. The oxygen in the water molecule is attached to a carbon atom, and one of the hydrogen molecules is separated from the water molecule. As a result, dextrin molecules are formed, which are hydrolyzed by the same mechanism to form maltose molecules. The final product of starch hydrolysis is an alpha-glucose molecule. Starch is a very popular vegetable polysaccharide with excellent film-forming properties. However, some hydroxyl groups can be replaced with ether or ester groups. In this case, water will not be able to easily affect the polymer. To increase the heat resistance of polymers, acid resistance, and shearing force, additional chemical treatment is required, which makes it possible to create additional bonds between different parts of the polymer - starch [20].

The excellent properties of starch as a natural multi-tonnage polymer arouse the interest of researchers and large manufacturers for the development and production of various starch-based products.

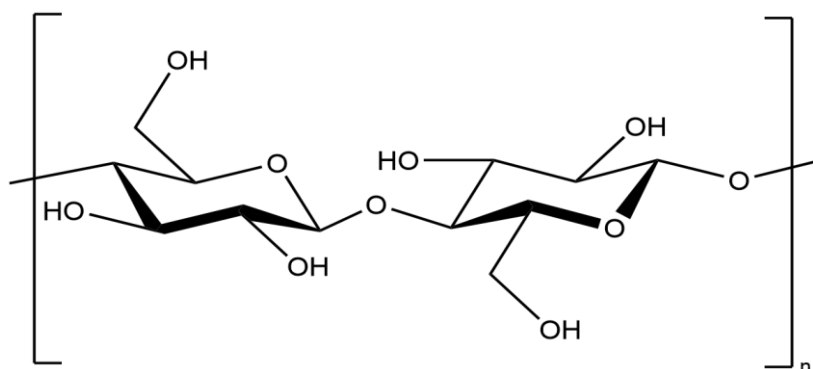The main advantages of starch as a natural polysaccharide [21]:

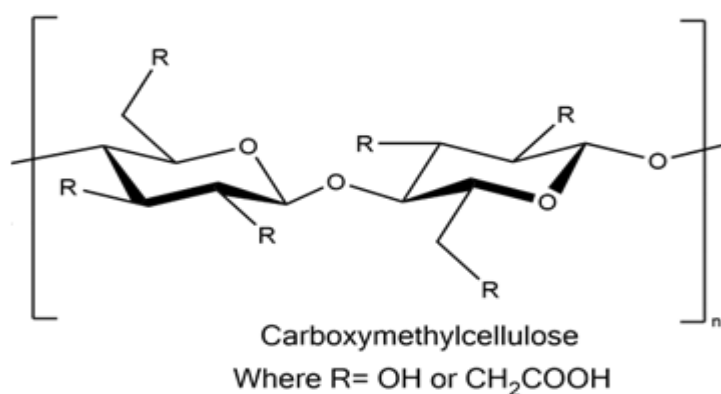**Figure 2**- The chemical structure of Cellulose

Figure 3 - The chemical structure of Carboxymethylcellulose

− the renewability and inexhaustibility of raw materials from year to year, such as potatoes, corn, wheat, rye, etc. This raw material has a huge advantage over cellulose obtained from wood, which takes at least 17-20 years to grow.

− easy modification and giving valuable characteristics through chemical, physical, biological, or combined interaction.

− a wide range of reactions with starch related to the chemistry of low molecular weight compounds.

− the ability to give biodegradable properties to synthetic polymers using starch.

− environmental friendliness, no toxicity and convenience of working with starch.

Cellulose (Figure 2) is a fascinating natural polymer that contains reactive OH groups. The molecular structure of starch and cellulose are identical; cellulose is a polysaccharide. The d-glucose units in starch are connected to -glycosidic bonds, but they are not present in cellulose.

Cellulose has high mechanical strength, does not dissolve in water and organic solvents, and also does not melt. Cellulose, when interacting with acid, is easily hydrolyzed. It is known that to obtain cellulose gum, it is necessary to dissolve cellulose in a solution of sodium hydroxide and carbon disulfide. Then it is converted to sulfuric acid and a cellophane film is obtained [22]. The simplest cellulose derivative is methylcellulose. It has high film-forming properties, good solubility, and low oxygen permeability. Methylcellulose has all the prospects as a raw material for biodegradable materials [23]. The characteristics of edible films made of methylcellulose were studied with the introduction of special extracts saturated with polyphenols and antioxidants into the mixture [24]. A film packaging made of cellulose glued with starch, with high resistance to fats, allowed for direct contact with food products, was obtained. This packaging is resistant to high or low temperatures and is used when baking products in the oven or microwave [25].

A method is known for producing biopolymers by the interaction of cellulose with an epoxy compound and dicarboxylic acid anhydrides. As a result, the obtained biomaterials are completely biodegraded in compost in 4 weeks. Products such as disposable tableware, films, bottles, etc. are made by molding [26].
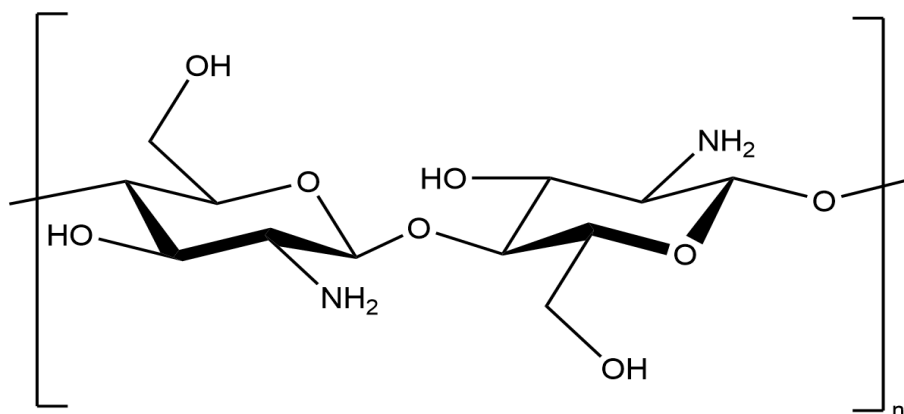
Figure 4- The chemical structure of Chitosan

The carboxyl methyl group (-CH$_2$-COOH) of carboxymethylcellulose (CMC; Figure 3) is linked by the hydroxyl groups of glucose monomers. CMC is readily soluble in water, possesses strong film-forming abilities, and gets along well with other biomolecules [22].

There is a nitrogen-containing polysaccharide from the residues of n-acetyl glucosamine, interconnected by β-glycoside ties which are called chitin. It can be obtained by fungi or in the sea (the shells of shrimps, crabs, and lobsters). The predominant characteristics of chitin are low density, layered structure of the polysaccharide, high ability to form a film, selectivity of interaction with bacteria, and radio-absorbing and radioprotective properties. All these important properties of chitin make it possible to develop biodegradable materials based on it when interacting with polyethylene [27]. Chitosan is an amino sugar, a linear polysaccharide derivative, whose macromolecules are made up of randomly bound β–(1-4) D-glucosamine units and N-acetyl-D-glucosamine (Figure 4). It is a chitin derivative.

The main advantages of Chitosan to produce edible films are non-toxicity, environmental friendliness, biocompatibility, biodegradability, and the ability to form films [28]. It has been established that chemical and physical modifications are used to improve the technological properties of chitosan in the manufacture of biofilms. For example, mixing chitosan with starch or protein [29]. Starch is the most suitable biopolymer for mixing with chitosan because it is available as a raw material and has excellent physical characteristics (tasteless, odorless, and transparent) [30].

Agar — a mixture of agarose polysaccharides and agaropectin obtained by extraction from red algae (Rhodophyta) is an excellent alternative for obtaining biodegradable polymers. Agar compositions with synthetic polymers (polybutylene adipate-terephthalate (PBAT), low-density polyethylene (LDPE) and polyvinyl alcohol (PVA)) have been studied [31].

Pectin is a polysaccharide formed mainly by galacturonic acid residues. High-strength and flexible films with heat resistance up to 180 °C are obtained from a mixture of citrus pectin components and high-amylose starch [32]. The structure of galacturonic acid is shown in Figure 5.

Protein is a high molecular weight organic substance consisting of alpha-amino acids connected to a chain of peptide bonds. It is a natural polymer made from vegetables and animals. Soy protein, gluten, etc. are also of interest to produce biopolymers [33]. The cohesiveness of the protein, its adhesiveness, the ability to absorb water and fat, as well as the ability to texture, give a high degree of film formation to biodegradable polymers [34]. Soy products such as soy milk, soy flour and fractionated soy proteins have also been studied [35]. There are two main factors in the production of biopolymers based on soy: this is the concentration of protein and the pH of the film-forming mixture. When casting the film, the protein concentration is 4-5%, when using the "dry" technology; the protein concentration is 80% [36].
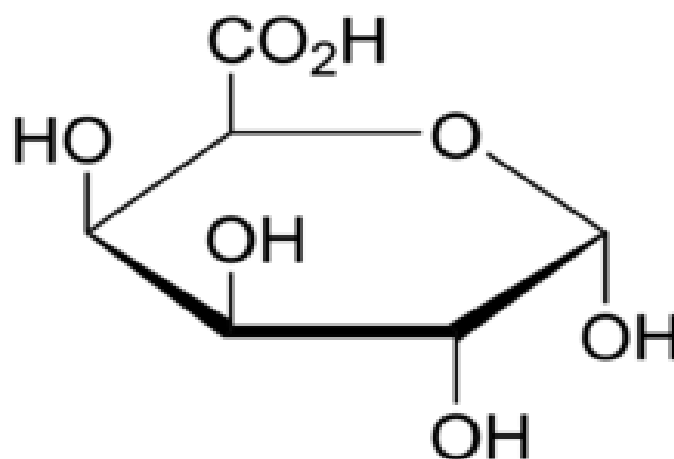
Figure 5 - The chemical structure of Galacturonic acid

Figure 6 - Microorganism: a) Paracoccus, b) Bacillus, c) Spirullum

Bioplastics from Naturally Occurred or Genetically Engineered Microorganisms

Biopolymers, such as Paracoccus, Bacillus, and Spirillum (Figure 6), are created by living microbes. One such biopolymer is poly (3-hydroxybutanoic acid), which is produced from glucose by certain microorganisms. PHB is a biopolymer with similar properties as synthetic polymers, but under aerobic conditions, it can completely decompose to water and carbon dioxide molecules. This biopolymer is obtained by fermentation of glucose strains or wastewater. Cane sugar and starch are the most affordable and suitable carbon sources to produce PHB. According to the LCA categories, the production of PHB is less environmentally harmful than the production of polypropylene (PP). The demand for crude oil in the production of PHB is much lower; accordingly, this significantly reduces the impact on the environment. If we consider the production of PE and PHB, then PE has a lower environmental impact in terms of acidification and eutrophication, but if we consider the utilization of polymers - the burning of synthetic polymers, this will significantly increase the environmental burden [22]. Within 9 months after disposal, PHB can be broken down by microorganisms in the soil and natural water sources. PHB costs 15 times as much as polyethylene, though.

Poly(3-hydroxybutyrate)-hydroxy valerate (PHBV) is a copolymer comprising hydroxybutyrate (PHB) and hydroxy valerate (HV). It crystallizes strongly. The tensile strength and crystallinity of polymers decrease while the impact strength increases with the development of HV, the melting point, and the glass transition temperature. PHB is more delicate than PHBV. PHBV breaks down more quickly than PHB [24].

Light-sensitive functional groups, such as carbonyl groups, are integrated into the polymer chains of photodegradable polymers. These groups will collect solar energy and use it to disrupt the polymer's chemical connections, resulting in tiny pieces that break down more quickly than lengthy strands. However, these polymers and synthetic biodegradable polymers have the same problem - both are obtained from materials that were derived from fossil fuels [23]. Photodegradable plastic bags are shown in Figure 7.

Figure 7 - Photodegradable plastic bags

A significant role is played by the issue of giving biodegradable properties to existing industrial polymers such as Polyethylene (PE), Polypropylene (PP), polystyrene (PS) and polyethylene terephthalate (PET). The strategy to get photo-degradable or oxo-biodegradable plastics is to add to standard conventional plastics such as PE, PP, PET etc. some photodegrading additives. These additives are added in at the extrusion stage, they help to attack free radicals on the polymer and initiate degradation. The chain breaks with the formation of smaller fragments, where bacterial degradation starts. Polymers can be decomposed within a few months [24].

These additives are mainly based on transition metals of cobalt (Co), magnesium, manganese, zinc, iron, or nickel. These metal ions have a high susceptibility to light, heat, and moisture. These factors lead to mechanical stress and weaken the tensile strength of the chain [24].

Synthetic Biodegradable Plastics

Synthetic biodegradable materials can be obtained by polymerization, such as aliphatic polyesters, polylactic acid-based polylactic acid copolymers, and others [26]. Polylactic acid is linear aliphatic polyester. Polylactic acid is obtained by polymerization of lactic acid made on the basis of fermentation of corn sugars or other biological mass. The breakdown of polylactic acid proceeds in two stages. In the first stage, the ester groups are hydrolyzed with water to form lactic acid and other small molecules. Next comes their decomposition in the presence of advising microorganisms in a certain environment. Polylactic acid reaches 72% decomposition within 45 days under favorable composting conditions [37]. To date, polylactide is one of the promising bios-destructive polymaterials for use as a packaging material. Polycaprolactone is biodegradable synthetic aliphatic polyester with a low melting point and high mechanical strength, as well as high barrier properties to water and fats. Biodegradation of this polymer occurs by 75% after 28 days of contact with relevant microorganisms and fungi [38]. Shtilman and other authors obtained biodegradable copolymers of the product of the co-polymerization of ethylene with caprolactone using the grafted copolymerization method [39]. There are companies "El-Batyr Biopolymer" LLP and "Eco Products" LLP which produce biodegradable bags based on PLA in Astana (Kazakhstan).

PVA is a synthetic polymer with biodegradable properties, high mechanical characteristics, good film-forming properties, and high thermal stability, and PVS has the property of high bonding. PVA has mainly C-C connections in its chain. They activate rapid biodegradation [40].

PVA is produced worldwide on an annual basis in quantities of several hundred tons. It is the largest quantity of water-soluble polymer currently manufactured. PVA is produced by hydrolysis of poly (vinyl acetate) in an alkaline medium, with a possibility of fluctuating the degree of hydrolysis as shown in Figure 8 [19].
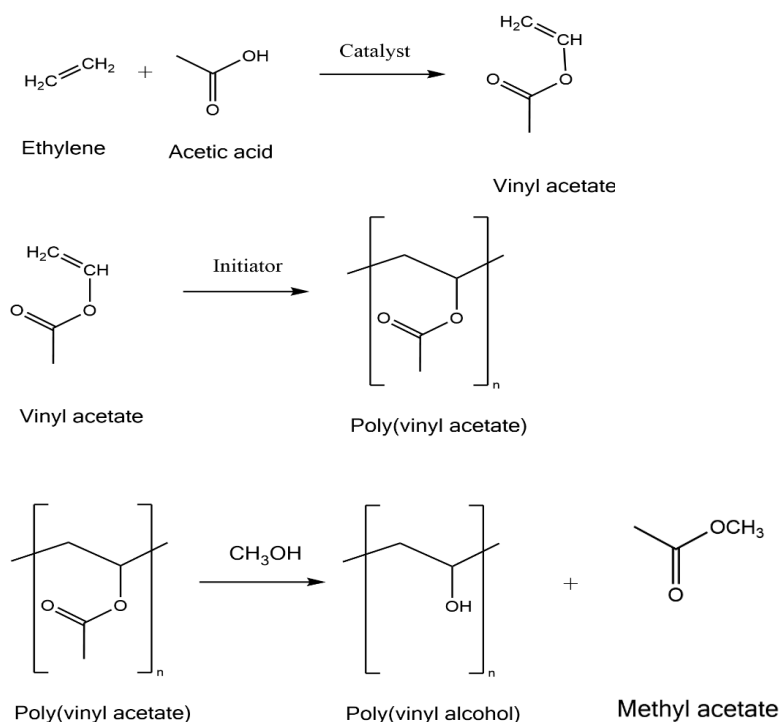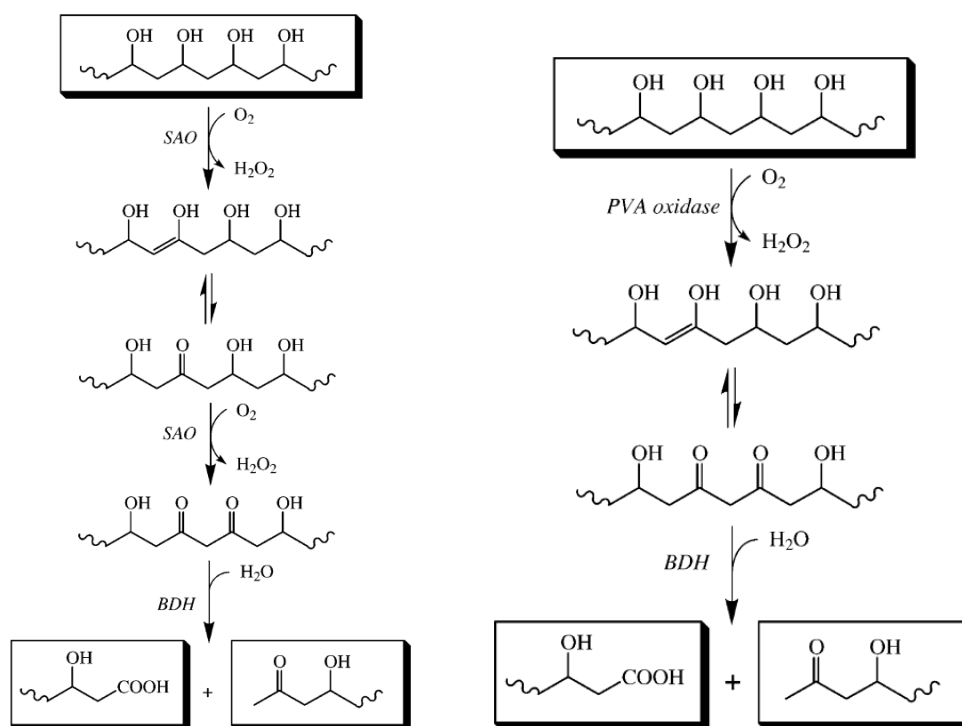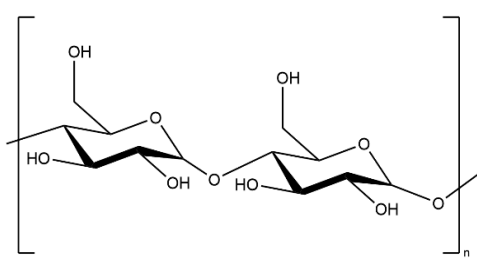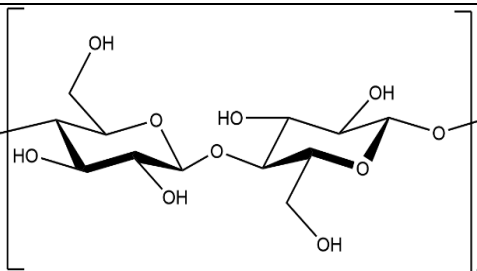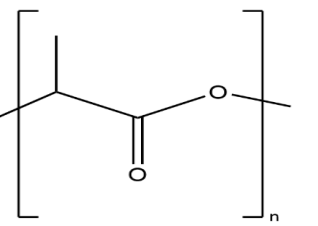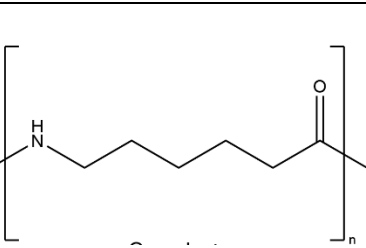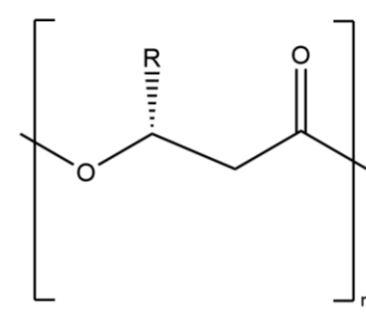
Figure 8 - Scheme of PVA production

Figure 9 - Metabolic pathways of PVA degradation

PVAc is obtained by free radical polymerization. Fully hydrolyzed PVA has higher performance characteristics compared to partially hydrolyzed PVA. The molecular weight of PVA is regulated by the time of polymerization in the reactor, the rate of supply of vinyl acetate, the amount of solven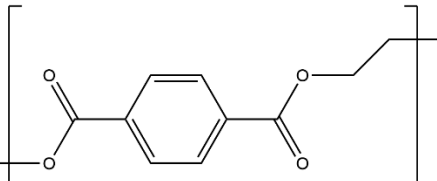t (methanol), the concentration of the radical initiator, and the temperature of polymerization. The degree of PVAc hydrolysis is regulated by the time of presence, the concentration of the catalyst, and temperature [41].

Watanabe and his associates explored the PVA depolymerization mechanism in the 1970s. Their

Table 2 - Characteristics of the main biodegradable polymers.

Starch-based biopolymers		
	In terms of mechanical properties, they are close to conventional polymers and resistant to fats and alcohol. A significant difference in properties depends on the ratio of amylopectin and amylose, as well as other additives. Subject to composting	Packaging of food and personal hygiene products, medical and sports products
Cellulose-based biopolymers		
	They have a sufficiently high mechanical strength; they are easily hydrolyzed under the influence of acids. Varieties: acetyl cellulose, carboxymethyl cellulose, celluloid, etc.	Products for household use, construction and sports purposes, toys
Polylactic acid, polylactide (PLA)		
	The properties depend on the stereochemical composition and may approach the properties of polypropylene, polystyrene, polyvinyl chloride	Packaging for household and construction purposes, biocomposites
Polycaprolactam, polycaproamide, Capron (PCL)		
	High mechanical strength and good barrier properties (concerning water and fats), low melting point (50 °C). It can be composted or recycled.	Packaging, fibers for textiles
Polyhydroxyalkanoates (PHA)		
	The physicochemical properties depend on the composition. The presence of properties characteristic of both thermoplastics and elastomers. High barrier properties. They are subjected to composting.	Packaging of food and personal care products, biocomposites, foams

Continued Table 2

Aliphatic-aromatic Copolymer (AAC)		
	Combines the biodegradability properties of aliphatic parts with the high mechanical properties of aromatic parts.	Packaging, laminates, and material for storing products in agriculture and construction.
Modified Polyethylene terephthalate (pet)		
	High mechanical strength and good barrier properties (in relation to water and fats). It can be subjected to composting and recycling.	Packaging, agricultural products

further investigation revealed that the compound's bonds cleave at random, thus grafting won't significantly affect the polymer chain's biodegradability. Numerous metabolic pathways exist, some of which are depicted in Figure 9. Typically, neither the degree of polymerization nor the degree of hydrolysis affects how quickly PVS degrades [33].

Polyvinyl alcohol dissolves well in water, and successfully undergoes final biodegradation due to the corresponding microorganisms. Therefore, great interest is shown in the production of environmental materials based on polyvinyl alcohol, and their use in a wide range of applications. The main characteristics of the most popular biodegradable polymers are shown in Table 2.

The Dependence of the Structure and Properties of Polymers on Biodegradation

The dependence of the structure and properties of polymers on biodegradation based on:

- Molecular weight. It was found that with a decrease in the molecular weight of macromolecules, the ability of polymer biodegradation increases.
- Crystallinity of polymers. It has been proved that by increasing the degree of crystallinity, the ability of biodegradation of polymers decreases, i.e., polymers with an amorphous structure are destroyed better than polymers with a crystalline structure. Also, the biodegradability of low-molecular polymers with a crystalline structure is better than high-molecular polymers. The ability to biodegrade is higher when branching in polymer macromolecules is formed. The introduction of various modifying additives into polymers significantly affects the ability to biodegrade [21].

For example, ester plasticizers increase the biodegradability of PVC on the one hand, however, uneven dispersion on the polymer surface of a biodegradable plasticizer -dibutyl phthalate can lead to a low biodegradability of PVC. The rate and outcome of polymer biodegradation are complicated processes that are influenced by environmental factors such as humidity, temperature, pH, light, contact with soil, and type of soil, in addition to the polymer's structure and qualities [21].

Oxybiorestructive Additives

There are special oxybiorestructive additives based on modified starch, lactic acid, and cellulose, which contain metal ions - carboxylates, which accelerate photo- and thermal oxidation in polymer materials (Table 3). The main difference between these additives from conventional ones is the high efficiency at low doses of concentration from 1 to 3%, as well as their decomposability by two factors: UV radiation and the action of microorganisms.

The mechanism of biodegradation due to oxybioregosing additives is that salts of transition metals (cobalt, zinc, iron, etc.) contribute to the appearance of free radicals that create hydroxides and peroxides as esters, aldehydes, ketones, alcohols, and carboxylic acids. These compounds are easily biodegradable. Microbes and fungi spread on the folds of the film and throughout its thickness. In the process of biodegradation of polymers, three stages are distinguished: stage 1 – oxidative processes (exposure to UV light, high temperature); Stage 2 – reduction of physical characteristics (fragility and size reduction); stage 3 – decomposition into molecules and a further chain of transformations to carbon dioxide and water.

Table 3 - Characteristics of oxybiorestructive additives

Name	Properties
PDQ-H	An additive whose principle of operation is based on the reduction of the molecular weight of the main polymer (to improve biological decomposition) under the action of UV radiation and oxidizing media. Decomposes by UV radiation and microorganisms
ECM	The additive is decomposed by microorganisms
Bio-Batch	The additive is decomposed by microorganisms
Renatura	It contains a unique iron-based ingredient (the company's development) and is mainly used for the biodegradation of polyolefins
Reverte	Additives and masterbatch mixtures containing prodegradants from metal ions impart photo- and thermal decomposition to the base polymer. It also contains a unique biodegradation booster of the second stage, which uses a reaction rate modifier to control
D2w	the initiation and timing of oxybioregradation
P-Life	Prodegradant additives based on masterbatch polyester, polypropylene, or polystyrene. The company also supplies fully degradable polymer materials
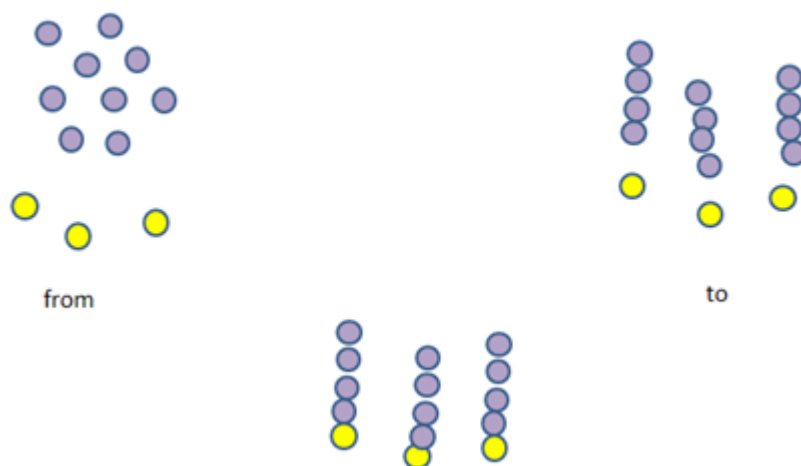
Figure 10- Schematic illustration of two types of graft-copolymerization

Grafting Copolymerization

Grafting copolymerization is a type of polymerization, where one or several blocks of homopolymer are grafted onto a main backbone like branches. This approach of modification of polymer allows upgrading properties of main chain with growing of grafted chain of another polymer.

There are the most popular grafting techniques: "grafting from" and "grafting to" techniques. The schematic illustration of two types of graft copolymerization is shown in Figure 10. The "Grafting from" method is the initiation of polymerization of the main chain with monomer solution by the special catalyst and the "grafting to" technique uses a special coupling agent [27].

Synthesis of Biodegradable Starch-Based Materials

Obtaining biodegradable starch-based materials boil down to several principles [30]:

– the creation of thermoplastic starch and its derivatives.

– the creation of a mixture of synthetic and natural polymers.

– the creation of starch products by extrusion method.

Methods of obtaining and characteristics of the obtained materials are widely covered in many publications and reviews. Thanks to the processing, starch is modified, can decompose in the environment, and has the properties of the necessary thermoplastics. The equipment to produce modified starch is the same as to produce ordinary plastic. Modified starch can be dyed, and it can also be printed using all standard technologies. This material is antistatic. The physical properties of modified starch are still inferior to the properties of resins – low and high-pressure polyethylene, and polypropylene. Starch decomposes at a temperature of 30 °C in two months [[30], [31], [32]].

Methods of producing extrusion-blown and injection-molded films containing 50% starch have been studied. The water resistance of these films was achieved by applying polyvinyl chloride to the surface of the film [40]. Mixing urea with polyols helped to improve starch plasticization and obtain high-quality films [41]. It has been established that to improve the technological properties of starch for the manufacture of biofilms, various modifications are used, such as mixing with other compounds, and grafting-copolymerization [42]. Due to intermolecular and intramolecular hydrogen interactions between the amino and hydroxyl groups of the major chains of the two components, chitosan/starch combinations produce films with a high degree of film formation. The physicomechanical, water-barrier, and miscibility characteristics of biodegradable films are influenced by the ratio of starch and chitosan [43]. Films based on starch and agar were investigated. It was found that the addition of agar improves the microstructure Mirzoerova et al. used calcium carbonate as a plasticizer to produce a film based on starch and polyvinyl alcohol (60:40 wt. %) by mechanical mixing. It is revealed that with an increase in the concentration of calcium carbonate, the mechanical properties of the film increase, in particular, the tensile strength. The degrees of biodegradation of films in the soil were determined. It turned out that with an increase in the percentage of the plasticizer - calcium carbonate in the mixture, the degree of biodegradation increases [42].

Starch can serve as a filler to produce reinforced plastics. For this, a little starch is added to the synthetic polymer, giving these polymer biodegradable properties. Starch is modified in various ways to produce plastic masses based on it. The starch solution is cast to create the film. However, this method has not been widely applied due to the high expense of manufacturing starch solutions. The thermomechanical processing techniques (wet starch compression, extrusion, and injection molding) have received most of the attention in studies related to starch products. The article shows the results of research and characteristics of polymer compositions based on starch and calcium chloride. It has been known the thermal stability of this composition reduced with the rising of calcium chloride [44]. According to the publication [45], starch was modified directly in extruders, starch esters and esters, grafted copolymers, and oxidized and cationic starches were obtained.

To produce biodegradable polymers, starch is mixed with aliphatic polyesters or polyvinyl alcohol. Main et al. synthesized polyesters as polyhydroxyalkanoates by microbes and polylactide by chemical polymerization [46]. It is noted that among the above-mentioned synthetic polymers, polyvinyl alcohol is the most popular in use. PVA has excellent qualities such as high compatibility with starch, ease of preparation, absence of carcinogens, relative cheapness, good biocompatibility, and biodegradability in nature. It was found that the usual mixing of polymers strongly affects the quality of the resulting films. PVA and starch interact well with each other, forming intermolecular and intramolecular hydrogen bonds due to the excess of hydroxyl groups in both polymers (Figure 11).
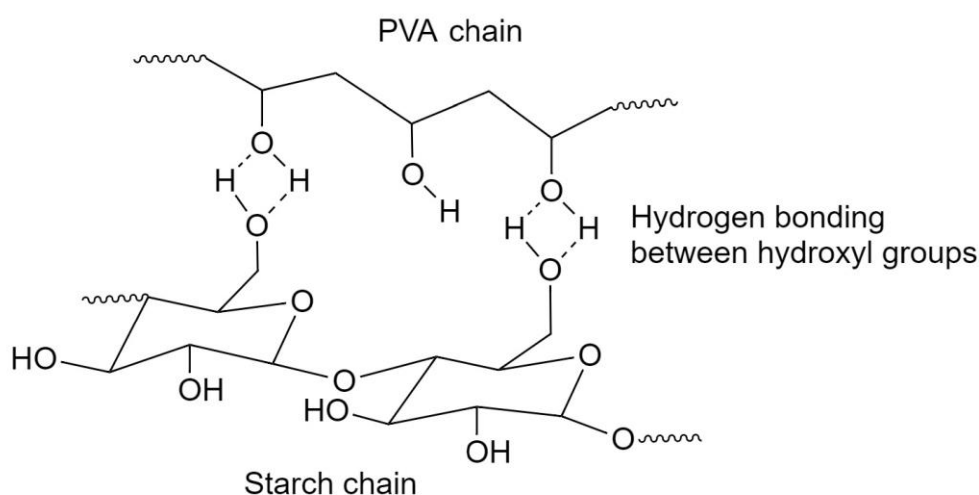
Figure 11 - Hydrogen bonding between PVA and Starch chains.

This contact causes the films to absorb more water. However, chemical starch modification can be used to enhance the water-resistant qualities of films made of a PVA/Starch (PVA/C) combination. The most popular technique for enhancing the qualities of natural polymers like starch is grafting. In addition, it is assumed that the film from the PVS/K mixture is biodegradable since both components easily degrade in the bacterial environment. In this regard, scientists are faced with the task of improving the structural integrity of the polymer mixture. There are various crosslinking agents for starch crosslinking [21]. A method is known for producing a biofilm-based on starch and PVA, a mixture of which was modified with silicon dioxide nanoparticles. The results were improved mechanical properties, water resistance, and light transmission of the films [47].

Crosslinking agents are not safe and toxic, respectively, and have limitations for their use both in everyday life and for medical purposes. In scientific work, maleic acid was used as a crosslinking agent between starch and PVA using esterification to increase the physical and mechanical properties and to create a high-quality polymer. Maleic acid is a common food additive, nontoxic, and biologically pure. These characteristics are favorable for obtaining biomaterial being a dicarboxylic acid, the starch esterification reaction with PVA proceeds through the substitution of carboxyl groups of maleic acid with free hydroxyl groups of starch and PVA [48].

Plasticizers, namely their carboxyl and hydroxyl groups, are utilized to increase molecular dynamics and provide flexibility. Additionally, crosslinking changes significantly enhance the tensile strength, elastic modulus, heat, and water resistance, swelling capacity, and antibacterial activity of biofilms. Gas tightness, mechanical rigidity, transparency, and thermal stability are enhanced thanks to the filler. Chemical and physical modifications make it possible to improve films by changing the molecular structure during esterification, esterification, due to the formation of hydrogen bonds and oxidation [22].

Gulati et al. analyzed the effect of carboxymethyl cellulose (CMC) on the thermal and mechanical properties of PVS/starch films, which were synthesized and obtained by casting. Glycerin is a plasticizer. Citric acid is a crosslinking agent. It was revealed that with an increase in the concentration of CMC, the thermal stability of PVS/starch films increased. The PVA/starch/CMC film had a maximum tensile strength of 36.56 ± 1.54 MPa and was used for testing when adding walnut shell flour (WSF). The PVA/starch/CMC films reinforced with WSF have improved thermal stability and water resistance. However, this also led to a decrease in the film's biodegradability [23].

Incorporating -polylysine into maize starch/polyvinyl alcohol (PVA)/glycerin films was studied by Bin Liu et al. The hydroxyl group of the starch/PVA combination and the amino group of -polylysine interacted, according to FTIR studies. The films' thermal stability increased with the addition of -polylysine. It was also looked at if adding -polylysine produced a flatter surface. The tensile strength and elongation at the break of films, as well as other strength characteristics, have improved. The films' antibacterial and water absorption capacities have also improved [24].

Intelligent Films Based on Starch

Today, starch-based packaging materials are being developed with new features that control the quality of the food packaged inside or determine the environment of the food. This is how packaging is called smart packaging. For this, natural active substances with antibacterial and antioxidant activity are used.

In comparison to other biodegradable polymers, the fundamental benefit of starch-based film is its lack of color and transparency. Changes in factors like color can be visibly identified thanks to the content of indicators in intelligent packaging. The freshness indicator reacts with some of the gases released during food storage to reveal the shelf life of food goods. The shelf life of food goods is also shown by a temperature-time indicator, which considers the effects of both time and temperature accumulation [30].

Films constructed of PVA and starch were deemed sensible packaging by Abedi-Firoozjah et al. Due to the chemicals found in PVA/starch films' antioxidant and antibacterial properties, these films can be utilized as a sign of the quality and safety of food. It should be emphasized that the source, kind, quantity, and composition of the active chemicals determine how effective these packing sheets are. The way different polymers and components interact inside the film structure is also crucial. The PVA/starch film is given colorimetric characteristics by the addition of natural food dyes. Products containing food may benefit from such clever packaging [25].

Indicator of Freshness

The biopolymer is in a great position to create intelligent colorimetric films thanks to starch's high capacity for film formation. These days, there is a lot of interest in the creation of intelligent pH-sensitive starch-based films. Changes in pH are the main indicators of food freshness. When food begins to rot due to microbial action, the environment begins to change, and therefore the freshness and quality of food can be determined by changing pH values. The environment and the human body are both safe around organic pH monitors. Curcumin (CR), carotenoids, anthocyanins (ATH), and others are some of the well-known natural markers. Electrochemical and colorimetric methods are used to determine the pH values [31].

Ammonia, dimethylamine, triathalon, and other gases that alter the pH level around the food are produced as a result of rotting food. Additionally, in accordance with its function, the organic indicator present in the packing film will change color in response to the pH shift. A strong color intensity results from the high anthocyanin concentration. The high starch content's porosity results in great sensitivity. The mechanical strength of the sensor increases with cellulose binder concentration. The color of anthocyanins changes from mauve to blue-violet to blue-green as the pH rises. The customer assesses the product's freshness based on the color shift [30].

A colorimetric pH agar/potato starch/anthocyanin indicator film was created by Choi et al. This film was used to package pork, and as the meat's quality declined and the pH altered, the film's color changed from red to green [32]. The pH of logs made from chitosan/cornstarch/purple cabbage extract was examined by Silva-Pereira et al. This is how they established the fish's breakdown [33]. Liu et al. (2017) studied PVA/starch film containing purple yam for quality control of pasteurized milk. They kept the milk in this package for 48 hours, after which the color of the smart film changed from purple to red, indicating spoilage of milk at room temperature [36]. To ascertain the deterioration of pasteurized milk, Mustafa et al. (2020) investigated a film based on PVA/starch/propolis/red cabbage extract. The color of the film quickly and clearly changed from pink to light purple and then to yellow when the pH value changed from an acidic to an alkaline environment [37].

Manufacturers of Biodegradable Plastic Materials

The largest manufacturers of biodegradable plastic materials are Nature Works (USA), BASF (Europe), Novamont (Europe), and Mitsubishi Chemicals (Japan).

Popular brands on bioplastics:

1) Novon™ is a starch-based biopolymer; modified polysaccharide derivatives are often added. Products: disposable tableware, egg packaging, cosmetics, wrapping films for textiles and clothing, medicinal capsules, diapers for children, women's tampons, etc.

2) Biopac™ is a starch-based biopolymer with a content of 87-94%. Products: packaging of bakery products, cereals, eggs, etc.

3) Bioceta™ is a cellulose-based biopolymer with additives. Products: Packaging of batteries for household electrical appliances.

4) Bioflex™ is a starch-based biopolymer with the addition of plasticizers such as alcohols, sugars, fats, wax, and aliphatic polyesters.

Film material decomposes in compost at a temperature of 30 °C in 56 days with the formation of products favorable for plant growth.

Market Development for Biodegradable Polymers

European Bioplastics gave a positive forecast for the world bioplastics industry. There was no dynamic plastics production in 2020, mainly because of Covid-19. But now there is a new impulse for global bioplastics manufacturing. It is a positive outlook for the capacity from 2.23 million tons of bioplastics production in 2022 to 6.3 million tons -in 2027. The data was done with the cooperation of the Nova-Institute (Hürth, Germany) and European Bioplastics [49].

According to data [50]. In 2021 world plastic production increased by 4% and accounted for around 390 million tons. The reason is the growing demand for and development of more sophisticated applications and products. Over the next five years, manufacturing capabilities will continue to rise dramatically and diversify as a result of the strong development of polymers such polyhydroxyalkanoates (PHA), polylactic acid (PLA), and polyamides, as well as the steady expansion of polypropylene (PP).

Nowadays the world produces annually more than 1.1 million tons (51%) of biodegradable plastics based on PLA, PHA, starch blends, and others. The capacity of bioplastic production will increase due to the rapid development of PHA (polyhydroxyalkanoates), polylactic acid (PLA), and others. In 2027 it is predicted to produce more than 3.5 million tons based on these polymers. Global production of non-biodegradable plastic materials such as biobased PE, biobased PET, and biobased PA has amounted to almost 1.1 million tons (48%) annually. In 2027 it is expected decrease in these materials will be around 44% [51]. Bioplastics are widely used in various sectors such as food packaging, children's toys, consumer electronics, auto manufacturing, agriculture, and textiles. In 2022 packaging will be the largest bioplastics application sector with almost 1.1 million tons (48%) of the total bioplastics market [52].

Asia is the largest player in this industry and produces about 41% of eco-plastics. Now, more than 25% of production capacity remains in Europe. According to forecasts, in 2027 the share of Europe and other regions of the world will decrease significantly while production capacity in Asia will grow to almost 63% [53].

In 2022, the world's agricultural area is 5 billion hectares, of which only 0.8 million hectares or 0.015% is allocated to land for the cultivation of renewable raw materials to produce bioplastics. Simultaneously with the forecast of a significant increase in global bioplastics production until 2027, the earth is projected to grow by up to 0.06%. This proves that the production of bioplastics does not interfere in any way with the use of land for growing food and feed [54].

Conflicts of interest. The authors declare no conflicts of interest, financial or otherwise.

Қаптама пленкаларына арналған крахмал негізіндегі биологиялық ыдырайтын полимердің синтезі: Шолу

1*Искалиева А.Ж, ²Оразалин Ж.Қ., ²Елигбаева Г.Ж., ³Ирмухаметова Г.С., ⁴Табурова С.Н., ⁴Тоқтар Т.А.

¹Химиялық инженерия мектебі, Қазақ-Британ техникалық университеті, Алматы, Қазақстан
²Мұнай өнеркәсіп мектебі, Сәтбаев университеті, Алматы, Қазақстан
³Химия және химиялық технология факультеті, әл-Фараби атындағы ҚазҰУ, Алматы, Қазақстан
⁴ Энергетика және мұнай-газ индустриясы мектебі, Қазақ-Британ Техникалық Университеті, Алматы, Қазақстан

ТҮЙІНДЕМЕ

Өзінің маңызды қасиеттері мен функционалдық мүмкіндіктеріне байланысты полимерлерге соңғы жылдары азық-түлік орауыш материалдары ретінде көп көңіл бөлініп жатыр. Бұл сипаттамаларға уытты еместігі, қолжетімділігі, биоүйлесімділігі және биоыдырағыштығы жатады. Бұл оларды қоршаған ортаға әсері бұрыннан зерттелген дәстүрлі пластикалық қаптамаға балама етеді. Қазіргі уақыттағы тұрақты дамуды ескере отырып, биополимерлерді тамақ өнімдерін орау үшін экологиялық таза және тұрақты материалдар ретінде зерттеу өте маңызды. Крахмал негізіндегі биологиялық ыдырайтын полимерлерді синтездеу маңызды қадам болып табылады. Экологиялық таза материалдарға жаһандық сұраныс өсіп келе жатқандықтан, осы саладағы үздіксіз зерттеулер мен инновациялар қасиеттері жақсартылған және кең қолданылатын крахмал негізіндегі орау пленкаларын кең өндіруге әкелуі мүмкін. Осыған байланысты, бұл шолудың негізгі мақсаты пластикалық пакеттерде пайдалану үшін жоғары физика-механикалық сипаттамалары бар жүгері крахмалы мен ПВА негізіндегі биологиялық ыдырайтын полимерді жасау болып табылады.

Түйін сөздер: Полимерлер, биологиялық ыдырағыштық, қаптау, пластикалық пакеттер.

Авторлар туралы ақпарат:

Искалиева Асылзат Жамбуловна	*Ph.D., Қазақстан-Британ техникалық университеті, Химиялық инженерия мектебінің студенті, Төле би көшесі, 59, Алматы 050000, Қазақстан. Email: asylzat@bk.ru*
Оразалин Жандос Қайратұлы	*Мұнай инженериясы кафедрасы, Сәтбаев университеті, Сәтбаев көшесі, 22, Алматы 050013, Қазақстан. Email: zhandos1403@bk.ru*
Елигбаева Гульжахан Жакпаровна	*Мұнай инженериясы кафедрасы, Сәтбаев университеті, Сәтбаев көшесі, 22, Алматы 050013, Қазақстан. Email g.yeligbayeva@satbayev.university*
Ирмухаметова Галия Серикбаевна	*Органикалық заттар, табиғи қосылыстар және полимерлер химиясы және технологиясы кафедрасы, Химия және химиялық технология факультеті, әл-Фараби атындағы ҚазҰУ 71, әл-Фараби даңғылы, 050040, Алматы, Қазақстан. Email: Galiya.Irmukhametova@kaznu.kz*
Табурова Ситора Нематовна	*Энергетика және мұнай-газ индустриясы мектебінің бакалавриат студенті, Қазақ-Британ Техникалық Университеті, Төле би көш.,59, 050000, Алматы, Қазақстан. Email: s_taburova@kbtu.com*
Токтар Томирис Алтайқызы	*Энергетика және мұнай-газ индустриясы мектебінің бакалавриат студенті, Қазақ-Британ Техникалық Университеті, Төле би көш.,59, 050000, Алматы, Қазақстан. Email: t_toktar@kbtu.com*

Синтез биоразлагаемого полимера на основе крахмала для упаковочных пленок: Обзор

1*Искалиева А.Ж, ²Оразалин Ж.К., ²Елигбаева Г.Ж., ³Ирмухаметова Г.С. ., ⁴Табурова С.Н., ⁴Токтар Т.А.

¹Школа химической инженерии, Казахстанско-Британский технический университет, Алматы, Казахстан
² Кафедра Нефтяной Инженерии, Сатбаев Университет, Алматы, Казахстан
³ Факультет химии и химической технологии Казахский национальный университет им. аль-Фараби, Алматы, Казахстан
⁴Школа Энергетики и нефтегазовой индустрии, Казахстанско-Британский технический книверситет, Алматы, Казахстан

Аннотация

Благодаря своим качествам и функциональным возможностям в последние годы полимерам уделяется большое внимание в качестве материалов для упаковки пищевых продуктов. Эти характеристики включают нетоксичность, доступность, биосовместимость и способность к биоразложению, что свидетельствует об их перспективности в качестве альтернативы традиционной пластиковой упаковке, воздействие которой на окружающую

среду уже давно исследуется. Учитывая нынешний упор на устойчивое развитие, исследования биополимеров как экологически чистых и устойчивых материалов для упаковки пищевых продуктов имеют решающее значение. Синтез биоразлагаемых полимеров на основе крахмала представляет собой значительный шаг на пути к экологичным упаковочным решениям. Поскольку глобальный спрос на экологически чистые материалы продолжает расти, текущие исследования и инновации в этой области могут привести к разработке упаковочных пленок на основе крахмала с улучшенными свойствами и широким коммерческим применением. В связи с этим основной целью данного обзора является создание биоразлагаемого полимера на основе кукурузного крахмала и ПВС с высокими физико-механическими характеристиками для использования в пластиковых пакетах.

Ключевые слова: Полимеры, биоразлагаемость, упаковка, пластиковые пакеты.

	Информация об авторах:
Искалиева Асылзат Жамбуловна	*Ph.D. докторант школы химической инженерии, Казахстанско-Британский технический университет, ул. Толе би, 59, Алматы 050000, Казахстан. Email: asylzat@bk.ru*
Оразалин Жандос Кайратулы	*Кафедра Нефтяной Инженерии, Сатбаев Университет, ул. Сатбаева 22а, 050013, Алматы, Казахстан. Email: zhandos1403@bk.ru*
Елигбаева Гульжахан Жакпаровна	*Кафедра Нефтяной Инженерии, Сатбаев Университет, ул. Сатбаева 22а, 050013, Алматы, Казахстан. Email g.yeligbayeva@satbayev.university*
Ирмухаметова Галия Серикбаевна	*Кафедра химии и технологии органических веществ, природных соединений и полимеров Факультет химии и химической технологии Казахский национальный университет им. аль-Фараби, пр. аль-Фараби, 71, 050040, Алматы, Казахстан. Email: Galiya.Irmukhametova@kaznu.kz*
Табурова Ситора Нематовна	*Баклавриат, Школа Энергетики и нефтегазовой индустрии, Казахстанско-Британский технический книверситет, Толе би, 59, 050000, Алматы, Казахстан. Email: s_taburova@kbtu.com*
Токтар Томирис Алтайкызы	*Баклавриат, Школа Энергетики и нефтегазовой индустрии, Казахстанско-Британский технический книверситет, Толе би, 59, 050000, Алматы, Казахстан. Email: t_toktar@kbtu.com*

References

[1] Volkova TG. Destructible microbial polyhydroxyalkanoates as a technical analogue of indestructible polyolefins. Journal of the Siberian Federal University. Biology. 2015; 8(2):131-151.

[2] UNEP (Piece ed Nations Environmental Program). 2004. The African 10-Year Framework Programme (10YFP) on Sustainable Consumption and Production.http://www.unep.org/ru/Projects_Programmes/10YFP/index.asp. Accessed April 2010.

[3] Scott G. Degradable polymers. Principles and applications. Nederlands: Kluwer Academic Publ. 2002, 500.

[4] Potapov AG, Parmon VN. Biodegradable polymers – forward to the future. Ecology and industry of Russia. 2010; 5:4-8.

[5] Kaza Silpa, Yao Lisa C, Bhada-Tata Perinaz, Van Woerden Frank. What a Waste 2.0: A Global Snapshot of Solid Waste Management to 2050. Urban Development; Washington, DC: World Bank. 2018. https://openknowledge.worldbank.org/handle/10986/30317 License: CC BY 3.0 IGO

[6] 125 mln tonn tverdykh bytovykh otkhodov nakopilos v Kazakhstane [125 million tons of solid household waste have accumulated in Kazakhstan]. (Electron resource). 2021. https://www.inform.kz/ru/125-mln-tonn-tverdyh-bytovyh-othodov-nakopilos-v-kazahstane_a3800662

[7] Kongjan P, O-Thong S, Angelidaki I. Performance and microbial community analysis of two-stage process with extreme thermophilic hydrogen and thermophilic methane production from hydrolysate in UASB reactors. Bioresour. Technol. 2011; 102: 4028–4025.

[8] The source of this information is the letter written by Tim Krupnik of the Berkeley Ecology Center to Dr A. N. Bhat of the Indian Centre for Plastic in the Environment (ICPE), supporting the attempt to ban disposable plastics in India, on 15 March 2001. Courtesy Bharati Chaturvedi, Director, Chintan Environmental Organisation, New Delhi.

[9] Gordon SH, Imam SH, Greene RV. Starch-based plastics-measurement of biodegradability. In J. C. Salamone (Ed.), Boca Raton: CRC Press, Polymeric materials encyclopedia. 1996, 7885–7901.

[10] Strength of biodegradable polypropylene flat tapes filled with modified starch. Mechanics of composite materials. 2006; 42(3):389-400.

[11] Sherieva ML, Shustov GB, Beslaneeva ZL. Biodegradable compositions based on high-density polyethylene and starch. Plastic masses. 2007; 8:46-48.

[12] Bazunova MV, Bakirova ER, Bazunova AA, Kulish EI, Zakharov VP. The study of biodegradation of biodegradable polymer composites based on primary and secondary polyolefins and natural fillers of plant origin. Bulletin of the Technological University. 2018; 21(1):43-46.

[13] Suvorova AI, Tyukova IS, Trufanova EI. Biodegradable polymer materials based on starch. Uspekhi khimii. 2000; 69(5): 494-504.

[14] Lyubimtseva EC, Chursin VI. Multicomponent biopolymer compositions and films based on them. E.C. Lyubimtseva, Design and technologies. 2017; 57(99):6573.

[15] Iskalieva A, Yesmurat M, Al Azzam KM, Ainakulova D, Yerbolat Y, Negim E-S, Ibrahim MNM, Gulzhakhan Y. Effect of Polyethylene Glycol Methyl Ether Methacrylate on the Biodegradability of Polyvinyl Alcohol. Starch Blend Films. Polymers. 2023; 15:3165. https://doi.org/10.3390/polym15153165

[16] Ermolovich OA, Makarevich AV. The effect of the additives of the compatibilizer on the technological and operational characteristics of biodegradable materials based on starch-filled polyethylene. Journal of Applied Chemistry. 2006; 79(9):1542-1547.

[17] Krutko ET, Prokopchuk NR, Globa AI. Technology of biodegradable polymer materials: studies - method.manual Chemical technology of organic substances, materials and products. Technology of plastic masses. Minsk: BSTU. 2014, 105.

[18] Vlasov SV, Olkhov AA. Biodegradable polymer materials. Polymer materials: products, equipment, technologies. 2006; 7: 23-26, 2006; 8:35-36, 2006; 10:28-33.

[19] Opredeleniye i klassifikatsiya biopolimerov [Biopolymers and promising materials based on them]. (Electron resource). 2017. https://studref.com/694707/tovarovedenie/opredelenie_klassifikatsiya_biopolimerov

[20] Berketova LV, Polkovnikova VA. On the issue of eco-, edible and rapidly decomposing packaging in the food industry. Bulletin of Science and practice. 2020; 6(10):234-243.

[21] Maolin Zhai, Fumio Yoshiib, Tamikazu Kume «Radiation modification of starch-based plastic sheets». Carbohydrate Polymers. 2003; 52: 311–317.

[22] Barendswaard W, Litvinov VM, Souren F, Scherrenberg R L, Gondard C, Colemonts C. Crystallinity and Microstructure of Plasticized Poly(vinyl chloride). A 13C and 1H Solid State NMR Study. Macromolecules. 1999; 32:167–180.

[23] Felix H Otey, Richard P Westhoff. Biodegradable Films from Starch and Ethylene-Acrylic Acid Copolymer. American Chemical Society, Chicago. 1977; III(A):305-308.

[24] Pat. 2019/0017 Kazakhstan. El-Sayed Negim, Lyazzat Bekbayeva, Mun GA. Biodegradable plastic based on starch.

[25] De Moraes JO, Scheibe A.S, Sereno A, and Laurindo JB. Scale-up of the production of cassava starch based films using tape-casting. Journal of Food Engineering. 2013; 119(4):800-808. [Online]. Available: http://dx.doi.org/10.1016/j.jfoodeng.2013.07.009

[26] Wang S, Li C, Copeland L, Niu Q, and Wang S. Starch Retrogradation: A Com- prehensive Review. Comprehensive Reviews in Food Science and Food Safety. 2015; 14(5):568–585.

[27] Pither RJ. in Encyclopedia of Food Sciences and Nutrition (Second Edition) 2003.

[28] Mitrus M, and Mo´scicki L. Thermoplastic Starch. Extrusion-Cooking Techniques: Applications, Theory and Sustainability. 2011, 177-189.

[29] Ismail NA, Mohd Tahir S, Yahya N, Abdul Wahid MF, Khairuddin NE, Hashim I, Rosli N, and Abdullah MA. Synthesis and characterization of biodegrad- able starch-based bioplastics. Materials Science Forum. 2017; 846:673–678.

[30] Thawien Bourtoom, Manjeet S. Preparation and properties of rice starche-chitosan blend biodegradable film. LWT - Food Science and Technology. 2008; 4:1633- 1664.

[31] Shogren RL, Fanta GF, Doane WM. Development of starch based plastics– a reexamination of selected polymer systems in historical perspective. Staerke. 1993; 45:276-280.

[32] Doane WM. USDA research on starch-based biodegradable plastics. Staerke. 1992; 44:293-295.

[33] Lu DR, Xiao CM, Xu S. Starch-based completely biodegradable polymer materials. Polymer Letters. 2009; 3(6):366-375.

[34] Mani R, Bhattacharya M. Properties of injection moulded blends of starch and modified biodegradable polyesters. European Polymer Journal. 2001; 37:515-526.

[35] Bourtoom T, Chinnan MS. Preparation and properties of rice starch-chitosan blend biodegradable film. LWT-Food Science and Technology. 2008; 41:1633-1641.

[36] Wu Y, Geng F, Chang PR, Yu J, Ma X. Effect of agar on the microstructure and performance of potato starch film. Carbohydrate Polymers. 2009; 76:299-304.

[37] Ghanbarzadeh B, Almasi H, Entezami AA. Physical properties of edible modified starch/carboxymethyl cellulose films. Innovative Food Science & Emerging Technologies. 2010; 11(4):697-702.

[38] Suvorova AI, Tyukova IS, Trufanova EI. Biodegradable starch-based polymeric materials. Russian Chemical Reviews. 2000; 69:451-459.

[39] Gutierrez TJ, Alvarez VA. Properties of native and oxidized corn starch-polystyrene blends under conditions of reactive extrusion using zinc octanoate as a catalyst. React. Funct. Polym. 2017; 112:33-44.

[40] Tharanathan RN. Biodegradable films and composite coatings: past, present and future. Trends in Food Science & Technology. 2003; 14:71-78.

[41] Swin SN, Biswal SM, Nanda PK, Nayak PL. Biodegradable soy-based plastics: opportunities and challenges. Journal of Polymers and Environment. 2004; 12:35-42.

[42] Legonkova O, Melitskova E, Peshekhonova A. The future of biodegradation. Packaging and packaging. 2003; 2:62-63.

[43] Schmidt-Rohr K, Spiess HW. Multidimensional Solid-State NMR and Polymers. Academic Press: London. 1994; 9:187-215.

[44] Tang H, Xiong H, Tang S, Zou P. A starch-based biodegradable film modified by nano silicon dioxide. Journal of Applied Polymer Science. 2009; 113(1):34-40.

[45] Mukhiddinov BF, Alikulov FZh, Juraev ShT. Derivatographic study of thermal characteristics of compositions based on technical starch with calcium chloride. Universum: technical sciences. 2022; 2-5(95):48-52.

[46] Mirzoerova VA, Mukhamadiev MG. Obtaining biodegradable composite films based on starch and polyvinyl alcohol. Universum: chemistry and biology: electron, scientific. Journal. 2022;11(101). URL: https://7universum.com/ru/nature/archive/item/14511

[47] Morgacheva AA. Hydrogels based on modified polyvinyl alcohol and modified 2-hydroxyethyl starch. Moscow. 2019.

[48] Rath SK, Singh RP. On the characterization of grafted and ungrafted starch, amylose and amylopectin. J Appl Polym Sci. 1998; 7:1795-1810.

[49] Chiellini E, Corti A, D'Antone S, & Solaro R. Biodegradation of poly (vinyl alcohol) based materials. Progress in Polymer Science. 2013; 28(6):963-1014. https://doi.org/10.1016/s0079-6700(02)00149-1

[50] Averous L. Biodegradation multiphase systems based on plasticized starch. A review. J Macromol Sci Polym Rev. 2004; 44:231-274.

[51] Negim E, Rakhmetullayeva R, Yeligbayeva G, Urkimbaeva P, Primzharova S, Kaldybekov D, Khatib J, Mun G, and C W. Improving biodegradability of polyvinyl alcohol-starch blend films for packaging applications. International Journal of Basic and Applied Sciences. 2014; 3(3):263-273.

[52] Negim ESM, PI U, Bekbayeva L, BHO M, Mohamad MN, Irmukhametova G, & GA M. Effect of acrylic acid on the mechanical properties of PVA-starch blend films. Egyptian Journal of Chemistry. 2020; 63(5):1911-1919.

[53] Byrn SR, Xu W, Newman AW. Chemical Reactivity in Solid- State Pharmaceuticals. Formulation Implications. Adv. Drug Delivery Rev. 2001; 48:115-136.

[54] Thakur R, Pristijono P, Scarlett CJ, Bowyer M, Singh SP, and Vuong QV. Starch-based films: Major factors affecting their properties. International Journal of Biological Macromolecules. 2019; 132:1079-1089. [Online]. Available: https://doi.org/10.1016/j.ijbiomac.2019.03.190

МАЗМҰНЫ
СОДЕРЖАНИЕ
CONTENTS

Техникалық редакторлар:
Г.К. Қасымова, Н.М.Айтжанова, Т.И. Қожахметов

Компьютердегі макет:
Г.К. Қасымова

Дизайнер:
Г.К. Қасымова, Н.М.Айтжанова

Металлургия және кен байыту институты; Сәтбаев Университеті
050010, Қазақстан Республикасы, Алматы қаласы, Шевченко к-сі, 29/133

Жариялауға 14.09.2023 жылы қол қойылды

Технические редакторы:
Г.К. Касымова, Н.М. Айтжанова, Т.И. Кожахметов

Верстка на компьютере:
Г.К. Касымова

Дизайнер:
Г.К. Касымова, Н.М.Айтжанова

Институт металлургии и обогащения; Сатпаев Университет
050010, г. Алматы, Республика Казахстан. ул. Шевченко, 29/133

Подписано в печать 14.09.2023г.

Technical editors:
G.K. Kassymova, N.M. Aitzhanova, T.I. Kozhakhmetov

The layout on a computer:
G.K. Kassymova

Designer:
G.K. Kassymova, N.M. Aitzhanova

Institute of Metallurgy and Ore Benficiation; Satbayev University,
050010, Almaty city, the Republic of Kazakhstan. Shevchenko str., 29/133

Signed for publication on 14.09.2023